SOME   STUDIES   OF   VIBRATIONAL   RELAXATION

USING   A   SHOCK   TUBE

by

R. GUTTERIDGE

A thesis submitted to the University of Keele
in partial fulfilment of the requirements for
    the Degree of Doctor of Philosophy

DEPARTMENT OF CHEMISTRY

UNIVERSITY OF KEELE   SEPTEMBER 1972

ACKNOWLEDGMENTS

In presenting this thesis I would like to thank the following:

All the work reported in this Thesis

was carried out by the author under the

supervision of Dr. P. Borrell

ABSTRACT

The vibrational relaxation of HCl, HBr, HI or DCl has been studied either as a pure gas or in mixtures with argon, nitrogen or carbon monoxide. Infrared radiation from the second or third vibrational levels was used to follow the relaxation process.

Measurements on pure HCl and HBr only allowed upper limits for the Napier times to be given because of the rapidity with which vibrational energy is taken up. A lower limit for the Napier time of HCl was obtained by diluting it with argon. Collisions of argon with HCl were assumed to be completely ineffective in causing T→V energy transfer. Subsequently published values fell within the range obtained (0.2 - 0.6 atm s at 1850 K).

Dilution of HCl by nitrogen was only moderately effective in slowing down the rate of relaxation. Analysis showed that the Napier time for the V→V process is about 50 times longer than that for the T,R→V process in pure HCl. The value agrees with the recently published Napier time for the N_2/HI system.

For mixtures of hydrogen halides with CO, emission from the predominant component, CO, was monitored. Even with small amounts of halide, the relaxation was considerably faster than that of pure CO. The measurements, analysed using the equations of Bauer, showed that the V→V and T,R(CO)→V(halide) processes were approximately equally

efficient. Limiting values of these rate constants were set for CO/HCl, CO/HBr, CO/HI and CO/DCl systems. They indicate that the smaller the energy difference, the faster the rate for V→V energy exchange.

All the measurements are compared with theoretical predictions for the systems. The Napier times for pure HCl and HBr agree with the predictions of the Moore theory better than with those of SSH and support the idea of R→V energy transfer being important for molecules containing hydrogen.

For mixtures of halide with CO, the rates of vibrational energy exchange are predicted moderately well by the SSH near resonance theory. However values of τ_{HCl-CO} are poorly predicted by both theories for they both neglect the rotation of the activated molecules.

UNITS

During the writing of this thesis, some of the accepted units of measurement have been changed. The relevant ones are listed below together with the factor by which the measurement is multiplied to convert it to the appropriate S.I. unit.

	Previous Unit	S.I. unit	Conversion factor
Pressure	mm Hg	Nm^{-2}	133.3
	bar	Nm^{-2}	10^5
Temperature	$^{\circ}K$	K	1
Length	$\overset{\circ}{A}$	m	10^{-10}
Capacity	litre	dm^3	1
Energy	cal	J	4.186
Planck's Constant	$erg\ s^{-1}$	Js	10^{-7}
Boltzmann Constant	$erg\ deg^{-1}$	JK^{-1}	10^{-7}
Gas Constant	$cal\ deg^{-1}\ mole^{-1}$	$J\ mol^{-1}\ K^{-1}$	4.186

C O N T E N T S

1. INTRODUCTION

1.1 Historical

Space research brought a fresh impetus to the study of gases at high temperatures for vehicles re-entering the earth's atmosphere are preceded by shock waves in which temperatures of several thousand degrees are common. Under these conditions, molecules contain appreciable amounts of vibrational energy and are sometimes sufficiently excited for dissociation to occur. Prediction of their behaviour from low temperature data is inaccurate and it is better to derive high temperature data by measurement rather than extrapolation.

The exploitation of shock waves to study gases at elevated temperatures is essentially a post Second World War phenomenon. Vielle[1] described the production of shock waves in shock tubes as long ago as 1899 but little use was made of them for several decades when the rapid developments in electronics during the war period and the advent of supersonic flight spurred on the use of shock tubes as a tool for aeronautical research. Since about 1953, papers have been published reporting new applications of the shock tube in the fields of aeronautics, chemistry and physics.

Heating of gases in shock waves is very rapid; the energy is taken up by the molecules as translational motion causing, for all but nonatomic gases, a disequilibrium between the various modes of energy. The relaxation of vibrational energy to equilibrium is a gradual process which has been quantitatively described by Schwartz, Slawsky and Herzfeld[2] from theoretical considerations (SSH theory). Moderately good agreement was found between theoretical calculations and experimental values which are mostly for air gases having attracted a great deal of attention due to their obvious importance.

However measurements of the rate of vibrational relaxation are important not only on account of space research for the way in which energy is transferred between molecules may be important for an understanding of how a molecule can take up sufficient energy to dissociate. This is presumably a preliminary step in some chemical reactions.

A further reason for investigating vibrational relaxation is to help the interplay of theory and experiment. By referring to measured values, theories can be refined and made applicable to a wider range of molecules over a wider range of temperatures.

Of gases not found in the atmosphere, hydrogen halides with their high force constants and large dipole moments provide a severe test of SSH theory which only considers important energy

transfer between the translational and vibrational modes. Cottrell and his co-workers[3] and Moore[4] suggest that transfer between rotational and vibrational modes may be important for molecules which, like hydrogen halides, have a low moment of inertia. This mechanism would affect the rate at which the pure gas relaxes and indirectly the rate at which vibrational energy can be transferred from a hydrogen halide to a second diatomic molecule. For these reasons, hydrogen halides are interesting molecules on which to make measurements. It was decided therefore to study some systems which incorporated these molecules.

The rest of the introduction contains the background information against which the measurements were made. The value of the shock tube as a technique for making such measurements is assessed in section 1.2 and its operation is described in sections 1.3 and 1.4. Sections are devoted to the measurements, available at the commencement of this study, of relevant Napier times (sections 1.5, 1.6) and the theories for calculating them (section 1.7). Section 1.8 summarises the problems on which it was hoped to shed some light.

1.2   The Shock Tube as a Technique for Measuring Vibrational

Relaxation

Methods for measuring the rate of vibrational relaxation
have been described by Read,[5] by Gordon, Klemperer and Steinfeld[6]
and more recently by Borrell.[7]   Many techniques such as ultrasonic
absorption and dispersion, are only suitable for measurements within
a few hundred degrees of room temperature even though furnaces can
be constructed, albeit with some difficulty, which will maintain
the temperatures of the subsequent study (up to 3000°K).

Production of a disequilibrium between the modes of energy
is a prerequisite to observing vibrational relaxation.   Sound waves
of the correct frequency do this repeatedly but flash photolysis
and shock waves are single event phenomena.

In flash photolysis, the reactant is subjected to a short
pulse of a highly intense light.   An upper limit to the fastest
observable rate of relaxation is set by the duration of the pulse,
usually a few microseconds.   Sometimes an absorbing species must be
introduced although this complicates the system.   But even if one
is not added, the quantity of energy taken up by the system cannot
be predicted.

For a shock wave the amount of thermal energy imparted to
the system is varied simply by changing the downstream pressure thus
altering the speed and strength of the shock wave.   This quantity of

energy can be calculated precisely for a diatomic gas where only translational, rotational and vibrational excitation need be considered; the accuracy is the same as the accuracy of the equations of state (the gas law and the caloric equation of state). A second advantage of using shock waves is that the rate of heating is very rapid being approximately the time it takes to convert directed momentum into randomised motion. Only a few collisions are needed and the process is often complete in less than a nanosecond. Relaxation is followed by observing the rate at which vibrational levels are populated but very slow rates are excluded as the total time of uniform heating rarely exceeds a millisecond. In spite of this restriction, the simplicity with which any gas can be rapidly heated over a wide range of temperatures makes the shock tube a very attractive tool for measuring the rate of vibrational relaxation.

1.3 Performance of a Shock Tube

Becker[8] produced a simple picture for the formation of a plane shock wave which has been reiterated in the standard texts of Gaydon and Hurle,[9] Greene and Toennies[10] and Bradley.[11] It shows that the pressure, density, temperature and velocity of the gas change rapidly across the shock front although for a diatomic gas,
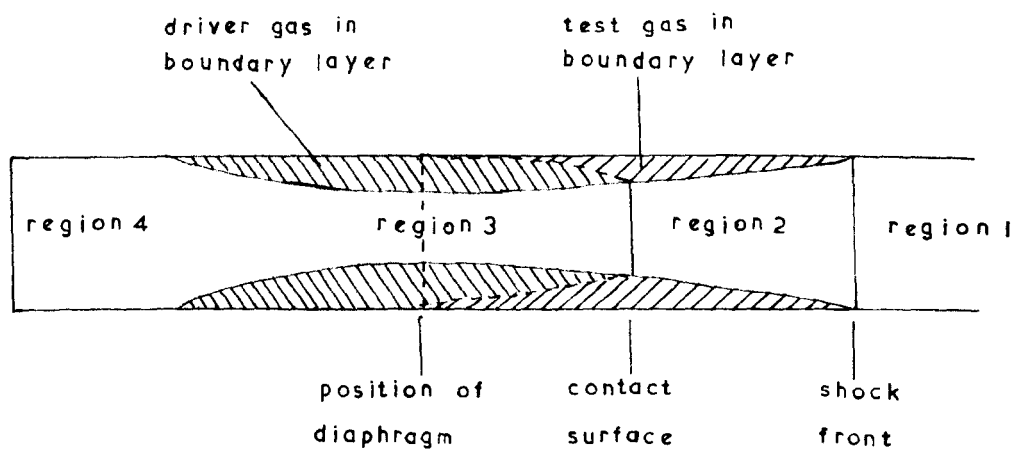
Figure 1.1 Boundary layer in a shock tube

complete equilibrium may take thousands of collisions.

Ideally, the shocked gas has one-dimensional character
for non-planarity of the shock front would invoke a pressure
gradient across the gas flow which is insupportable in a fluid.
The latter situation does occur but only momentarily near the
diaphragm so a distance of several tube diameters is allowed
before any measurements are taken to ensure that the shock wave
is fully formed. Downstream, deviation from being one-dimensional
occurs due to the viscous nature of gas. The shocked gas cannot
move in the whole cross-section of the tube as a boundary layer
is formed in the flow behind the incident shock. Its thickness
gradually increases from zero at the shock front (fig. 1.1). The
boundary layer which is the leading cause of non-idealities that
complicate quantitative shock tube work, removes test gas from the
flow. A direct result of this is a decrease in the area of the
contact surface, in extreme cases to zero, so reducing the driving
force for the shock which will consequently attenuate. That the
boundary layer is not complicating measurements is most easily
indicated by monitoring the shock speed between several points;
it should be unvarying. As constant speed implies constant enthalpy
behind the shock front, a photoemissive gas which relaxes rapidly
should give a constant light output. Both these characteristics
were observed in the subsequent experiments except perhaps when

| moving gas ③ | →v_2 | shock wave ② P_2, ρ_2, T_2 | →u_1 | stationary test gas ① P_1, ρ_1, T_1 |

contact
surface
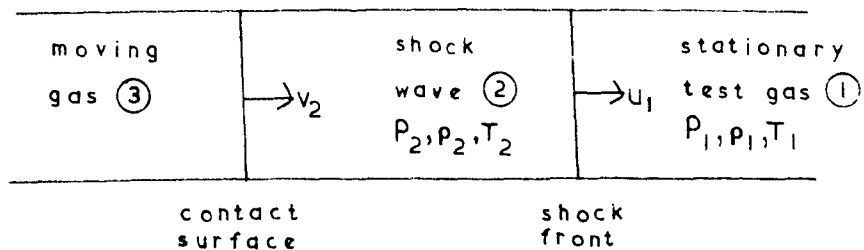
shock
front

Figure 1.2 Laboratory fixed coordinates:
shock tube at rest.

←
$u_2 = u_1 - v_2$ ←—u_1
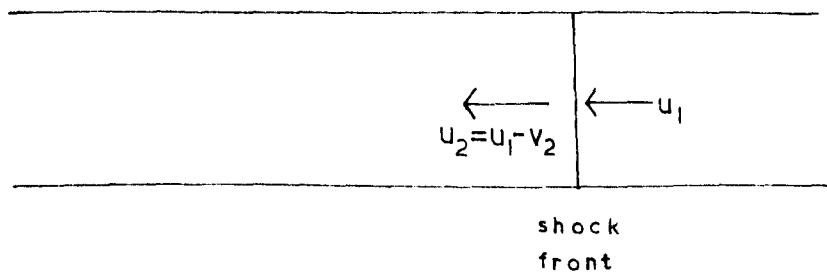
shock
front

Figure 1.3 Shock-fixed coordinates:
shock front at rest

the lowest downstream pressure, 1.3 mm Hg, was tried (section 3.1.2).

Projections into the gas stream are another reason for non-uniform flow. Windows inserted into the tube are obvious and crucial places where such projections may be found. Using a glass shock tube and observing only harmonic radiation from HCl, HBr and CO avoided the need for windows. Joints in the sections of tubing were made as smooth as possible.

1.4 Calculation of Conditions in the Shock Wave

Passage of the shock front down the shock tube is represented in figure 1.2; the cold test gas, which is stationary is designated as region 1 and the shocked gas as region 2. It is easier to work in shock-fixed coordinates in which case the shock front is considered at rest (fig. 1.3).

Relationships between the parameters P, ρ, u and H, the pressure, density, speed and enthalpy of unit mass respectively, are obtained by application of the conservation equations for mass (1.1), momentum (1.2), and energy (1.3), (see for example page 14 ref. 9).

For unit mass of gas passing through the shock front

$$\rho_1 u = \rho_2 u_2 \qquad\qquad 1.1$$

$$P_1 + \rho_1 u_1^2 = P_2 + \rho_2 u_2^2 \qquad\qquad 1.2$$

$$H_1 + \tfrac{1}{2} u_1^2 = H_2 + \tfrac{1}{2} u_2^2 \qquad\qquad 1.3$$

Of the above parameters, only P_1 and u_1 are measured. This leaves six unknowns: ρ_1, ρ_2, u_2, P_2, H_1, and H_2. The density is related to pressure by the gas law. For an ideal gas,

$$P = \rho RT \qquad\qquad 1.4$$

where R is the gas constant for unit mass of gas and T is the absolute temperature. Substitutions for ρ_1 and ρ_2 in equations 1.1 and 1.2 eliminates two unknowns but introduced two others, T_1 and T_2. The initial temperature, T, is measured leaving five unknowns.

The above conservation equations (1.1, 1.2, 1.3) are true for all gases whereas equation 1.4-4 is only true for ideal gases. Greater accuracy when dealing with real gases would be achieved by using a gas law such as Van der Waal's, which represents the behaviour of the gas more exactly than the ideal gas law. However for the low densities found in the shock tube, the difference between the two is negligible (page 33, ref. 10).

Values for the enthalpy can be obtained by using the caloric equation of state. The form of it applicable to this study is

$$H = E_{tr} + E_{rot} + E_{vib} + RT \qquad 1.5$$

where the energy terms, E, are for translational, rotational and vibrational motion respectively. Even at room temperature the first two have their classical values, $3/2RT$ for E_{tr} and RT for E_{rot}. For the molecules considered (HCl, HBr, CO, N_2), the vibrational energy is negligible at room temperature but must be considered at higher temperatures. For an harmonic oscillator

$$E_{vib} \simeq \frac{Nh\nu}{\exp(h\nu/kT)-1} \qquad 1.6$$

where h, ν and k have their usual significance and N is the number of molecules in unit mass of gas. The expression needs to be modified for real effects such as anharmonicity. In general, it is more accurate to use standard enthalpy tables (such as JANAF tables[12]) and use a curve fitting procedure to obtain an equation for the way in which the enthalpy varies with temperature. By substituting expressions in terms of T for H_1 and H_2 in equation 1.3, only three unknowns, P_2, u_2 and T_2 remain and there are three equations with which to solve them.

Computer Program 1 (Appendix A) calculates the coefficients for the power equation used to express the enthalpy of the gas or gas mixture. These are fed into Computer Program 2 (Appendix A) which has an iterative routine based on the procedure of Gaydon and

Hurle (page 37, ref. 9) to obtain values for the ratios ρ_2/ρ_1, T_2/T_1 and P_2/P_1. For a relaxing gas, the enthalpy, H_2, is constant but since the vibrational energy increases, the translational energy, which the temperature, T_2 reflects must fall. The ratios are calculated for two conditions: firstly when there has been no vibrational relaxation and secondly when the relaxation is complete.

1.5 Non-equilibrium Processes in the Shock Wave

The transition from gas in region 1 at equilibrium to gas in region 2 at equilibrium (fig. 1.2) must be brought about by molecular collisions. For a two state system, the relaxation may be characterised by a quantity τ known as the relaxation time defined by the equation

$$\frac{dx(t)}{dt} = \frac{x(\infty) - x(t)}{\tau} \qquad 1.7$$

Here $x(t)$ is the value of a relaxing physical quantity at time t, $x(\infty)$ is the equilibrium value.

For a monatomic gas, only translational energy increases across the shock front and so only a translational relaxation time exists.

For a diatomic gas, rotational and vibrational energy increase and so rotational and vibrational relaxation times can

also be given. Since rotational energy increases at the expense

of translational energy, and vibrational at the expense of

rotational and translational "equilibrium value" must be used in

the restricted sense of the value to which the energy tends should

a subsequent process not occur.

The rate of relaxation can also be quantified by quoting

the number of collisions, Z_{tr}, Z_{rot} or Z_{vib}, associated with the

relaxation time.

When considering rotational and vibrational energy, it

is necessary to consider energy transfer in multistate systems and

it becomes possible to distinguish three types of experiments in

which one measures:

(1)   a specific rate of transition from state 1 to state 2

(2)   a net rate of removal of species from state 1 to any
      other state

(3)   a net relaxation effect averaged over some distribution
      of states.

Measurements of relaxation times are usually compared

directly without regard to which category the experiments belong

or whether the energy levels were observed directly, by spectroscopic

measurements, or indirectly by density measurements.

1.6   Relaxation Measurements

The problems of energy transfer between atoms and molecules have been the subject of many studies (section 1.6.1). Evidence is presented to show that translation → translation energy transfer is very rapid for all molecules (section 1.6.2) and transfer from translation → rotation is only a little slower for most molecules (section 1.6.3). Equilibrating translational with vibrational energy is generally a much slower process (section 1.6.4). If however the species is a vibrationally excited molecule, the activation can occur by rapid vibration → vibration energy exchange (section 1.6.5).

The mechanism by which upper vibrational levels are populated is the subject of the last part of this section (section 1.6.6).

1.6.1   Literature

Greene and Toennies[10] tabulated physico-chemical shock tube literature up to 1963 and Strehlow[13] extended the review to 1966. Bauer[14] covered the period from the middle of 1963 to the end of 1964.

Herzfeld and Litovitz[15] and Cottrell and McCoubrey[16] restrict the field to relaxation phenomena but increase the range of measurements with the inclusion of non-shock tube data. Literature

up to 1964 has been reviewed by Read,[5] Takayanagi,[17,18] Callear[19] and Stevens[20] and up to 1967 by Borrell[7,21] and Gordon, Klemperer and Steinfeld.[6]

1.6.2   Translational Relaxation

Kohler[22] interpreted viscosity, η, as due to the existence of a relaxation time, τ_{tr}, for the adjustment of translational energy to that of the new environment. He writes

$$\eta \quad = \quad P \, \tau_{tr} \qquad\qquad 1.8$$

$$\text{where} \quad \tau_{tr} \quad = \quad 1.271 \, \tau_c \qquad\qquad 1.9$$

where τ_c is the time between collisions. The factor 1.271 is due to the persistence of velocities.

Figure 1.3 shows that the situation at the shock front can be considered as a gas moving with speed u, suddenly being brought nearly to rest. Because most of the directed momentum need to be randomized, it would be anticipated that a number of collisions greater than 1.271 will be needed to relax the translational energy.[14]

Several theoretical papers such as those by Mott-Smith,[23] Zoller,[24] Gustafson[25] and Gilbarg and Paolucci,[26] have predicted a shock front thickness of only a few collisions. Andersen and Hornig[27] reflected light from the shock front and found about 11 collisions were needed for argon at $500^{\circ}K$. The number decreased

with increasing temperature.

The situation for polyatomic gases is complicated by the need for the redistribution of energy among translation, rotation and vibration. However values of Z_{tr} for N_2, CO and HCl have been measured over the temperature range $340-400^{\circ}$K.[27] They are similar to Ar and show the same trend with temperature. Linzer and Hornig[28] have extended the measurements on N_2 to Mach 3.7 (1060°K) when only 2.5 collisions were needed. The measurements were in good agreement with the calculations of Muckenfuss[29] whereas the previous results[27] fitted the calculations of Gilbarg and Paolucci.[26]

As the time for a few collisions is so small (usually <1 ns at 1 atm) the relative merits of the theories are of no importance when considering vibrational relaxation. For N_2, CO and HCl, translational energy can be considered to respond instantly to any adjustment in the distribution of energy. Although HBr has not been observed, there is no reason to expect any great difference in its behaviour.

1.6.3 Rotational Relaxation

Transfer of translational to rotational (T→R) energy increases the rotational quantum number by at least unity and often more (30, 31). Consider HCl at 2000°K: the average molecular kinetic

energy, $^3/_2$ kT, is 0.041 aJ molecule^{-1}; the separation of

rotational lines is approximately 20.8 cm^{-1} [32] so the quantum

for the J = 0 → 1 transition is 0.00083 aJ. Therefore most

molecules will have sufficient energy for redistribution to

take place.

Ehrenfest (cf. ref. 15, page 62) showed that for a near

adiabatic change, when the change in a force is relatively small

during a period of motion, it is unlikely that the quantum number

will be affected. For T → R transitions to occur frequently, it

means that the time during which the exciting and excitable molecule

interact must be short compared with the period of rotation. Again

consider HCl at 2000°K: the arithmetic mean relative speed[33] is

$(8kT/\bar{m}\pi)^{\frac{1}{2}}$ which is 1.832 km s^{-1} so for a characteristic length,

l', of 120 pm (ref. 15, sections 56, 58), the time of interaction

is 65.5 fs. The frequency for the J = 0 → 1 transition is 624 GHz

which means a period of rotation of 1.60 ps. As this is 25 times

larger than the period of interaction, the collision is relatively

nonadiabatic.

The above two reasons that most molecules of hydrogen

chloride have sufficient kinetic energy and the collision is non-

adiabatic, suggest that few collisions should be required for a

T → R energy transfer. As HCl is a particularly unfavourable case

with the spacing of rotational lines being so large (for example,

the spacing for N$_2$ is 4.0, CO is 3.8 and HBr 16.7 cm^{-1} [32]), the

conclusion should be valid for most molecules.

Experiments show that values of Z_{rot} greater than 10 are uncommon except for hydrogen and deuterium which have values of 200-300.[6,14,15,16]

To predict values for Z_{rot} at the temperatures in shock waves requires knowledge of Z_{rot} at some temperature and also the temperature dependence of Z_{rot}. Raff[34,35] made calculations for two systems (H_2, He) and (D_2, He) and showed τ_{rot} decreased as the temperature increased. Zeleznik[36] found the antithesis for polar molecules, while Berend and Benson[37] agreed with Raff for (H_2, He), (H_2, H_2) and (D_2, He) but with Zeleznik for (O_2, O_2) and (N_2, N_2) between 100° and 700°K, while expecting a negative temperature dependence above 700°K. This theoretical uncertainty is paralleled by the experimental results. A positive temperature dependence has been measured for H_2, D_2, O_2, N_2, NH_3, SO_2[38,39,40,41] and a negative temperature dependence for H_2O, D_2O, CH_4, CD_4, HCl, DCl, HF, DF, NH_3.[42,43,44,45] Hydrogen sulphide exhibits both.[45]

Results for Individual Molecules used in this Study

Nitrogen

Table 1.1

Technique	$T^{O}K$	Z_{rot}	Reference
Acoustical	302	6.0	46
"	293	3.6	47
"	298	4.6	48
"	293	5.5	49
"	295	5.3	50
"	295	5.5	51
"	303	4.7	52
"	Room Temp.	4.4	39
"	295	3.6	38
Shock thickness		5.5	28
Recovery factor	279	7.2	53
Thermal transpiration	280	3.3	54
" "	495	4.4	55
" "	500	3.8	56
Free jet	300	4.2	57

Carnevale, Grey and Larson[39] and Winter and Hill[38] showed that Z_{rot} for N_2 increased with temperature. The latter paper gave a value of 15.4 collisions at $1072^{O}K$.

Carbon Monoxide

Andersen and Hornig[27] showed that carbon monoxide was more than 90% towards rotational equilibrium within 20 collisions. Tip, Los and de Vries[56] measured Z_{rot} as 1.9 at 500°K. Bauer and Kosche[58] gave a value of 2.1 at room temperature.

Hydrogen Chloride

Andersen and Hornig[27] showed that HCl had taken up more than the equilibrium amount of rotational energy within 20 collisions. Breazeale and Kneser[59] measured Z_{rot} as 7 at 273°K. Baker and Brokow[43] measured a value of 6.2 at 300°K falling to 3.0 at 471°K; Barua, Manna and Muckhopadhwyay[45] measured it as 6.6 at 273°K falling to 2.2 at 473°K.

Summary of Measurements

The rotational collision numbers for HCl, N_2 and CO are known to be less than 10 at room temperature and it is presumed that the value for HBr will be similar. Indications are that Z_{rot} will increase with temperature for N_2 but decrease for HCl, HBr, and CO. Even at the highest temperatures in this study (3000°K), it is not anticipated that τ_{rot} will be greater than 10 atm ns for any molecule. When measuring vibrational relaxation, this is sufficiently small for the rotational and translation energies to be

considered continuously coupled, instantly adjusting to changes in the environment.

1.6.4 Vibrational Relaxation of a Gas with Either Itself or a Monatomic Gas as Collision Partner

In section 1.6.3 it was shown that the average molecular kinetic energy of HCl at 2000°K is 0.041 aJ. As a quantum of vibrational energy, frequency 2886 cm^{-1}, [32] is 0.052 aJ, many molecules do not have sufficient kinetic energy to effect a T $\rightarrow$ V transfer. Suppose 0.041 aJ molecule^{-1} corresponds to a relative velocity ω_o. From the Maxwell distribution law for one-dimensional motion, N', the number of molecules per unit mass with a relative velocity greater than ω_o is:

$$N' = \int_{\omega_o}^{\infty} N \, \omega \, \frac{\tilde{m}}{kT} \, \exp\left(-\frac{\tilde{m}\,\omega^2}{2kT}\right) \cdot d\omega \qquad\qquad 1.10$$

where N is the total number of molecules per unit mass. Performing the integration gives $\frac{N'}{N} = 0.15$. Thus for HCl at 2000°K, only 15% of the molecules have the energy sufficient to transfer to vibrational energy.

The frequency of HCl, 2886 cm^{-1} (86.5 THz) corresponds to a vibration period of 11.6 fs. As this is only a factor of 5.7 smaller than the time of interaction (section 1.6.3), the molecular
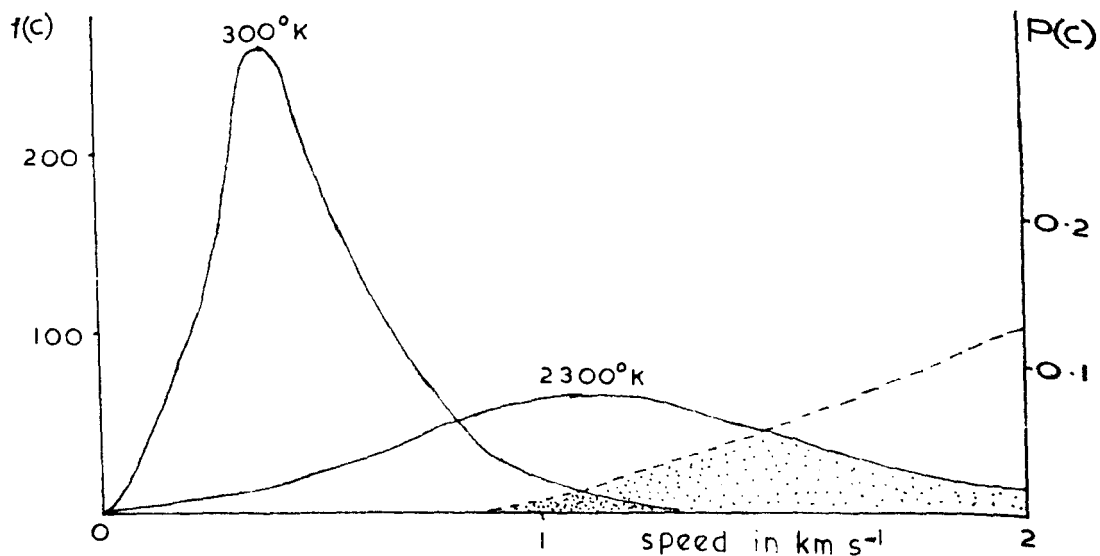
Figure 1.4 Schematic representation of the distribution of molecular speeds, $f(c)$, and the probability of vibrational de-excitation, $P(c)$, for nitrogen. (After Millikan[60])

collisions are more adiabatic than when rotational energy is being transferred.

The above reasons suggest that a large number of collisions are required for vibrational relaxation. More detailed theoretical calculations show (section 1.7) and experimental observations confirm this to be the case.

Measured vibrational relaxation times are usually corrected to a standard pressure of one atmosphere. Henderson[61] has pleaded that the quantity should be known as the "Napier Time". This notation will be used in this thesis.

Johanneson and his co-workers[62,63,64] recognized that any temperature dependence of the Napier time must be partly due to a decrease in the number of molecules when temperature is increased and pressure kept constant. They prefer to eliminate this effect presenting values of relaxation frequency (the reciprocal of relaxation time) at a standard density in units of $Amagat^{-1}s^{-1}$. This convention has not achieved general acceptance and in this thesis the previous system will be followed.

Raising the temperature of a gas leads to a greater fraction of molecules having sufficient kinetic energy and hence the relaxation process is accelerated. This is illustrated in figure 1.4. The temperature dependence, which exhibits the form $\log \tau_{vib} \alpha\ T^{-\frac{1}{3}}$, is that predicted by SSH theory (section 1.7).

Napier Times for Gases Used in this Study

      Several authors have collated Napier times.[5,7,10,13-22]
The review by Borrell[7] is both recent and extensive and most of the
values contained therein are still accepted. It has been used as
a source of values for nitrogen, carbon monoxide, hydrogen chloride
and hydrogen bromide.

Nitrogen

      Many early measurements are suspect due to the presence
of water to which the relaxation is particularly sensitive.[65,66]
Blackman's values[67] for the higher temperature (5000°K) still appear
to be valid but at lower temperatures those of Gaydon and Hurle[68,69,74]
and Millikan and White[70] are better.

Table 1.2 Napier Times for Nitrogen $N_2(N_2)$

Temperature (°K)	Napier Time (atm μs)
1500	4680
2000	854
2500	143
5000	5.5

Hurle[68] has shown that concurrent results are given by three methods of observing vibrational relaxation of nitrogen: interferometry (Blackmann), interferometry and sensitised infrared emission from 1% CO (Millikan and White), and sodium-line reversal (Hurle). Levitt and Sheen[71] also obtained similar values after replacing CO by SO_2 as the tracer gas.

The Napier times for $N_2(N_2)$ fit the equation:

$$\log_{10} \quad \tau(\text{atm s}) = 102 \, T^{-\frac{1}{3}} - 11.24 \quad (1500\text{-}6000^\circ K) \qquad 1.11$$

Measurements in expansion experiments of the V → T rate (as opposed to the T → V rate observed above) lead to Napier times which are anomolously short, often a factor of 70 smaller. A satisfactory vindication of these values has not yet been advanced although it may be that the conclusion of Von Rosenberg, Jr., Taylor and Teare for CO (next subsection) are applicable to N_2. They will be disregarded here.

Carbon Monoxide

The first study of CO in a shock tube was made by Windsor, Davidson and Taylor[72] who observed the infrared emission at 2.3 μm from the gas in the reflected shock. Their times were found to be a little long by later workers who also were extremely careful about impurities, especially water, to which Windsor and his co-workers had shown the Napier time to be sensitive. Matthews[73] used

interferometry, Gaydon and Hurle[74] the line reversal technique
and Hooker and Millikan[75,76] observed the infrared emission from
the fundamental band.

Table 1.3 · Napier Times for Carbon Monoxide, CO(CO)

Temperature ($^{\circ}$K)	Napier Times (atm µs)
1000	2000
1500	257
2000	74.1
2500	29.5
5000	2.3

The Napier time[73-75] for CO(CO) is given by the quation:

$$\log_{10} \tau(\text{atm s}) = 75.8T^{-\frac{1}{3}} - 10.16 \quad (1000\text{-}6000^{\circ}\text{K}) \qquad 1.12$$

Measurements in expansion experiments give anomolously
short values being sometimes one thousandth the T $\rightarrow$ V rate.
Von Rosenberg, Jr., Taylor and Teare[77] have reduced the ratio to
a factor of 5 by careful purification of the gas giving particular
attention to hydrogen. They have shown that the rate of relaxation
is extremely sensitive to presence of hydrogen atoms.

The effect of additives on the relaxation has been extensively studied by Millikan and White.[75,78,79] The equations for Napier times are:

$$CO(He) \quad : \quad \log_{10} \quad \tau(atm\ s) = 37.8T^{-\frac{1}{3}} - 8.30 \quad (580-1500^{\circ}K) \quad 1.13$$

$$CO(Ne) \quad : \quad \log_{10} \quad \tau(atm\ s) = 61.7T^{-\frac{1}{3}} - 9.16 \quad (1400-3000^{\circ}K) \quad 1.14$$

$$CO(CO) \quad : \quad \log_{10} \quad \tau(atm\ s) = 69.5T^{-\frac{1}{3}} - 9.65 \quad (1400-2900^{\circ}K) \quad 1.15$$

$$CO(Ar) \quad : \quad \log_{10} \quad \tau(atm\ s) = 79.1T^{-\frac{1}{3}} - 9.74 \quad (1700-2700^{\circ}K) \quad 1.16$$

$$CO(Kr) \quad : \quad \log_{10} \quad \tau(atm\ s) = 81.8T^{-\frac{1}{3}} - 9.70 \quad (2100-7000^{\circ}K) \quad 1.17$$

The atomic masses of the colliding partners He, Ne, CO, Ar, Kr are 4, 20, 28, 40 and 84 respectively. There is a definite correlation between τ and mass: the lighter the activating atom, the more rapid is the process of relaxation.

Hydrogen Chloride, Hydrogen Bromide

At the commencement of this study, the only high temperature values of Napier times for these hydrogen halides had been made by Borrell.[80] The measurements for both gases show some scatter but an average value for HBr (from the fundamental emission) is 16 atm μs at $1000^{\circ}K$ and an average for HCl (for both fundamental and first overtone emission) is 8 atm μs at $2000^{\circ}K$. Subsequent measurements by Bowman and Seery and Breashers and Bird (Section 5.1) have shown the actual values to be somewhat shorter than these.

1.6.5 Mixtures of Two Polyatomic Gases

When a mixture of two polyatomic gases is shocked, both components can take up energy by a $T \to V$ process. The molecule causing excitation can be of the same or the complementary species to that being excited.

$$AB(v = 0) \quad + \quad AB \quad \rightleftharpoons \quad AB(v = 1) \quad + \quad AB \qquad T \to V \qquad \qquad 1.18$$

$$AB(v = 0) \quad + \quad CD \quad \rightleftharpoons \quad AB(v = 1) \quad + \quad CD \qquad T \to V \qquad \qquad 1.19$$

$$CD(v = 0) \quad + \quad CD \quad \rightleftharpoons \quad CD(v = 1) \quad + \quad CD \qquad T \to V \qquad \qquad 1.20$$

$$CD(v = 0) \quad + \quad AB \quad \rightleftharpoons \quad CD(v = 1) \quad + \quad AB \qquad T \to V \qquad \qquad 1.21$$

A fifth reaction, involving vibration-vibration energy transfer, is also possible:

$$AB(v = 0) \quad + \quad CD(v = 1) \quad \rightleftharpoons \quad AB(v = 1) \quad + \quad CD(v = 0) \qquad V \to V \qquad 1.22$$
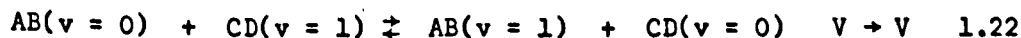
Evidence of this process has been indirectly presented in the preceding section (1.6.4). Firstly, the sensitivity of CO and N_2 to H_2O is thought to be due to $V \to V$ transfer although it might result from $R \to V$ transfer. Secondly, the use of CO to indicate the extent to which N_2 has relaxed must depend on a $V \to V$ exchange of the type

$$N_2(v = 1) \quad + \quad CO(v = 0) \quad \rightleftharpoons \quad N_2(v = 0) \quad + \quad CO(v = 1) \qquad \qquad 1.23$$
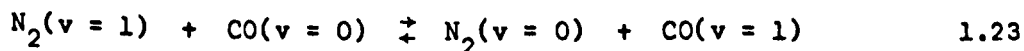
Millikan and White studied the effect of additives on the vibrational

relaxation of CO[76,78,78,81] using as diluents not only monatomic, but also some diatomic gases. For $CO(H_2)$ the Napier time is given by:

$$\log_{10} \tau(\text{atm s}) = 29.1 T^{-\frac{1}{3}} - 8.49 \quad (500\text{-}2000^\circ K) \qquad 1.24$$

This is much faster than any CO (monatomic gas) system but can be explained by a mass effect. However deuterium (mass 4) effects the Napier time below $1600^\circ K$ to exactly the same extent as helium (mass 4) but between $1600^\circ K$ and $2800^\circ K$, D_2 is a more effective collision partner. White[79] has suggested that this may be due to V → V exchange pointing out that only above $1600^\circ K$ is there any appreciable population in the vibrational states of D_2.

From their work on air, which is a special mixture of O_2 and N_2, White and Millikan[81] concluded that O_2 relaxed quickly via a rapid T → V process which then supplied energy to N_2 via a V → V process. Nitrogen relaxes more rapidly when it is in air than as a pure gas.

In a series of flash photolysis experiments, Basco, Callear and Norrish[82,83,84] have estimated the V → V exchange process between NO-CO and NO-N_2 at room temperature.

Taylor, Camac and Feinberg[85] studied NO-CO, NO-N_2 and CO_2-N_2 in the shock tube. They found that the component with the faster T → V energy exchange rate (NO or CO_2) initially relaxed

rapidly to some fraction of its final equilibrium energy. At that point the $V \rightarrow V$ process causes the two components to subsequently approach equilibrium at the same rate. Small amounts of NO or CO_2 were shown to dramatically reduce the relaxation time of the major component, CO or N_2.

The effect of hydrogen halides as a component in a mixture of diatomic molecules had not been studied in the shock tube although Eucken and Becker[86] had shown by ultrasonic measurements that HCl is an effective collision partner for Cl_2 and CO_2 at lower temperatures.

1.6.6 Mechanism for Populating Upper Vibrational Levels

It is generally assumed that vibrational energy maintains a Boltzmann distribution during relaxation. Zitlau and Moore[87] treated the problem theoretically and have calculated that relaxing CO maintains a Boltzmann distribution to within 2%.

Few observations of upper vibrational levels have been made. Hooker and Millikan[75] observed simultaneously fundamental and first overtone emission from CO. They considered two mechanisms for population of the second level.

$$CO(v = 1) \ + \ M \ \rightarrow \ CO(v = 2) \ + \ M \qquad\qquad 1.25$$

$$\text{or} \ \ CO(v = 0) \ + \ M \ \rightarrow \ CO(v = 2) \ + \ M \qquad\qquad 1.26$$
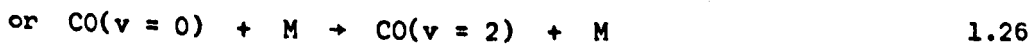
If in equation 1.25 M is a molecule of vibrationally excited CO, the reaction would be expected to be rapid, due to its being a resonance type, but with favourable collisions infrequent. The authors concluded that no more than 10% of the population of v = 2 was by the direct mechanism (1.23). They fitted the shape of the overtone emission to:

$$I = I_{\infty} (1 - \exp(-t/\tau\exp))^2 \qquad 1.27$$

where I was the intensity of emission at time t, I_{∞} being the equilibrium value of I. This form was assumed by Windsor, Davidson and Taylor.[72]

Chow and Greene[88] observed 10% HI diluted in Ar monitoring the population of the v = 1, 2, 3 and 4 states by ultraviolet absorption. All levels approached equilibrium exponentially (as for the first level of CO in the study of Hooker and Millikan) and all at approximately the same rate. The authors proposed the mechanism:

$$HI(v = 0) + M \overset{k_1}{\rightleftharpoons} HI(v = 1) + M \overset{k_2}{\rightleftharpoons} HI(v = 2) + M \overset{k_3}{\rightleftharpoons}$$

$$HI(v = 3) + M \text{ etc.} \qquad 1.28$$
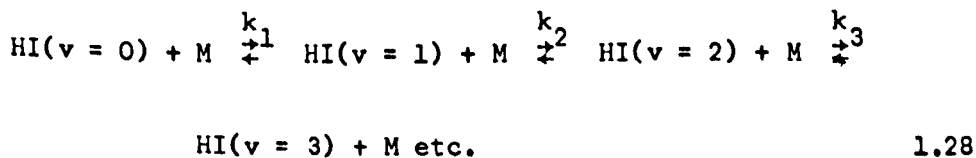
with $k_1 \ll k_2$, k_3 etc.

The observed emission could be explained by assuming direct quantum

jumps with $k_{01} = k_{02} = k_{03} = k_{04}$ but Chow and Greene consider unsatisfactory the explanation of the shape of the observed emission by direct quantum jumps with $k_{01} = k_{02} = k_{03}$ for they thought that the corollary, $k_{30} > k_{32}$ and $k_{20} > k_{21}$, was particularly unreasonable. However they failed to suggest a reason why k_2 and k_3 are much faster than k_1.

For it to be due to resonance exchange of the type,

$$HI(v = 1) + HI(v = 1) \quad \overset{fast}{\underset{\leftarrow}{\rightarrow}} \quad HI(v = 2) + HI(v = 0) \qquad 1.29$$
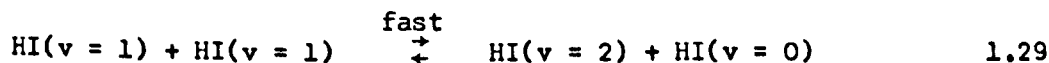
the rate of populating of HI(v = 2) would be proportional to the square of the concentration of HI(v = 1) and the rise of the emission would therefore not be of the simple exponential form. This is discussed further in section 5.1.

Thus evidence on the mechanism for populating upper vibrational levels appears a little confusing. Further light on this problem was considered to be valuable.

1.7 Theoretical Calculations of Napier Times

Vibrational relaxation measurements by experimentalists have stimulated theoreticians and vice versa. Two standard texts on relaxation theory are those by Herzfeld and Litovitz[15] and Cottrell and McCoubrey.[16] Takayanagi[17,18] has written two review papers and the theory of vibrational energy transfer between simple molecules

in nonreactive collisions has been recently appraised by Rapp and Kassal.[89]

A major contribution to the early work was by Landau and Teller[90] who considered initially the simple case of an atom approaching a molecule along its axis leading to a head on collision. They treated the problem of $T \rightarrow V$ energy transfer classicaly pointing out the importance of Ehrenfest's principle (section 1.6.3). By using a better interaction potential than previous workers and taking Maxwell's distribution law of velocities into account, they were able to deduce the correct temperature dependence for τ but unable to calculate actual values as they lacked the parameters necessary to describe the intermolecular potential.

Herzfeld and his co-workers[2,15] adopted a quantum-mechanical approach. They used a more refined intermolecular potential, the Lennard-Jones 12-6 equation, whose well depth, ε, was found, as was the molecular cross section, σ, from viscosity measurements. (Both ε/k and σ are tabulated in Hirschfelder, Curtiss and Bird (Table I-A, ref. 91)). Their expression for Z, the number of collisions required for the vibrational relaxation of BC by A is:
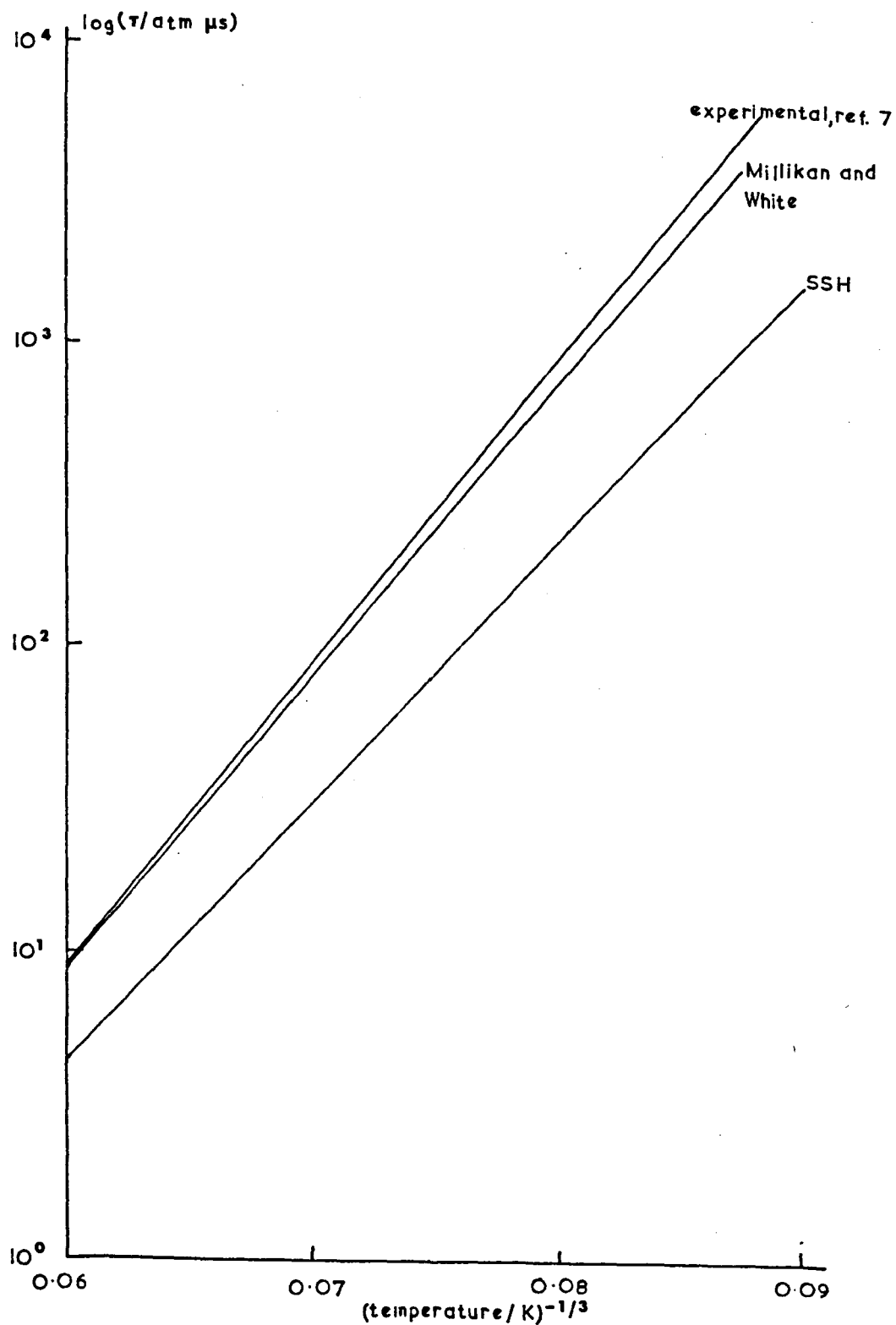
Figure 1.5 Napier Times of Pure Nitrogen

$$Z = 1.017 \left(\frac{ro}{rc}\right)^2 Zo \ Zosc \ Z_{tr}' \ Y(2,2) \ e^{-\varepsilon/kT} (1-e^{-\theta/T})^{-1} \qquad 1.30$$

where Zo is a steric factor taken as 3

$$Zosc = \frac{M_B M_C (M_A + M_B + M_C)}{(M_B^2 + M_C^2) M_A} \cdot \frac{1}{\pi^2} \cdot \frac{\theta'}{\theta} \qquad 1.31$$

$$Z_{tr}' = \pi^2 \left(\frac{\theta}{\theta'}\right)^2 \sqrt{\frac{3}{2\pi}} \left(\frac{T}{\theta'}\right)^{\frac{1}{6}} \exp\left[\frac{3}{2} \left(\frac{\theta'}{T}\right)^{\frac{1}{3}} - \frac{\theta}{T} \right] \qquad 1.32$$

and $Y(2,2) = 0.76 (1 + 1.1 \ \varepsilon/kT)$ \qquad 1.33

Values of Z and hence Napier times are calculated by Computer Program 3 (Appendix A). Most experimentalists compare their values with those predicted by the above SSH theory. Good agreement is found in many cases. Figures 1.5, 1.6, 1.7 and 1.8 show the comparison of experimental results and the values calculated by equation 1.16 for pure N_2, CO, HCl and HBr. It can be seen and it is a general feature, that the predictions of SSH theory is not good for hydrogen containing molecules.

When the incident molecule can not be treated as an atom but is a diatomic molecule of frequency ν_2, then the energy to be transferred from translation is $\frac{1}{2}h(\nu_1 - \nu_2)$ where ν_1 of the frequency of the relaxing diatomic. Some of the approximations used in deriving $Zosc$ and Z_{tr}' are no longer valid and the expression for them must be
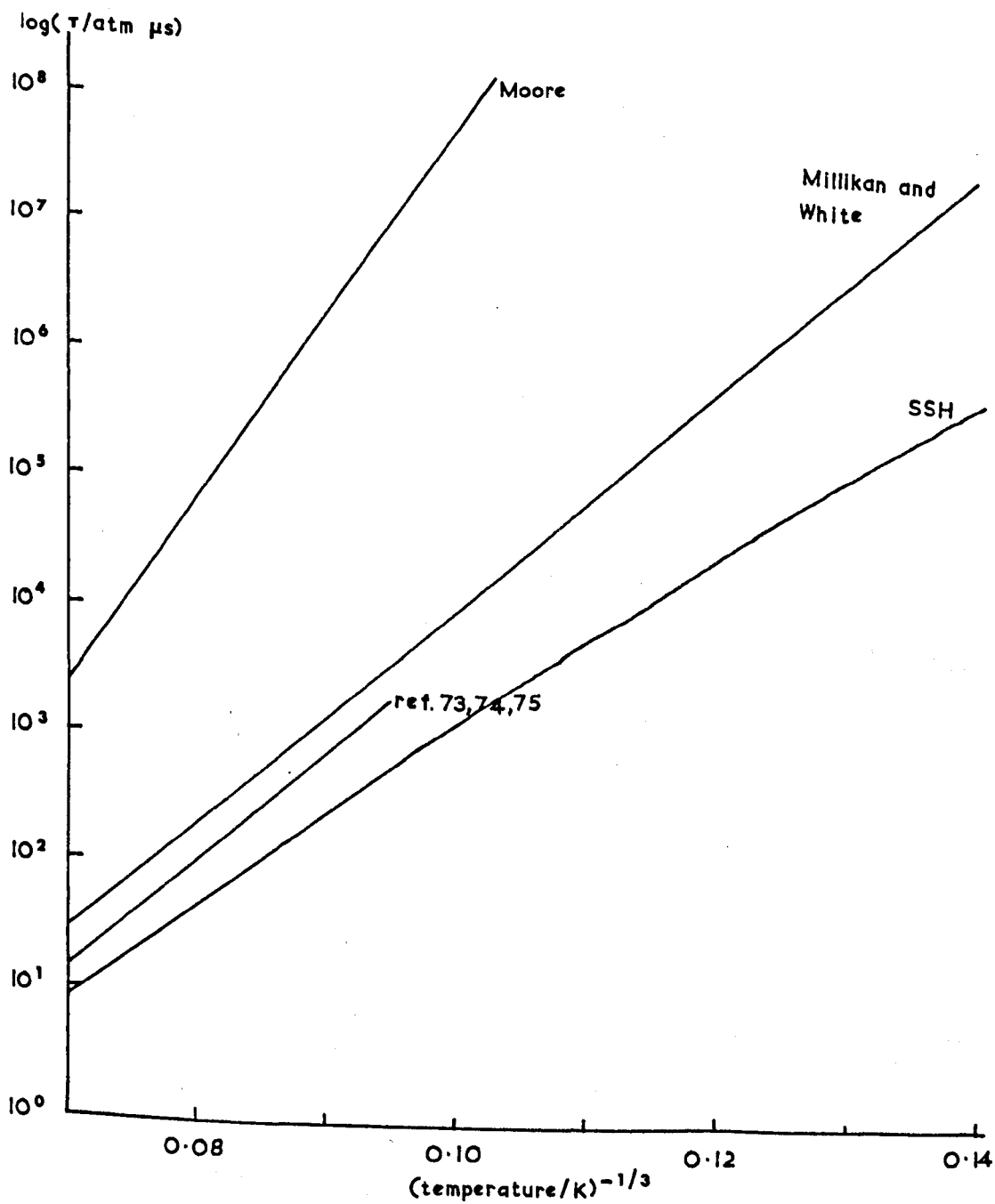
Figure 1·6   Napier Times of Pure CO
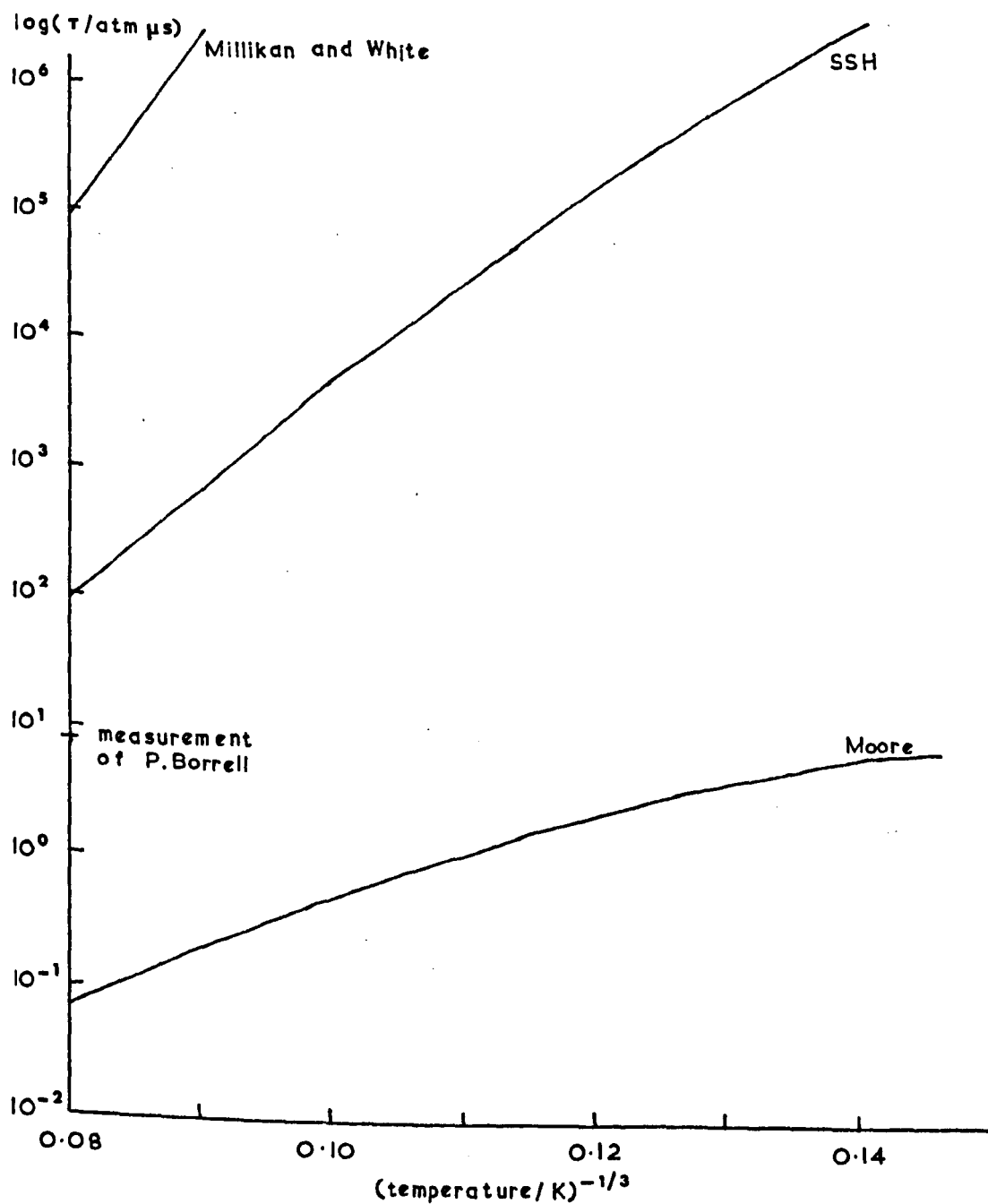
Figure 1·7 Napier Times of Pure HCl
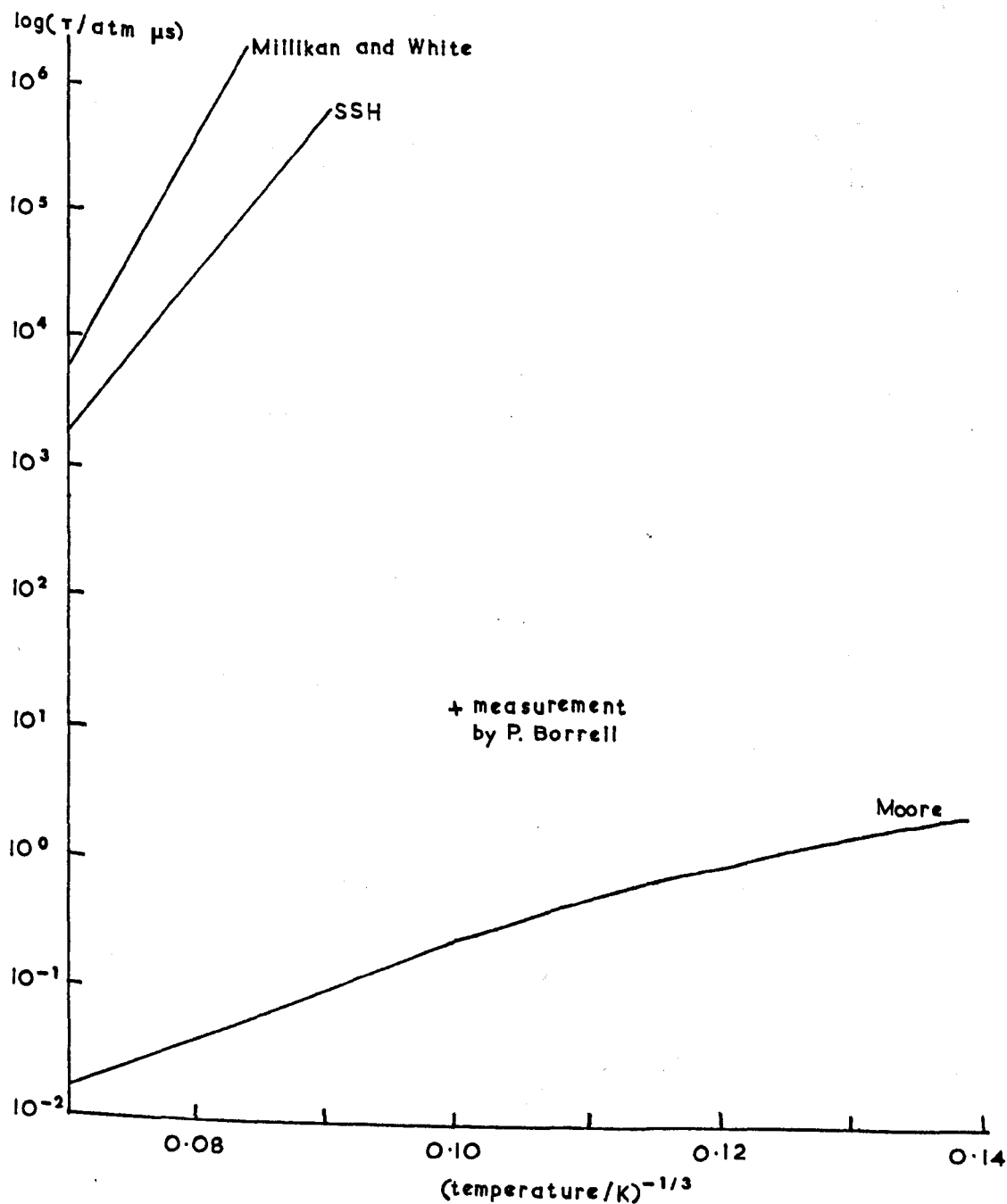
Figure 1·8 Napier Times of Pure HBr

modified. For near resonance ($\nu_1 \neq \nu_2$), Herzfeld and Litovitz[15] derive:

$$Z_{tr}' = \pi^2 \sqrt{\frac{3}{2\pi}} \left(\frac{T}{\theta_{12}'}\right)^{\frac{1}{6}} \left(\frac{\theta_1 - \theta_2}{\theta_{12}'}\right)^2 \exp\left[\frac{3}{2}\left(\frac{\theta_{12}'}{T}\right)^{\frac{1}{3}}\right.$$

$$\left. \pm \frac{\theta_1 - \theta_2}{2T} - \frac{\varepsilon}{T}\right] \qquad \qquad 1.34$$

where $\theta_{12}' = 16\pi^4 \tilde{m}_{12} 1^2 (\nu_1 - \nu_2)^2$. $\qquad\qquad$ 1.35

$$Z_{osc} = \frac{1}{4\pi^4}\left(\frac{4M_B M_C}{M_B{}^2 + M_C{}^2}\right)_1 \left(\frac{4M_B M_C}{M_B{}^2 + M_C{}^2}\right)_2 \frac{\theta_1'}{\theta_1} \cdot \frac{\theta_2'}{\theta_2} \qquad 1.36$$

and $Z_o = 9$

θ_1' and θ_2' are for the pure gases, but with the common 1.

For exact resonance, ($\nu_1 = \nu_2$):

$$Z_{tr}' = \frac{\pi^2}{4} \cdot \frac{\theta^2}{\theta_{12}' T} \cdot e^{-\varepsilon/kT} \qquad\qquad 1.37$$

and Z_{osc} and Z_o are as for the near resonance case.

Computer Program 3 compares, where appropriate, results

obtained by all three sets of equations: the incoming particle is treated firstly as an atom, secondly as a near resonant vibrator, and thirdly as an exactly resonant vibrator.

Cottrell and McCoubrey[16] have demonstrated that the equation they derive from $T \rightarrow V$ energy transfer agrees with that of Herzfeld and Litovitz to within an order of magnitude. This they consider the accuracy of their calculations.

Discrepancies between theoretical and measured values for a number of hydrides were reported by Cottrell and his co-workers.[3,92,93] They suggested that exchange between rotational and vibrational energy occurs, particularly where the velocity of the peripheral atoms is high due to a low moment of inertia. Moore adopted this suggestion[4] and made semi-classical, semi-empirical calculations which were applied to a large number of molecules with some success. Computer Program 4 calculates values of Z_{10} for each of Moore's three equations (4, 8 and 9). Of these he seems to prefer his equation 4:

$$\frac{1}{Z_{10}} = \frac{1}{Z_0} \; \frac{17.1\, I^{\frac{13}{6}}\, \nu^{\frac{4}{3}}}{d^{\frac{13}{3}}\, T^{\frac{1}{6}}\, \tilde{M}_a^{\frac{7}{3}}} \; \exp\left[-1.78\left(\frac{I\nu^2}{d^2\alpha^2 T}\right)^{\frac{1}{3}}\right] \exp\frac{0.7194\nu}{T} \qquad 1.38$$

where mass is in atomic mass units and length in Angstroms. Z_0 is a steric factor and α is the potential-energy range parameter which are found by comparison of calculated and measured values of

relaxation times to be 4.97 and 2.94 $A^{o}{}^{-1}$ respectively. When relaxation times from Moore's theory are plotted, the values are obtained by using equation 1.34 (equation 4 of Moore).

Millikan and White[94] were able to fit a large number of experimental relaxation times to the empirically derived formula

$$\log_{10} \tau(\text{atm s}) = (5.0 \times 10^{-4})\dot{m}^{\frac{1}{2}} \theta^{\frac{4}{3}} (T^{-\frac{1}{3}} - 0.015\dot{m}^{\frac{1}{4}})-8.00 \qquad 1.39$$

Its failure for a number of hydrides is taken by Millikan[60] as illustrating the use of the correlation to indicate the presence of a new factor or possibly a different mechanism.

Theoreticians have little to say about the size of quantum jumps. The Landau-Teller model for an harmonic oscillator assumes that $\Delta v = \pm 1$ (as in spectroscopy) and that

$$k_{01} : k_{12} : k_{23} \text{ etc.} = k_{10} : k_{21} : k_{32} \text{ etc.} = 1 : 2 : 3 \text{ etc.} \qquad 1.40$$

There is little evidence (section 1.6.6) as to whether or not molecules obey these rules but the presence of anharmonicity may increase as in spectroscopy, the probability of multi-quantum transitions.

1.8 Summary

Of the molecules whose rate of vibrational relaxation
had been measured at the commencement of this study, hydrogen
chloride and hydrogen bromide appeared to have Napier times which
were shorter than predicted by both SSH theory and the Millikan
and White correlation. The failure of these may be due to some
feature of the molecules, such as their dipole moments, or that
the basic assumption of T → V energy transfer is incorrect. Much
shorter theoretical Napier times for hydrogen halides are predicted
by the theory of Moore which is based on R → V energy transfer. A
crucial test between the two propositions is the ratio of
τ_{HCl}/τ_{HBr} which is less than unity if SSH theory of T → V energy
transfer is correct but greater than unity if Moore's theory of
R → V energy transfer better represents the situation. It was
hoped to decide which of these two mechanisms is important for
hydrogen halides by measuring the ratio of the Napier times for
pure hydrogen chloride and pure hydrogen bromide.

By deriving these values from observations on upper
vibrational levels, it was felt it may be possible to also decide
whether the higher levels are populated by a stepwise mechanism or
by multi-quantum transitions.

In gas mixtures, the presence of small amounts of fast
relaxing hydrogen halides would be expected to accelerate the slow

relaxation of N_2 and CO. By measuring Napier Times for a range of concentrations of added halide, it was hoped to elucidate the mechanism which is responsible for the acceleration. This could be either by the $T \rightarrow V$ (or $R \rightarrow V$) energy transfer or by $V \rightarrow V$ energy transfer.

The above problems lend themselves to investigation by the shock tube technique which can produce with ease a wide range of operational temperatures. Section 2 of this thesis describes the actual shock tube and its associated equipment used in this study.

2. EXPERIMENTAL

2.1 Introduction

The experimental section describes the materials (Section 2.2) and apparatus (Section 2.3) used in this study. Both the equipment used to produce the shock waves and the instruments for making the essential measurements of initial pressure, shock speed and radiation are discussed. Calibration of these instruments is described in Section 2.4 and the adjustments for optimising the experimental conditions in Section 2.5. The last section (2.6) briefly sets out the procedure according to which the shock tube was operated.

2.2 Materials

Small amounts of impurities, especially water, will generally speed up the vibrational relaxation of a gas. This effect is greatest on those gases which have a long relaxation time and for these, purity is more important than for those having a short relaxation time.

In general, cylinder gases were used although some carbon monoxide was purchased in litre glass bulbs.

Hydrogen chloride (Air Products Limited) was quoted as being 99% pure and hydrogen bromide (B.D.H. Limited) as 99.8% pure. Water was removed from the gases by passing them over phosphorus pentoxide on entry to the system. Non-dondensable impurities were removed by freezing the gases in a liquid nitrogen cooled trap and pumping on them until the pressure was below 1 μm Hg. The solid was then distilled into another trap, rejecting the initial and final fractions. The pumping and distilling were repeated several times.

Nitrogen (B.O.C. Limited) was white spot quality indicating freedom from oxygen, an impurity which reduces its relaxation time. Drying was again by passing over phosphorus pentoxide. As the relaxation time of the pure gas was not measured and the effect of hydrogen halides on it was very great, the highest purity nitrogen was not necessary.

Carbon monoxide was obtained both in cylinders and litre glass bulbs. It was Grade X quality from B.O.C. Limited and no attempts were made to increase its purity above the quoted 99.95%.

Hydrogen was purchased from Air Products Limited in preference to B.O.C. Limited as the water content is slightly lower. Less moisture could then be adsorbed onto the shock tube wall reducing any possible effect on subsequent shocks.
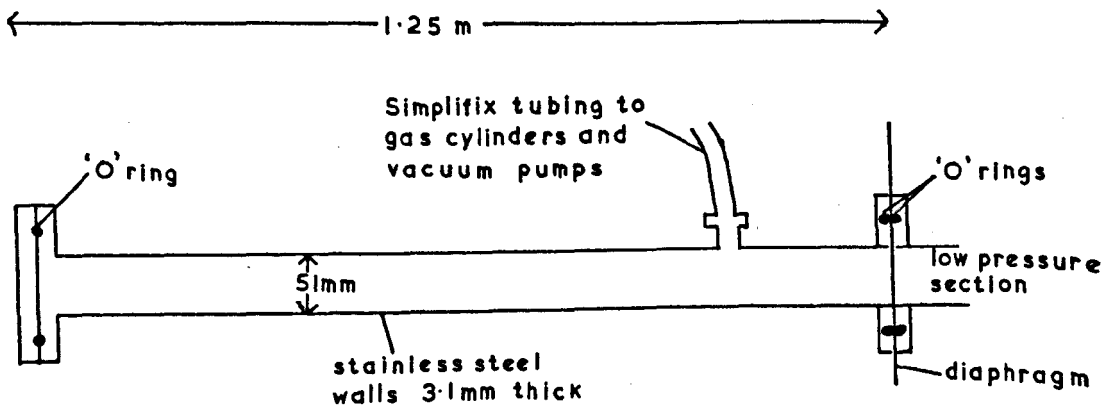
Figure 2·1 High Pressure or Driver Section
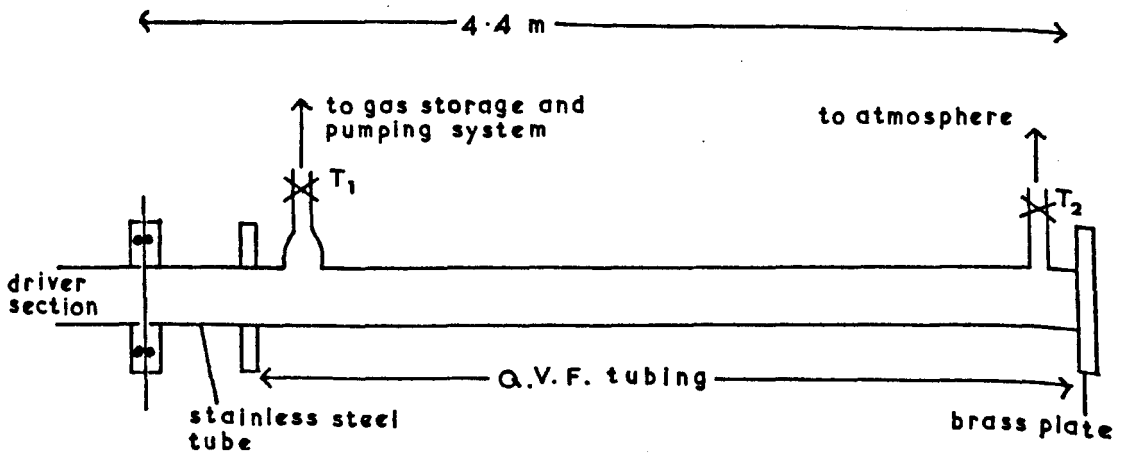
Figure 2·2 Low Pressure Section

2.3 Apparatus

2.3.1 The Shock Tube

The bore of the shock tube was approximately uniform and was nominally 2 inches (51 mm); the overall length could be varied but was usually 4.65 m. Diaphragm material divided it into two sections.

The high pressure or driver section was 1.25 m long and was contructed of stainless steel tubing having walls of 3.1 mm and a flange each end (Fig. 2.1). Simplifix nylon tubing (9.6 mm o.d.) conveyed gas from cylinders via a manifold to the driver section. Simplifix couplings secured the tubing at each end. Roller mountings facilitated smooth separation of the driver and low pressure sections and close fitting pins ensured alignment of the two sections, pivoted bolts with butterfly nuts clamping them together.

Stainless steel tubing was also used for the initial 100 mm of the low pressure or test section. Q.V.F. pyrex tubing was used for the remainder of the shock tube, (Fig. 2.2). T1, a Q.V.F. tap with teflon diaphragm, led to the pumping and gas handling system. T2 led to the outside atmosphere. Corrosive and poisonous gases were blown from the shock tube via T2 so reducing damage to the pumps and avoiding toxic gases leaking to the environment when a diaphragm was changed. Standard Q.V.F. joints were employed: three bolts between a pair of plastic backing
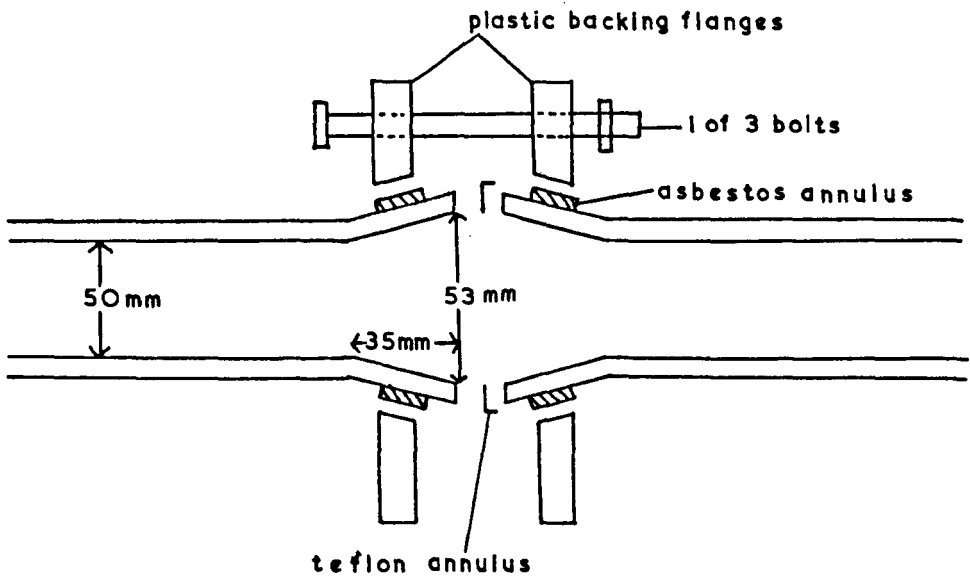
Figure 2·3 Exploded View of a Q.V.F. Joint
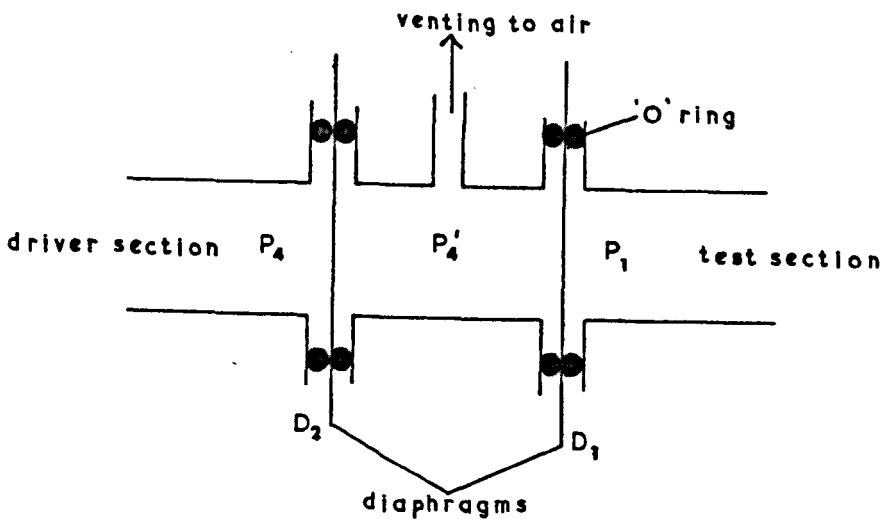
Figure 2·4 Double Diaphragm Technique

$P_4 - P_4'$ is insufficient to burst D_2;

$P_4' - P_1$ is insufficient to burst D_1;

P_4 – atmospheric pressure is sufficient to burst D_2 then D_1

flanges with asbestos inserts provided the longitudinal pressure between the buttress end of the pipe sections which were vacuum sealed by a teflon gasket (Fig. 2.3). To attain an acceptable vacuum, good alignment was necessary and the bolts needed retightening intermittently. Overtightening caused breaking of a backing flange; overtightening of the alternative cast iron backing flanges resulted in fracture of the glass section at the collar. Figure 2.3 also shows how the tubing splays at each end to facilitate jointing. Since the transition was smooth, it was felt that the effect on flow characteristics due to the non-uniform cross-section would not be great. When the emission from a fast relaxing gas was monitored, the level of emission was fairly constant indicating no great deviation from ideal flow.

The low pressure section was terminated by a brass plate. No corrosion was observed on either the brass or stainless steel.

Two concentric viton rubber O rings of equal size held the diaphragm material between the driver and test sections. This technique was satisfactory for a single thickness of material but not when several thicknesses were used. (A later shock tube has shown that a pair of concentric O rings of unequal size helps in this respect).

When a high or predetermined driver pressure was required, a double diaphragm technique was adopted (Fig. 2.4). In this case the pressure difference $P_4' - P_1$ was a little less than required to

burst diaphragm D1 and $P_4 - P_4'$ insufficient to burst D2. P_4 was above atmospheric pressure so that when the middle section was vented to the atmosphere, D2 burst quickly then D1 causing propagation of the shock wave. Melinex (I.C.I.) and aluminium foil of various thicknesses were used. Table 2.1 list their approximate breaking pressures.

TABLE 2.1

Diaphragm Bursting Pressures

Material	Supplier	Thickness	No. of Thicknesses	Bursting Pressure above atmospheric	
				bar	lb in^{-2}
Melinex	1	50 gauge	1	0.55	8
Melinex	1	100 gauge	2	1.93	28
Aluminium	2	Baking foil	2	-0.30	-10
Aluminium	2	Baking foil	3	-0.65	-5
Aluminium	2	0.008 mm (.003")	1	2.76	40
Aluminium	2	0.013 mm (.005")	1	5.52	80
Aluminium	2	0.013 mm (.005")	1	4.48	65
Aluminium	3	0.013 mm (.005")	1	1.79	26

1. I.C.I. Limited

2. British Aluminium Foils Limited

3. Alcan Polyfoils Limited

Plate 1. The shock tube as originally built with its low pressure section foremost. The instrumentation is above the tube. Two light screens and the infrared sensitive photomultiplier are shown exposed. Modifications as described in the text were incorporated when the tube was resituated.
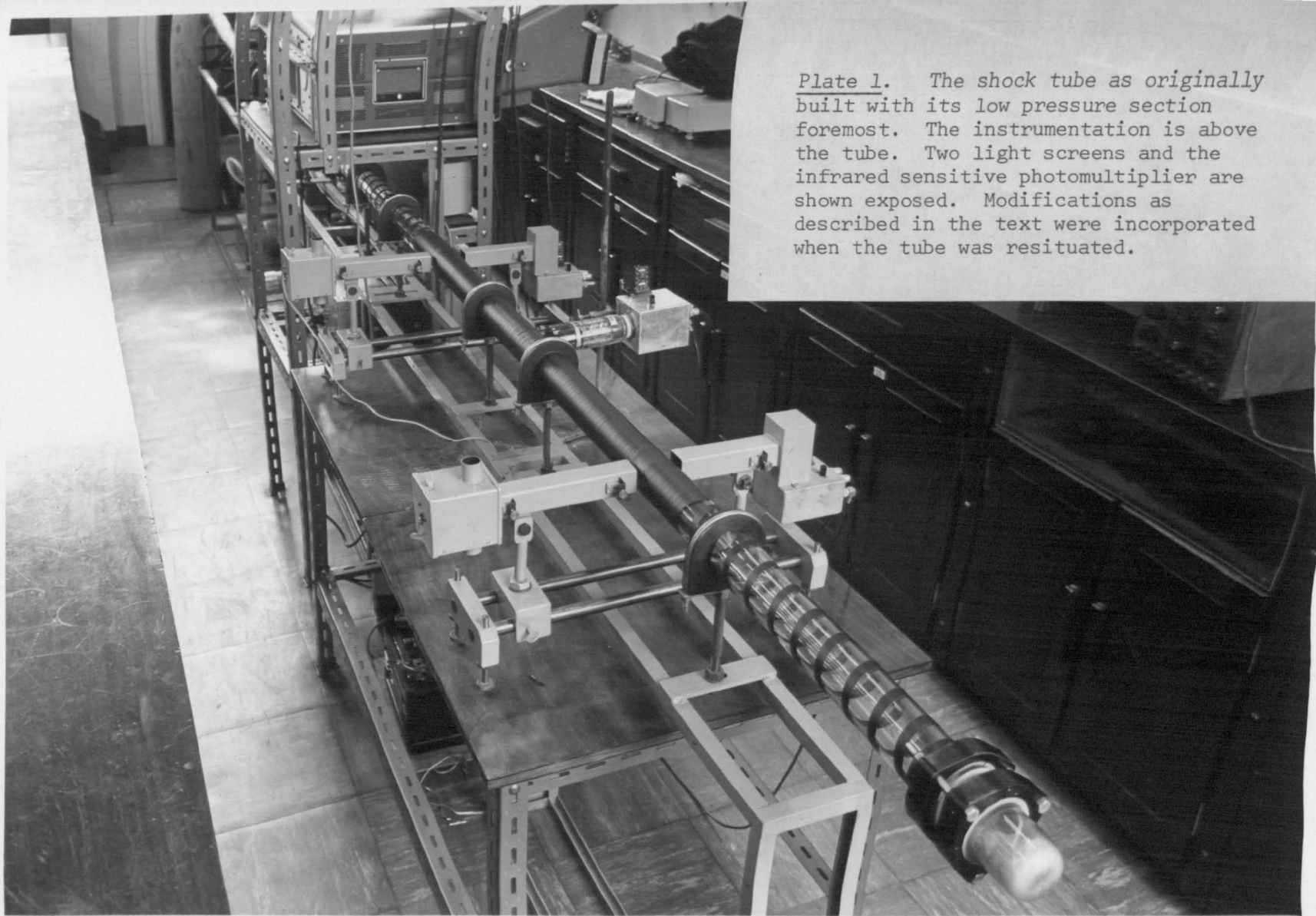
The bursting pressure was found to be much lower before the inside edge of the shock tube at the diaphragm had been bevelled: the diaphragm tore rather than burst.

54

Q.V.F. tubing to gas storage and test section

copper tubing

25mm 12mm 6mm

Simplitix tubing to driver section

Pirani gauge

nitrogen cylinder air double diaphragm section

hydrogen cylinder pressure gauge

Penning gauge

Simplitix tubing to rotary pump

to laboratory

glass trap

diffusion pump
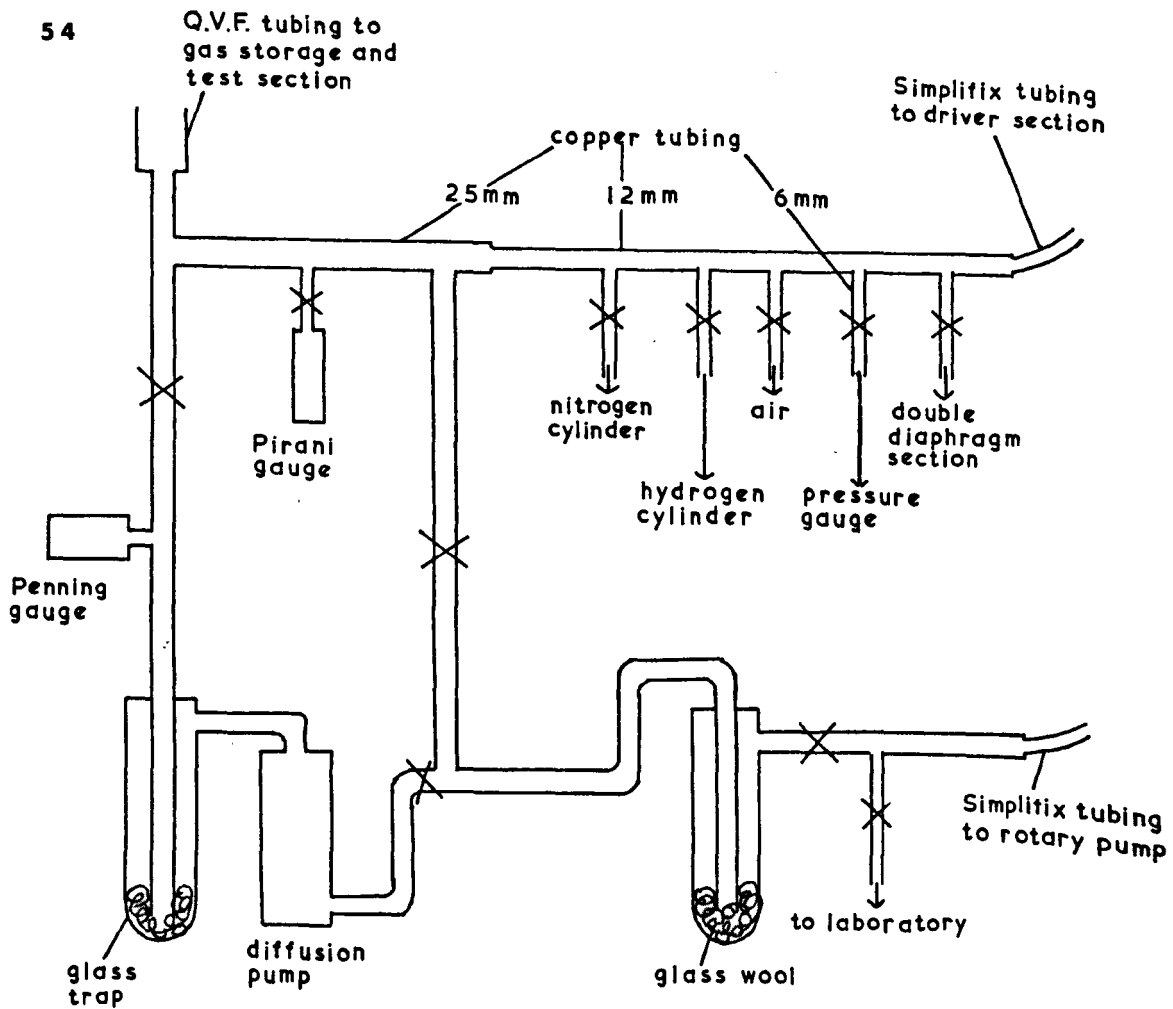
glass wool

Figure 2·5 Vacuum and Pressure System

Glass wool was inserted into the traps to help the vapours condense.

2.3.2 Vacuum and Pressure System

Figure (2.5) illustrates the vacuum and pressure system in relation to the shock tube. Copper tubing formed the majority of the system which was mounted on a vertical board. Joints were of Yorkshire fittings; isolation of various sections was by Edwards Speedivalves.

Flexible connections were of Simplifix nylon tubing. Between the gas cylinders and driver section, the system was designed to easily withstand pressures of 8.2 bar (120 lb in^{-2}). Initially a single needle Budenberg gauge indicated the pressure in the driver section. A subsequent gauge was equipped with a second needle which only moved manually or with increasing pressure. This recorded the bursting pressure permanently which could hence be read more accurately.

An Edwards ED35 two stage rotary pump created the backing vacuum for an Edwards oil diffusion pump. The rotary pump alone was originally able to achieve a vacuum of 1 μm Hg after prolonged pumping although its performance gradually deteriorated with age. Full gas ballast was needed when corrosive gases were passed through the pump and the ultimate attainable vacuum was considerably reduced (20 μm Hg). Prolonged pumping with the diffusion pump achieved a vacuum of 0.3 μm Hg. Glass traps cooled by liquid nitrogen were fitted adjacent to each pump to trap out pump oil and condensable vapours, and to increase pumping speed.

Pressures between 1 mm and 1 µm Hg were measured by an Edwards Pirani Gauge (Model M6A) and pressures below 10 µm Hg by an Edwards Penning Gauge (Model 5MF). The accuracy of the gauges was checked by comparison with a McCleod Gauge when nitrogen was the residual gas. Agreement was good and since extreme accuracy was not required, it was assumed that the gauges gave a sufficiently accurate measurement of pressure whatever the residual gas. (An idea of the possible magnitude of the error was obtained by reference to the data sheet[95] where the calibration curves for various gases are given).

to the test
section of the
shock tube

Edwards
capsule
dial gauge

I litre SB

to the gas
inlet
system

D

mercury
manometer

I litre SB

EI
to atmosphere

5 litre SB

to the
copper
vacuum
system

20 litre SB

SB = storage bulb

gas inlet system

to D

glass wool

trap

P_2O_5

silica gel

E2
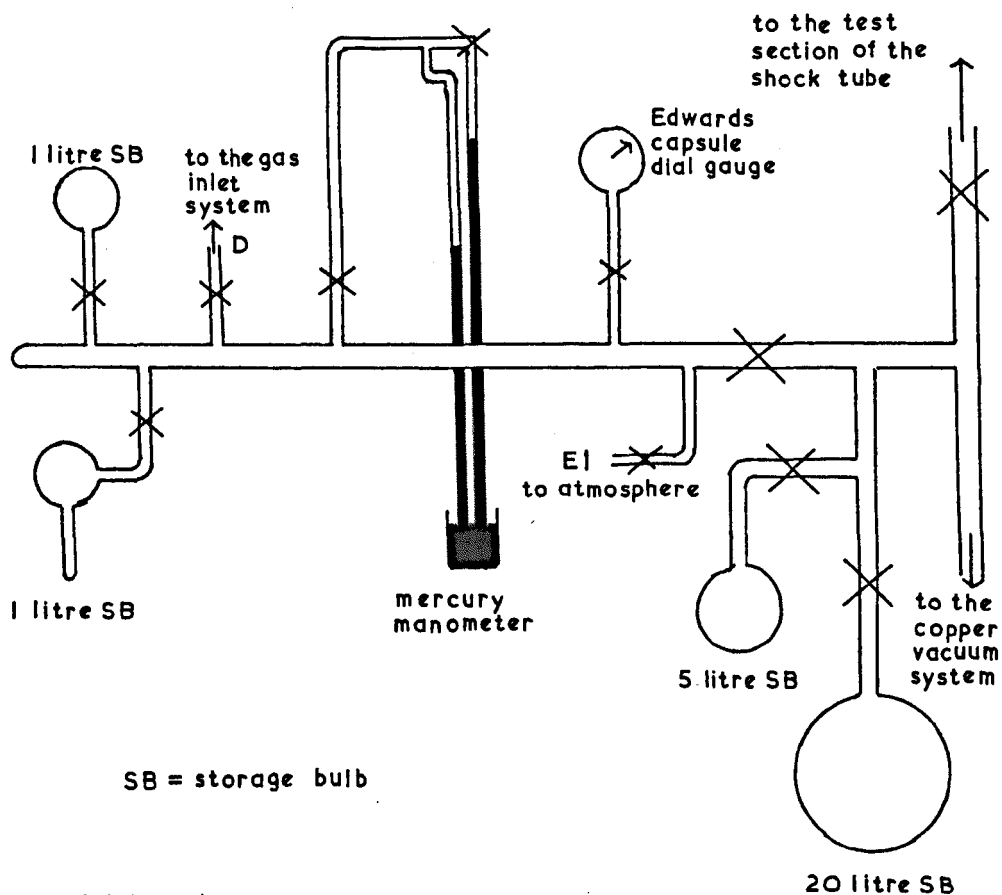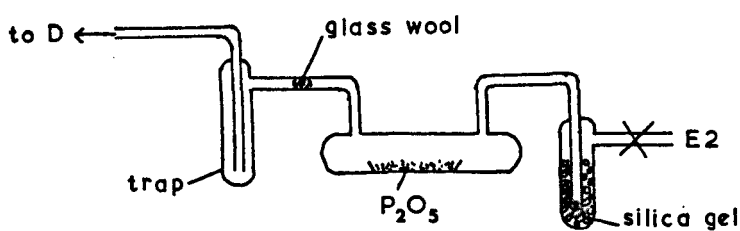
glass wool was used to trap any P_2O_5

Figure 2·6 Gas Handling System

2.3.3   Gas Handling System

Large quantities of test gases were stored in two Q.V.F. storage bulbs, one of 5 litre and the other of 20 litre capacity. Q.V.F. tubing connected these with the shock tube and pumping system (Fig. 2.6). Smaller amounts of test gases were stored in litre storage vessels which were glass blown onto a system that was joined to the Q.V.F. tubing by a B24 cone and socket sealed with Piescein Wax.

Taps on the glass blown system were from Springham having viton A diaphragms; the objective was to minimise the number of greased joints.

Test gases entered by either E1 or E2 (Fig. 2.6). Entry via E2 dried the gas by passage through silica gel and over phosphorus pentoxide. Silica gel was omitted when hydrogen halides used this route as they reacted with the indicating agent.

To the manifold was blown a manometer for measuring pressure. Also attached was an Edwards capsule dial gauge for low pressure measurements (0 - 20 mm Hg); it was only satisfactory for inert gases as the corrosive halide gases attacked the mechanism.
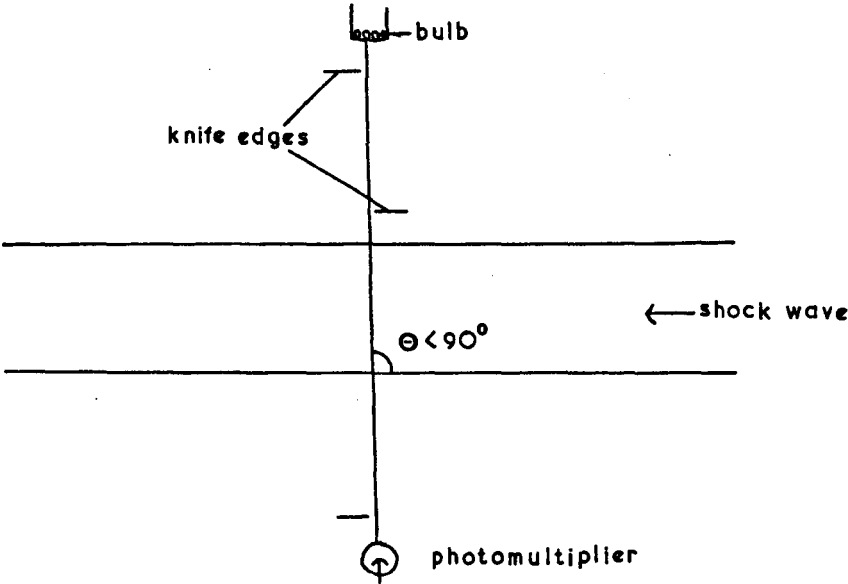
Figure 2·7a A Light Screen using a Bulb
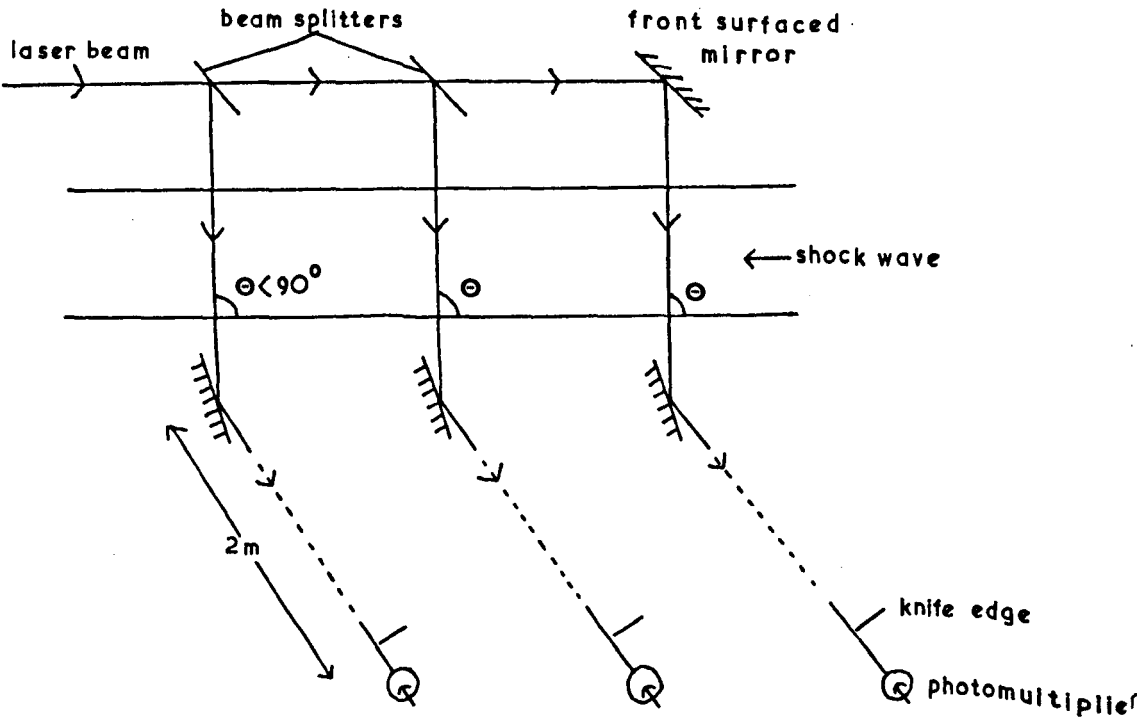
Figure 2·7b Light Screens using a Laser

2.3.4 Light Screens

Light screens were designed to operate on the principle
that the change in refractive index at a shock front deflects a
transverse light beam. The change in light intensity at a
particular position is registered photometrically.[9,10,11,96]

Three knife edges were aligned so that light from a
battery driven 12 volt lamp just failed to reach a photomultiplier,
E.M.I. 9660B (Fig. 2.7). Deflection of the light beam caused a
pulse of light to be detected by the photomultiplier giving a
negative electrical pulse which, after modification, operated
a timer. One light screen activated the timer and a second light
screen situated about 1 m downstream of the first, stopped it. A
third light screen placed just before the observation station was
useful in checking attenuation and predicting the arrival time of
the shock front at the observation point.

In later work, a Ferranti model GP1 laser was used for the
source of light and this being nearly parallel, required only one
knife edge positioned just before the photomultiplier (Fig. 2.7b).
Two "half" silvered mirrors split the beam into three approximately
intense parts. All reflections were from front surfaces so reducing
interference effects. The first mirrors used were produced by
depositing gold on microscope slides in a Edwards Speedivac Coating
Unit (Model 6E2). Later ones, purchased from Optical Works Limited,
were aluminium coated. The commerically half silvered mirrors split

the laser beam more equally and the surfaces were less affected
by the atmosphere compared with those made in the coating unit.
Advantage was taken of the small angular divergence of the laser
beam in the long optical lever and this, together with the
increased intensity, accounted for the greater sensitivity and
ability to detect weaker shocks.
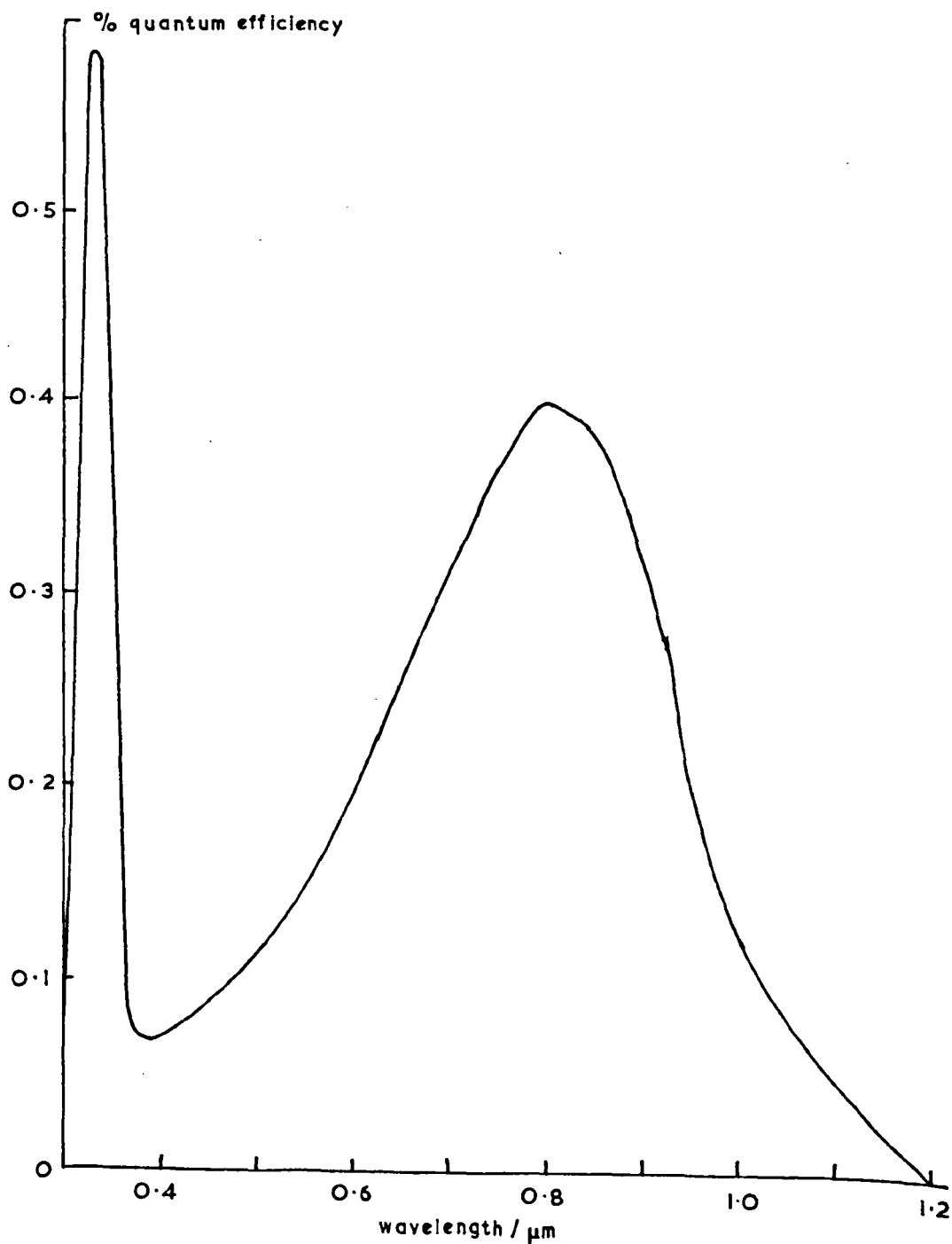
Figure 2·8 Spectral Sensitiviy Curve for the 9684 B Photomultiplier

2.3.5 Infrared Detectors

A molecule of HCl in the third vibrational level emits light of wavelength 1.19 µm when it undergoes a transition to the first vibrational level. This should be detectable with an E.M.I. 9684B photomultiplier which is quoted as having a long wavelength threshold of 1.20 µm (Fig. 2.8). The photocathode, described as S1 type, is of AgOCs and is 44 mm in diameter. Changes in voltage across the load resistor were monitored on an oscilloscope.

Light from molecules whose vibrational quantum number decreases by two can not be detected by a photomultiplier and an indium antimonide detector was used (Mullard, RPY36). The detector is sensitive to visible light and infrared radiation extending to 7.5 µm (Fig. 2.9). Detection is by a thin 6 mm x $\frac{1}{2}$ mm specimen of the semiconducting material situated inside the vacuum of a dewar vessel cooled with liquid nitrogen (Fig. 2.10). An Exide battery (H1006) with resistors provided a steady bias current of approximately 1mA (Fig. 2.11). Radiation incident on the element decreases its resistance leading to a change in voltage which was monitored on an oscilloscope containing a differential amplifier unit. The resistance of the cell varies inversely with temperature being between approximately 15 kΩ at 77°K and 26 Ω at ambient temperature. Large resistors in the bias circuit guard against a damagingly large current (>5mA) should the cell inadvertently not be cooled.

Figure 2.9 Spectral Sensitivity Curve
for the RPY 36 Detector

% response

100

10

1

0

2

4

6

8

wavelength / μm
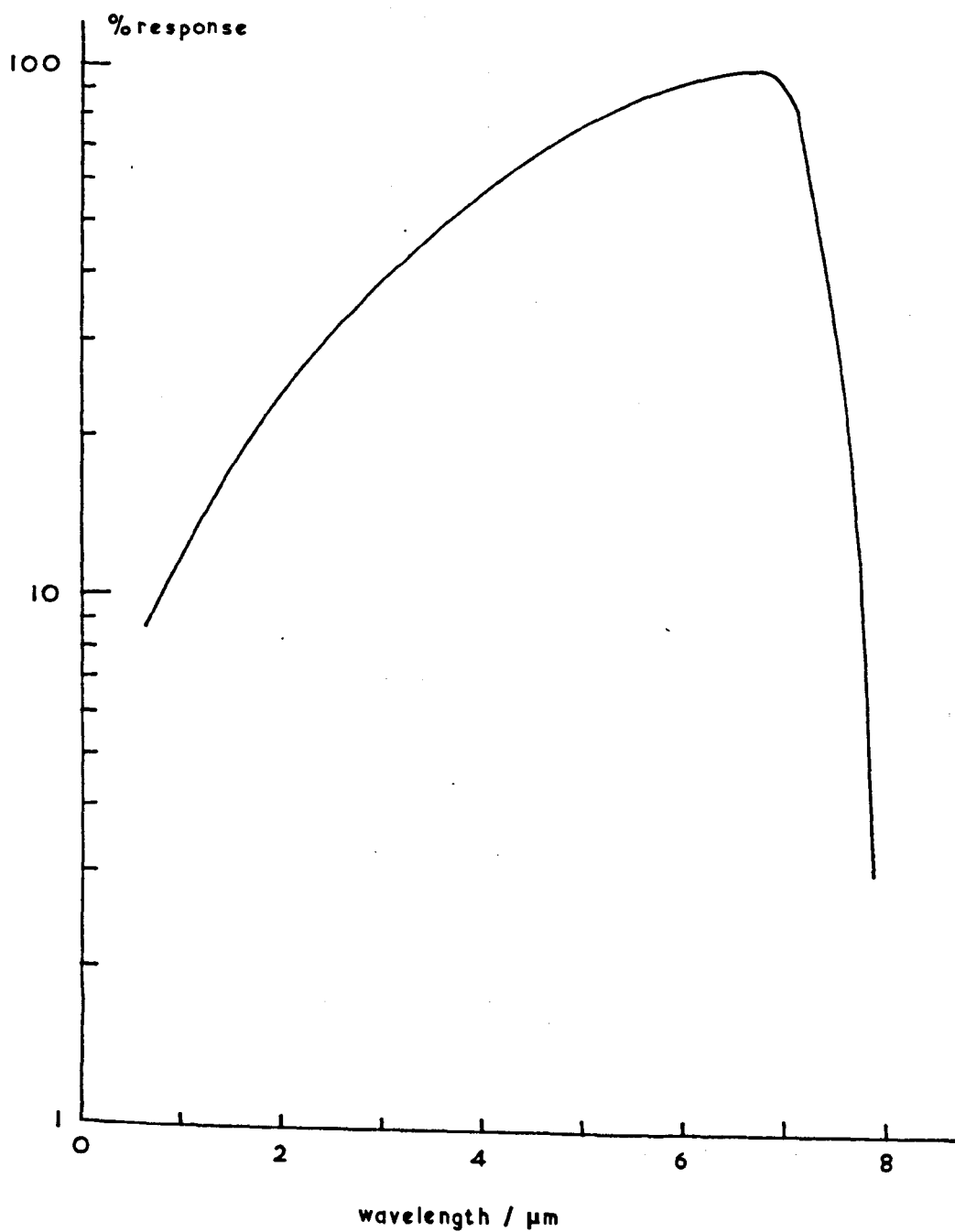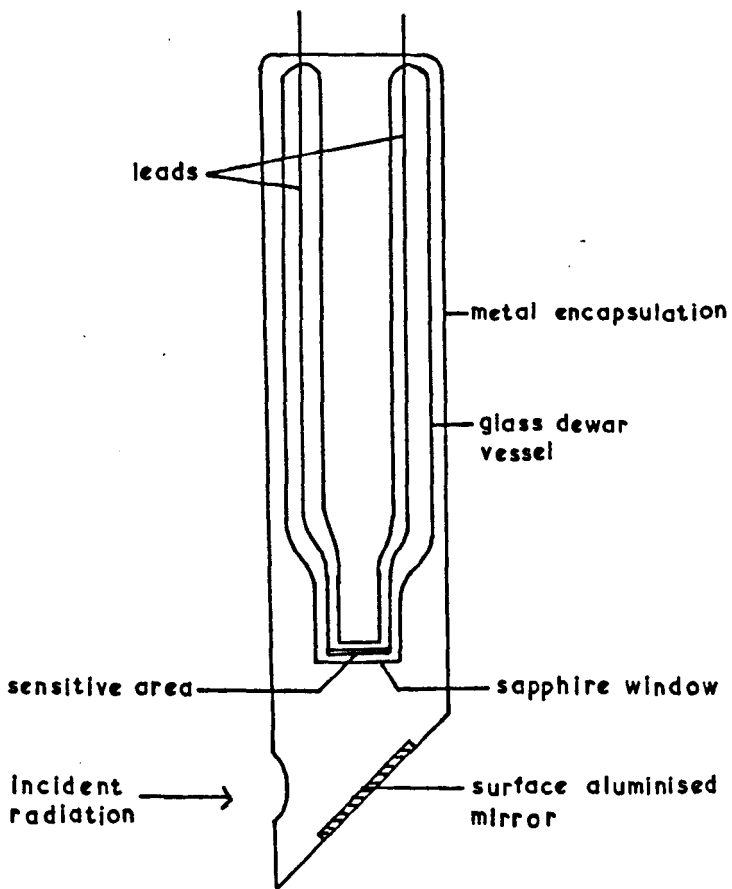
Figure 2·10   Indium Antimonide Detector, RPY 36

In operation, the dewar is filled with liquid nitrogen.
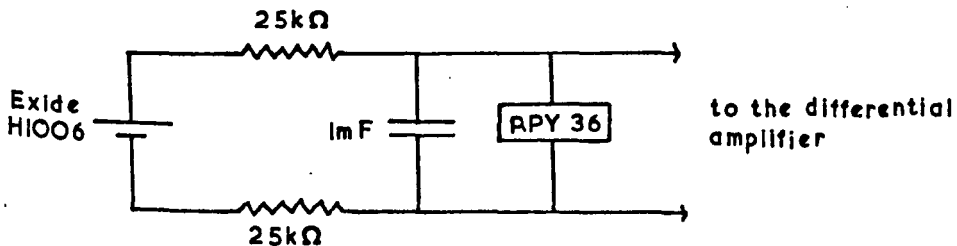
Figure 2·11 Biasing Circuit for the RPY 36

The resistors are wire wound to reduce noise.
The capacitor decouples the battery and hence reduces low
frequency noise which causes a vertical displacement of
the oscilloscope trace.
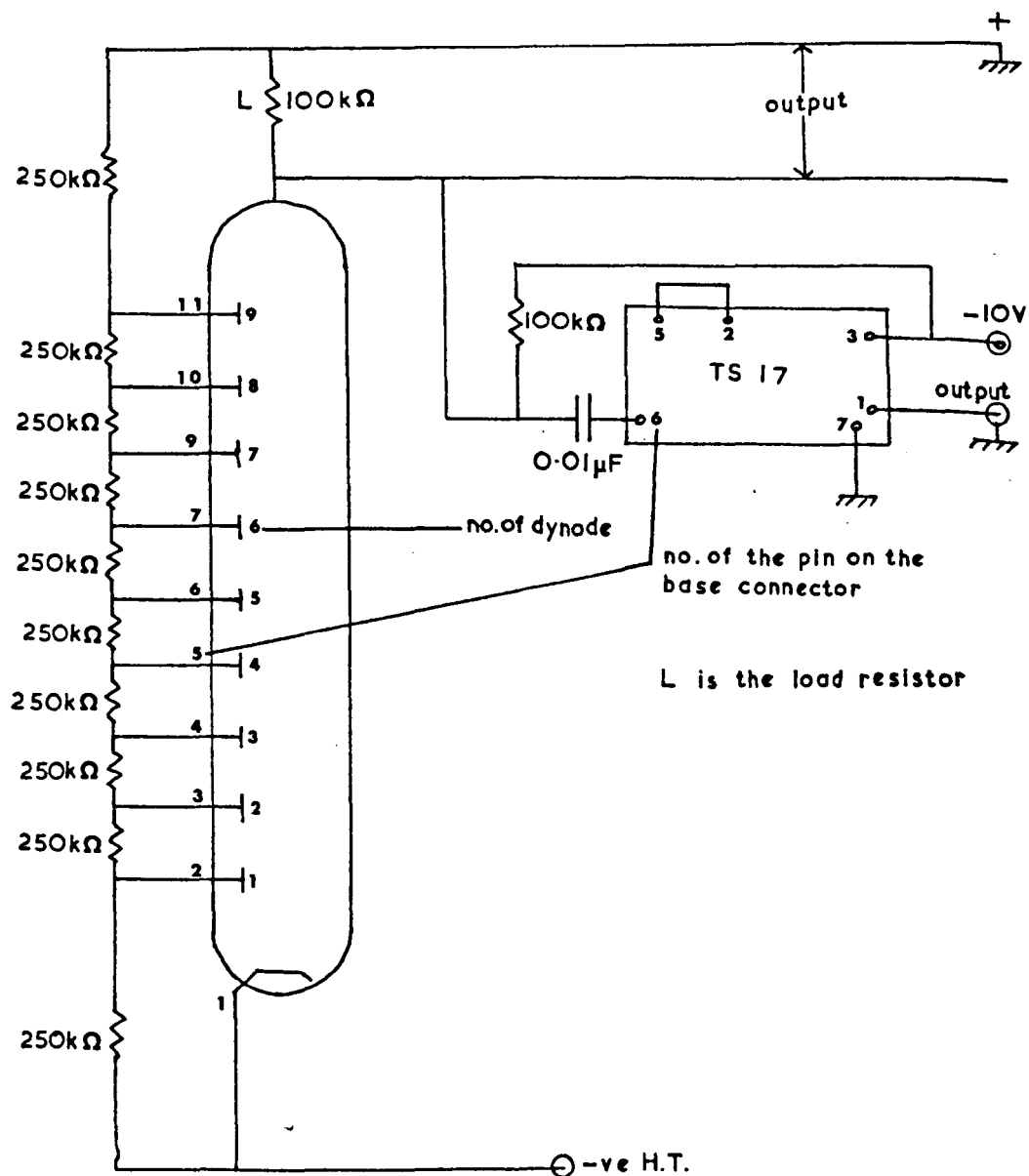
Figure 2·12 Circuit for Light Screen Photomultipliers
(E.M.I. 9660 B) with Emitter Follower TS 17

2.3.6 Instrumentation and Circuitry

Photomultipliers detect light by electro-magnetic radiation of sufficiently high energy impinging on a photocathode which emits an electron. This is amplified by successive accelerations between dynodes which are secondary emitters, until the electrons reach the anode. Hence photomultipliers are current producing detectors; their output is usually fed across a load resistor creating voltage changes which are more easily monitored. Figures 2.12 and 2.13 show the circuits used for the two types of photomultipliers.

A Brandenburg Power Supply, Type PM2500/R provided the high tension to operate the photomultipliers. Different operating voltages from the one output were achieved by splitting the output and reducing the voltage by passing the current through a resistor.

Venner emitter followers, TS 17, modified the photomultiplier outputs for connecting to remote low input impedence instruments. With both stages cascaded, the output impedence of the photomultipliers was reduced by a factor of approximately 1500.

Output from the RPY 36 detector was monitored without modification.

Signals from the photomultiplier and indium antimonide detector were observed on Hewlett-Packard oscilloscopes, one of model 140A and two of model 141A. Observation of single transients was greatly eased by the arrival of the later model which incorporates a storage facility.

Figure 2·13 Circuit for the Infrared Sensitive Photomultiplier with Emitter Follower (E.M.I. 9684B with TS17)

Three amplifiers were used: HP 1402A, HP 1405A, and HP 1400A. The initial pair have bandwidths greater than 5MHz and so do not noticeably distort the output from the emitter followers which have a bandwidth of only 1.8MHz. Their maximum sensitivity is 5mV cm^{-1}. Model HP 1400A is a differential amplifier sensitive down to 10μV mm^{-1} and a maximum bandwidth of 400kHz. All amplifiers can be AC or DC coupled to the input signal.

Only one model of time base was used, HP 1421A. Sweep speeds vary from 200 ns cm^{-1} to 1 s cm^{-1}. An extensively used feature was the delayed sweep when the visible sweep was not commenced until a predetermined interval had elapsed since the main sweep had started. Calibration of the oscilloscope is discussed in section 2.4.3.

An additional facility was a positive pulse which was available at the end of the delay period. This was used to stop a time interval meter when measuring the period of delay.

Two Venner timers, TSA 5536 and TSA 625, measured the interval between successive pairs of light screen pulses. The former had slope and level controls so light screen pulses could operate the timer directly although an amplifier was often used, especially when dealing with weak shocks, to increase the pulse to the 1 volt necessary to trigger the timer. The latter instrument required positive pulses of 5-10V to operate the start and stop gates.

Light screen pulses 25mV more negative than a reference
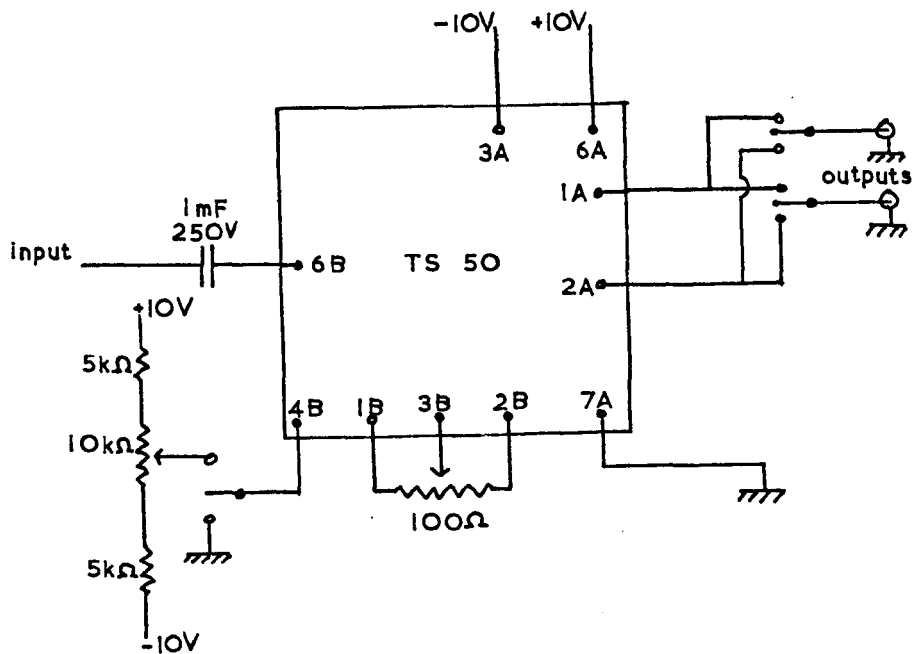
Figure 2·14 Trigger Level Comparator Unit

voltage operated a trigger unit whose output provided the necessary input for the timer. The trigger unit was constructed from a Venner Transistorised Trigger Level Comparator Unit, TS 50 (Fig. 2.14). Power for their operation came from a Venner Power Supply Unit, TS 20/C; its -10 volt output was used for the emitter followers. Operation of the controls associated with the trigger unit are described in Section 2.5.3.

It was the output from the second trigger unit that was usually fed into the lockout. This was made from a Venner Binary Unit, TS 2B, and D.C. Relay Stage, TS 9 (Fig. 2.15). Unless the lockout was reset manually, only one output pulse (positive or negative) was provided. Its operation and usefulness in diagnosing a fault in one of two light screens is described in Section 2.5.3.

A pulse after a period of delay could be obtained by using a Venner Delay Unit, TS 48 (Fig. 2.16). The delay time was not continuously variable but was nearly so.

Sine and square waves of less than 2.5V amplitude were provided by a Venner oscillator, TSA 625. The frequency range was from 10Hz to 1MHz.
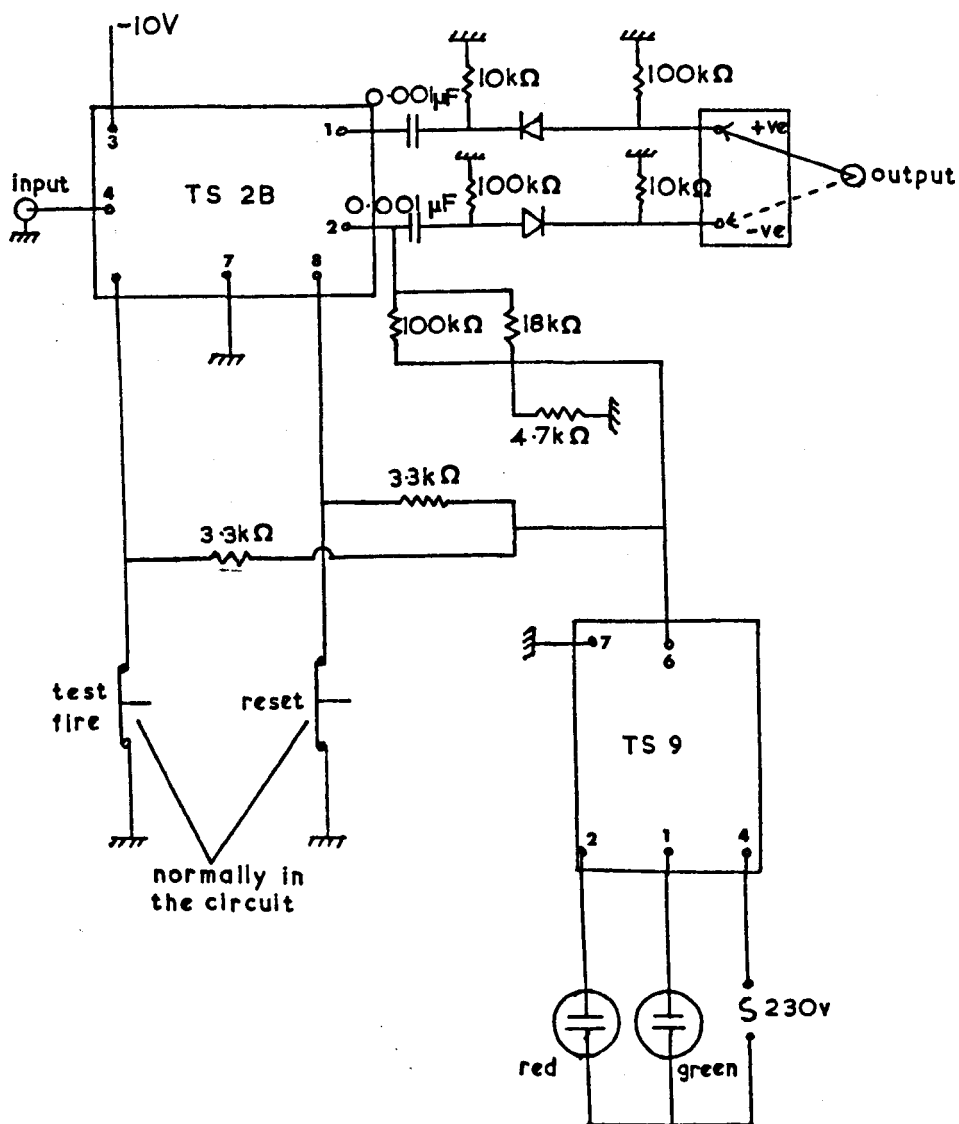
Figure 2·15 Lock Out Unit

Red light on: circuit fired; green light on: circuit ready.
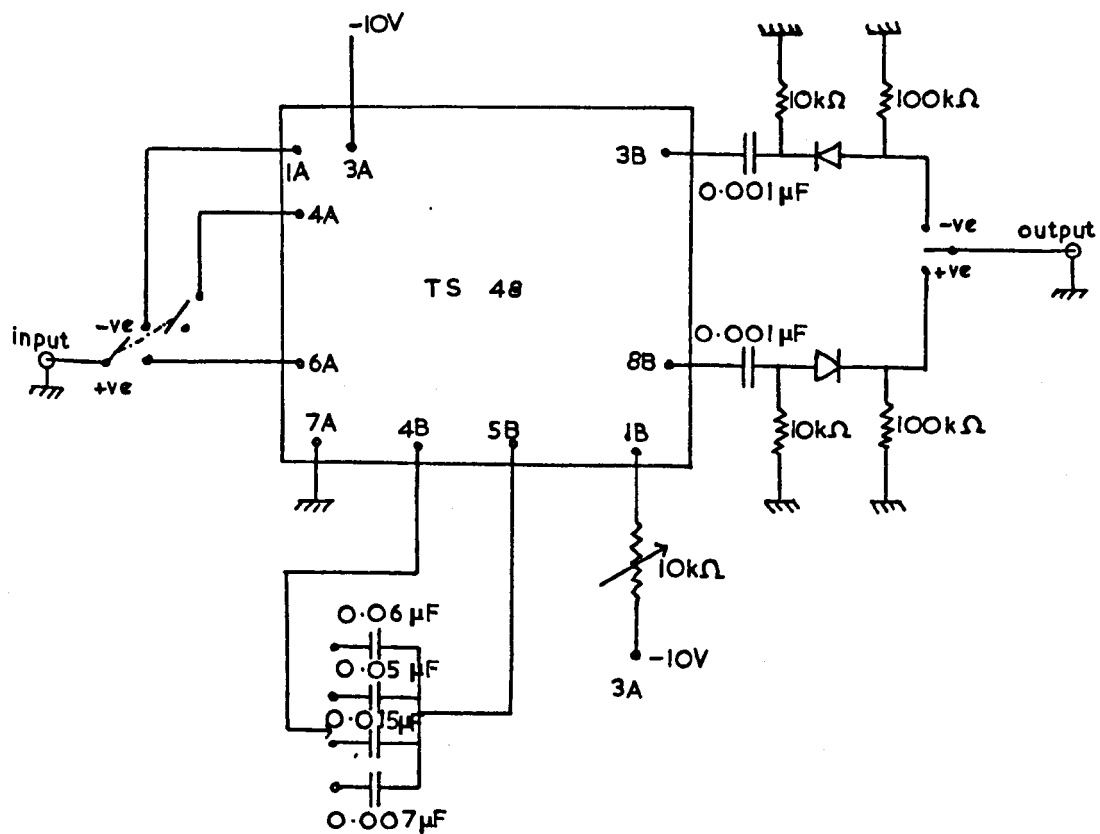
Figure 2·16 Delay Unit

2.3.7A Optical System: General Considerations

Observation of light from an infinitely thin cross-section
of the shock tube as the gas flows past is an ideal way of following
the time history of a shock heated gas. In practice it is necessary
to observe light from a section of finite thickness. Figure 2.17
shows the simplest way, a pair of parallel plates, of defining a
small "cylinder" of gas.

It is not possible to detect all the light emitted from
the cylinder for since molecules radiate light in all directions,
much will be directed away from the detector. Neither is it possible
to receive only light from the cylinder for there is no way of
distinguishing between light differing only in its origin (cp. ray 1
and ray 2, Fig. 2.17). Hence a "cone" of light is observed; this
is defined by limiting rays 3 and 4.

The angle of the cone decreases when depth of the plates,
s, increases which means that molecules outside the cylinder contribute
a smaller fraction to the total light detected.

The angle of the cone also affects the optical rise-time
of the system. Some confusion exists because rise-time itself has
several definitions. Common usage (which is adopted below) is that
for measured properties which rise in an exponential manner: the
rise-time is taken as the time to reach a fraction, $1/e$, of the
equilibrium. For non-exponential instances, the rise-time is taken

Figure 2·17 Plates defining the Light seen by a
Large Detector (Photomultiplier)

Only light from the hatched part should be monitored but all
light in the cone defined by rays 3 and 4 is detected.
AB = CD = BC if the distance S is also the diameter of the tube.

as the time required for the property to increase from 10% to 90%
of its equilibrium value. The optical rise-time is an example of
the latter case being related to the time taken for the shock front
to traverse the cone which is observed. In figure 2.17, the base of
the cone (ABCD) is 6 mm. For a shock of speed 2 mm μs^{-1}, the time
taken to traverse the cone is 3 μs. However areas a and b are each
only $^1/16$ of the total area, and so each contribute less than 6%
of the total light. Hence the optical rise-time (10 - 90%) must
be less than 2 μs. A faster shock gives a slightly shorter rise-
time and a slower shock a slightly longer one.

The rise-time observed on an oscilloscope is a combination
of the optical rise-time and the rise-time of the detector with its
associated electronics.

2.3.7B Optical System: Consideration for a Photomultiplier Detector

A previous study[80] indicated that the relaxation time of pure hydrogen chloride was fast and so it is desirable to have a rise-time that is as short as possible consistent with an adequate signal. Due to the low intensity of the emission, the optical rise-time was the principal contribution to the overall rise-time. The 9684B photomultipliers has a rise-time of 7 ns;[97] a 5MHz bandwidth amplifier has a rise-time of less than 0.05 μs; an emitter follower of bandwidth 1.8 MHz has a rise-time of less than 0.15 μs. These are negligible compared with the optical rise-time of 2 μs which results from using 2 mm slits. Hence the overall rise-time of system is approximately 2 μs.

2.3.7C Optical System: Considerations for an Indium

Antimonide Detector

The rise-time of the RPY 36 detector is specified as less than 2 μs[98] which is comparable with the optical rise-time. The oscilloscope amplifier used for monitoring the detector only has a bandwidth of 400kHz; rise-time is 0.6 μs.

The overall rise-time, τ_o, is largely determined by the optical rise-time, τ_{op}, and the detectors rise-time, τ_d: τ_o can be defined by

$$\tau_o^2 = \tau_{op}^2 + \tau_d^2$$

Reduction of τ_{op} below 1 μs has little effect on τ_o so as in Section 2.3.7B, slits of 1 - 2 mm are the optimum giving a rise-time of 2 - 3 μs.

2.3.8 Filters

So that the effect of stray light and spurious emission
is minimised, filters were employed to isolate narrow regions of
the spectrum. Of the test gases, only three show infrared activity:
HCl, HBr and CO. Table 2.2 lists their fundamental spectroscopic
constants (Table 39, Herzberg (ref. 32)).

TABLE 2.2

Spectroscopic Molecular Constants

Molecule	ω_e / cm^{-1}	$\omega_e x_e$/cm^{-1}	B_e/ cm^{-1}	α_e / cm^{-1}
H^1Cl^{35}	2989.74	52.05	10.5909	0.3019
H^1Br	2649.67	45.21	8.473	0.226
$C^{12}O^{16}$	2170.21	13.461	1.9314	0.01749

The values in Table 2.3 are calculated from the above data using
equations (III, 81), (III, 116), (III, 171) of Herzberg.[32] They
incorporate a first order correction for anharmonicity.

Transmission Curves
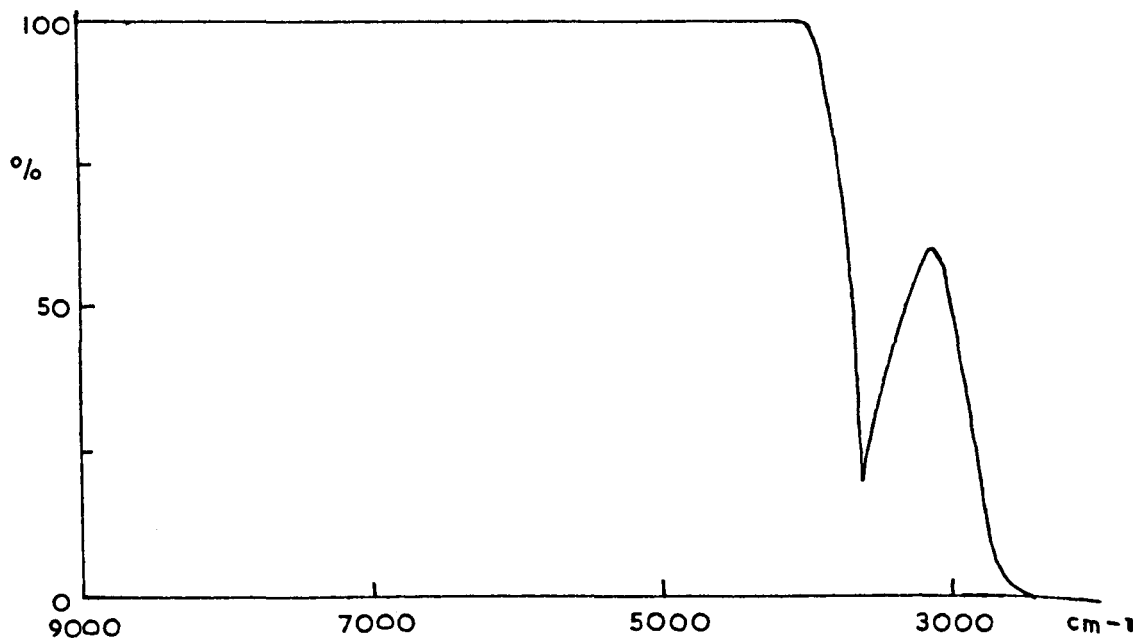
Figure 2.18 Pyrex
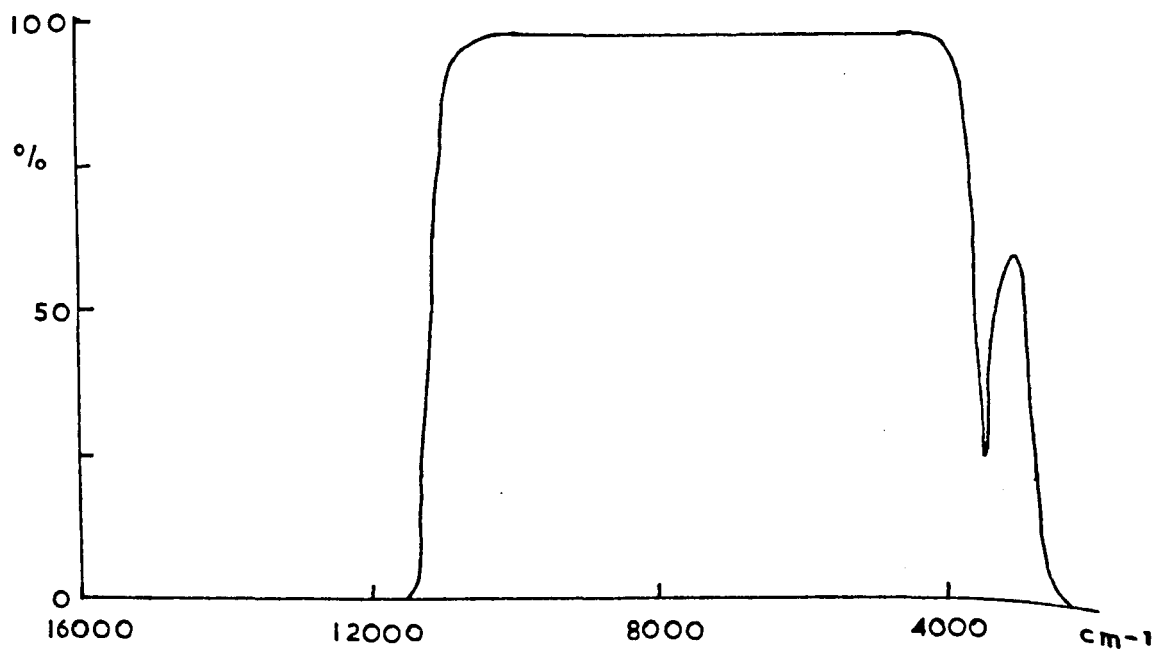
Figure 2.19 Chance OX5

TABLE 2.3

Vibrational Spectra

	1 → 0			2 → 0			3 → 0			4 → 0		
	cm^{-1}	μm	Δ^* (cm^{-1})	cm^{-1}	μm	Δ^* (cm^{-1})	cm^{-1}	μm	Δ^* (cm^{-1})	cm^{-1}	μm	Δ^* (cm^{-1})
HCl	2886	3.465	681	5667	1.836	671	8345	1.198	661	10918	0.916	651
HBr	2559	3.907	618	5028	1.989	609	7406	1.350	601	9694	1.032	593
CO	2143	4.666	292	4260	2.348	291	6349	1.576	290	8412	1.189	288

* Δ gives a measure of the width of the vibration-rotation band. It is twice the separation of the two most intense vibration-rotation lines at 2000°K.

The pyrex glass of the shock tube acts as a filter absorbing radiation of wavelength longer than 2.7 μm (Fig. 2.18). Thus without the use of windows, no emission which is due to a single quantum transition can be observed.

A band filter (Chance 0x5) which transmits between 850 nm and 2700 nm (Fig. 2.19) excluded all visible light from the detector so reducing the effect of stray light and spurious emission. A second band filter which cuts off at 800 nm (Fig. 2.20) was inserted in the light beam of the light screen situated at the observation station to ensure none of the infrared

Transmission Curves
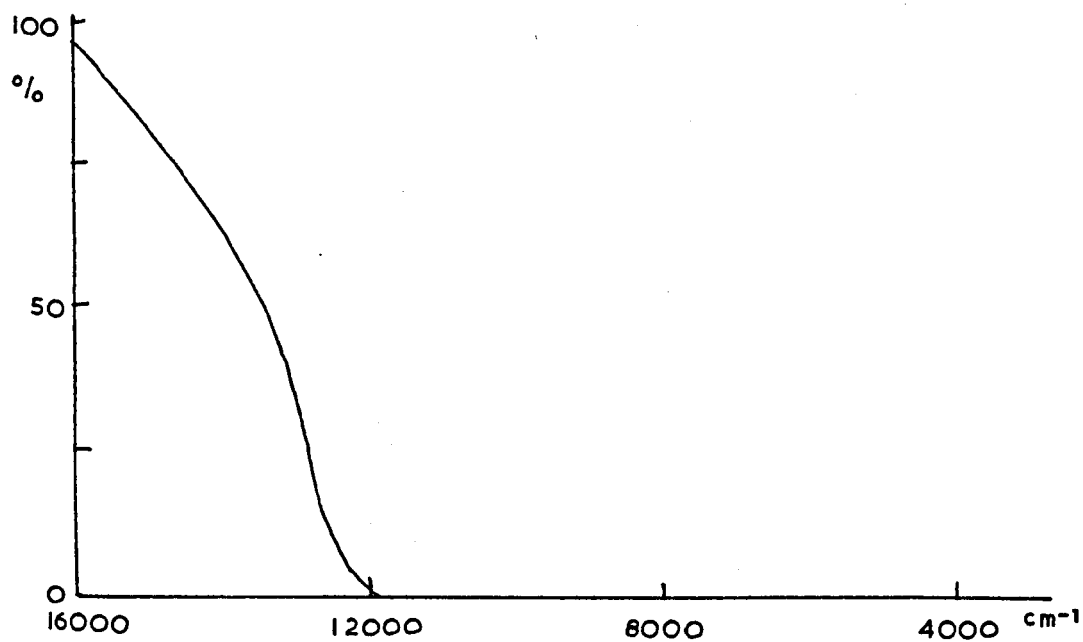
Figure 2.20 "Clear Filter"
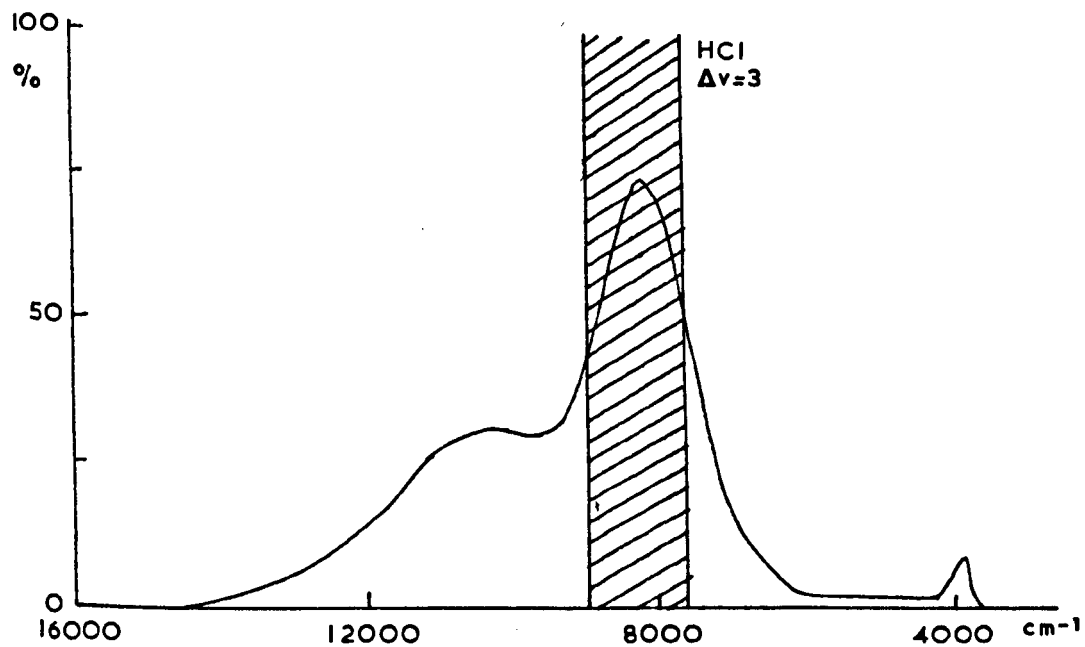
Figure 2.21 Filter No. 2

Transmission Curves
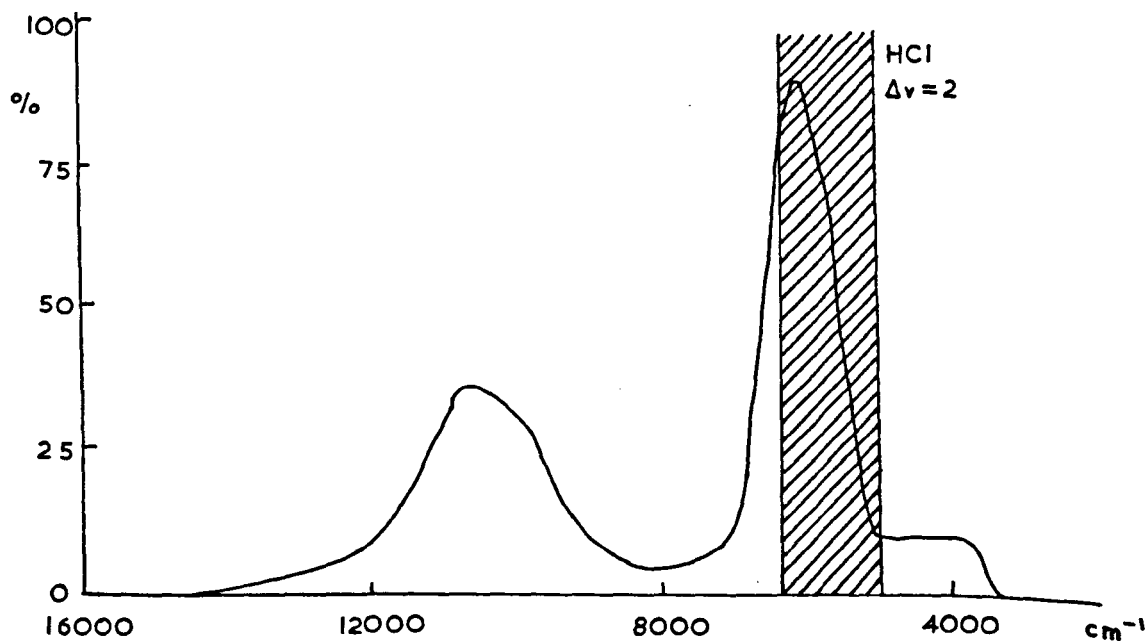
Figure 2·22   Filter No. 15
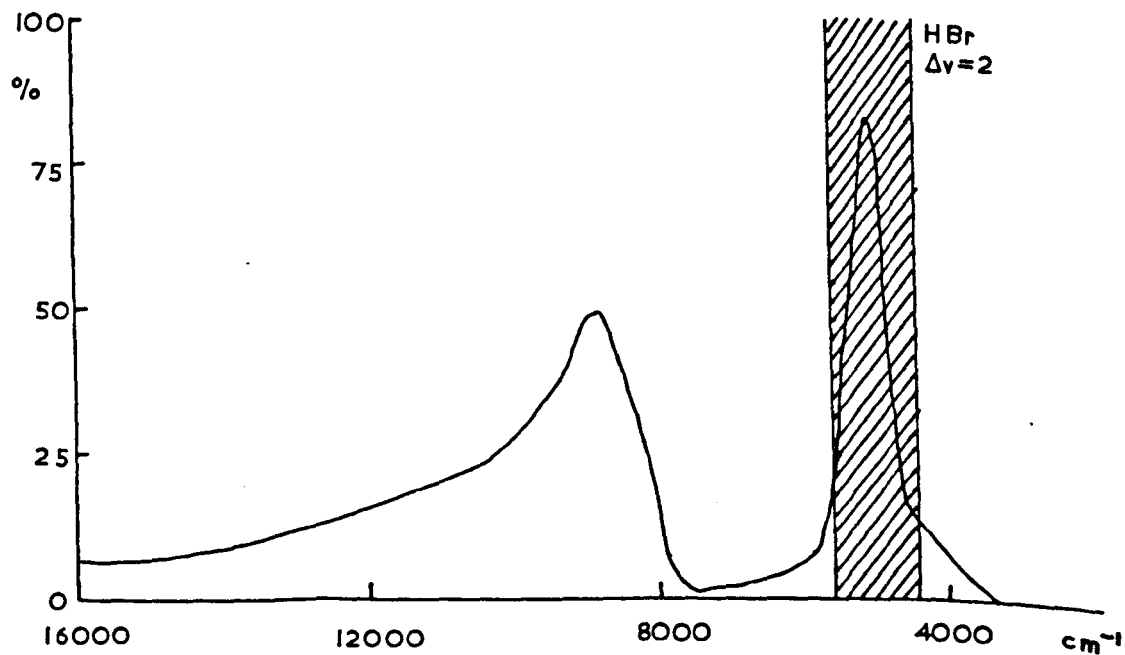
Figure 2·23   Filter No. 14

radiation observed was from this source.

Mr. A. Reid of A.W.R.E., Aldermaston kindly supplied
transmission filters which isolated individual lines.

Filter No. 2 was used to isolate the 3 → 0 transition
of HCl (Fig. 2.21). In this case, the long wavelength limit was
determined by the sensitivity of the photomultiplier detector
and was 1.2 μm.

Both the filters for isolating the 2 → 0 transitions
allowed through a considerable percentage of the 3 → 0 transition
(Figs. 2.22 and 2.23). However the intensity of the latter transition
is much the weaker of the two and its contribution to the total
intensity was neglected.[32,99] (Section 3.1.2)

2.4   Calibration of Measuring Instruments

2.4.1   Preliminary Remarks

The essential measured parameters of pressure and shock speed depend for their accuracy on the measurement of time and length. The timers, being crystal controlled, measure time intervals to ± 1 µs. Length was measured with a metre rule.

2.4.2 Pressure Gauges

Both the Pirani and Penning gauges were checked against McCleod gauge (Section 2.3.2). As they served only to indicate the amount of residual gas in the shock tube, an accurate calibration was not necessary.

Similarly, the Budenburg gauge served to show whether the bursting pressure was different from the norm. Its accuracy was not checked.

The pressure of the test gas was recorded by a mercury manometer or by the Edwards Dial gauge when non-corrosive gases at low pressures were being used. To measure more accurately small pressures of corrosive test gases, gas was introduced initially only into the glass blown section adjacent to the manometer. After measuring the pressure, it was expanded into the shock tube. The final pressure was about $1/6$ that of the unexpanded gas; it could be calculated accurately knowing the expansion factor. This was obtained by using the above technique but with the initial pressure near atmospheric. Then initial and final pressures could be accurately measured on the manometer. A second expansion factor (for non-corrosive gases) was determined when the Edwards Dial gauge was connected into the system. By arranging expansion that made the final pressure between 0 and 20 mm Hg, the accuracy of the Dial gauge was confirmed.

2.4.3 Oscilloscopes

Hewlett-Packard quote 3% as the maximum inaccuracy in the horizontal and vertical deflections of the oscilloscope beam. Calibration procedure for the voltage (Y) sensitivity is given in the manual; it uses standard voltages available on the oscilloscope. (These were measured against a potentiometer). The X sensitivity was calibrated against a crystal controlled output from the TSA 625 timer. By frequent checking, the accuracy of the instrument appeared to be better than 1%.

2.5 Optimisation and Operational Conditions

2.5.1 Light Screens

The speed of the shock wave is one of the two measured
parameters used to calculate the thermodynamic conditions in the
shock heated gas. It is usually obtained from the time taken for
the shock front to travel between a pair of velocity measuring stations.
The choice of pyrex tubing for the low pressure section allowed
detection of the shock front by light screens; they avoid making
insertions into the shock tube with the inherent danger of flow
disturbance. Considerable effort was devoted to making the light
screens reliable as they originally operated intermittently.

Most descriptions of light screen operation (for example
refs. 9,10,11,98) show the light beam reflected from the front of
the shock front. Consideration of the physical principles suggest
operating them with reflection from the back of the shock front.

When light is incident on an interface between two media
(or two parts of a medium) having different refractive indices, some
light is usually transmitted with a change in its direction and
some is reflected. The relationship between the angles of incidence
and refraction is given by Snell's Law and between the intensities of
the transmitted and reflected component rays by Fresnel's Equations
(ref. 100, p. 370).

The above relationships show that, for a sufficiently large

reflected
ray

transmitted
ray

original direction

→ shock wave

shock
front
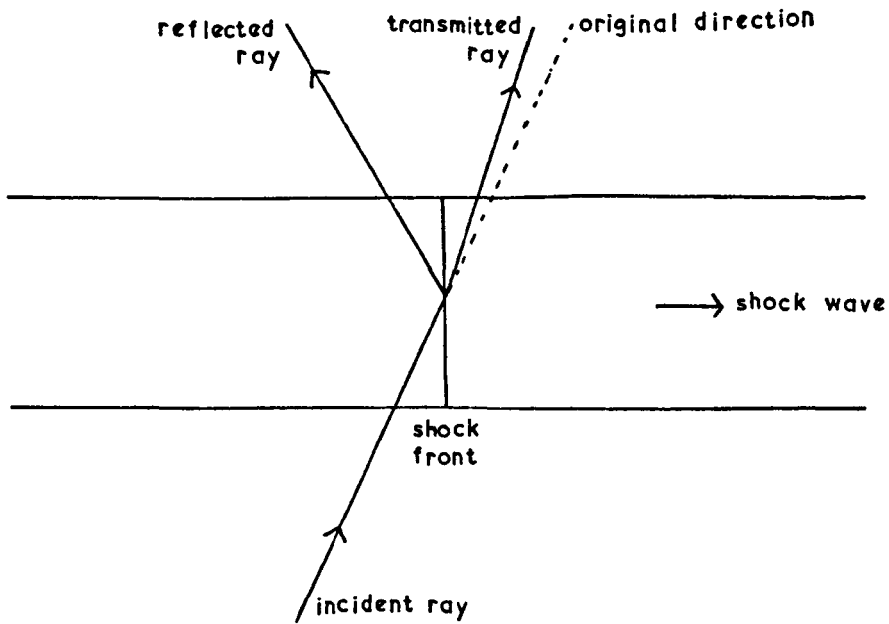
incident ray

Figure 2·24 Reflection from the Back of the Shock Front

transmitted
ray

original
direction

reflected
ray

→ shock wave

shock
front
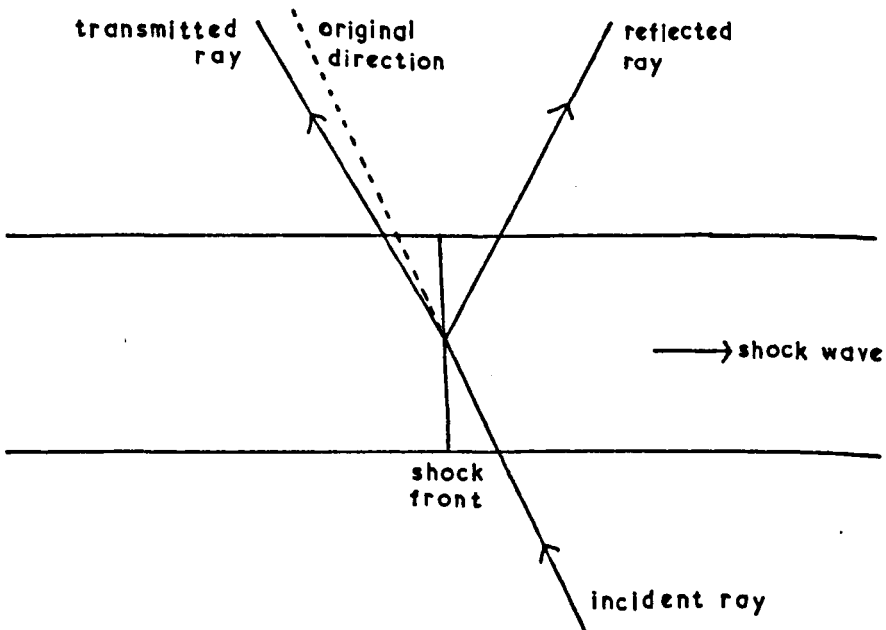
incident ray

Figure 2·25 Reflection from the Front of the Shock Front

incident angle, all light approaching the interface on the side

which is optically more dense will be reflected. The minimum angle

for total internal reflection to occur is related to the ratio of

the refractive indices. A typical value is calculated in Appendix B

to be 1.000015 which means the angle of incidence must be greater

than 89.95°. Although total internal reflection would be expected

to yield the highest signal, it is not easy to set the angle between

the light beam and the shock tube to this accuracy and also the shock

front can tilt by up to $1/15^{\circ}$.[11] Nevertheless, reflection from the

back with a high angle of incidence might lead to this condition being

met sometimes. To offset this, substitution of typical conditions

$(P_1 = 10 \text{ mm Hg}, \rho_2/\rho_1 = 5.5$ for a nitrogen shock) into Fresnel's

equations show that slightly less light is reflected from the back

of the interface compared with the front.

A second factor favouring reflection from the back can be

deduced by considering the direction in which the shock front deflects

the light (Fig. 2.24 and 2.25). For light incident on the back, both

reflected and refracted components are deflected in the same direction

so both can contribute to an increase in light reaching the

photomultiplier. In the alternative case, reflected and refracted

rays are deflected in opposite directions so only one of them is

detected.

A third factor recommending reflection from the back comes

deflected ray

original direction

shock wave

region of refractive index gradient

incident ray
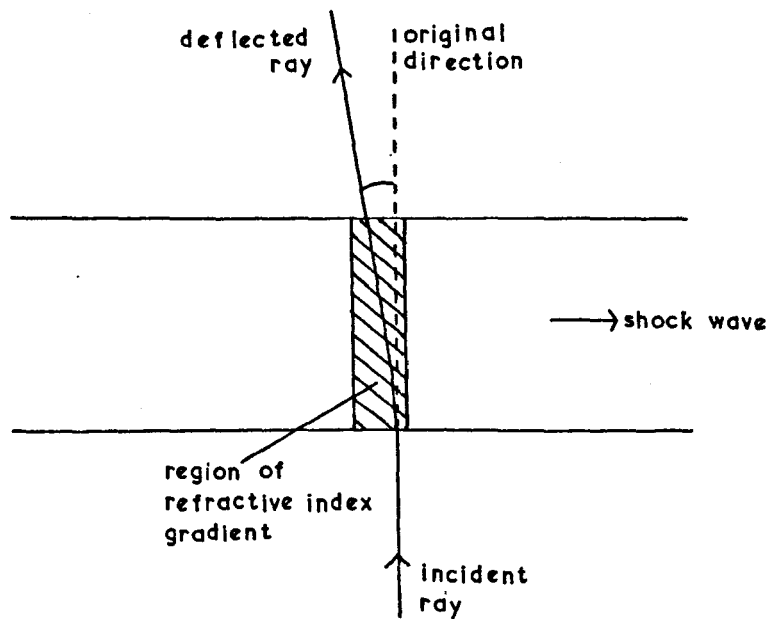
Figure 2.26 Light deflected in a Refractive Index Gradient

from considering the shock front as a region of changing refractive index as opposed to a discontinuity. Light traversing a medium perpendicular to a refractive index gradient is deflected towards the region of higher density (Fig. 2.26). The angle of deflection, α, is given by the formula[101]

$$\alpha = \frac{L}{n_o} \frac{\delta n}{\delta x} \qquad 2.1$$

where L is the distance travelled across the refractive index gradient, $\frac{\delta n}{\delta x}$, and n_o the refractive index of the air surrounding the shock tube. The direction of deflection is the same as for light reflected from the back of the shock front and so this effect could contribute to the light monitored by a photomultiplier set to observe "back reflection".

Even with "identical" shocks, the height of the light screen pulse was variable. It was therefore not possible to demonstrate experimentally from pulse height that reflection from the back was superior to reflection from the front nor which of the three effects was most important.

By considering the magnitude of the light beam's deflection, it is possible to say which effects are likely to be important. Take a beam incident to the interface at 89° for a typical nitrogen shock $(P_1 = 10 \text{ mm Hg}, \; ^{\rho_2}/_{\rho_1} = 5.5)$. Fresnel's equations show that 0.05% of light on the interface is reflected and 99.95% is transmitted. The angular deflection of the reflected component is 2° which, with an
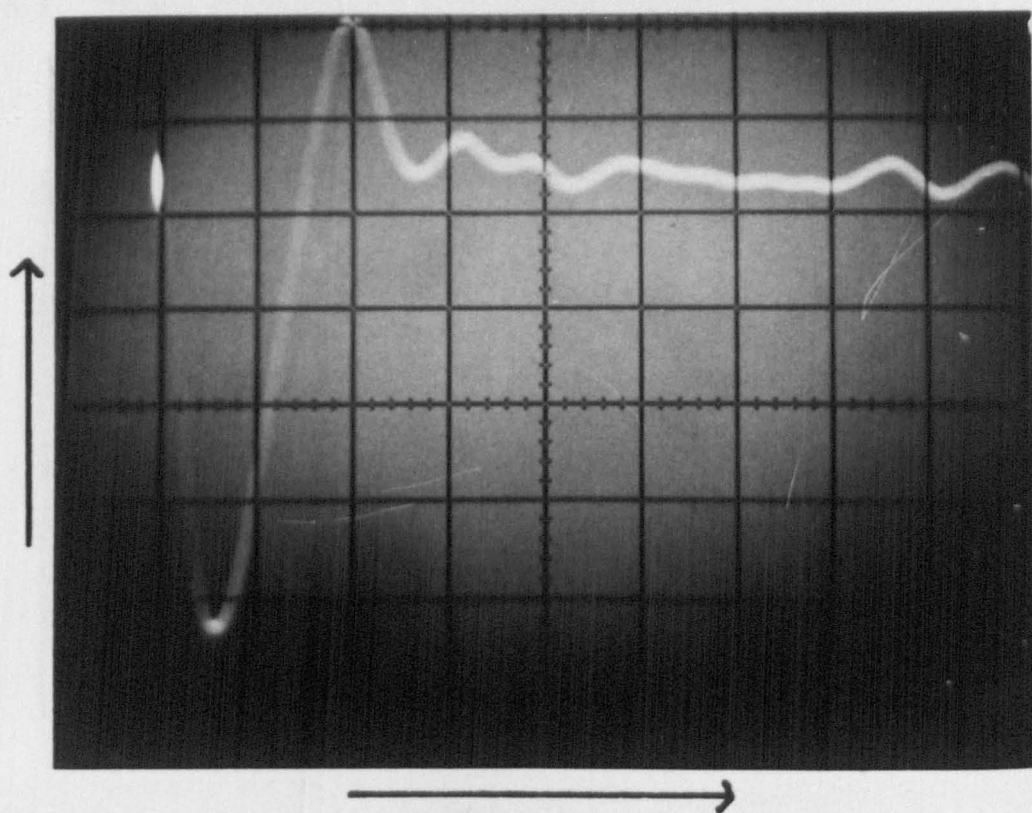
Figure 2·27 Light Screen Pulse
1 μs cm⁻¹ ; 0·2mv cm⁻¹.

optical lever of 2 m, gives a lateral displacement at the photo-
multiplier of 69.8 mm. The refracted component is deflected by
0.05^O leading to a lateral displacement of 1.7 mm. Since the light
screen pulse has only one peak (Fig. 2.27), the light must only move
onto the sensitive region of the photomultiplier and not across it.
It would seem therefore that the reflected ray contributes
insignificantly to the light reaching the photomultiplier.

The deflection due to the schlieren effect is a little
more difficult to calculate. Consider the beam parallel to the inter-
face. Figures for substituting in the preceding equation 2.1 include
$L = 50$ mm, $n_o = 1.0$, $\delta n = 1.5 \times 10^{-5}$. The distance, δx, over which
n changes rapidly is the distance taken for rotational relaxation.
Ordinarily this is about 10 collisions (Section 1.6.3). With the
mean free path calculated from equation 1.2.3,[91] a value for δx of
7.25 μm is obtained. Therefore α, the angle of deflection is 59.5^O
leading to a lateral displacement, d, of 207 mm. If instead of being
parallel, the light is again incident at 89°, L, the distance travelled
by the light while in the refractive index gradient, is drastically
reduced. The distance becomes $\delta x/\text{Sin } 1^O$ which is 0.415 nm which
leads to $\alpha = 0.05^O$ and d = 1.7 mm. It seems therefore that schlieren
effect could well be a major factor determining how much light reaches
the photomultiplier.

After deciding in which direction to expect the deflection,
the knife edges require setting accordingly. They were initially set
by eye so that the light did not quite reach the photomultiplier
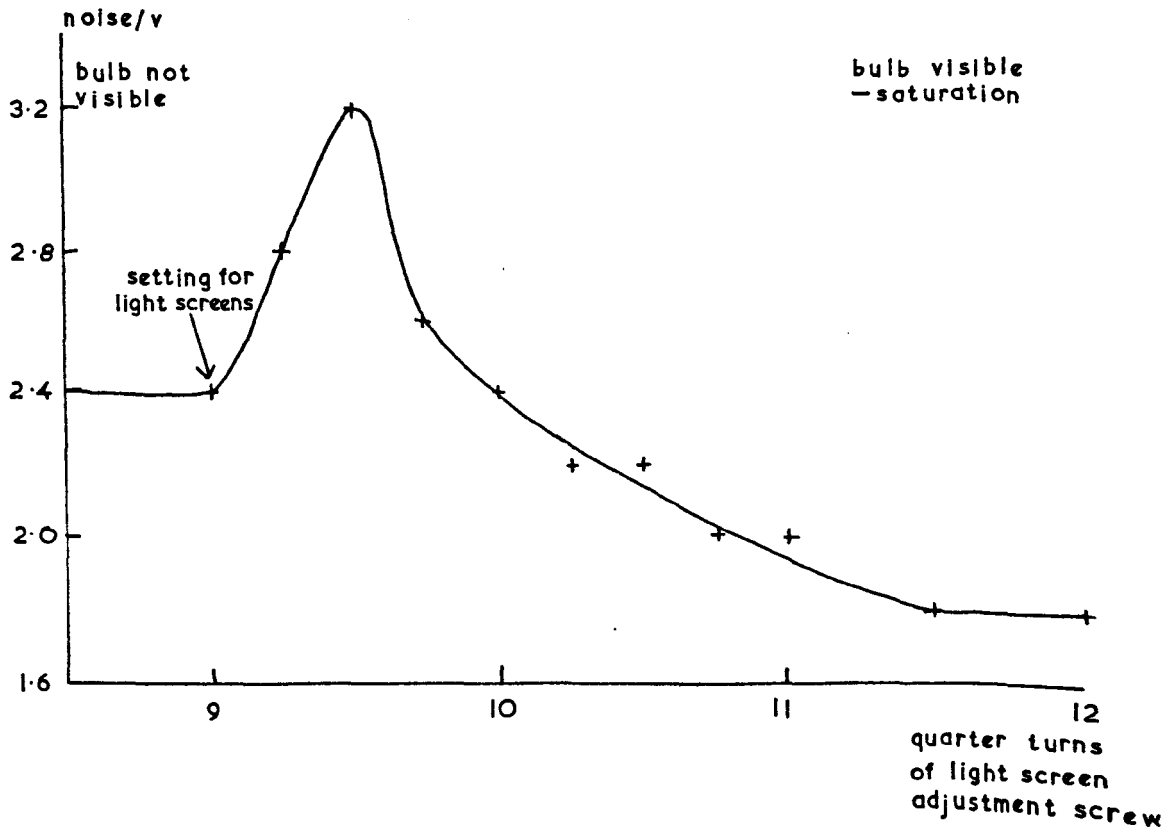
Figure 2.28 Noise of a Light Screen Photomultiplier on moving a Knife Edge

(Fig. 2.7); a piece of Polaroid was inserted into the laser beam to reduce its intensity to a safe level. It was found that the most critical setting was the position of the knife edge just before the photomultiplier; it was adjusted by rotating a knurled screw. Figure 2.28 shows how the intensity varies with the position of the knife edge, and the setting adopted for light screen operation. In practice, the long optical lever used in conjunction with the laser (Fig. 2.7) caused a large change in the position of the beam for a small adjustment in the mirror. In this case it was found better to maintain the relative position of knife edge and photomultiplier and obtain the effect shown in figure 2.28 by moving the whole housing.
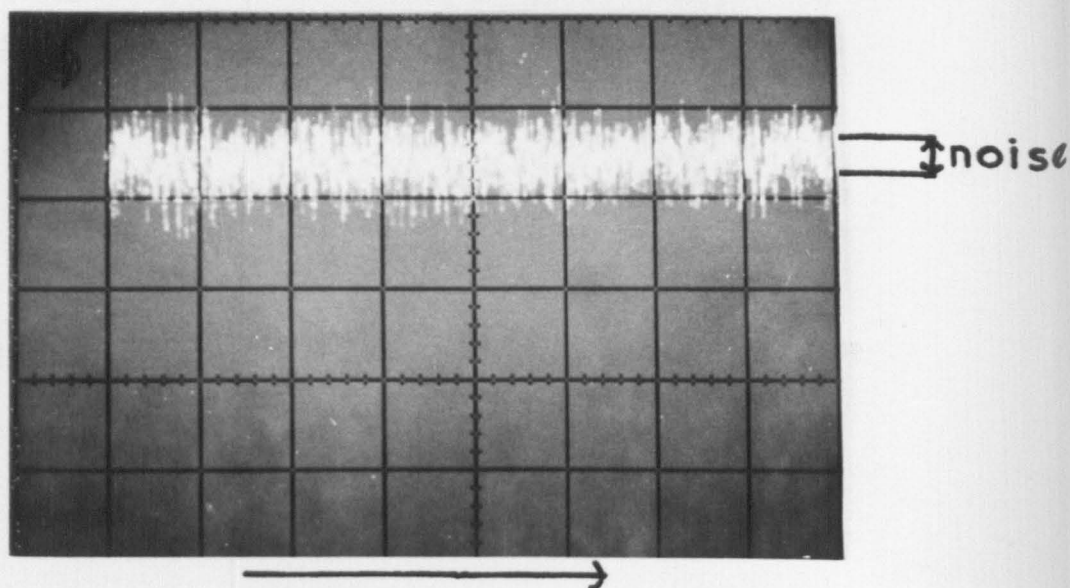
noise

Figure 2·29 Measurement of Noise
100 μs cm⁻¹.

2.5.2   Photomultipliers

E.M.I. suggest an operating voltage for each photomultiplier to give the best signal/noise (^{S}/N) ratio. So high was the level of stray light that when the light screen photomultipliers were operated at the recommended voltages, the noise was too large to be conventiently handled by the trigger units. Reducing the voltage to between 600 and 650 overcame this problem. Conversely, the intensity of light for detection by the infrared sensitive photomultiplier was so low that optimum conditions were essential.

Confirmation was sought that the voltage on the ticket was the optimum by measuring the ^{S}/N ratio at various voltages. Measurement of N, the dark current noise, presents a problem in that formulae containing N refer to its R.M.S. value which is extremely tedious to measure. An approximation was made by running the oscilloscope at 10 μs mm^{-1} and taking N as the voltage over which the trace was dense (Fig. 2.29). A low level signal, S, was applied by running a 12v projector bulb from the 6v output of a battery charger. ^{S}/N was plotted against various operating voltages (Fig. 2.30). The optimum value of 1450v was confirmed.

A further improvement in the ^{S}/N ratio for a fixed signal can be achieved by lowering the noise. The majority of the dark current noise at room temperature is due to thermionic emission; its magnitude is given by Dushman's Equation.:[102]
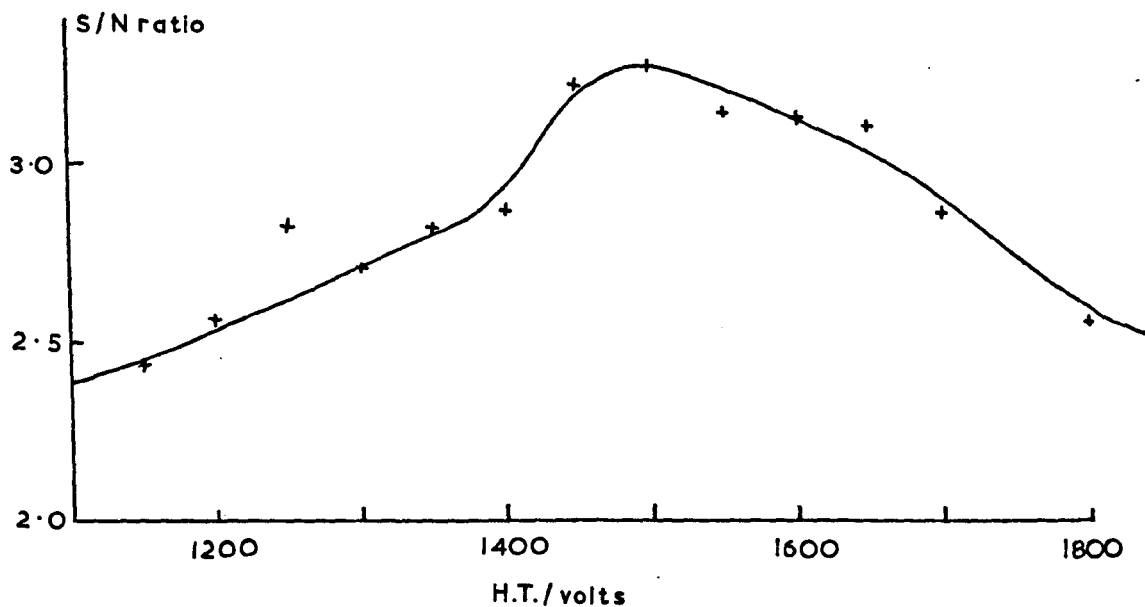
Figure 2·30   Signal to Noise Ratio (S/N)   v.   High Tension (H.T.) for the 9684B Photomultiplier at Room Temp.
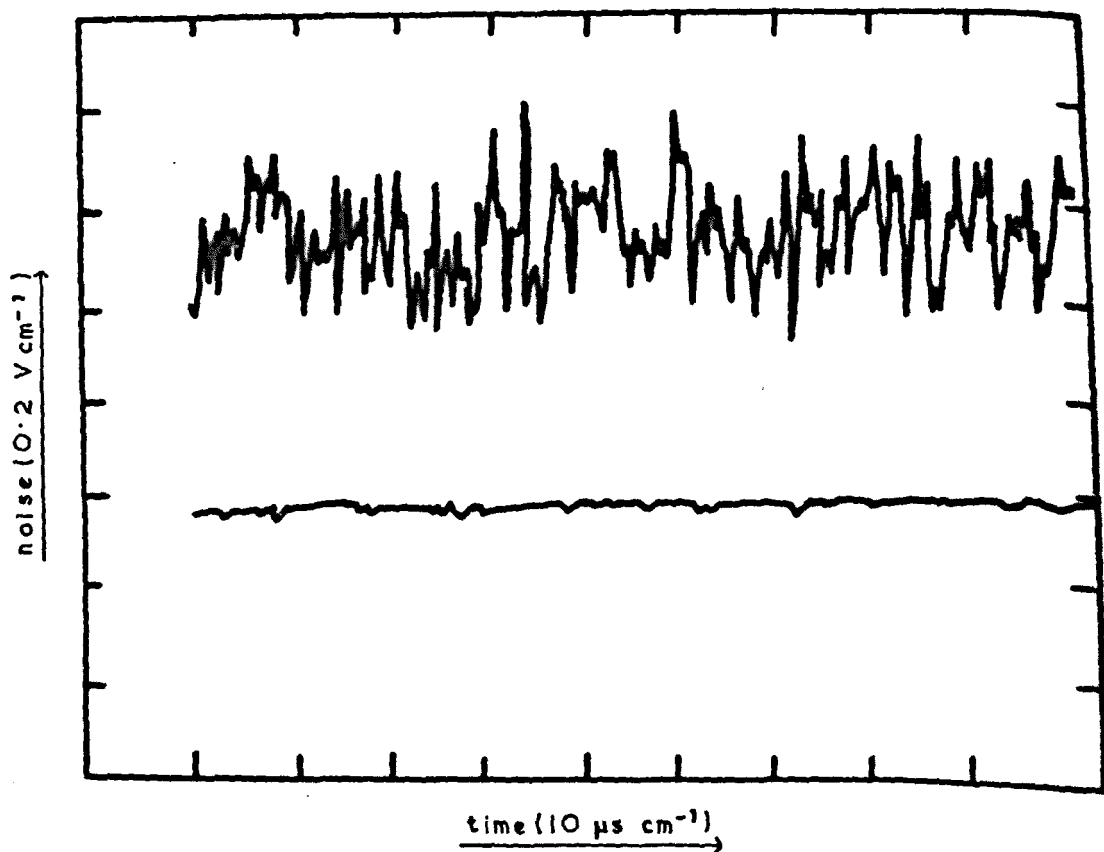
Figure 2·31 The Effect of Cooling on Photomultiplier Noise

Upper trace : room temperature.

Lower trace : −40 °C.

$$i = A_o T^2 e^{-\emptyset/RT} \qquad\qquad 2.2$$

where A_o is Richardson's constant, $\emptyset$ the work function of the surface, R the gas constant and T the absolute temperature. As T is contained in an exponential function, reduction of the photomultiplier's temperature dramatically reduces the dark current noise (Fig. 2.31). Cooling was initially with improvised equipment (Fig. 2.32) but subsequently a commercial instrument was purchased, model TE 200 from Products for Research Incorporated. Besides providing electrostatic and magnetic shielding, it had the advantage of maintaining a constant temperature $(-68^{o}C)$. Previously, the outer window dropped to as low as $-100^{o}C$ which is below the due point of commerical gases so it was impossible to prevent condensation. With the commercial cooler, intensity measurements of the emission were more reliable.

A minority of the temperature dependent noise is Johnson noise (also known as Nyguist noise and thermal noise). It originates from the statistical thermal fluctuations of electron density in a conductor; its magnitude, ΔV_J, is given by

$$\Delta V_J = (4k\ TR_o \Delta f)^{\frac{1}{2}} \qquad\qquad 2.3$$

Here k is Boltzmann's constant, R_o the resistance of the conductor and Δf the bandwidth over which the noise is measured. The temperature dependence is much weaker and ΔV_J is only reduced 20% by cooling from
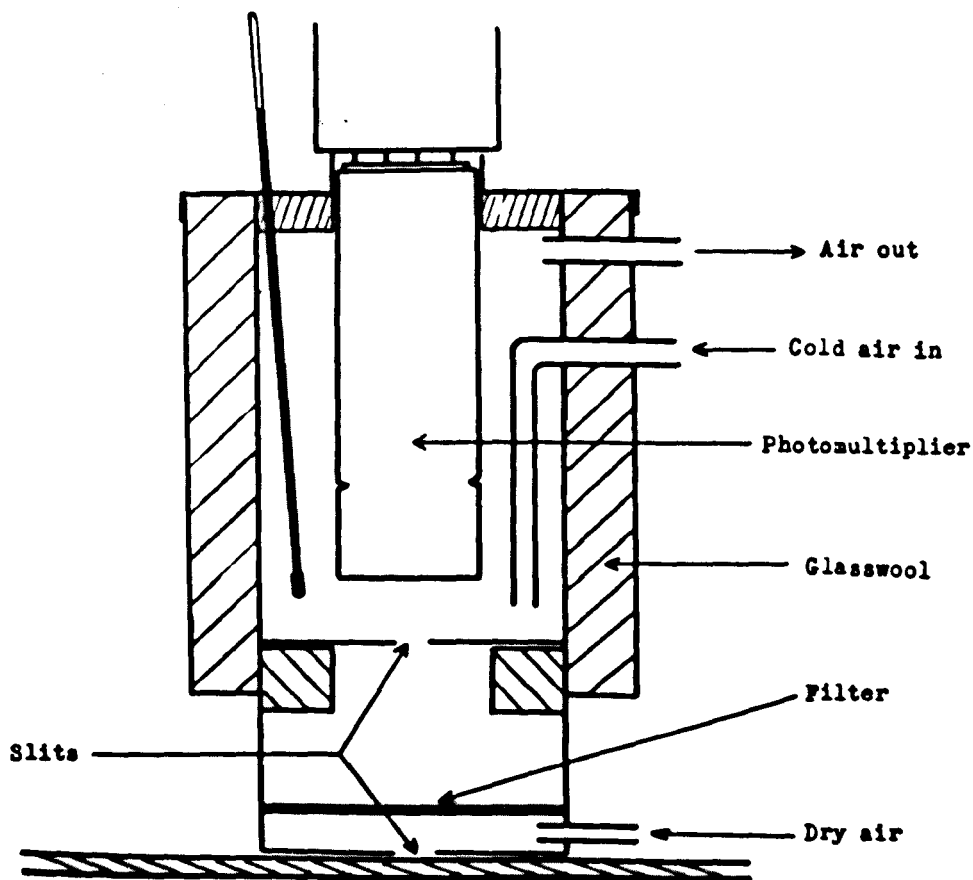
Figure 2·32 The Improvised Cooler for the Photomultiplier
The casing material was cardboard. The cool
air is passed through liquid nitrogen. The dry
air is necessary to prevent condensation on
the filter.
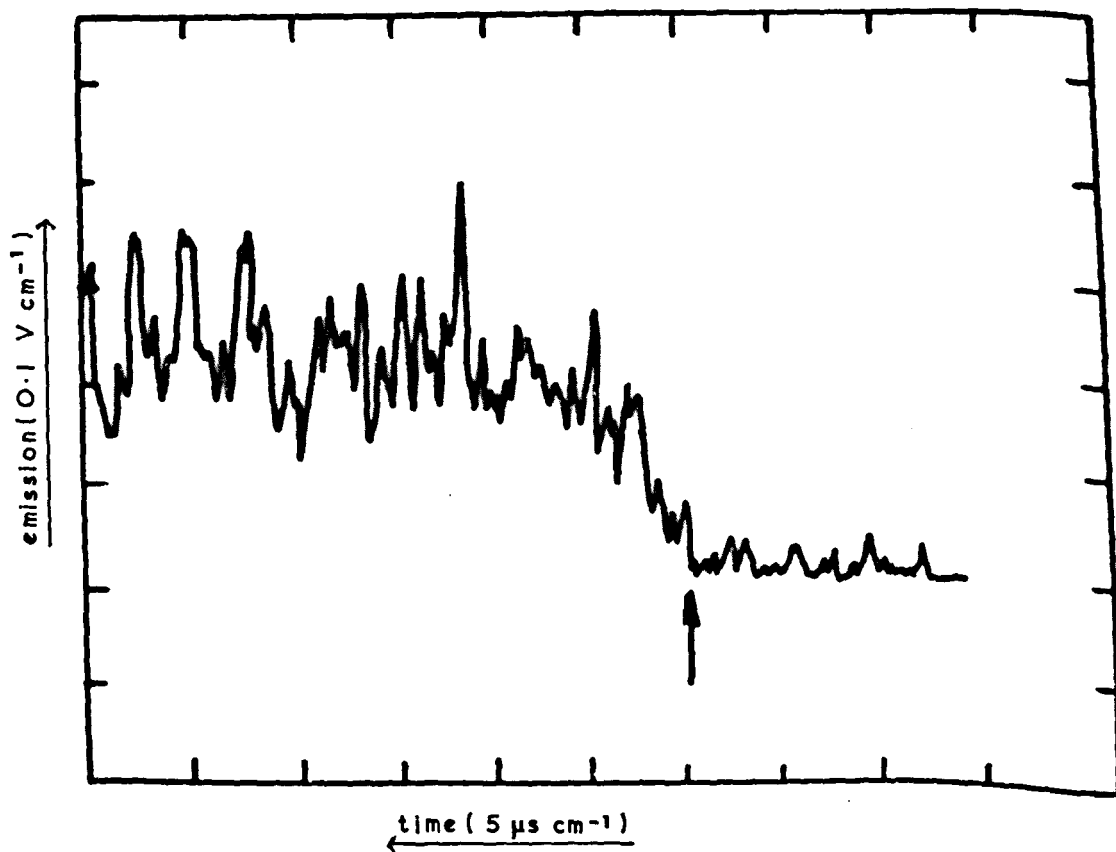
Figure 2·33 A Typical Trace for Δv = 3. Run 142
The arrow marks the arrival of the shock
front.

room temperature to dry ice temperature.

Not all noise is temperature dependent: for example current noise which can have many causes, one of which is contact resistance noise in hetrogenous materials.

Also noise due to the bubbling of the coolant can appear on lowering the temperature. Figure 2.31 shows however that these are all negligible when the detector is run at $-68^{\circ}C$ in the model TE 200 photomultiplier cooler.

Of greater importance is the noise associated with the signal (Fig. 2.33). It is mainly shot noise, due to the fact that current is carried by discrete elementary particles, and radiation noise, which is due to the random arrival of photons at the detector.[103]

2.5.3 Trigger and Lock Out Units

The trigger units provide output voltages of 8 volts for
an input signal 25 mV greater than a reference voltage which could
be set between 0 and -0.8 V by a variable resistor. Its value was
as low as possible consistent with the trigger units not being fired.

A delay between input and output pulses of 1 µs was allowed
for in measuring time intervals.

The stop pulse was fed to the timer via the lock out which
aided diagnosis of light screen failure. A fault in the first one
would cause the lock out to fire but the timer did not stop; a
fault in the second would give an unreasonable time.

2.5.4   Optical System

The basic optical system is described in Section 2.3.7 (Fig. 2.17) but several methods of improving the light collection were considered. A difficulty in predicting the value of a modification is that the shock tube itself acts as a diverging lens in the direction perpendicular to its length. Each effect was considered for the two extreme cases of light parallel and perpendicular to the shock tube.

A conventional way of increasing the light collection is to interpose a lens between the source and detector. So that the cone of acceptance is not enlarged it is necessary to retain the pair of slits. The width of the cone is 2 mm at the top and this gradually increases with increasing distance from the tube. As the photomultiplier has a sensitive area of diameter 44 mm, virtually no light is lost due to splaying out along the tube. A lens is not helpful. On the other hand, the RPY 36 detector has a width of only 0.5 mm and so a lens can be helpful in concentrating the diverging cone onto the element.

Light perpendicular to the length of the tube is diverged by it. Twice using conventional formula for single surface reflection (ref. 104, page 32) with $r_1 = 25$, $r_2 = 30$ and $n = 1.5$, showed the tube has a focal length of 480 mm. Hence it is advantageous to have the sensitive element and source as close as possible, viz. just above

Plate 2. The glass circle for collecting light from all round the shock tube.
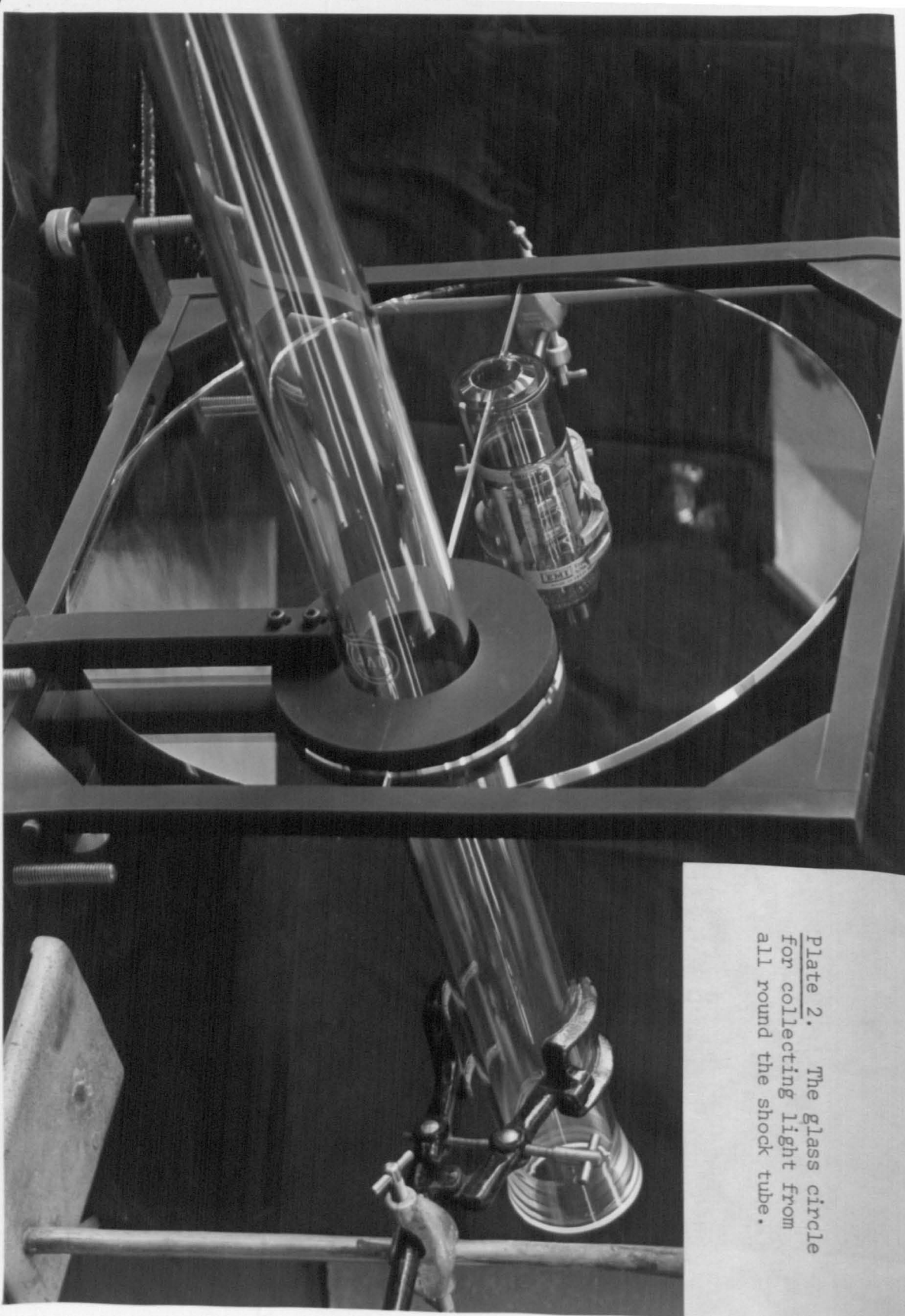
the slits. For the photomultiplier the angle of the cone in this direction was reduced by the aperture of the lens available and a decrease in signal was observed. Hence no lens was used in conjunction with the photomultiplier. For the RPY 36 with an element of length 6 mm, the angle was increased and more light was recorded with a lens of 50 mm focal length and 25 mm diameter. The position of the lens was such that a 1 mm image of the element was calculated to be formed at the centre of the shock tube (neglecting the divergence due to the tube). Slits on the tube were retained although theoretically unnecessary as the cone of acceptance was limited by the size of the element and the aperture through which it was viewed. They did however aid alignment of the detector: a light in the shock tube cast an image of the slits onto the element, which was viewed down the dewar of the detector.

A second attempt at improving the light collection involved trying to collect the light emitted around the whole circumference of the shock tube instead of just that part below the detector. Light emitted from one focus of an ellipse should be reflected to the other. By positioning the shock tube at one focus, it was felt that an increase in light would be detected by the photomultiplier sited at the other. Manufacturing difficulties caused the ellipse to be modified to a circle (Plate 2). Even though the edge of the glass was silvered to increase reflections, no nett increase in signal was observed presumably due to the diffuse nature of the source which caused light emerging from the disc to diverge rapidly.

2.5.5 Mixing of Gases

Gases were mixed in the litre storage bulbs. To condition them, a little of the minor component of the mixture was introduced into the bulb then pumped away. The correct pressure was then put in, usually by expansion from a smaller volume so the actual pressure was known more accurately. The second component was then introduced making sure the flow of gas was always into the bulb.

Gas mixtures were stored at least 24 hr before use to ensure homogeneity.

2.6   Procedure for Shock Tube Operation

Apart from details which were varied from time to time, the shock tube was operated by the subsequent procedure.

Pumping of the low pressure section of the shock tube was to below 1 μm Hg in order to maintain the purity of the test gas. Purity of the driver gas is not so important and evacuation to 10 μm Hg is sufficient.

Before making measurements all the glassware was conditioned for 30 sec by test gas (1 mm Hg pressure). After evacuation, more test gas was introduced into the glass blown section and its pressure measured before expansion into the shock tube itself (Section 2.4.2).

After isolating the tube, the pressure of hydrogen gas in the driver section was increased until the diaphragm ruptured. The output from the first light screen was fed into a trigger unit whose output started both timers and externally triggered an oscilloscope which, after a preset delay, displayed the output from the detector at the observation station. The middle light screen, via a trigger unit and lock out, stopped one timer (TSA 625), and the last light screen, via an amplifier, stopped the second timer. Thus all measurements depended on the correct operation of the first light screen.

Conditions in the shocked gas were computed from the shock speed and initial pressure. Analysis of the behaviour of the shock heated gas was from a photograph of the oscilloscope transient.

The presence of spurious emission was overcome by cleaning the shock tube between each run by pulling through it three times a cloth moistened with sodium dried ether. Flaming the tube while pumping helped to drive the ether from the walls speeding up the attainment of the required vacuum.

3. RESULTS

The results section deals with the actual measured relaxation times and the deduced Napier times. They are recorded under three categories: firstly, those obtained for pure gases, secondly those for gases containing an inert diluent, and thirdly those for gases containing a diatomic diluent.
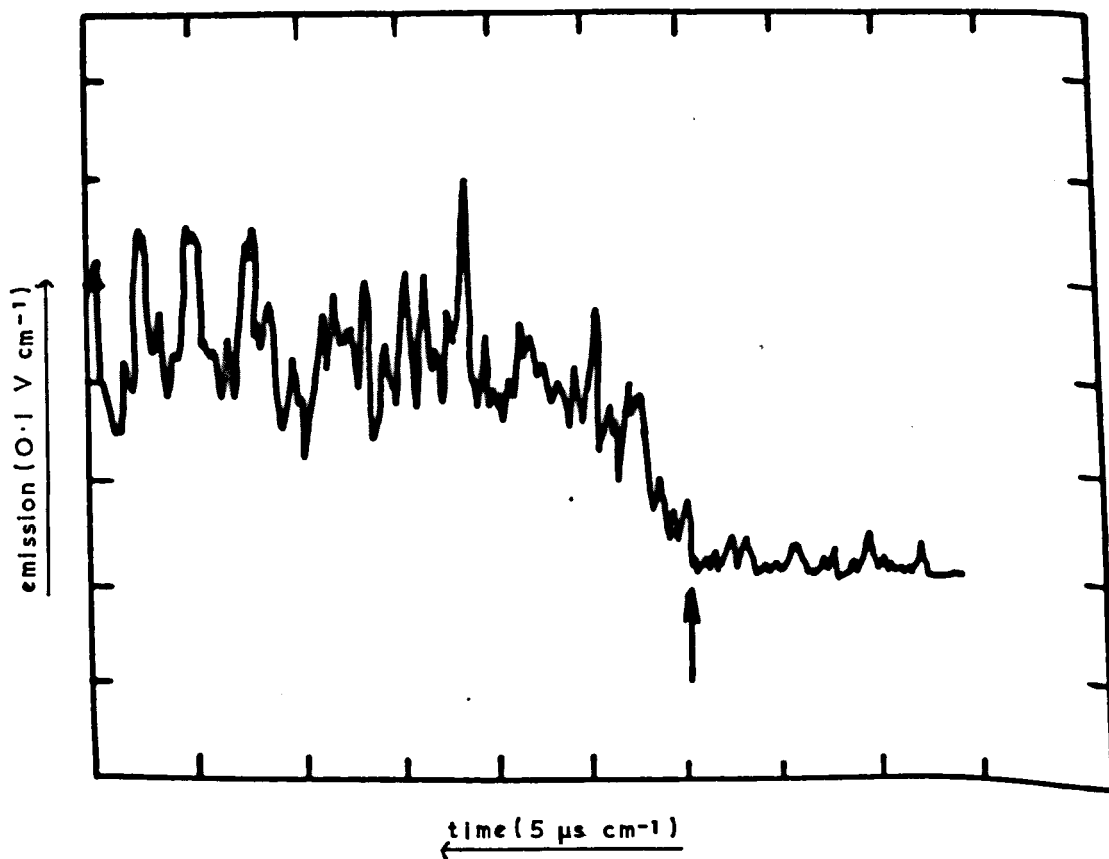
Figure 3·1 A Typical Trace for Δv ≑ 3 Run 142
The arrow marks the arrival of the shock
front.

3.1 Pure Gases

3.1.1 Relaxation of the Third Vibrational Level of Pure HCl

The first infrared detector available was the 9684B photomultiplier. It has a long wavelength cut off at 1.2 µm (Fig. 2.8) and so was used to monitor the population of the third vibrational level of HCl (Table 2.3).

With the improvised cooling system (Fig. 2.32), traces as shown in figure 3.1 were obtained. Analysis is made difficult by the shot noise but it was felt that the shape was roughly exponential which would suggest a two state system. Chow and Greene[88] obtained similar shapes for HI in argon but although they analysed their traces as for a two state system, they thought that upper vibrational levels were populated by a stepwise mechanism (Section 4.5).

For a two state system

$$\text{HCl (lower)} + \text{HCl (lower)} \quad \underset{k_{-1}}{\overset{k_{1}}{\rightleftarrows}} \quad \text{HCl (upper)} + \text{HCl (lower)}$$

$$3.1$$
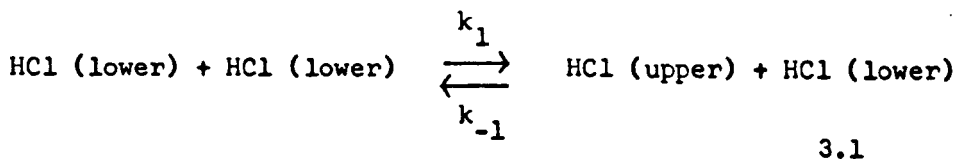
The population of the upper state, x_u, at time t is given by

$$x_u = x_{u\infty}(1-\exp(-t/\tau)) \qquad\qquad 3.2$$

where τ, the relaxation time is $(k_1 + k_{-1})$ and $x_{u\infty}$ is the equilibrium population of the upper state.

Figure 3.2 A Plot of Log($1-I_t/I_\infty$) versus t
for Run No. 142 (Figure 3.1)
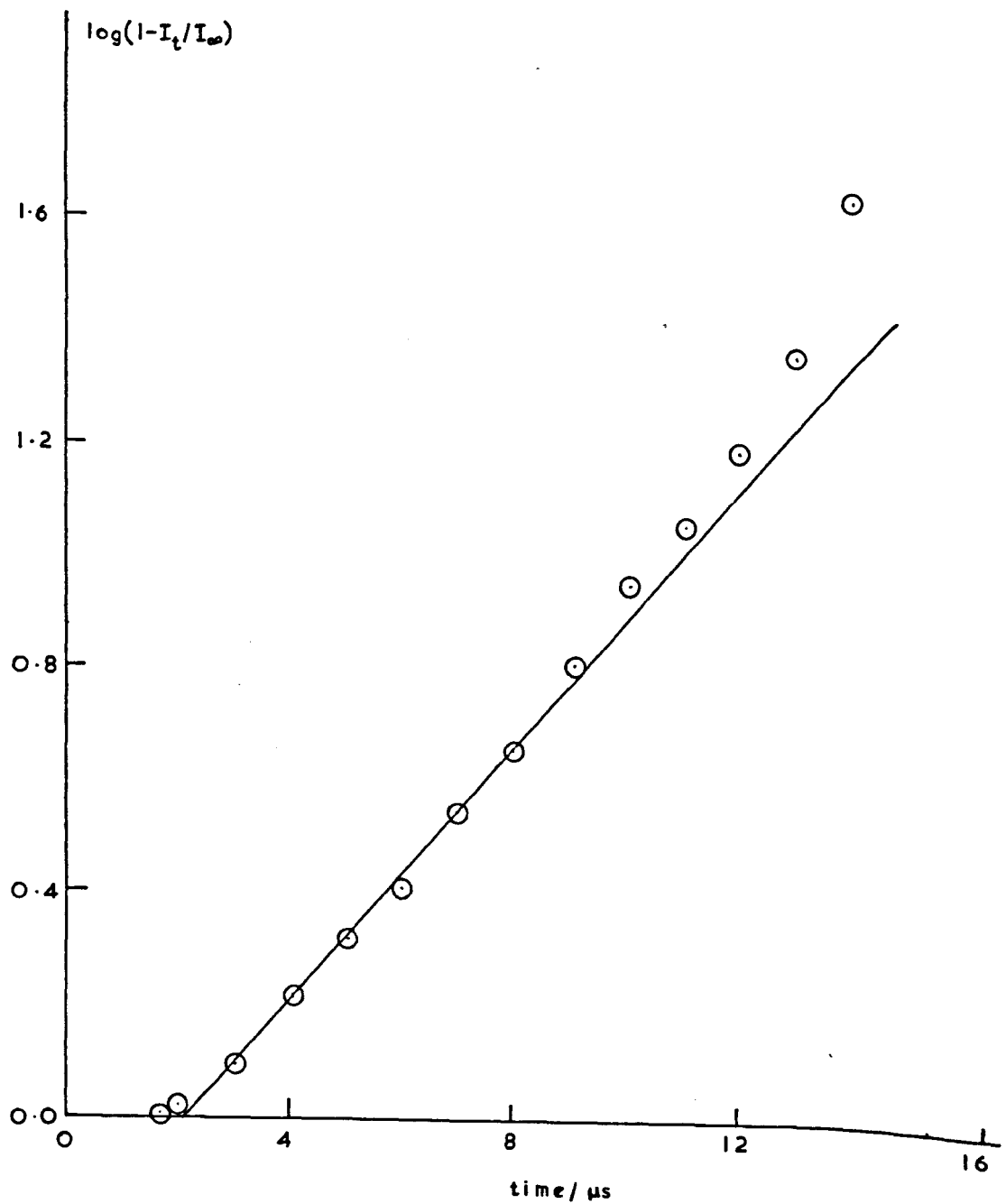
If the emission rises exponentially, a plot of $-\log_{10} (1 - I/I_\infty)$ against t should yield a straight line. Measurements were made by overlaying the photograph with a transparent graticule and drawing the best line, as judged by eye, through the trace. The appropriate plot yielded a straight line (Fig. 3.2), the gradient giving the experimental relaxation time, τ_{exp}, by

$$\tau_{exp} = \frac{-\log_e 10}{\text{gradient}} \qquad\qquad 3.3$$

Although drawing of the line through a trace is subjective, substantially the same result was obtained when several people analysed the trace in the above manner.

Experimental relaxation times were corrected to relaxation times at standard conditions (1 atmosphere) by

$$\tau = \tau_{exp} \frac{P_1}{760} \frac{P_2}{P_1} \frac{\rho_2}{\rho_1} \qquad\qquad 3.4$$

τ is the Napier time. The results are recorded in Table 3.1 and plotted in figure 3.3. The temperature at which the Napier time is plotted is T_{av}, the average of the temperatures of the gas when no and all vibrational relaxation has taken place.

Confirmation of the above results was sought when both slits and the commercial photomultiplier cooler were available. Experimental relaxation times were smaller ranging from 2.4 to 5.9 µs (Table 3.2).

TABLE 3.1

Napier Times of HCl using improvised photomultiplier cooler, $\Delta v = 3$

Run No.	P_1/mm Hg	Shock Velocity /mm μs^{-1}	$\frac{\rho_2}{\rho_1}$	$\frac{P_2}{P_1}$	τ /atm μs	T_{AV} /°K
P.B.155	10.3	1.82	5.56	41.65	11.0	2198
156	10.0	1.83	5.57	42.13	8.3	2218
158	10.2	1.80	5.54	40.75	6.7	2160
159	10.1	1.86	5.60	43.50	12.1	2280
162	10.2	1.82	5.56	41.65	10.0	2198
163	15.3	1.81	5.41	35.40	14.9	1920
164	15.1	1.68	5.40	35.00	19.3	1902
166	15.3	1.70	5.43	36.26	40.0	1958
167	14.8	1.70	5.43	36.26	48.0	1958
168	19.6	1.58	5.36	31.70	52.8	1755
169	19.6	1.60	5.31	32.20	84.6	1775
R.G.142	10.0	1.83	5.57	42.14	11.5	2218
143	11.9	1.78	5.51	39.80	7.4	2120
144	14.1	1.68	5.41	35.43	10.7	1920
147	16.0	1.67	5.39	35.00	45.0	1903
148	15.1	1.67	5.39	35.00	24.2	1903
149	18.1	1.60	5.31	32.13	62.4	1775
150	13.0	1.74	5.47	38.00	27.8	2035
151	11.0	1.78	5.51	39.80	24.1	2120
152	17.0	1.73	5.45	37.55	24.4	2016
153	10.0	1.65	5.37	34.20	28.1	1865
155	10.0	1.62	5.33	32.95	19.7	1812
156	10.0	1.64	5.38	33.75	33.7	1847
158	9.8	1.66	5.39	34.60	11.9	1984
159	10.0	1.64	5.38	33.75	15.8	1847
160	7.0	1.78	5.52	39.80	8.9	2118
161	8.0	1.68	5.41	35.40	10.7	1920
165	12.0	1.58	5.36	31.70	14.2	1848

The runs numbered P.B. 155 - 169 were made in collaboration with P. Borrell.

Figure 3.3 Napier Times for Pure HCl from Observations on the Emission from the Third Vibrational Level
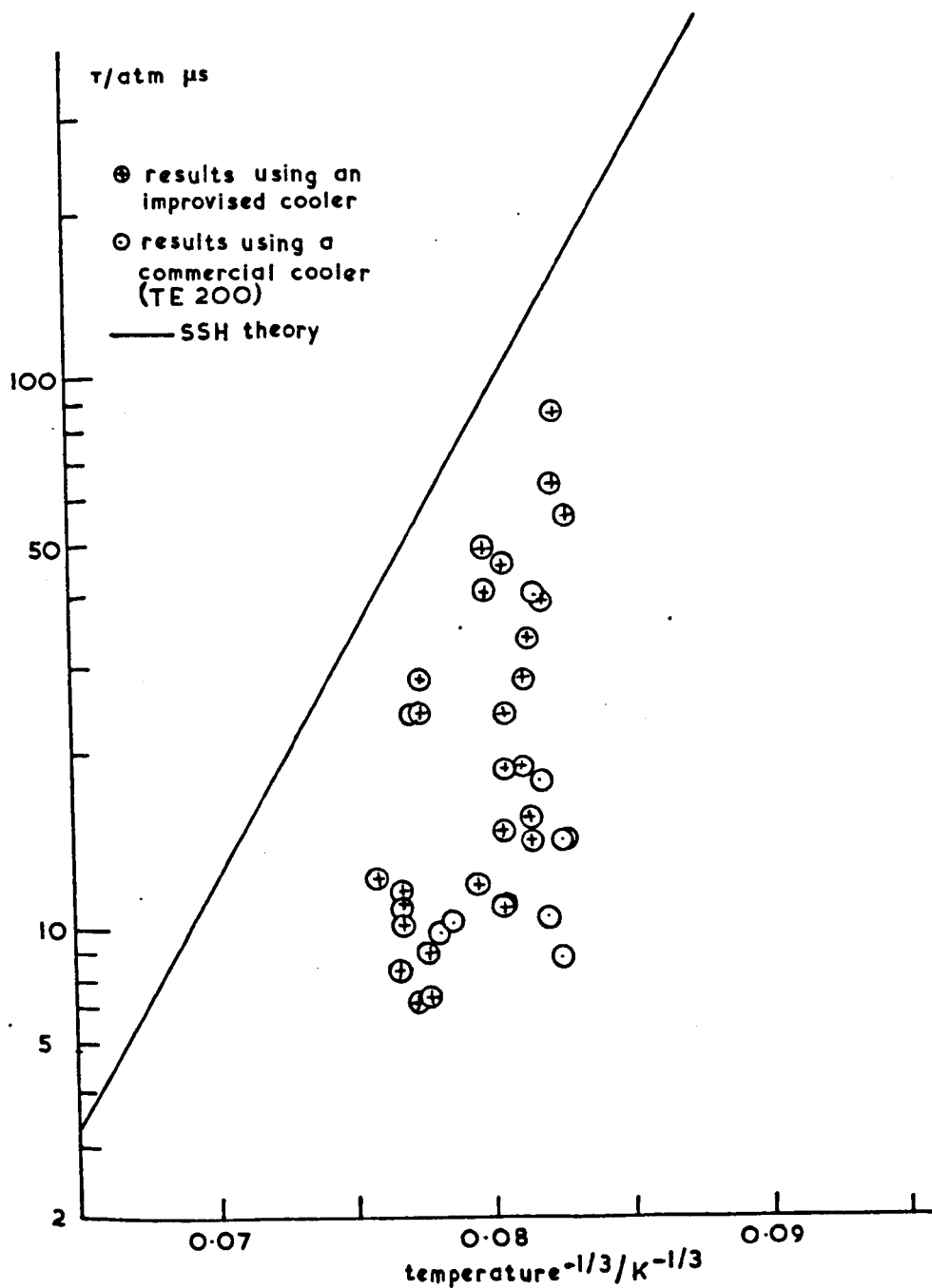
These are so close to the rise time of the system that the standardised relaxation times can only be considered as maximum values (Fig. 3.3). Borrell and Gutteridge have discussed this in their papers[105,106] and it is referred to again in section 5.1.2.

TABLE 3.2

Napier Times for HCl, using commercial photomultiplier cooler $\Delta v = 3$

Run No.	P_1/mmHg	Shock Velocity /mm μs^{-1}	$\dfrac{\rho_2}{\rho_1}$	$\dfrac{P_2}{P_1}$	τ_{exp} /μs	τ /atm μs	T_{AV} /$^\circ$K
325	13.1	1.772	5.801	38.95	2.51	9.8	2103
326	13.0	1.751	5.769	38.02	2.7	10.2	2062
329	18.7	1.618	5.553	32.36	2.4	10.6	1812
330	20.1	1.596	5.516	31.47	3.1	14.3	1772
333	13.0	1.623	6.562	32.58	5.9	18.5	1821
337	14.4	1.601	5.524	31.67	2.6	8.8	1781
338	14.4	1.608	5.537	31.97	4.2	14.3	1794

It has been assumed that the light intensity is proportional to the population of the third vibrational level. However the filter used, no. 2, can also transmit 4→0 emission as well as emission of wavelength close to the 3→0 transition such as 4→1 and 5→2 (Fig. 2.20). Polanyi's results for chemically produced vibrationally excited HCl suggest that there is virtually no 4→0 emission but there may be a

Figure 3.4 $\underline{\text{Log}(I_\infty/P_1 \cdot \frac{P_2}{P_1}) \text{ versus } T^{-1} \text{ for Pure HCl}}$

$\underline{(\Delta v = 3)}$
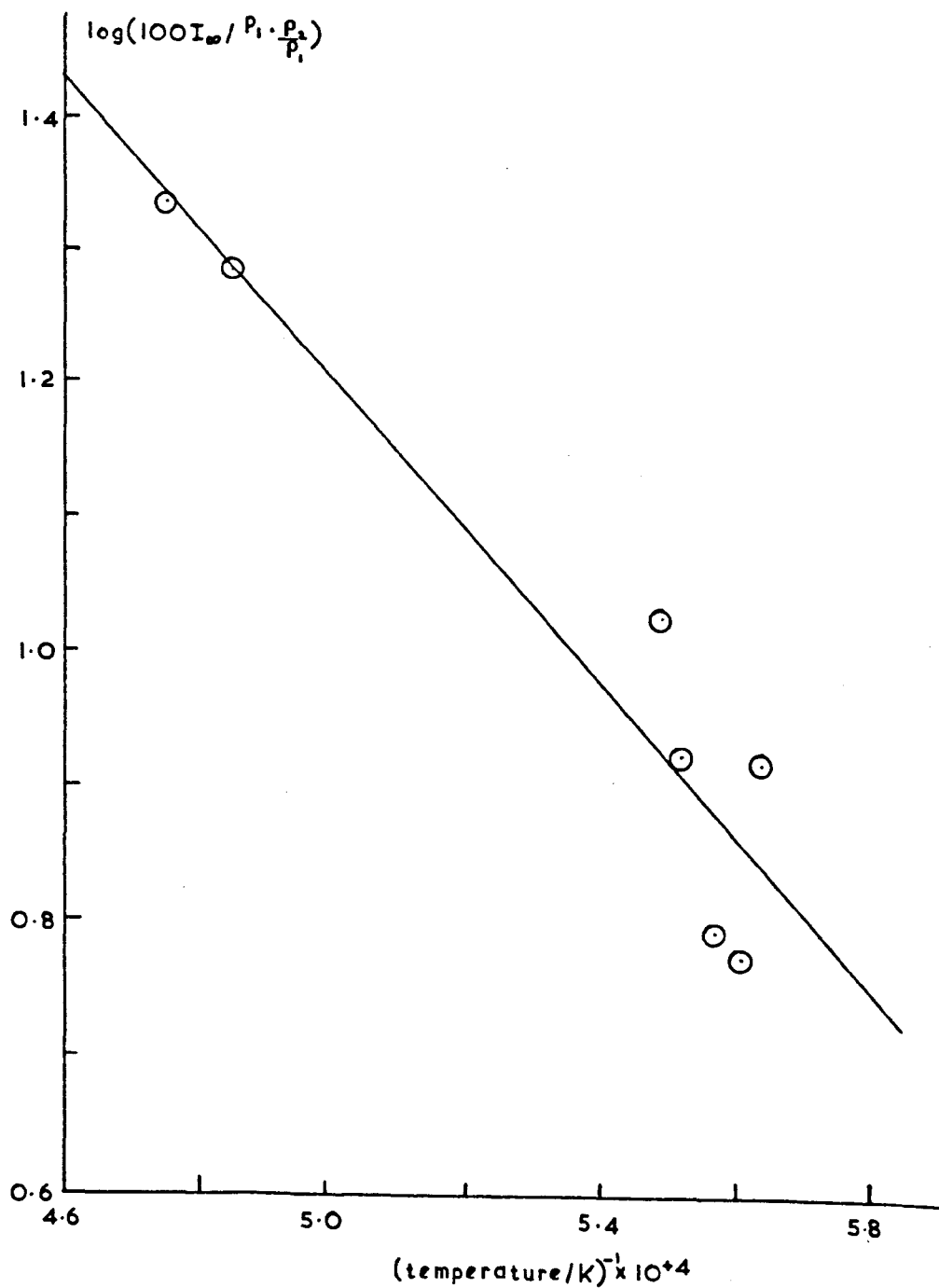
substantial amount of 4→1 emission.[99]

Statistical mechanics show that the temperature dependence of the population of the third vibrational level is different from that of the fourth. In general, for the ith vibrational level with energy ϵ_i, the equilibrium population is given by

$$n_i = N \exp(-\epsilon_i/kT)/p.f. \qquad 3.5$$

where N is the total number of molecules, k is Boltzmann's constant, T the absolute temperature. The partition function, p.f. for an harmonic oscillator is

$$p.f. = \exp(-\epsilon/2kT)/(1-\exp(-\epsilon/kT)) \qquad 3.6$$

where ϵ is the energy separation of the vibrational energy levels. The effect of temperature on the population is then given by

$$\frac{d \ln (\frac{n_i}{N})}{d(1/T)} = -(\epsilon_i - \epsilon/2)/k + (\epsilon/k)/(\exp(\epsilon/kT)-1) \qquad 3.7$$

If the second term is constant, then, since I_∞ is proportional to n_i and $P_1 \frac{\rho_2}{\rho_1}$ is proportional to N, a plot of log $I_\infty/P_1 \frac{\rho_2}{\rho_1}$ vs $\frac{1}{T}$ should yield a straight line. In fact the second term of the expression increases with temperature but only slightly. Theoretically it will lead to a curve which is slightly convex. However when the above function was plotted for the third level of HCl (Fig. 3.4), the scatter precluded any such detailed analysis. (The curvature would only alter the gradient by 2% over the range of temperature).

Using an average value for $\frac{1}{T}$, ε_i was calculated from the gradient to be 122 kJ mole^{-1} which compares favourably with the theoretical value for the third vibrational level of 121 kJ mole^{-1}. Thus all the emission monitored was for the $v = 3\rightarrow0$ transition.

Figure 3.5 $\underline{\text{Log}(I_\infty / P_1 \cdot \frac{P_2}{P_1}) \text{ v } T^{-1} \text{ for pure HCl}}$

$$\underline{(\Delta v = 2)}$$
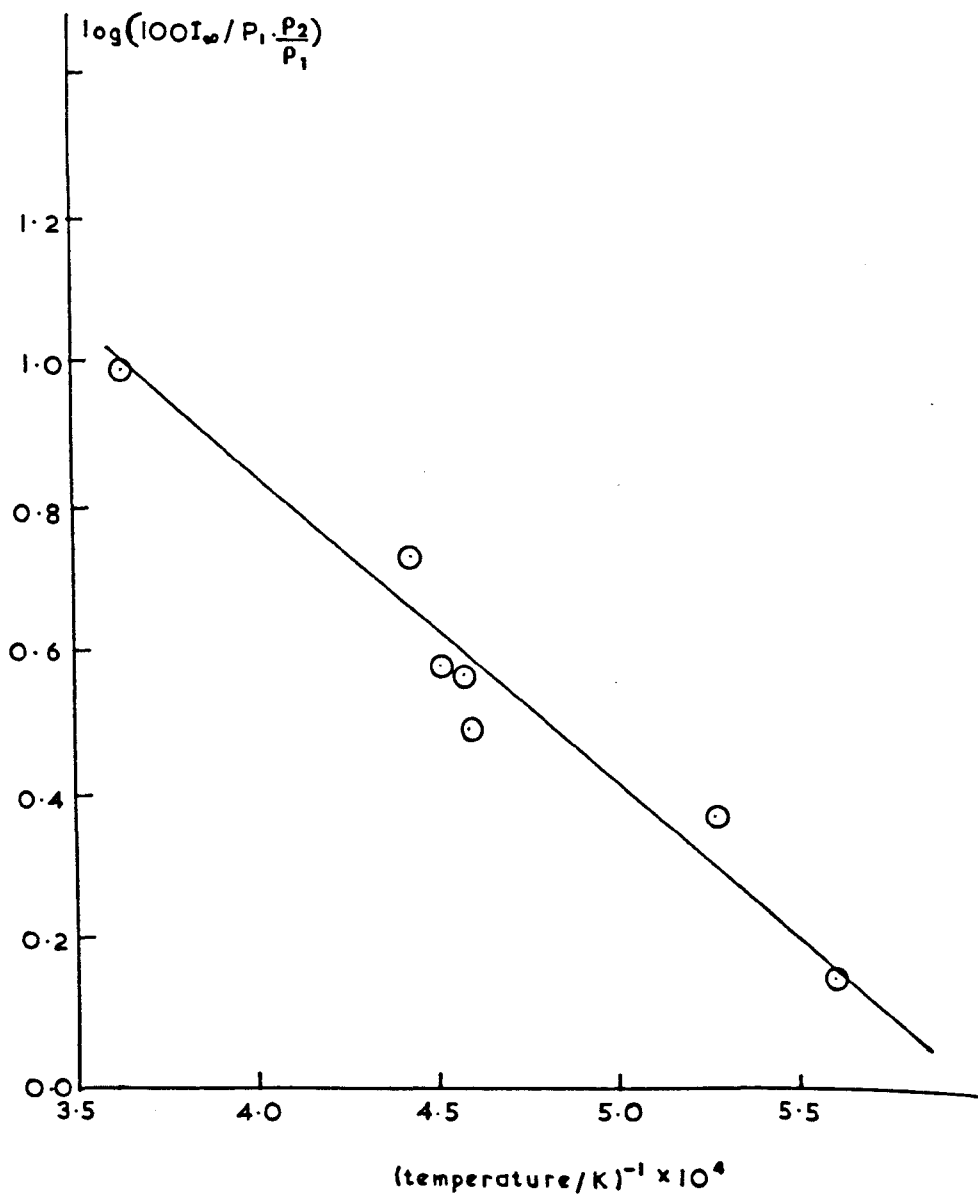
3.1.2 Relaxation of the Second Vibrational Level of HCl

The indium antimonide detector enabled monitoring the second vibrational level of HCl and the laser facilitated the use of low values of P_1. As the signal was much stronger, the slits were reduced to 0.5 mm. This meant that since the shock speeds were greater than 1 mm μs^{-1}, the rise time of the system was a function of the detector's rise time (2 μs) rather than the shock transit time across the slits.

For values of P_1 below 1.3 mm Hg, the light screens operated intermittently and there was indication of slight attenuation in that the "equilibrium" emission sometimes increased slightly as the shocked gas passed the observation station.

The rise time of the emission was never greater than 2 μs. Using this as the experimental relaxation time, a maximum value of the Napier time for pure HCl was found to be 0.6 atm μs at $1800^{\circ}K$.

Confirmation that it was the second level being monitored was sought by using the technique described in the previous section (Fig. 3.5). The energy of the level from which the emission originated was calculated to be 90.4 kJ $mole^{-1}$ which agrees with the theoretically calculated value for the second vibrational level of 86.0 kJ $mole^{-1}$.

3.1.3 Relaxation of the Second Vibrational Level of HBr

To isolate the second vibrational level of HBr, filter No. 15 was replaced by filter No. 14. The technique adopted was as described for HCl in section 3.1.2 and hence an upper limit for the Napier time of pure HBr could be set at 1.0 atm µs at 2300°K.
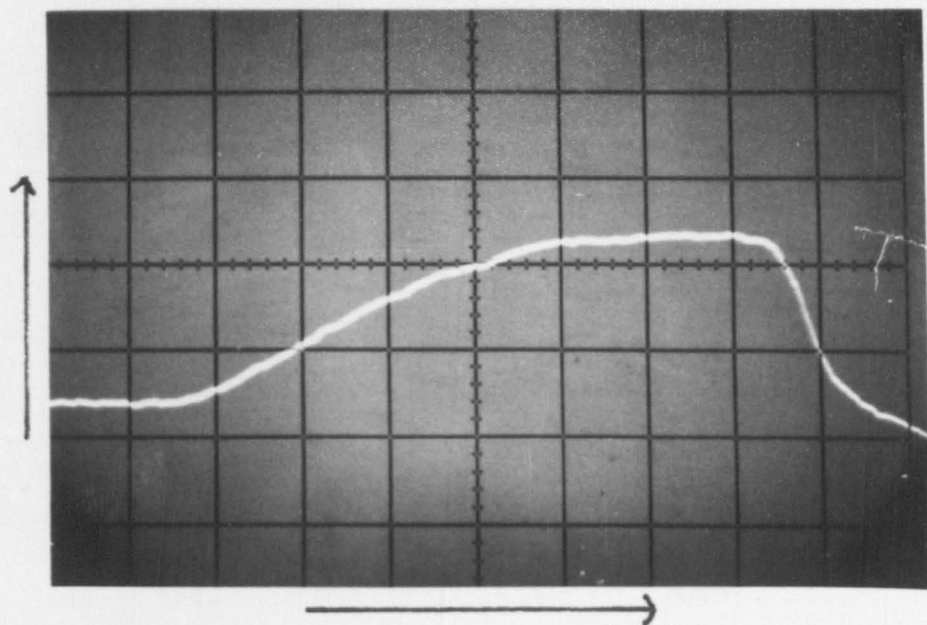
Figure 3·6 Emission from Pure CO
Run 429: 20 μs cm^{-1}; 1 mv cm^{-1}.

3.1.4   Relaxation of the Second Vibrational Level of CO

It is well known that the relaxation of CO is very
sensitive to the presence of certain impurities, especially
water.[72,77] Confidence that an acceleration in the relaxation
process is solely due to an added impurity is greater if it has
been demonstrated that the system is capable of measuring the
Napier time of pure CO. For this reason a few such observations
were made and a typical trace is shown in figure 3.6. The shape
is considerably different from a simple exponential curve and it
was analysed by assuming that the population of the second
vibrational level was by a two step process after the manner of
Windsor, Davidson and Taylor[72] and Hooker and Millikan.[75] Both
their methods for obtaining the experimental relaxation time
were tried: the gradient of the slope at $I_\infty/4$ was taken and plots
of $-\log (1-(I/I_\infty)^{\frac{1}{2}})$ against t were made. The two techniques, which
are discussed further in section 4.5 show the former being less
tedious, was more generally adopted. Values of the Napier times
for pure CO are given in Table 3.3 and plotted in figure 3.7.
They show good agreement with the generally accepted values of
Hooker and Millikan.[75]

Figure 3·7 Napier Times of Pure CO
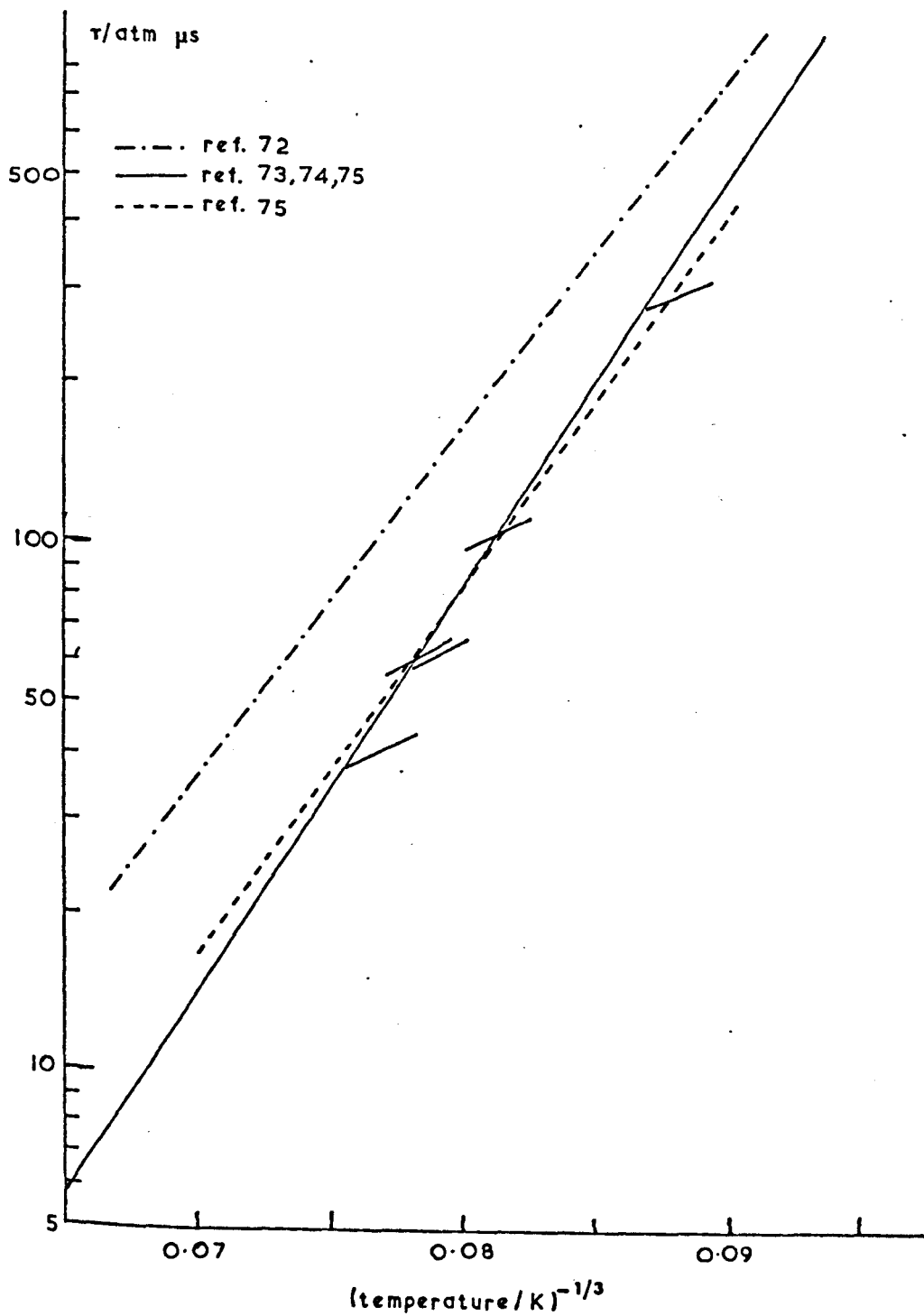
Figure 3.8 Log($I_\infty / P_1 \frac{P_2}{P_1}$) v T^{-1} for Pure CO

($\Delta v = 2$)
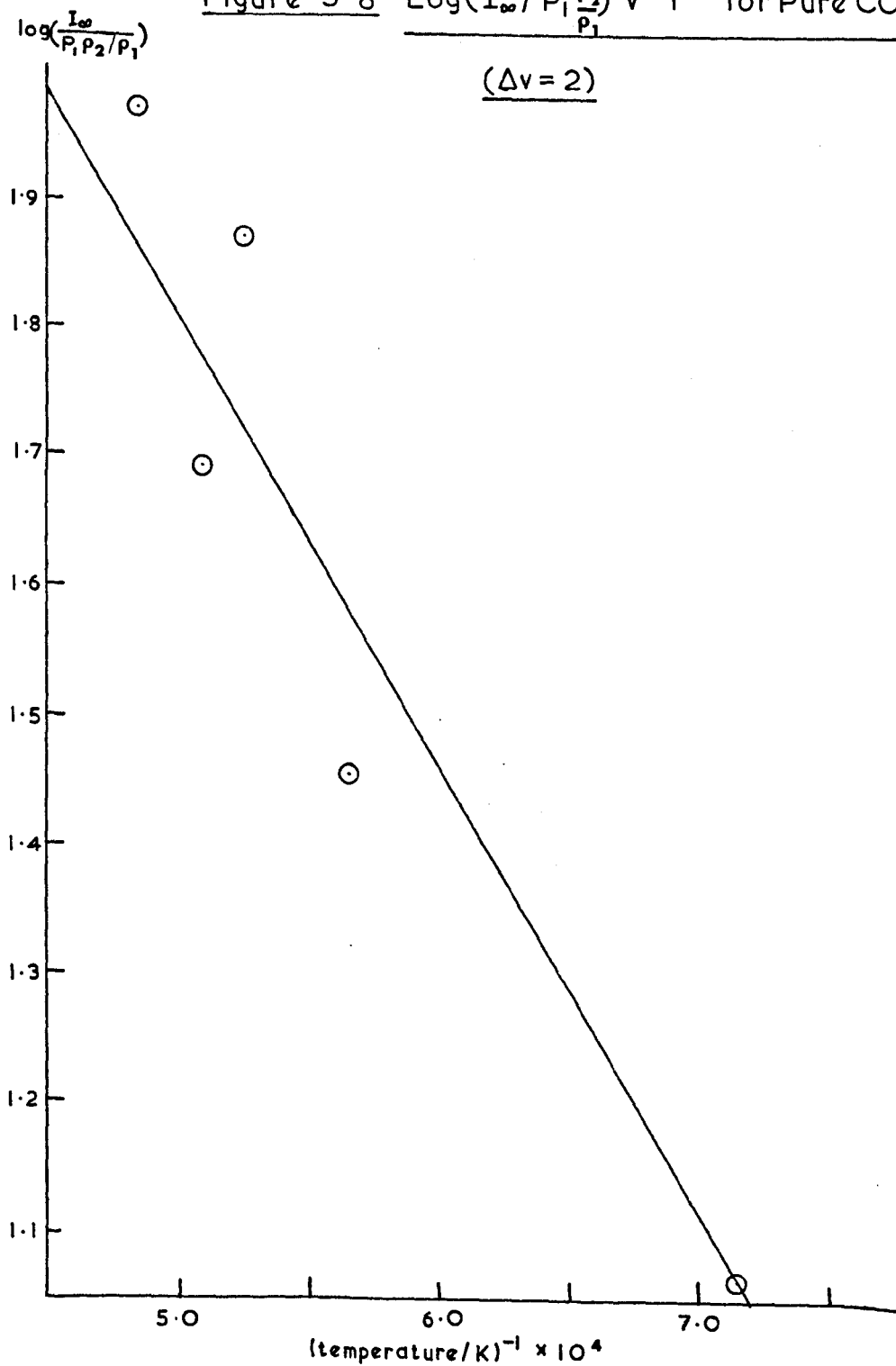
TABLE 3.3

Napier Times for Pure CO, $\Delta v = 2$

Run No.	P_1 /mm Hg	Speed /mm μs^{-1}	τ_{exp} /μs	τ_1 /atm μs	T_1 /$^\circ K$	τ_2 /atm μs	T_2 /$^\circ K$
484	10.95	1.614	160.5	272	1504	306	1399
485	9.2	1.880	46.4	92.7	1942	107	1765
489	6.5	2.012	33.4	57.5	2183	66.2	1963
492	9.4	2.073	14.0	37.0	2298	43.8	2057
493	11.2	1.970	20.0	56.0	2104	65.6	1899

The same technique as for HCl was used to show that the energy of the level from which the emission originated was 69.4 kJ mole^{-1} (Fig. 3.8). This compares favourably with the calculated value for the second vibrational energy level (64.5 kJ mole^{-1}).
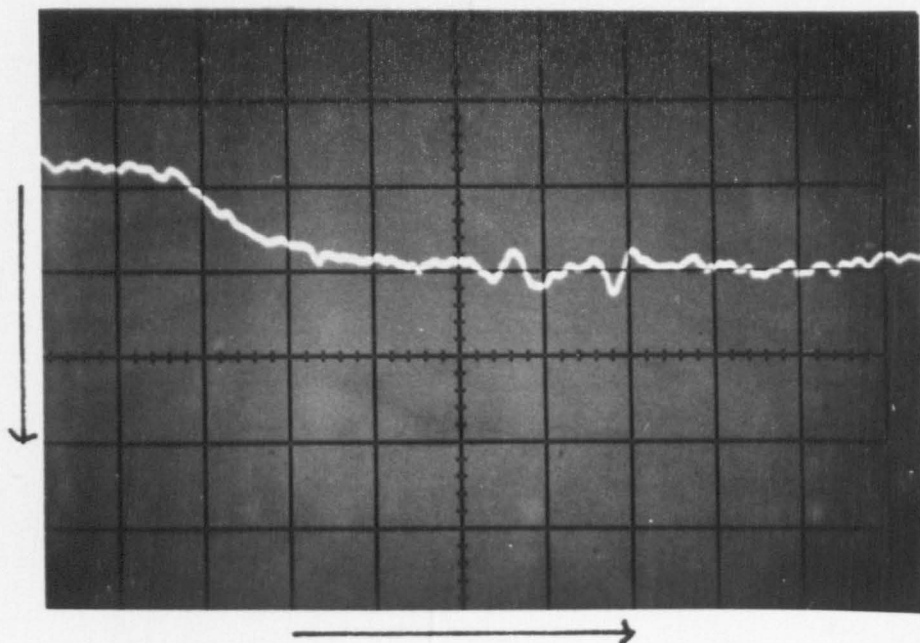
Figure 3·9 Emission from 5% HCl in Ar
Run 388: 5 μs cm⁻¹; 0·2 mv cm⁻¹.

3.2 Hydrogen Halides with Monatomic Diluent

3.2.1 Hydrogen Chloride in Argon

From the previous experiments, it was concluded that the conditions in shock heated hydrogen chloride could not be varied sufficiently to extend the experimental relaxation time of pure HCl beyond 2 µs. Addition of a heavy monatomic gas will usually slow down the relaxation process and by varying its concentration, the relaxation time for the pure diatomic gas can be calculated. Argon was chosen as diluent for this purpose.

With a mixture of 10.0% HCl in Ar, the rise time of the emission was still that of the detector, 2 µs.

With the concentration of HCl 5%, the experimental relaxation times began to lengthen but their measurement was more difficult because the intensity of emission was very low (Fig. 3.9). The traces were analysed as if they were simple exponentials and the results are given in Table 3.4 and plotted on figure 3.10.

Figure 3·10   HCl in Argon
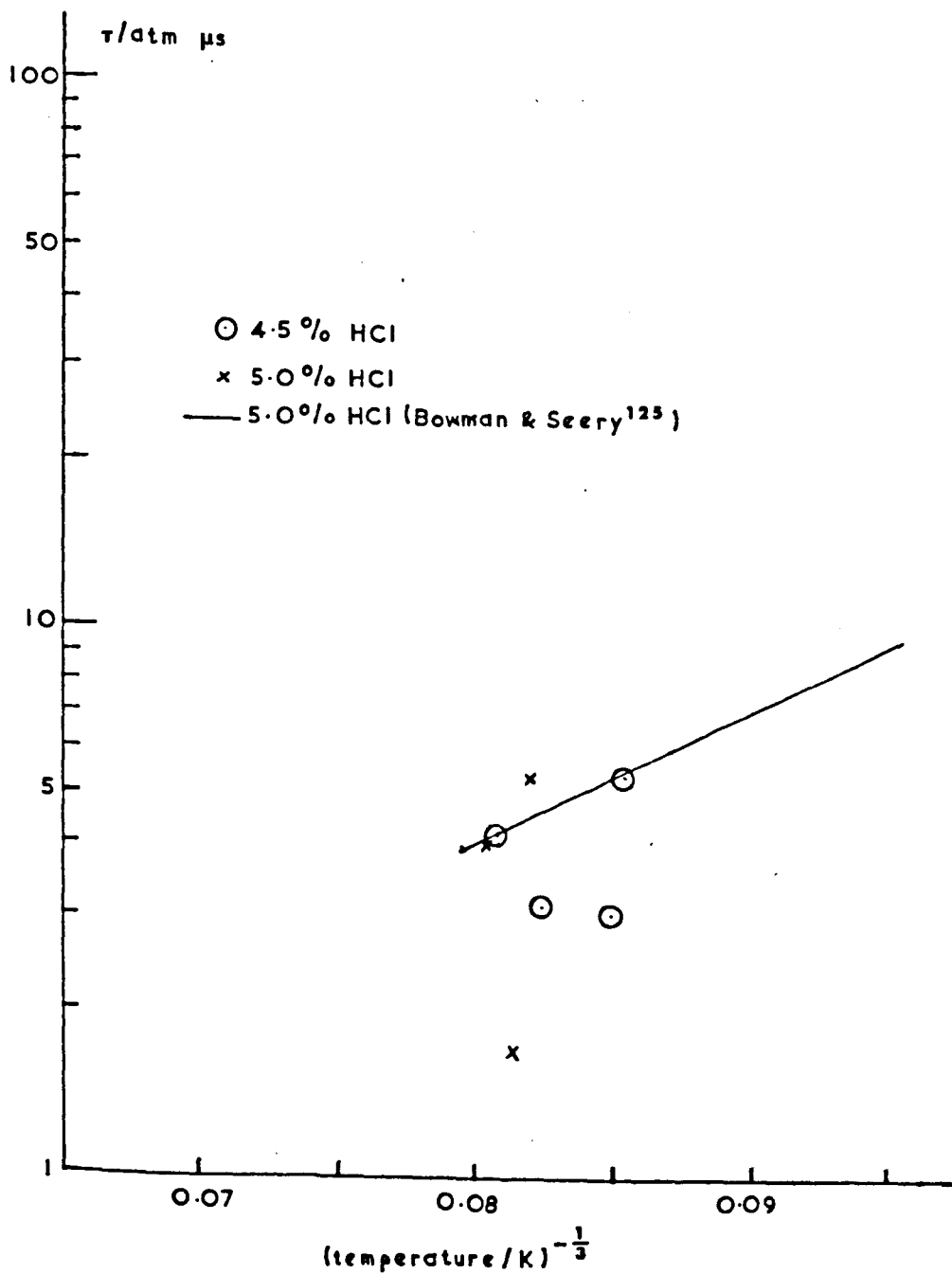
TABLE   3.4

Napier Times for HCl in Ar, $\Delta v = 2$

Run No.	%HCl	Shock Speed /mm μs^{-1}	P_1 /mm Hg	$\dfrac{P_2}{P_1}$	$\dfrac{\rho_2}{\rho_1}$	T_2 /$^\circ$K	T_{exp} /μs	T /atm μs
387	4.54	1.361	13.0	22.10	3.518	1895	3.1	4.2
388	4.54	1.239	14.3	18.28	3.410	1616	4.5	5.3
389	4.54	1.246	6.0	18.48	3.416	1631	6.1	3.0
390	4.54	1.315	5.0	20.63	3.480	1788	6.5	3.1
392	5.00	1.329	5.0	20.93	3.488	1810	11.1	5.3
397	5.00	1.344	5.7	21.57	3.505	1857	3.0	1.7
399	5.00	1.494	4.2	26.72	3.614	1926	7.6	4.0

3.3 Hydrogen Halides with Diatomic Diluents

The above experiments show that both hydrogen chloride
and hydrogen bromide relax quickly when pure which means that
HCl-HCl and HBr-HBr collisions are very efficient for increasing
the vibrational energy of the molecules. Mixed with a slow
relaxing diatomic gas such as CO or N_2, it would be expected that
the HCl would relax more slowly due to there being fewer of the
efficient HCl-HCl or HBr-HBr collisions and more collisions of
the type HCl-CO which are thought to be less efficient. Also the
hydrogen halide could lose vibrational energy in exciting the
diluent by vibration-vibration energy transfer. The converse
should be true for the diatomic diluent which will hence relax
more rapidly.
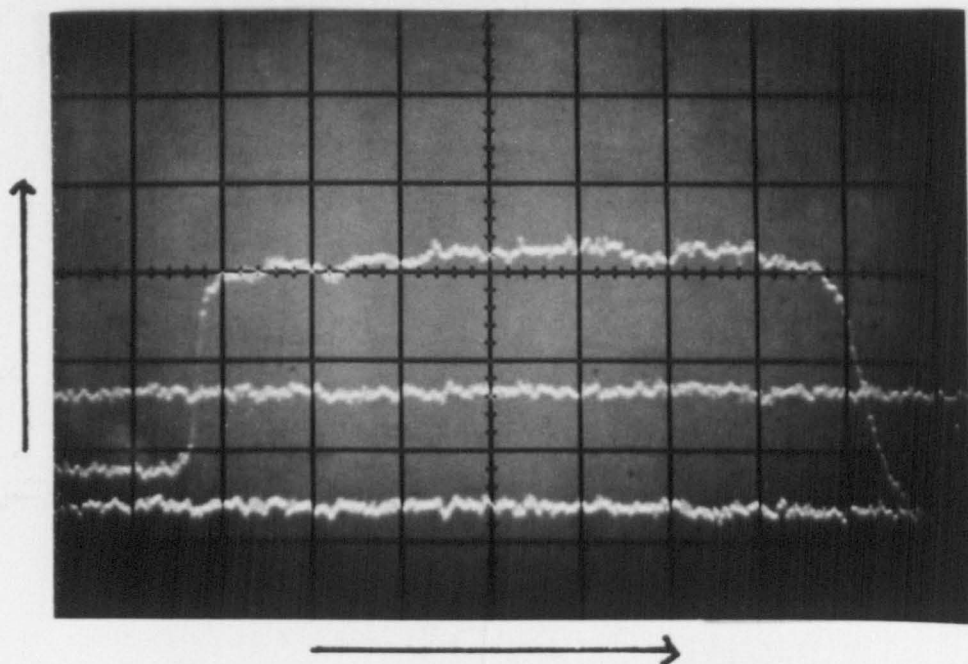
Figure 3·11 Emission from 10% HCl in N₂
Run 433: 20 μs cm⁻¹; 0·2 mv cm⁻¹

3.3.1 HCl in N_2

Mixtures of 10% HCl in N_2 were shock heated. The emission (fig. 3.11) is only from HCl as the N_2 is not infrared active. Over the range in which measurements were made (Table 3.5), the emission attained at least 90% of its equilibrium value within the rise time of the apparatus (2 µs). Attainment of complete equilibrium was a slower process.

TABLE 3.5

Napier Times for 10% HCl in N_2, $v = 2$

Run No.	P_1 /mm Hg	Shock Speed /mm µs^{-1}	$\frac{\rho_2}{\rho_1}$	$\frac{P_2}{P_1}$	τ_{exp} /µs	τ /atm µs	T_2 /^{0}K	I_∞ /µV
429	7.3	1.990	5.90	39.0	<2	<4.4	2088	0.44
432	7.3	2.050	5.98	41.5	<2	<4.6	2195	0.48
433	7.1	2.050	5.98	41.5	<2	<4.6	2195	0.46
437	3.8	2.300	6.28	52.5	<2	<2.9	2670	0.62
438	4.5	2.270	6.25	51.1	<2	<3.8	2610	0.68
440	6.2	2.130	6.09	45.8	<2	<4.4	2342	0.62
449	3.6	2.415	6.40	57.9	<2	<2.4	2906	0.70

Figure 3.12 is a plot to show from which energy level the emission originated. It was 84.4 kJ mole^{-1} which compares favourably with the calculated energy of the second vibrational level of HCl,

Figure 3.12 $\underline{Log(I_\infty/P_1^{\frac{P_2}{P_1}})}$ v. T^{-1} for $\underline{10\% \text{ HCl in } N_2}$

$log(\frac{I_\infty}{P_1P_2/P_1})$

(temperature/K)$^{-1}\times 10^4$
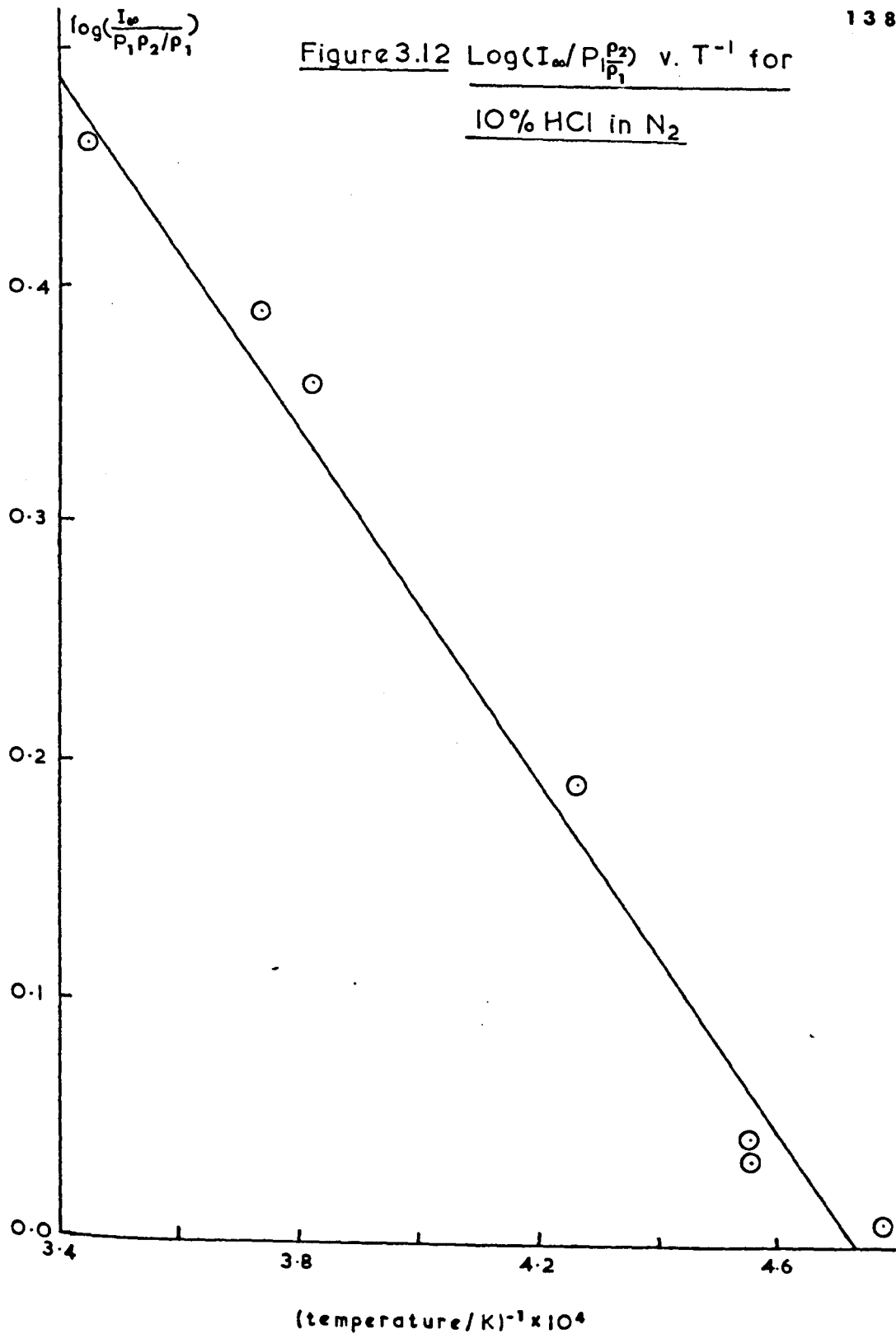
86.5 kJ mole^{-1}.
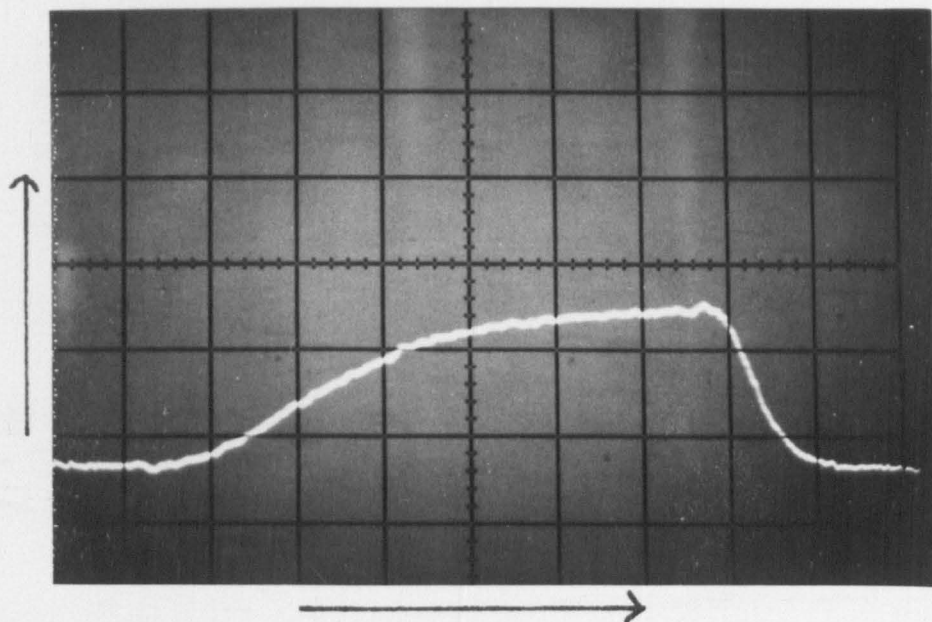
Figure 3·13 Emission from 2% HCl in CO
Run 526: 20 µs cm⁻¹; 0·2 mv cm⁻¹.

3.3.2 Hydrogen Chloride in Carbon Monoxide

Both these molecules are infrared active and the emission observed was from both of them as filters were not used to isolate the individual components. As however the CO is in great excess, the contribution from the HCl was ignored and the intensity of the emission was taken as indicating the population of the second vibrational level of CO.

Figure 3.13 shows a typical trace (2% HCl in CO). It exhibits a shape similar to that of pure CO and was analysed in the same way. (Section 3.1.4). Measurements were made on mixtures containing 2, 5, 7.5, 10 and 12% HCl.

Figure 3.14   2% HCl in CO
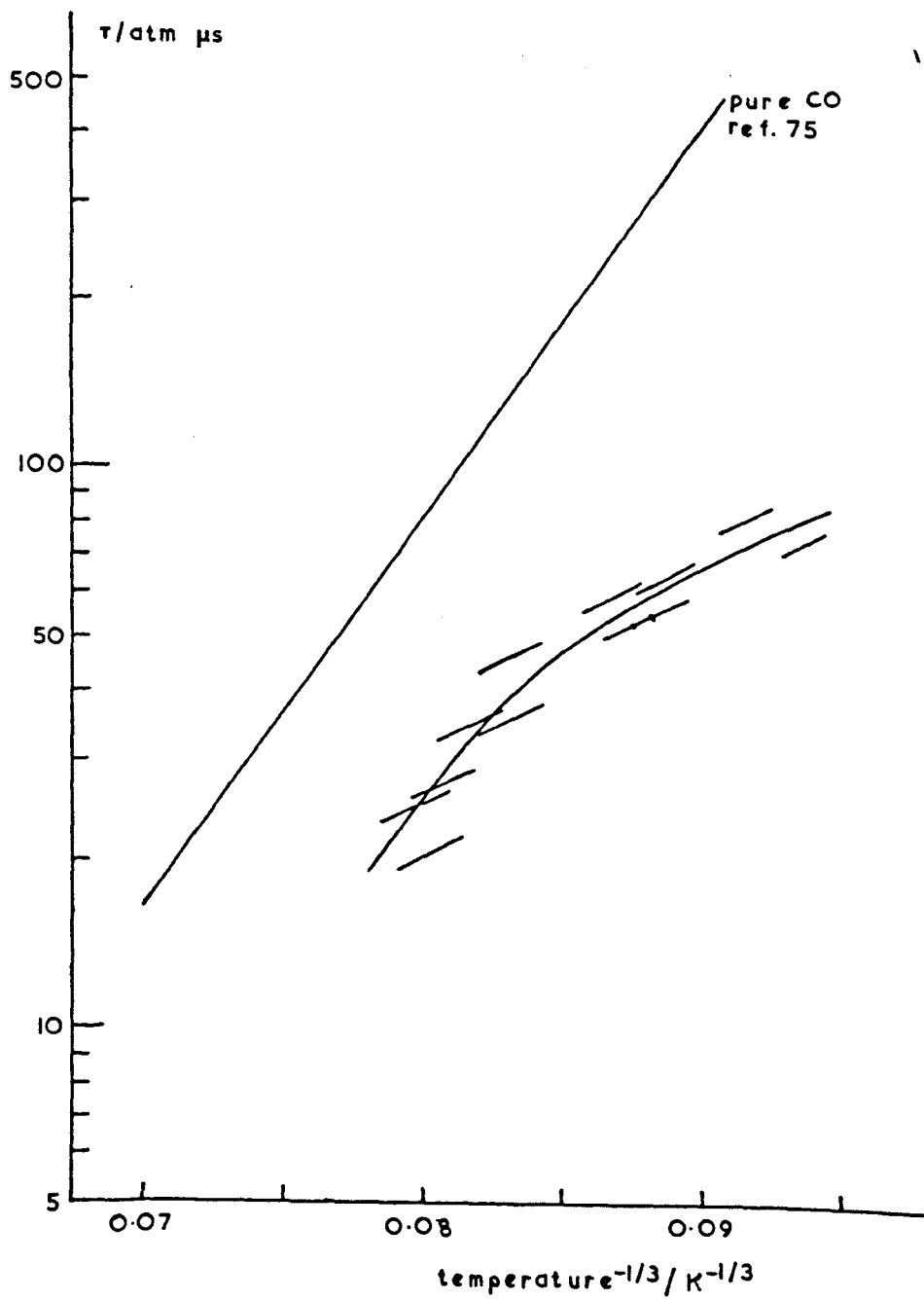
TABLE 3.6

Napier Times for Carbon Monoxide containing
2% HCl, $\Delta v = 2$

Run No.	P_1 /mm Hg	Speed /mm μs^{-1}	τ_{exp} /μs	τ_1 /atm μs	T_1 /$^{\circ}K$	τ_2 /atm μs	T_2 /$^{\circ}K$
517	13.38	1.435	45.0	70.2	1249	76.8	1181
518	9.64	1.659	35.9	57.4	1578	62.5	1462
519	8.05	1.637	37.7	49.1	1548	55.1	1436
521	5.52	1.861	27.1	32.5	1920	37.8	1748
523	6.55	1.795	25.4	33.8	1804	38.6	1652
522	4.59	1.944	21.0	23.2	2065	27.1	1868
524	8.89	1.493	67.4	77.4	1334	85.3	1255
525	8.33	1.599	41.3	52.5	1488	58.8	1386
526	3.56	1.908	23.5	19.4	2001	22.5	1815
528	9.55	1.673	35.2	57.2	1603	63.2	1483
530	5.47	1.805	38.8	43.2	1822	49.6	1667
531	7.39	1.596	54.0	60.5	1483	67.8	1382
532	3.84	1.906	28.4	26.0	1998	29.2	1812

144

Figure 3.15   5% HCl in CO
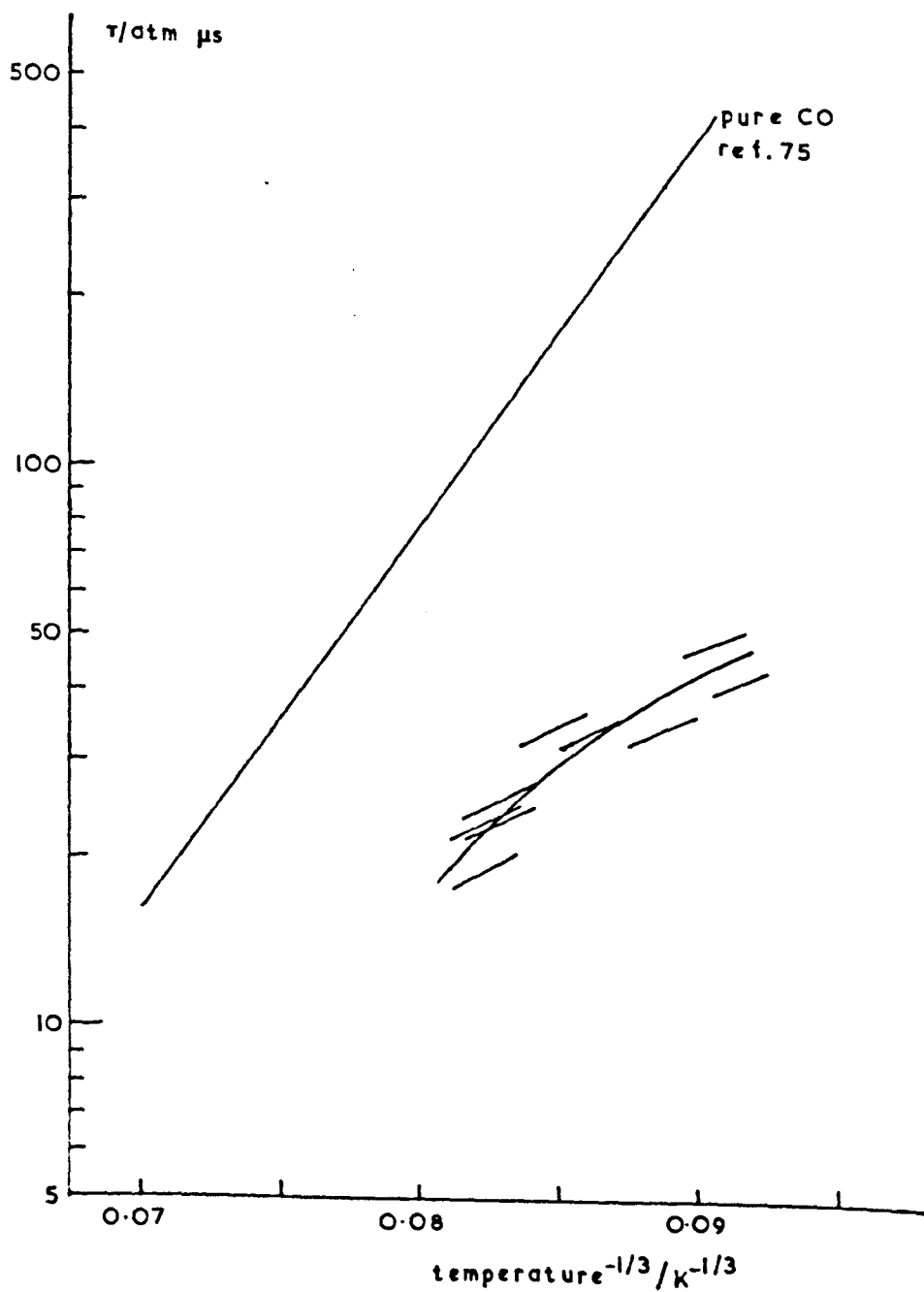
TABLE 3.7

Napier Times for Carbon Monoxide containing
5% HCl, $\Delta v = 2$

Run No.	P_1 /mm Hg	Speed /mm μs^{-1}	τ_{exp} /μs	τ_1 /atm μs	T_1 /^{o}K	τ_2 /atm μs	T_2 /^{o}K
541	14.13	1.530	23.7	46.5	1398	51.5	1310
542	5.80	1.827	17.6	21.6	1871	24.9	1708
543	7.77	1.727	22.1	31.9	1705	36.3	1570
545	9.55	1.681	19.0	31.6	1628	35.8	1505
546	11.23	1.493	27.0	39.7	1344	43.7	1264
547	4.40	1.833	19.0	17.8	1883	20.5	1718
548	6.55	1.801	16.2	21.7	1828	24.9	1673
549	8.24	1.597	26.0	32.6	1486	36.6	1384
550	5.5	1.810	20.9	23.7	1850	27.3	1690

Figure 3.16   7.5% HCl in CO
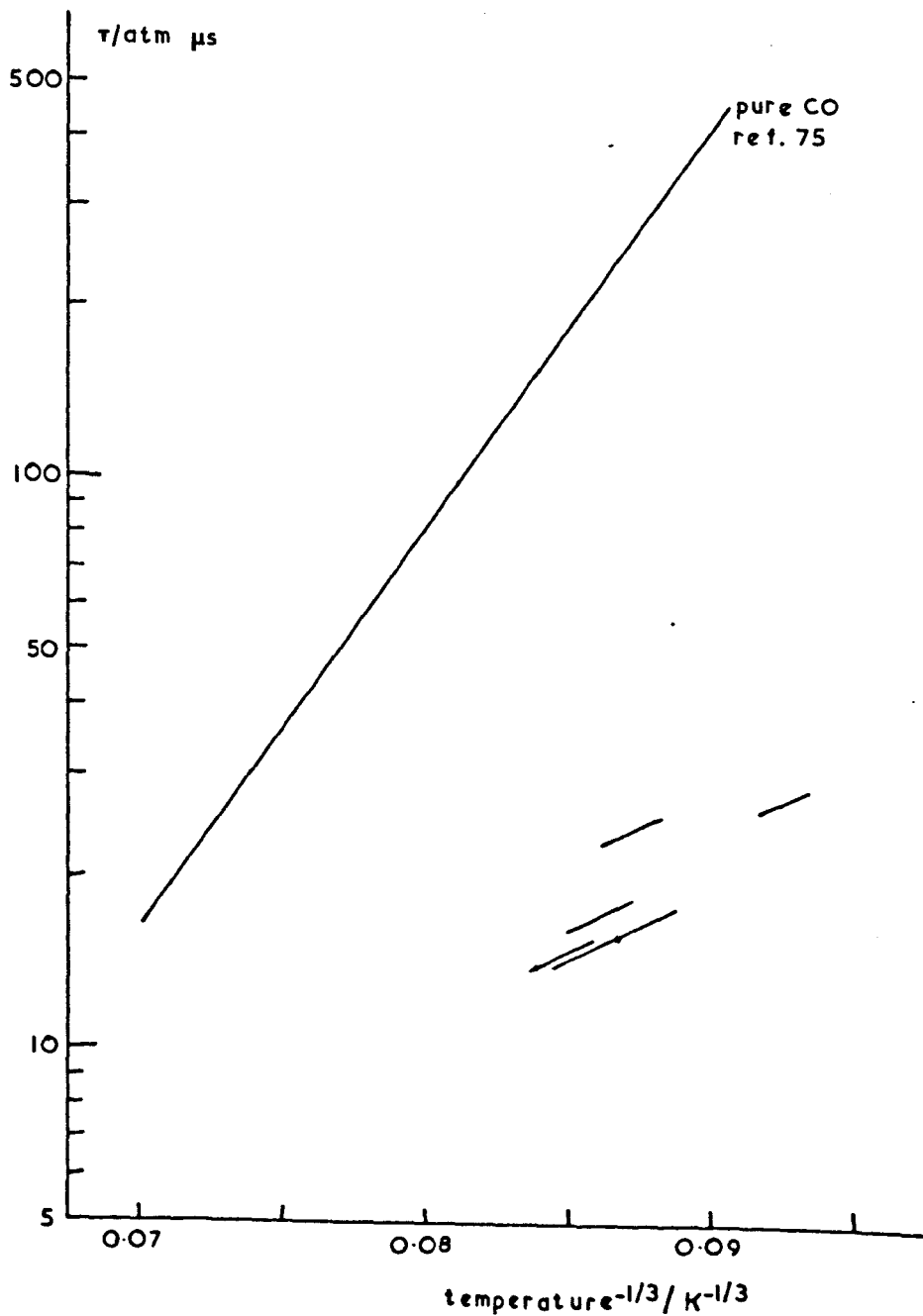
TABLE 3.8

Napier Times for Carbon Monoxide containing
7.5% HCl, $\Delta v = 2$.

Run No.	P_1 /mm Hg	Speed /mm μs^{-1}	τ_{exp} /μs	τ_1 /atm μs	T_1 /$^{\circ}K$	τ_2 /atm μs	T_2 /$^{\circ}K$
567	11.79	1.634	11.9	22.9	1559	25.7	1447
569	7.30	1.674	11.8	16.1	1622	18.3	1501
570	5.99	1.720	12.6	13.9	1699	15.8	1566
571	9.36	1.617	10.5	15.7	1531	17.6	1424
572	12.26	1.459	17.2	26.1	1300	28.6	1226
573	8.0	1.696	9.80	14.0	1659	15.9	1532

Figure 3.17   10% HCl in CO
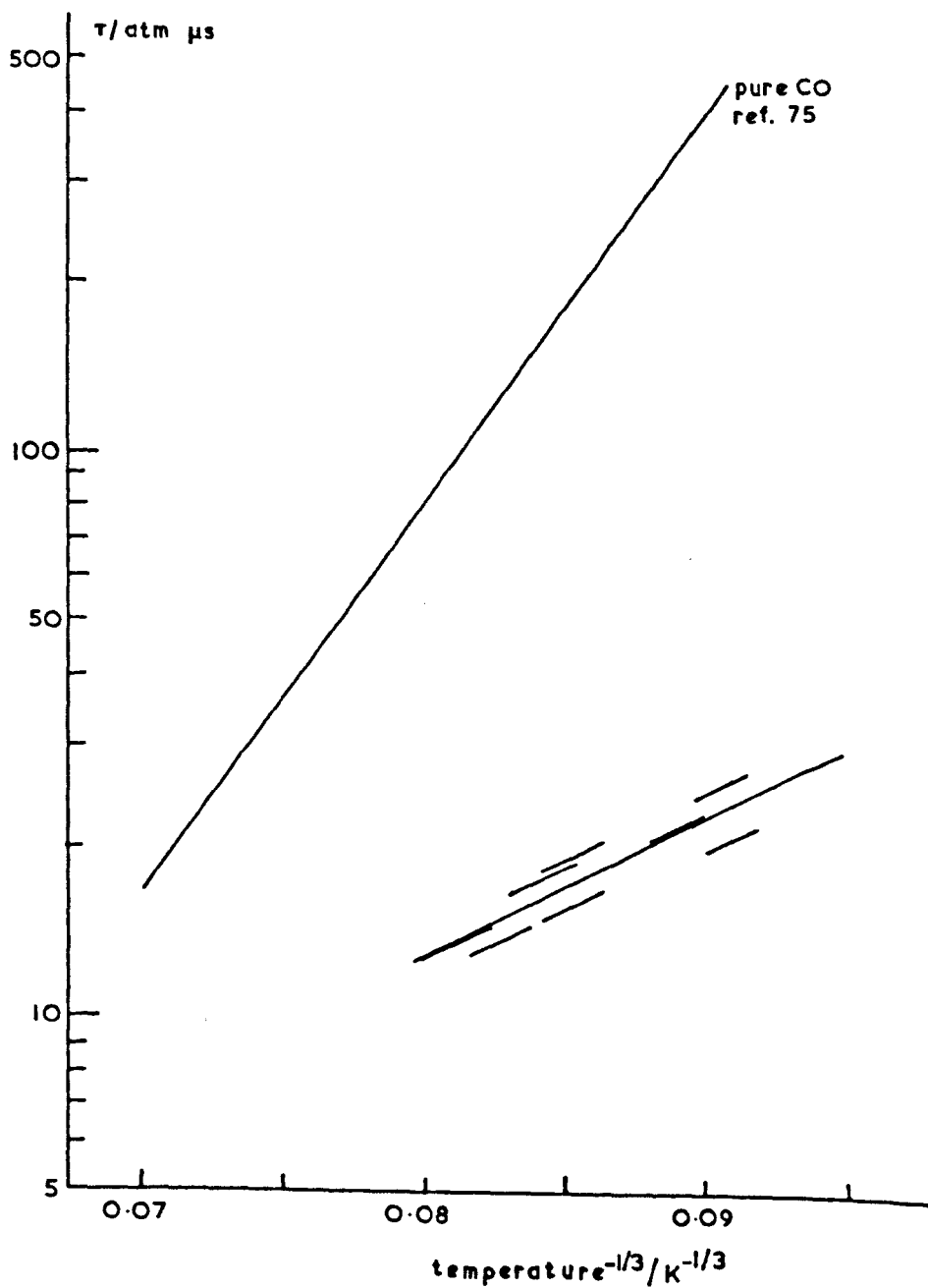
TABLE   3.9

Napier Times for Carbon Monoxide containing
10% HCl, $\Delta v = 2$

Run No.	P_1 /mm Hg	Speed /mm μs^{-1}	τ_{exp} /μs	τ_1 /atm μs	T_1 /$^\circ K$	τ_2 /atm μs	T_2 /$^\circ K$
551	11.89	1.511	15.0	24.4	1384	27.0	1300
552	7.86	1.696	10.6	15.1	1673	17.1	1545
553	5.52	1.571	25.0	20.7	1467	23.0	1370
554	5.80	1.783	10.8	12.9	1834	14.8	1680
555	4.87	1.739	18.0	16.8	1745	19.1	1605
556	9.36	1.496	15.9	19.9	1364	21.9	1283
557	7.68	1.693	13.4	18.5	1667	20.9	1540
558	5.5	1.858	10.4	12.8	1951	14.8	1777

Figure 3.18   12% HCl in CO
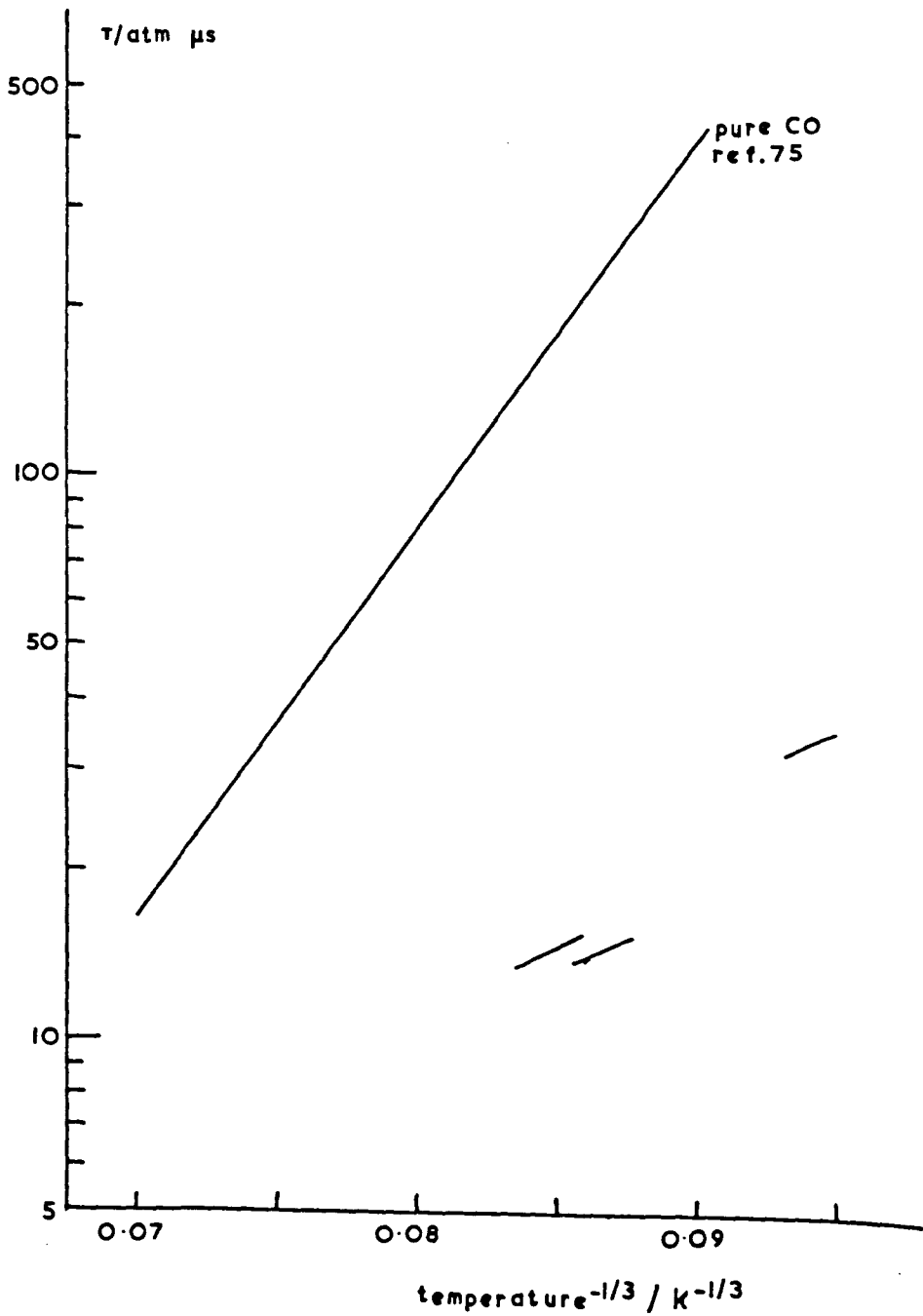
TABLE   3.10

Napier Times for Carbon Monoxide containing
12% HCl,   v = 2

Run No.	P_1 /mm Hg	Speed /mm μs^{-1}	τ_{exp} /μs	τ_1 /atm μs	T_1 /$^\circ$K	τ_2 /atm μs	T_2 /$^\circ$K
575	9.36	1.645	8.75	13.8	1592	15.5	1477
576	11.76	1.401	24.9	33.4	1232	36.4	1168
577	5.07	1.716	14.5	13.7	1710	15.6	1577
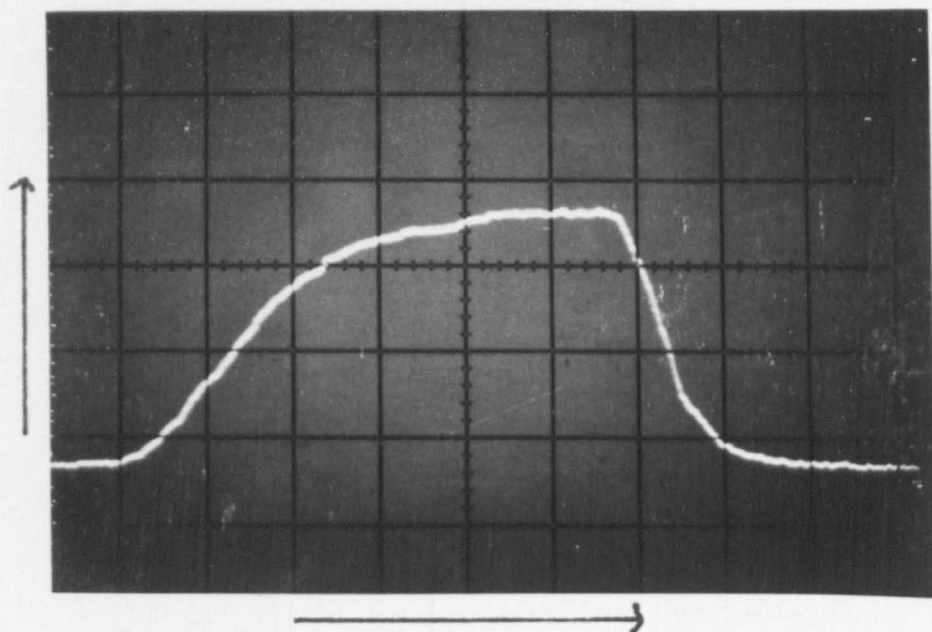
Figure 3·19 Emission from 2% HBr in CO
Run 513: 20 μs cm⁻¹; 0·2 mv cm⁻¹.

3.3.3 Hydrogen Bromide in Carbon Monoxide

Emission from this mixture was treated in the same way as HCl in CO (Section 3.3.2). Figure 3.19 shows a trace typical for mixtures containing 2, 5 and 10% HBr in CO.

Figure 3·20   2% HBr in CO
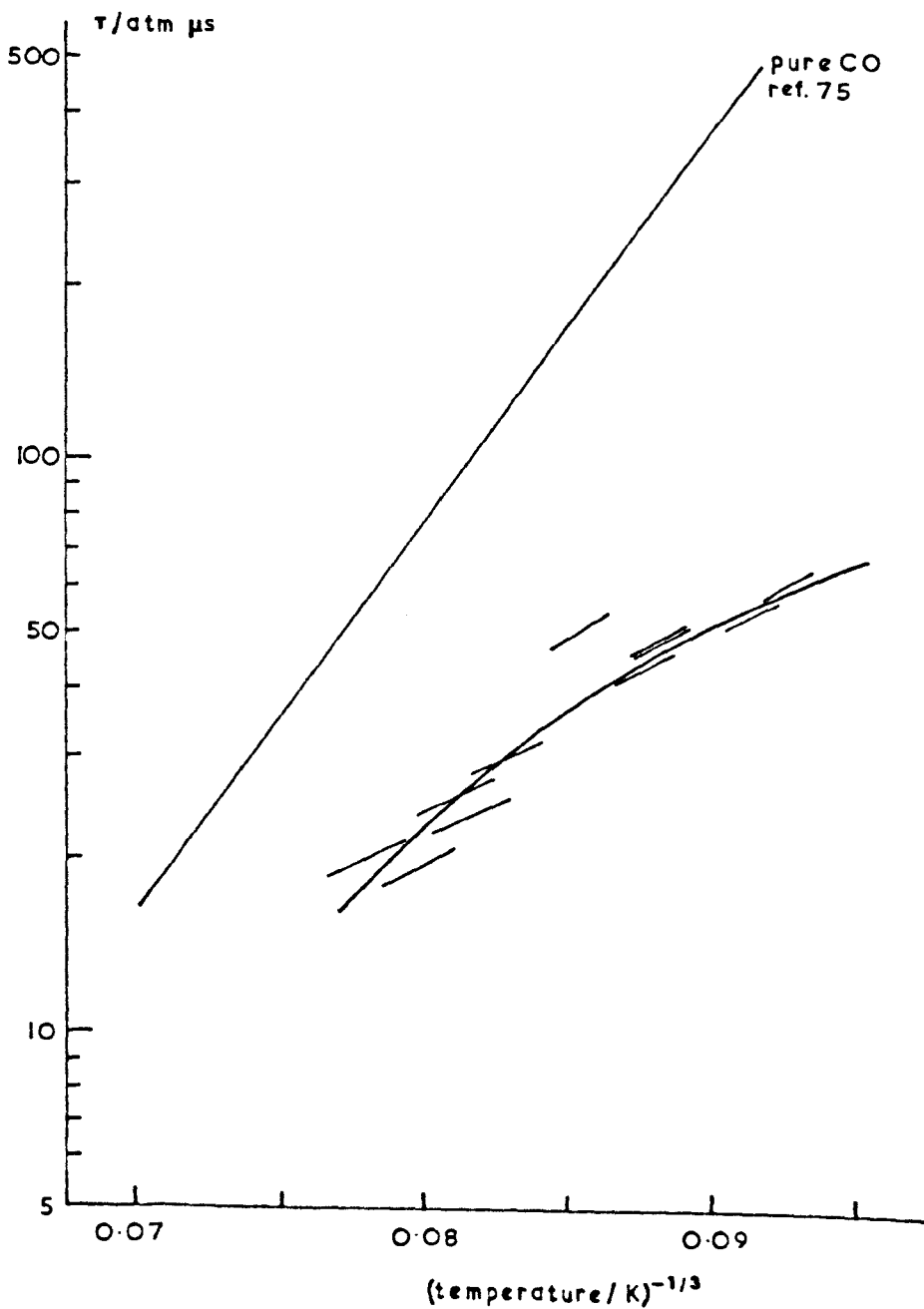
TABLE   3.11

Napier Times for CO containing 2% HBr, $\Delta v = 2$

Run No.	P_1 /mm Hg	Speed /mm μs^{-1}	τ_{exp} /μs	τ_1 /atm μs	T_1 /°K	τ_2 /atm μs	T_2 /°K
506	13.8	1.436	35.3	59.1	1285	65.1	1212
507	9.64	1.610	27.3	41.8	1542	46.2	1432
508	7.77	1.701	33.3	47.3	1690	54.0	1556
509	6.55	1.587	44.6	45.5	1510	51.0	1404
510	5.67	1.832	18.4	22.7	1917	26.3	1745
511	4.68	1.865	23.0	24.4	1976	28.4	1794
512	3.74	1.916	20.4	18.4	2072	21.5	1873
513	3.09	2.000	22.9	18.9	2230	22.2	2002
514	6.55	1.786	20.9	28.5	1834	32.8	1677
515	8.57	1.580	35.0	46.0	1497	51.6	1393
516	10.5	1.484	37.2	51.5	1354	57.5	1272

Figure 3.21   5% HBr in CO

τ/atm μs

pure CO
ref.75

temperature$^{-1/3}$ / K$^{-1/3}$
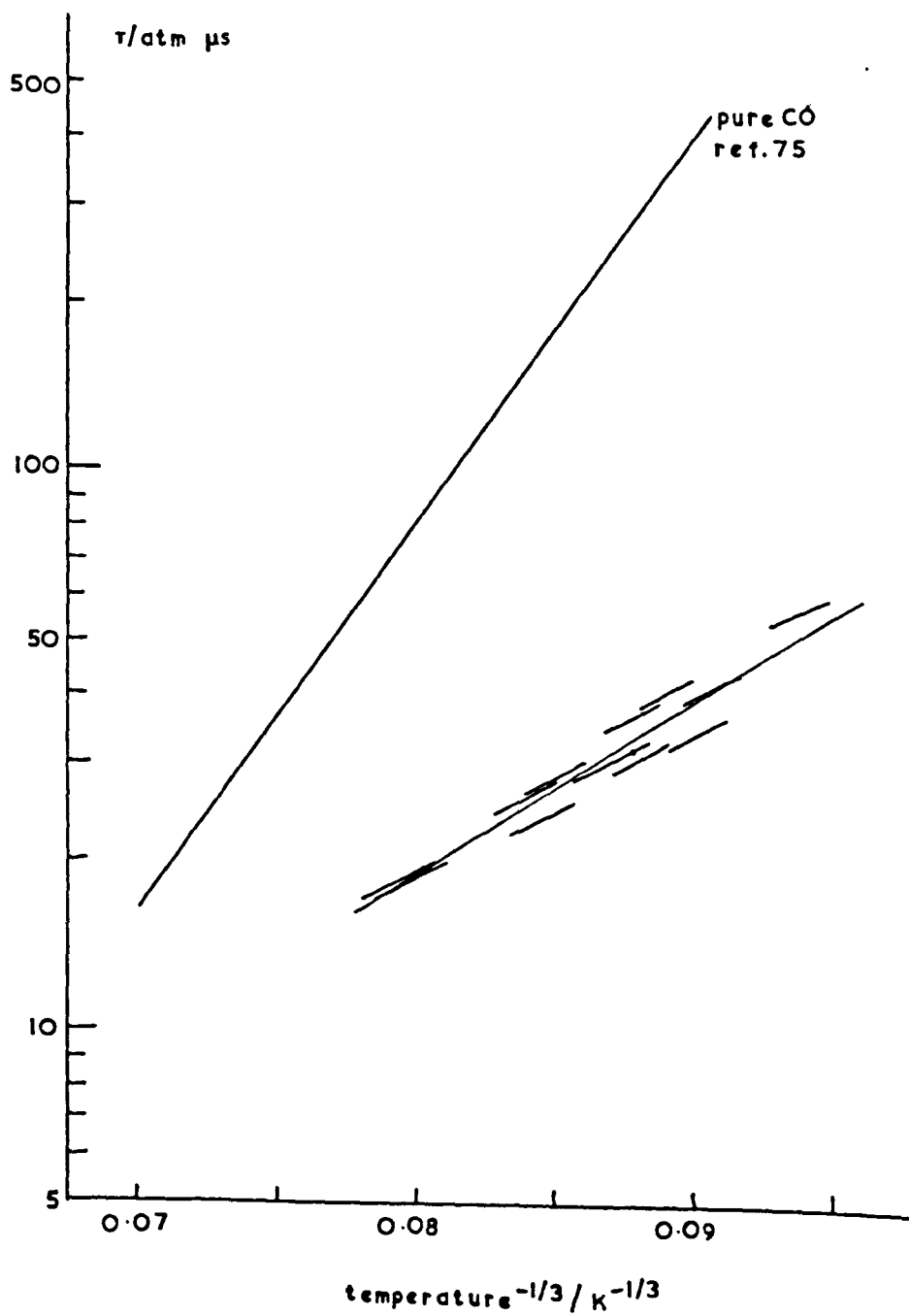
TABLE 3.12

Napier Times for CO containing 5.0% HBr, $\Delta v = 2$

Run No.	P_1 /mm Hg	Speed /mm μs^{-1}	τ_{exp} /μs	τ_1 /atm μs	T_1 /$^\circ K$	τ_2 /atm μs	T_2 /$^\circ K$
499	8.4	1.675	14.3	22.7	1722	25.8	1584
500	11.7	1.551	16.05	29.4	1515	33.0	1409
501	14.8	1.376	31.4	54.5	1254	59.8	1185
502	10.5	1.599	16.0	28.3	1597	32.0	1479
503	12.65	1.490	18.1	32.6	1420	36.0	1329
504	13.95	1.473	20.3	39.2	1395	43.4	1302
579	8.59	1.658	16.9	26.7	1693	30.4	1560
580	5.39	1.862	13.4	17.3	2062	20.2	1866
581	10.94	1.575	16.6	29.6	1556	33.3	1444
582	7.33	1.702	17.2	24.6	1769	28.2	1623
583	4.52	1.882	15.6	17.4	2101	20.3	1898
584	12.63	1.562	17.2	34.7	1534	39.0	1426
585	14.42	1.521	18.0	38.7	1467	43.2	1369
586	6.30	1.702	19.8	24.3	1789	27.9	1623

Figure 3.22   10 % HBr in CO
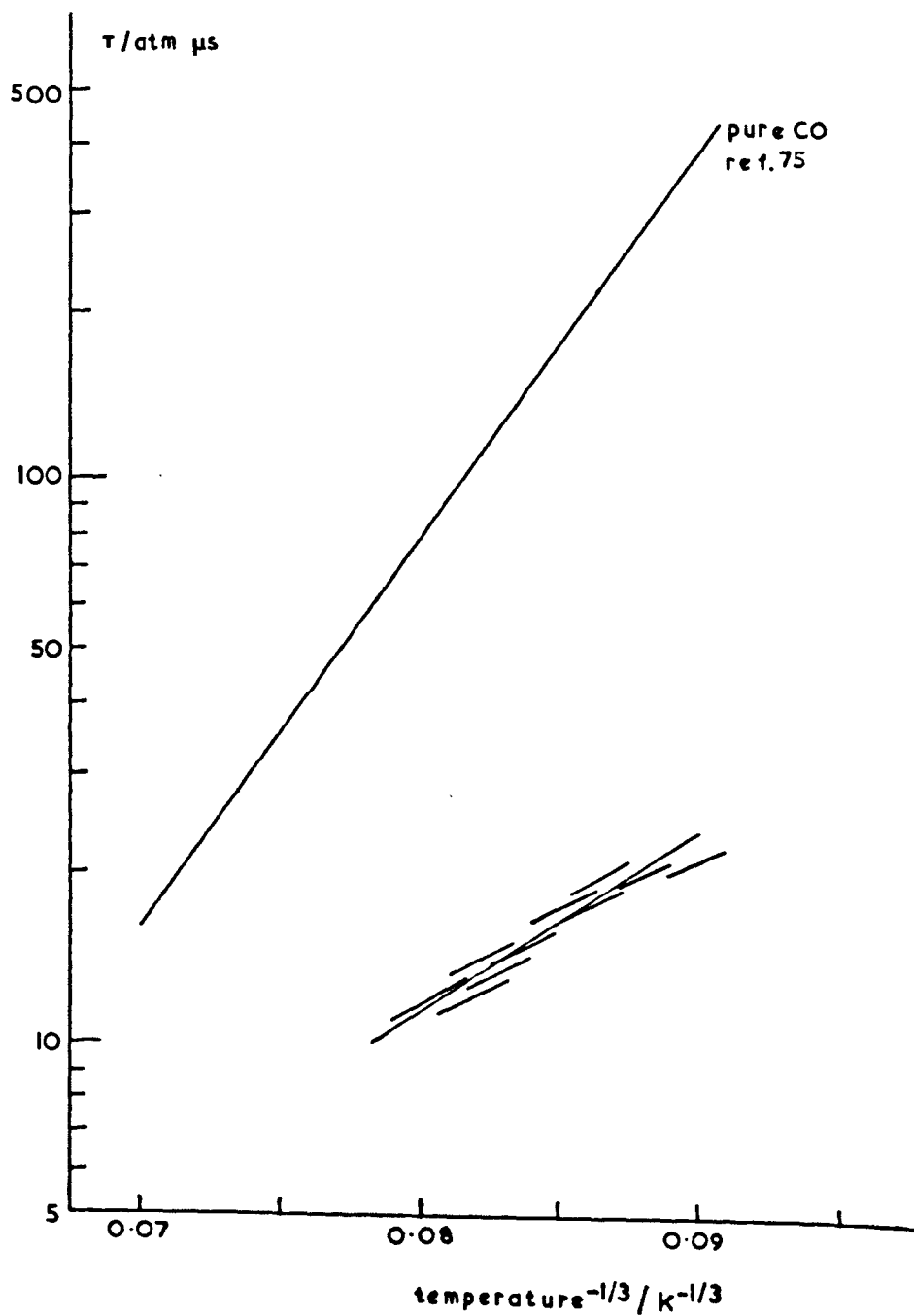
TABLE 3.13

Napier Times for CO containing 10% HBr, $\Delta v = 2$

Run No.	P_1 /mm Hg	Speed /mm μs^{-1}	τ_{exp} /μs	τ_1 /atm μs	T_1 /^{o}K	τ_2 /atm μs	T_2 /^{o}K
591	9.12	1.636	7.98	14.1	1735	16.1	1629
592	10.68	1.588	8.66	16.9	1687	19.2	1556
593	7.05	1.688	9.0	13.4	1871	15.4	1709
594	8.32	1.669	7.42	12.7	1834	14.6	1679
595	6.87	1.703	7.71	11.4	1901	13.2	1734
596	11.83	1.410	10.3	19.2	1523	21.6	1417
597	5.60	1.772	8.4	11.1	2033	13.3	1843
598	11.30	1.543	9.75	18.8	1608	21.2	1489
599	13.01	1.432	10.9	20.4	1425	22.6	1335
600	10.03	1.549	9.76	16.8	1619	19.1	1499

4. GENERAL COMMENTS ON THE EXPERIMENTS

Certain assumptions were made in measuring the Napier times and some of those are discussed in this part of the thesis. Sections 4.1 to 4.4 are concerned with ways in which the recorded emission may not accurately reflect the population of the vibrational level being monitored. Four sections (4.5 to 4.8) are devoted to the ways in which the traces were analysed, and two sections (4.9 and 4.10) to the conversion of experimental relaxation times to Napier times. The remaining sections assess the errors arising from non-ideal flow in the shock tube and from alternative methods by which theoretical collision numbers are compared with experimental Napier times.

161
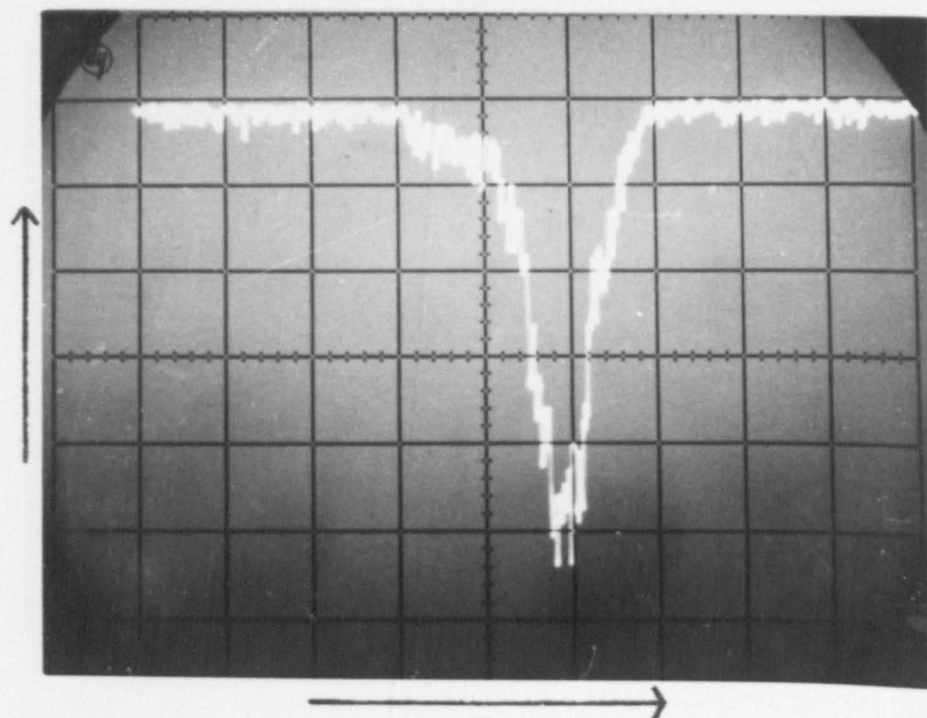
Figure 4·1 Spurious Emission
Run 126: 100 μs cm⁻¹; 0·1v cm⁻¹

4.1 Spurious Emission

Considerable difficulty was experienced in the initial stages with spurious emission. It was observed even when a non-radiative gas, such as nitrogen or argon, was shock heated the intensity appeared to be independent of both wavelength (over the region 0.8 nm and 1.8 nm) and temperature (as indicated by shock speed) but increased with consecutive shocks. Passing a damp cloth through the shock tube drastically reduced the level of emission thus indicating a wall effect. The shape of the photographic record (Fig. 4.1) seems to corroborate this; it shows a delay between passage of the shock front and the emission's reaching its most intense value.

The origin of the deposit on the wall could not be unambiguously elucidated. It seemed to be of an oily nature entering with the driver gas, so it may have been due to the hydrogen itself or impurities in the connecting tubes picked up by the passing hydrogen. Use of high purity (medical) hydrogen did not seem to help.

The difficulty was overcome by passing through the shock tube a cloth, moistened with ether dried over sodium, three times between each shock. If the tube was carefully flamed when pumping, the residual spurious emission was negligible (<10 μV).

4.2   Gas Adsorption by Walls

It would be expected that polar molecules, such as H_2O and HCl, would be particularly attracted to the shock tube wall. If this occurred to a serious extent, deduced Napier times would be too long, as the pressure in the tube would be lower than calculated, and if one of the gases were preferentially adsorbed, the composition of a gas mixture would not be as stated.

An estimate of the magnitude of the error due to this phenomenon was made by expanding small amounts of nitrogen and hydrogen chloride into the shock tube and measuring the final pressure with a McCleod gauge. Nitrogen, which is only adsorbed to a limited extent, at a pressure of 15 mmHg (measured by a mercury manometer) was expanded from a small glass section into the shock tube. The measured final pressure was 427 μmHg. Under the same conditions, expansion of 15 mmHg of HCl gave a final pressure of 327 μmHg. If however the previous gas in the tube was HCl and it was not flamed during pumping, the final pressure was 422 μmHg. It seems therefore that hydrogen chloride is adsorbed onto the shock tube walls but the phenomenon can be nullified by conditioning the tube with the gas beforehand. For this reason, a little test gas (1 mmHg) was allowed into the shock tube for a short period (1 minute was sufficient) before introducing the measured quantity of test gas.

Glass bulbs in which mixtures were made up were also conditioned by the hydrogen halide component in a similar way.

4.3 Dissociation

At high temperatures, all gases dissociate to some extent. If the amount is appreciable, the temperature will decrease and the decomposition products could affect the relaxation process.

The extent to which nitrogen is dissociated can be calculated from the equilibrium constant K_p given in JANAF tables[12] (Table 4.1).

Table 4.1   Dissociation Constant for Nitrogen

Temp.	$\log K_p$
500	-46.3
1000	-21.5
1500	-13.2
2000	- 9.0
2500	- 6.5
3000	- 4.9

It can be shown that even at $3000°K$ considerably less than 1% of nitrogen is in the form of atoms at one atmosphere pressure.

Measurements of dissociation show that for CO it is negligible below 3000 K.[107]

Hydrogen halides are less stable: values for HCl and HBr are given below (Table 4.2).

Table 4.2 Experimental Dissociation Measurements

Molecule	Temperature/$°K$	% Dissociation
HCl	500	1.92×10^{-8}
HCl	1000	1.34×10^{-3}
HCl	2000	4.1×10^{-1}
HCl	3000	1.30
HBr	1297	0.50
HBr	1381	0.73
HBr	1495	1.08

Reference Sidgwick[108]

The extent to which HCl dissociates would appear to give no cause for concern but indications are that the converse may be true for HBr at higher temperatures.
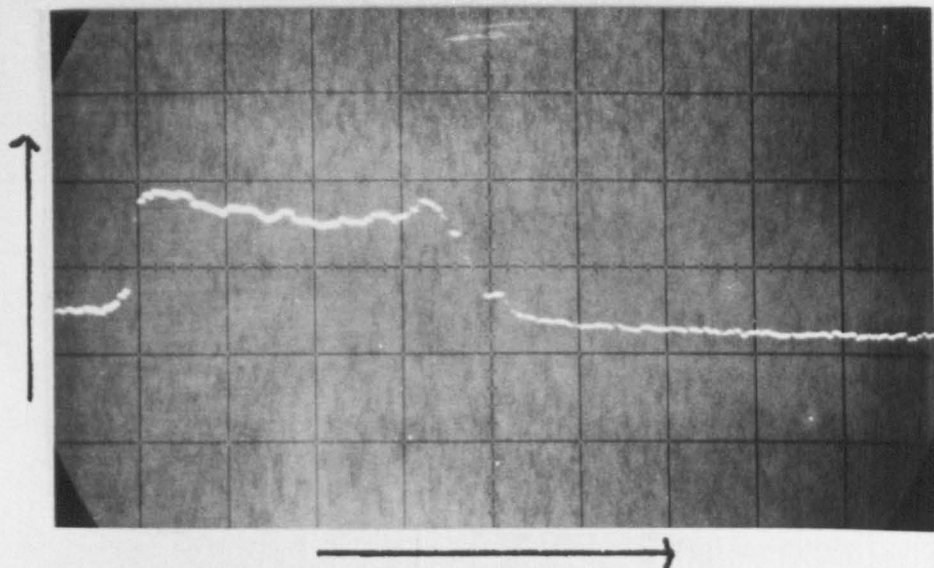
Figure 4·2 Dissociation of HBr
Run 587: 50 μs cm⁻¹; 0·5 mv cm⁻¹.
T_2, the temperature when the
gas is vibrationally relaxed
but not dissociated is 2448° K.

Confirmation that the above deductions for the infrared active molecules were correct was sought from the shock tube emission. For a non-attenuating shock where dissociation occurs, there is a reduction in the emission intensity behind the shock front for two reasons. Firstly, the quantity of emitting gas decreases and secondly, there is a fall in temperature in that region. When all the gas was vibrationally relaxed, constant emission was observed for CO and HCl over the whole range of temperature studied but this was not the case for HBr above 2300°K (Fig. 4.2). Hence to avoid complications, temperatures were kept below 2000°K when HBr was being shock heated.

4.4   Radiative Lifetimes

The emission monitored by the infrared detectors originated from vibrationally excited molecules with dipole moments which spontaneously emit radiation.   This process must be slow compared with the rate of excitation if it is not to affect the calculation of Napier times.

The chance of spontaneous emission occurring is given by a constant A_{nm} which is the probability that an atom in state n will emit a quantum of energy and pass to state m.   In a radiationless field, the mean life or radiative lifetime, τ_{rad}, is defined as the reciprocal of the transition probabilities from the state n to all states m (reference 109, page 94).   For state n,

$$\tau_{rad} \quad = \quad \frac{1}{\sum\limits_{m} A_{nm}} \qquad\qquad 4.1$$

Penner (reference 110, page 21) shows that if $h\nu_{nm} > kT$, A_{nm} is related to the line strength S_{nm} by

$$S_{nm} \ (cm^{-2} \ atm^{-1}) \quad = \quad 3.210 \times 10^{28} \ \frac{A_{nm}(s^{-1})}{\nu^{2} \ (s^{-2})} \qquad 4.2$$

For the first vibrational level $\sum\limits_{m} A_{nm} = A_{10}$, so

$$\tau_{rad} \quad = \quad \frac{3.210 \times 10^{28}}{S_{10} \ \nu^{2}_{10}} \qquad\qquad 4.3$$

Values of τ_{rad} (v=1) have been calculated using equation 4.3.

Table 4.3   Radiative Lifetimes (v=1)

Molecule	wavelength/cm^{-1}	S_{10}/cm^{-1} atom^{-1}	Reference	τ_{rad}/s
HCl	2886	130.0	111	0.033
HBr	2558	36.0	112	0.15
CO	2143	260	114	0.30

To obtain values for τ_{rad} (v=2) it is necessary to consider both the 2→0 and 2→1 transitions as $\sum_m A_{nm} = A_{20} + A_{21}$. The transition 2→0 is forbidden and so is very weak; most radiating molecules will emit a single quantum. If the Landau-Teller model is correct, $k_{21} = 2k_{10}$ and so τ_{rad} (v=2) will be half that of τ_{rad} (v=1). Windsor, Davidson and Taylor[72] arrived at this result for CO using measured line strengths.

Experimental confirmation of the calculated value of τ_{rad} for CO has been given by Millikan[78] and Doyennette, Margottin- -Maclon and Henry[113] who measured it to be 0.33 s.

The value for HCl however is less certain. Findlay and Polanyi[99] and Cabré and Henry[114] observed HCl produced in a vibrationally excited state but with a rotational temperature of only 600°K by reacting atomic and molecular hydrogen with molecular

chlorine at a pressure of 1 mm Hg. The former authors concluded that collisional deactivation was unimportant but the latter thought that vibrational energy was lost by both radiative and collisional processes. Findlay and Polanyi[99] believe that radiative transfer occurs within the time taken for 10^5 collisions which, at the pressure of the 1 mm Hg, places an upper limit to the radiative lifetime of 10^{-2} s. But even the shortest value for the radiative lifetime of HCl (that of Lukasik)[123] is more than an order of magnitude longer than the experimental relaxation time.

Although there is a lack of results for HBr, there is no reason to suppose that its radiative lifetime will be much shorter than that of HCl so a similar relationship between τ_{rad} and τ_{exp} would be expected.

Hence, since the experimental relaxation times are considerably less than the radiative lifetime of all three molecules, it was considered that the emission from upper vibrational levels can be used to monitor their population without its having a net effect on the population itself.

4.5 Analysis of Traces: Two Level System

When the rate of approach to a state is proportional to the deviation from that state, the relaxation can be characterised by a relaxation time, τ, defined by the equation

$$\frac{dx(t)}{dt} = \frac{x(\infty) - x(t)}{\tau} \qquad 4.4$$

where $x(t)$ is the value of x at time t and $x(\infty)$ is the value of x at $t = \infty$.

It is found that many systems, such as the population of the upper level of a relaxing two level oscillator, can be approximately represented by equation 4.4. That this should be so for the example quoted can be seen by a consideration of the mechanism by which the reaction can occur. The upper level of CO can be populated by

$$CO_{v=0} + CO \underset{k_{10}}{\overset{k_{01}}{\rightleftarrows}} CO_{v=1} + CO \qquad 4.5$$
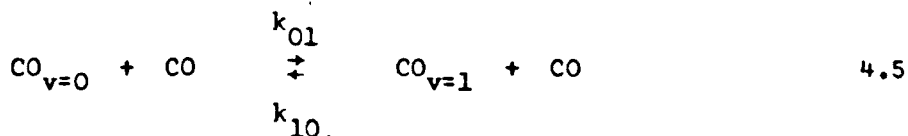
(CO represents a molecule in any unspecified vibrational energy state).

Then $$\frac{d[CO_{v=1}]}{dt} = k_{01}[CO_{v=0}][CO] - k_{10}[CO_{v=1}][CO] \qquad 4.6$$

$$= k_{10}[CO](\frac{k_{01}}{k_{10}}[CO_{v=0}] - [CO_{v=1}]) \qquad 4.7$$

But the equilibrium constant $K = \frac{k_{01}}{k_{10}}$ and is given by

$$K = \frac{[CO_{v=1}]_\infty [CO]_\infty}{[CO_{v=0}]_\infty [CO]_\infty} \qquad 4.8$$

Therefore equation 4.7 can be rewritten (as $[CO_{v=0}]$ constant)

$$\frac{d[CO_{v=1}]}{dt} = k_{10}[CO]([CO_{v=1}]_\infty - [CO_{v=1}]) \qquad 4.9$$

This is the same form as equation 4.4 where $k_{10}[CO]$ is equivalent to $1/\tau$. If the observed emission is proportional to $[CO_{v=1}]$, equation 4.9 can be written as

$$\frac{dI}{dt} = \frac{I_\infty - I}{\tau} \qquad 4.10$$

Integration, with the condition that $I = 0$ when $t = 0$, gives

$$I = I_\infty(1-\exp(-t/\tau)) \qquad 4.11$$

$$\text{or} \quad -\ln(1 - \frac{I}{I_\infty}) = t/\tau \qquad 4.12$$

Equation 4.11 is an exponential function whose shape seemed similar to that exhibited by the emission from the third vibrational level of pure HCl and the second vibrational level of HCl in argon. The traces were analysed by using the derived equation 4.12, plots of $-\ln(1-I/I_\infty)$ against t giving straight lines (fig. 3.2). Their gradients were taken to be $1/\tau exp$.

4.6 Analysis of Traces: Multi-level System

The analysis of a multi-level system is a little more complex than for a two level system. Consider CO having only three vibrational levels, the zeroth, first and second. For the population of the second vibrational level, three reaction schemes can be postulated.

$$
A \qquad CO_{v=0} + CO \; \underset{k_{20}}{\overset{k_{02}}{\rightleftarrows}} \; CO_{v=2} + CO \qquad\qquad 4.13
$$

$$
B \qquad CO_{v=0} + CO \; \underset{k_{10}}{\overset{k_{01}}{\rightleftarrows}} \; CO_{v=1} + CO \qquad\qquad 4.14
$$

$$
\text{and} \quad CO_{v=1} + CO \; \underset{k_{21}}{\overset{k_{12}}{\rightleftarrows}} \; CO_{v=2} + CO \qquad\qquad 4.15
$$

$$
C \qquad CO_{v=0} + CO \; \underset{k_{10}}{\overset{k_{01}}{\rightleftarrows}} \; CO_{v=1} + CO \qquad\qquad 4.14
$$

$$
\text{and} \quad CO_{v=1} + CO_{v=1} \; \underset{e}{\overset{e}{\rightleftarrows}} \; CO_{v=2} + CO_{v=0} \qquad\qquad 4.16
$$
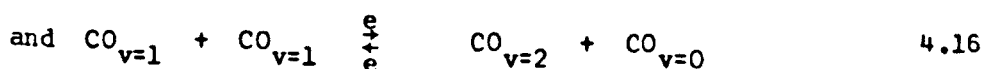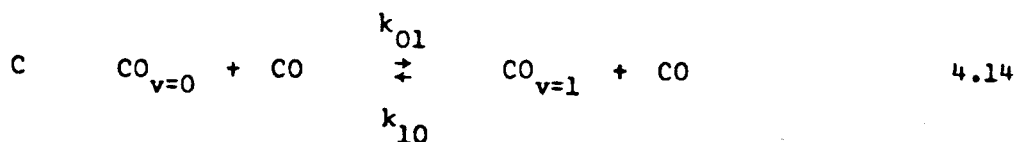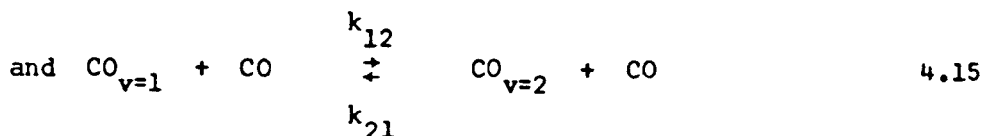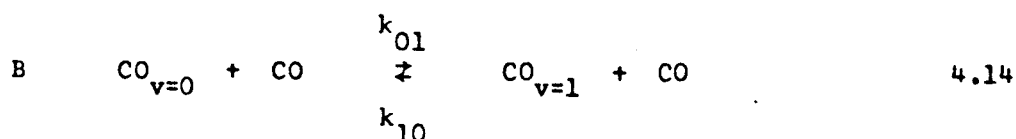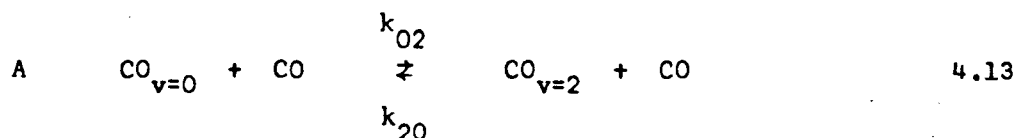
The approximation can be made that $[CO_{v=2}] << [CO_{v=1}] << [CO_{v=0}]$. By comparing equation 4.13 with 4.5 it can be seen that scheme A gives

Figure 4.3 Emission from the Second Vibrational Level
of Pure CO. Run No. 485.

$\odot \quad y = -\log[1-(I/I_\infty)^{1/2}]$

$x \quad y = -\log(1-I/I_\infty)$
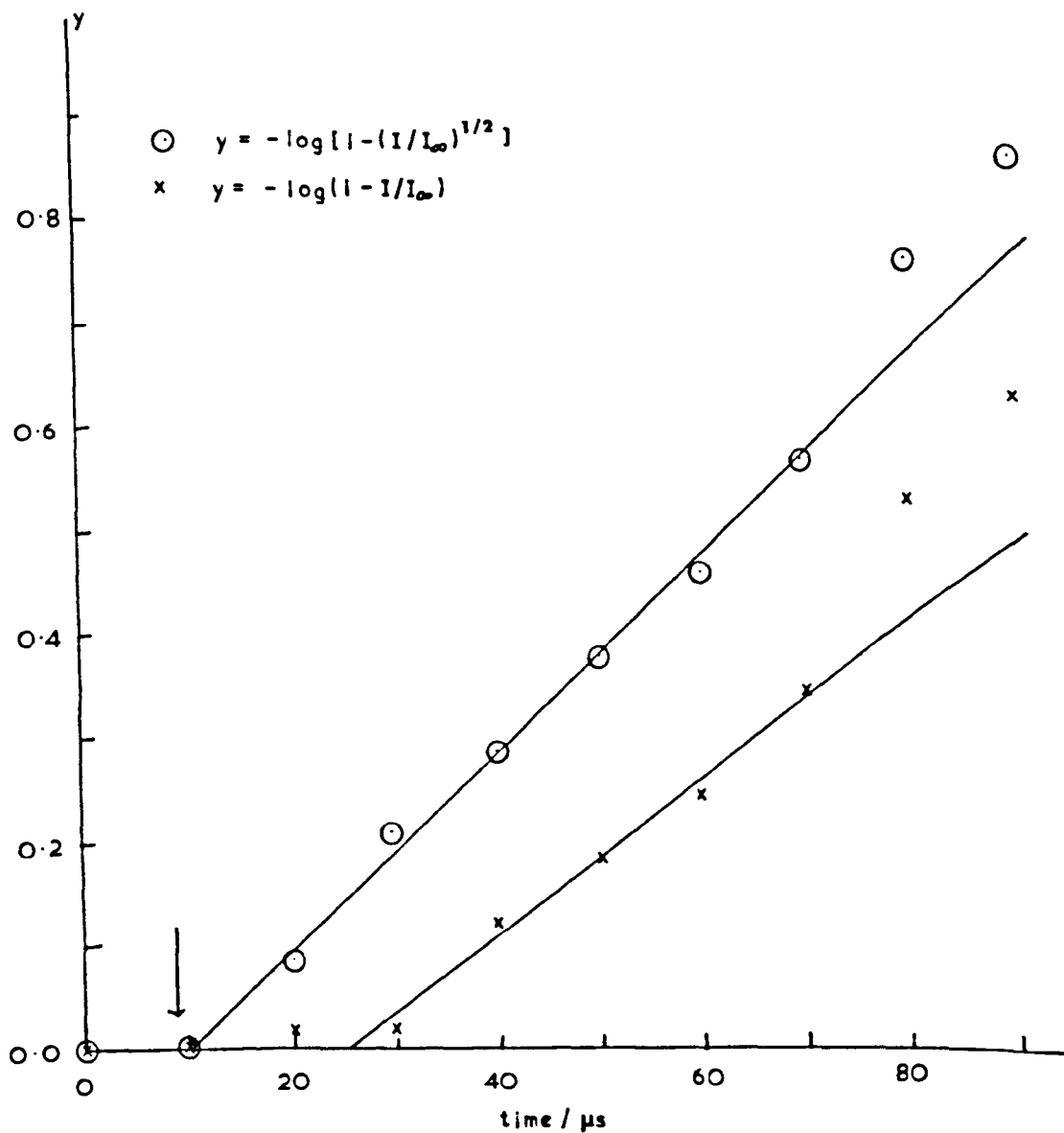
The arrow indicates the calculated time of arrival of the shock front at the observation station.

a simple exponential growth of $CO_{v=2}$.

Therefore the emission will fit an equation of the form given by equation 4.10, viz.

$$\frac{dI}{dt} = \frac{I_{\infty} - I}{\tau} \qquad 4.10$$

where $1/\tau = k_{02}[CO]$.

In the harmonic oscillator approximation, $k_{12} = 2k_{01}$, $k_{21} = 2k_{10}$. Then scheme B gives

$$I = I_{\infty}\{1-\exp(-t/\tau)\}^2 \qquad 4.17$$

where I is the intensity of emission from the second vibrational level and τ the relaxation time of the first level (equal to $1/k_{10}[CO]$). If in scheme C it is assumed that e is very large, then equation 4.17 again results.

When this equation is a fair representation of the shape of the trace, plots of $-\ln(1-(I/I_{\infty})^{\frac{1}{2}})$ against t are straight lines. Such was found to be the case for pure CO and CO with hydrogen halides (Fig. 4.3).

An alternative method of evaluating τ from a trace which is of the above shape is from the gradient. Differentation of equation 4.17 gives

$$\frac{dI}{dt} = \frac{2I_{\infty}}{\tau} \exp(-t/\tau) - \frac{2}{\tau} I_{\infty} \exp(-2t/\tau) \qquad 4.18$$
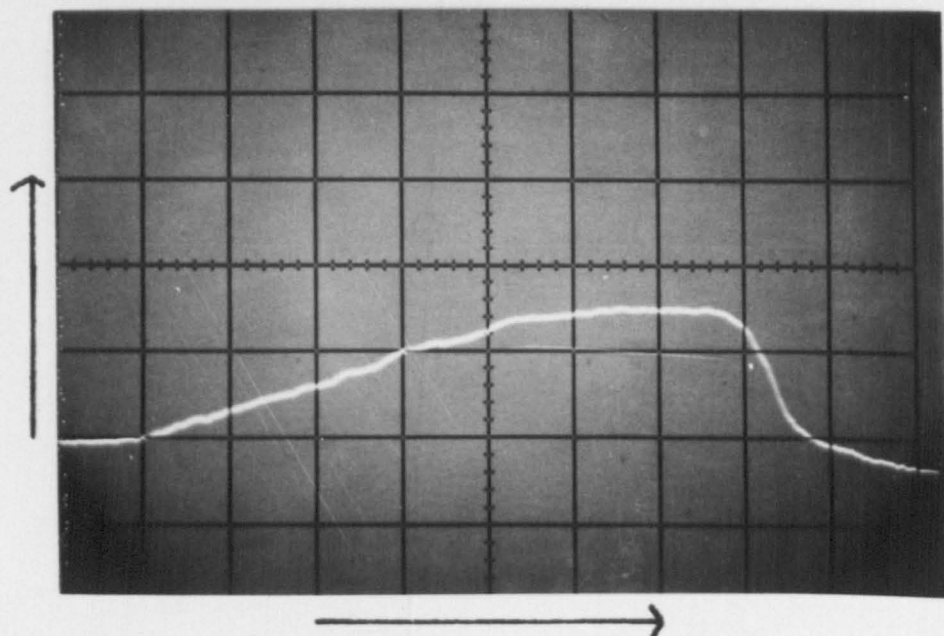
Figure 4·4 Emission from the Second
Vibrational Level of Pure CO.
Run 485: 20 μs cm^{-1}; 1 mv cm^{-1}.

and $\dfrac{d^2I}{dt^2}$ $=$ $-$ $\dfrac{2I_\infty}{\tau^2}$ $\exp(t/\tau)$ $+$ $\dfrac{4}{\tau^2}$ I_∞ $\exp(-2t/\tau)$ $\qquad$ 4.19

There is a point of inflexion where $\dfrac{d^2I}{dt^2}$ $=$ 0 i.e. when $\exp(-t/\tau) = \tfrac{1}{2}$. At that time,

$$\dfrac{dI}{dt} \;=\; \dfrac{I_\infty}{2\tau} \qquad\qquad 4.20$$

and the intensity at which it occurs is $I_\infty/4$. Therefore by measuring the gradient at $I = I_\infty/4$, the experimental relaxation time could be found by simply equating the gradient to $I_\infty/2\tau$.

Both gradient and plotting methods of analysis were tried for several traces and the agreement between them was within experimental error. For example, run number 485 (Fig. 4.4) which gave a value for τ_{exp} of 46 μs for the plotting method (Fig. 4.3) and 47 μs by the gradient method.

The latter method, being less tedious was more frequently adopted. The former was preferred when points from the trace could be taken by a D-Mac and the coordinates fed into a computer which was used to calculate points and plot them (Appendix A, Program 5).
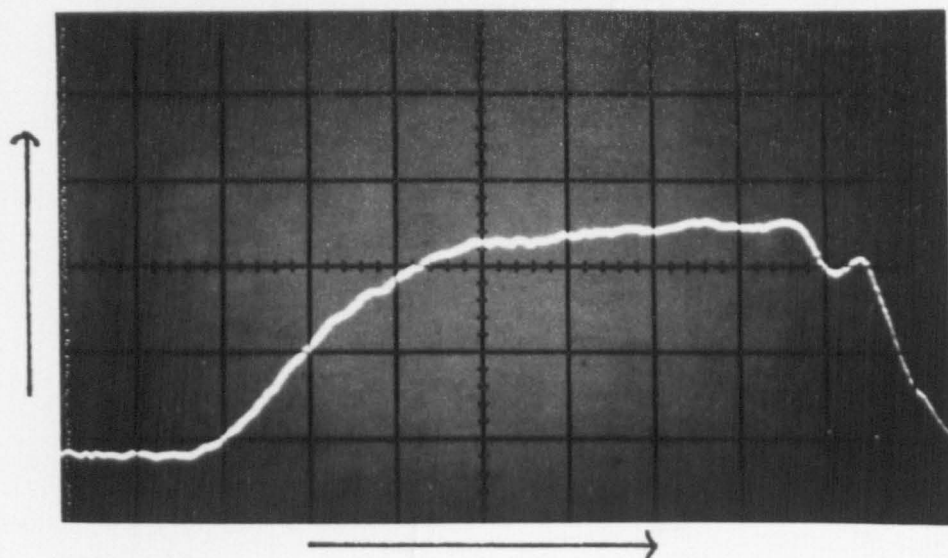
Figure 4·5 Emission from 2% HBr in CO.
Run 511: 20 µs cm⁻¹; 0·2 mv cm⁻¹.

4.7 Analysis of Traces: Choice of I_∞

Sometimes traces exhibited deviations from the ideal shape and the choice of I_∞ was not unambiguous. In run number 511, (Fig. 4.5) there is a slight fall in I around 40 mm from the start of the emission. As the shock velocity was 1.9 mm μs^{-1} and the sweep speed 2 μs mm^{-1}, the length of shocked gas between the two regions (40 x 2 x 1.9) equals 150 mm. This multiplied by the density ratio (5.9) gives the distance upstream from the observation of the place at which the deviation occurred. This distance, 890 mm corresponds approximately to a joint in the shock tube which was measured as 910 mm upstream of the observation station.

Such deviations make the choice of I_∞ a little difficult so it was decided to investigate what was the effect on τ of an inaccurate choice of I_∞. Two cases were tested: firstly for a simple exponential trace (equation 4.12) and secondly for a two step mechanism (equation 4.17). Values of I at times t were calculated for the equations using I_∞ = 30 mm and τ_{exp} = 100 μs. Plots of $-\ln(1 - I/I_\infty)$ vs t and $-\ln[1 - (I/I_\infty)^{\frac{1}{2}}]$ vs t were made for each case, the points being calculated for several values of I_∞ between 24 and 36 mm. The shape of the curves are illustrated schematically in figure 4.6.

Relaxation times were measured from the gradient near the origin and the error in τ_{exp} (compared with the correct value of 100 μs)
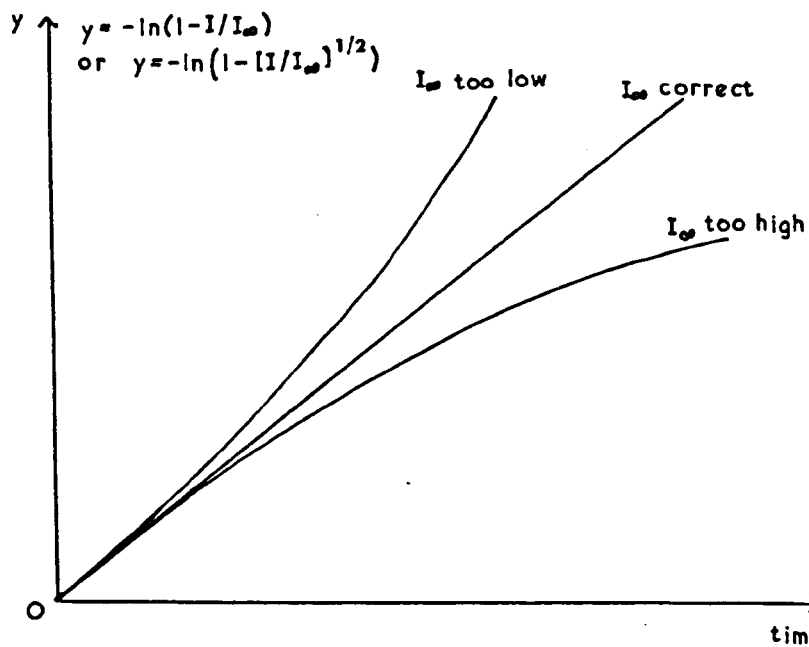
Figure 4·6 Effect on Plots of an Incorrect I_∞

The curvature increases with increasing error in I_∞
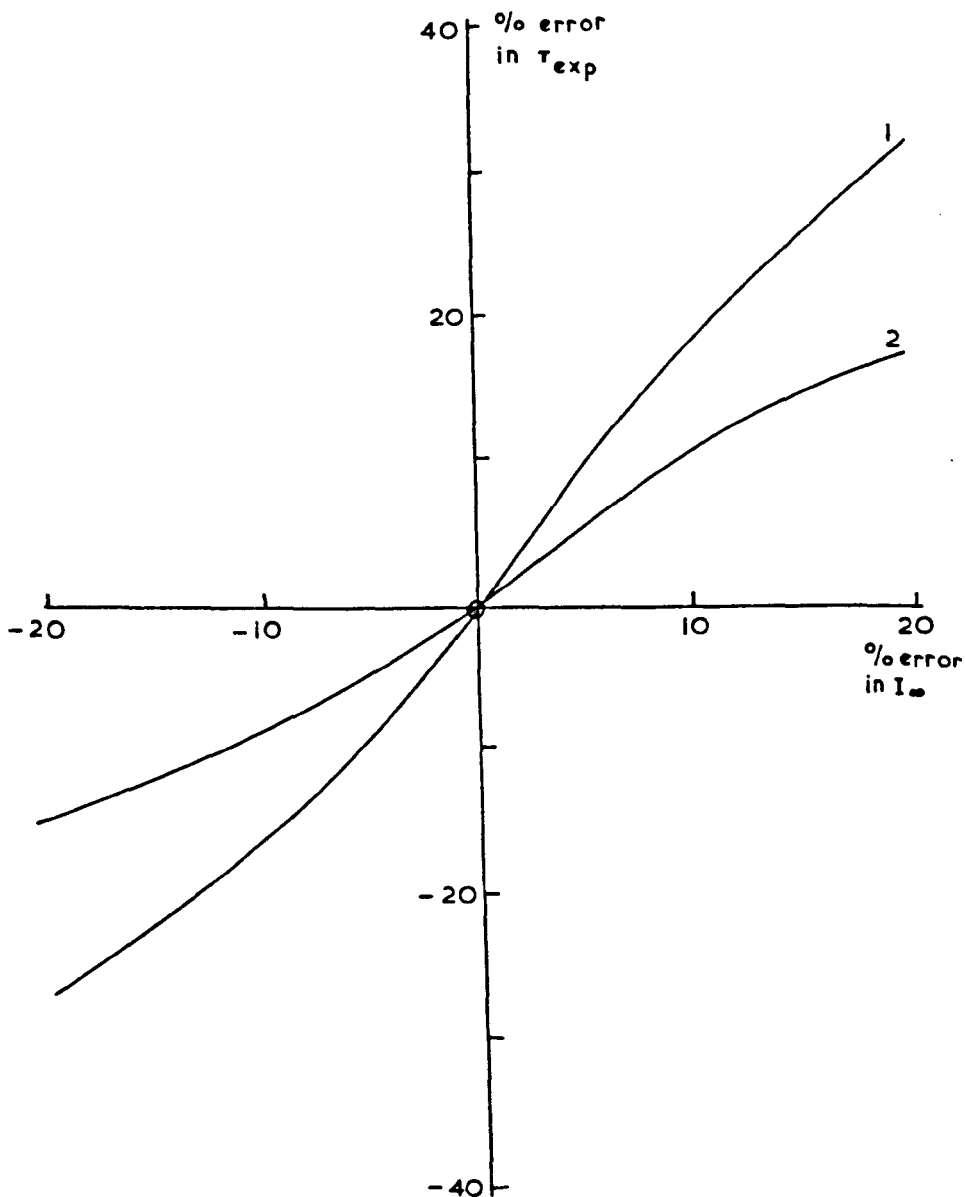
Figure 4·7 Effect on τ_{exp} due to an Error in I_∞

1 Assuming a simple exponential rise in emission.
2 Assuming stepwise population of the second level.

was plotted against the error in I_∞ (Fig. 4.7). For both cases considered, τ_{exp} is sensitive to I_∞ especially if the trace is a simple exponential.

Values of I_∞ under estimated by x% lead to an error in τ_{exp} of less than x%. So with the traces obtained, incorrect evaluation of I_∞ should contribute less than 5% to the error of τ_{exp}.

Greater errors than this could be avoided by plotting $-\ln(1 - I/I_\infty)$ versus t or $-\ln[1-(I/I_\infty)^{\frac{1}{2}}]$ versus t for several values of I_∞ seeing over estimating I_∞ produces a curvature different from when I_∞ is under estimated (Fig. 4.6).
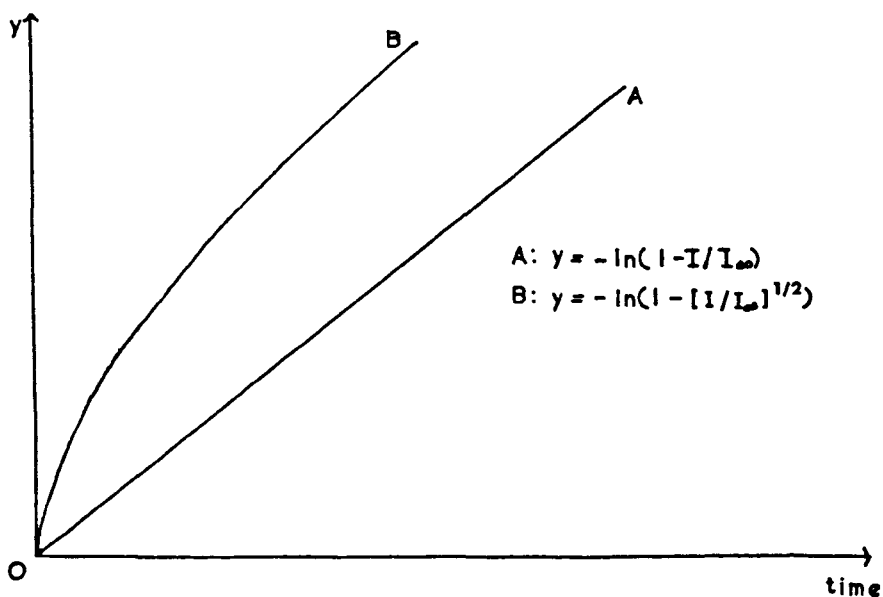
Figure 4·8 Schmatic Plots for an Ideal Simple Exponential Trace (Case 1) τ_{exp} = 1 / gradient

In the figure:

A: $y = -\ln(1 - I/I_\infty)$

B: $y = -\ln(1 - [I/I_\infty]^{1/2})$
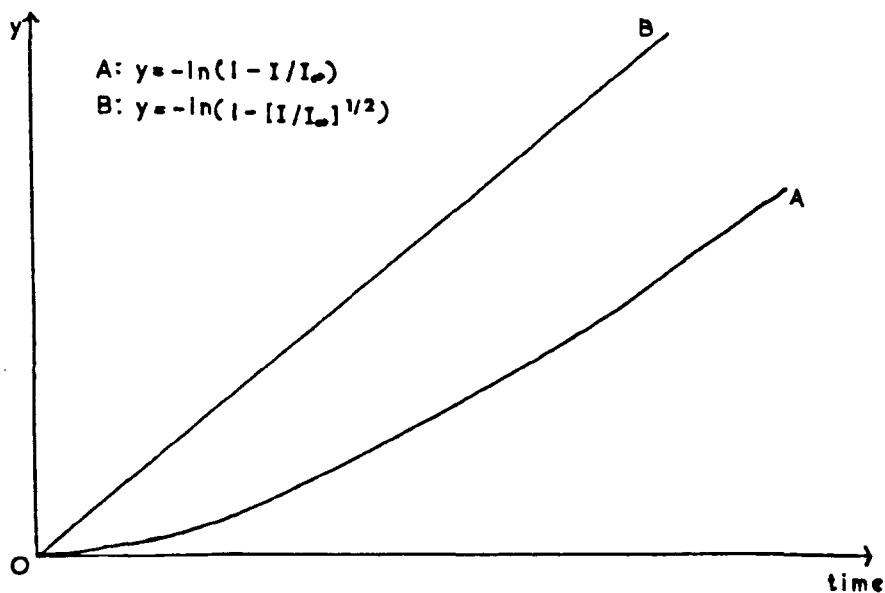
Figure 4·9 Schematic Plots of an Ideal Two Step Process accurately represented by Eqn. 4·28 (Case 2) τ_{exp} = 1 / gradient

In the figure:

A: $y = -\ln(1 - I/I_\infty)$

B: $y = -\ln(1 - [I/I_\infty]^{1/2})$

4.8 Analysis of Traces by Incorrect Model

Differing values of the Napier time are obtained depending
on whether the trace is analysed as for a two step process by
equation 4.17 or is treated as a simple exponential by equation 4.12.
Figure 4.3 shows that for the second vibrational level of CO, equation
4.17 fits better than equation 4.12. By drawing the best line through
the points of each plot, the former equation leads to a value for
τ_{exp} of 46 µs compared with a value of 56 µs by the latter. This
appears to be similar to the work of Windsor, Davidson and Taylor[72]
and contrasts with that of Hooker and Millikan[75] where it is stated
that the results obtained by the two methods differ by a factor of two.

The above experimental observation is confirmed by plots of
ideal curves. For a simple exponential, analysis by equation 4.17
yields a value for τ_{exp} a little shorter than the correct value
(Case 1, Fig. 4.8). (Curvature of the plot prevents quoting a
meaningful quantitative relationship). Conversely, if the trace is
exactly represented by the equation for a two step process (4.17),
then analysis as if it were a simple exponential trace by equation 4.12
gives a value for τ_{exp} a little longer than the correct one. (Case 2,
Fig. 4.9)

A second feature of the plots for the theoretical curves,
shown in figures 4.8 and 4.9, is that only the line for the correct
plot intercepts the axes at the origin. In case 1, the wrong line

would intercept the time axis at a negative value whereas in case 2, the wrong line would intercept at a positive value. The experimental plot for CO (Fig. 4.3) illustrates this point when due allowance is made for the origin for the plot being the commencement of the trace (Fig. 4.4) rather than the start of the emission. This time interval can be calculated in several cases for sometimes the sweep was triggered by a pulse from the middle light screen which was positioned a measured small distance (14 mm) upstream of the observation station. Thus for run number 485 (Fig. 4.4) when the shock speed was 1.88 mm μs^{-1}, the time interval is 8 μs. Therefore the correct plot should intercept the time axis at t = 8 μs. That this is approximately true (Fig. 4.3) is further confirmation of the adequacy of two step model for analysing second harmonic radiation from CO.

It seems therefore that there are two safeguards against chosing the wrong model for analysing a trace: firstly the closeness with which the calculated points lie on a straight line and secondly the position of the intercept. Should however an incorrect choice be made, the error in τ_{exp} is not liable to be large.

4.9 Conversion of Experimental Relaxation Times to Napier Times

Napier times are vibrational relaxation times at one atmosphere and are obtained by standardising experimental values. Allowances are made for the pressure at which they are measured, P_2, not being unit atmosphere and for a "time compression effect".

As τ is inversely proportional to pressure,[15,72] τ_{exp} must be multiplied by $P_2/760$ if the value of P_2 is in mm Hg ($P_2 = P_1 P_2/P_1$).

The second factor can be appreciated by considering a point in the shock heated gas a distance q behind the shock front and which passes the observation station a time t after it. If the shock speed is v, then

$$t = \frac{q}{v} \qquad\qquad 4.21$$

The gas at q must have been a distance upstream of the observation station of $q\,\rho_2/\rho_1$ before being compressed in the shock wave so the time, t', taken for the shock to travel between these two points is $\frac{q}{v} \cdot \frac{\rho_2}{\rho_1}$ and this is the length of time for which the gas has been shock heated. Therefore "laboratory time" is a factor of ρ_2/ρ_1 less than "particle time".

Hence $\quad \tau(1\ atm) = \tau_{exp} \cdot \dfrac{P_1}{760} \cdot \dfrac{P_2}{P_1} \cdot \dfrac{\rho_2}{\rho_1} \qquad 4.22$

This relationship was used to calculate the Napier times of pure HCl, pure HBr and HCl in Ar.

Since the temperature falls as vibrational energy increases (e.g. for pure HCl, Mach No. = 5.3, the temperature falls from 1920 to 1785°K), the Napier time was taken to correspond to a temperature T_{av} which is the average of two extreme conditions: firstly T_a, when the gas contained no vibrational energy (in the above example 1920°K) and secondly T_2, when the gas was in vibrational equilibrium (in the above example 1785°K). It was felt that for the pure hydrogen halides, the measurements were not sufficiently accurate to warrant the subsequent treatment used for CO and CO mixtures. For 5% HCl in Ar, the decrease in temperature due to vibrational relaxation is very small and again the subsequent treatment is of little value (e.g. Mach No. 4.1, $T_a = 1814^{\circ}$K, $T_2 = 1793^{\circ}$K).

For gases containing CO, there was plotted, in preference to a point, a line (Fig. 3.7) which has as its extremities the values of τ calculated for temperatures T_a and T_2 by the equations:

$$\text{At } T_a, \ \tau(1 \text{ atm}) = \tau_{exp} \cdot \frac{P_1}{760} \cdot \frac{P_a}{P_1} \cdot \frac{\rho_a}{\rho_1} \qquad 4.23$$

$$\text{and at } T_2, \ \tau(1 \text{ atm}) = \tau_{exp} \cdot \frac{P_1}{760} \cdot \frac{P_2}{P_1} \cdot \frac{\rho_2}{\rho_1} \qquad 4.24$$

The line represents the range over which the Napier time would vary from a particular shock if τ_{exp} were constant over the whole period of vibrational relaxation.

4.10   Change of Experimental Relaxation Time over the

      Vibrational Relaxation Region

      Although the fall in temperature during vibrational

relaxation is often $100^{\circ}K$, the experimental relaxation time does

not vary a great deal.   Its variation is considerably less than

the change in Napier time over the same temperature range.

      Consider a shock in pure CO of mach number 5.3:

T_a = $1920^{\circ}K$ and T_2 = $1834^{\circ}K$.   If the Landau-Teller equation 1.11

accurately represents the Napier time of CO, its value at $1920^{\circ}K$

is 87.0 atm μs and at $1834^{\circ}K$ 109.8 atm μs.   Using equations 4.23

and 4.24 with an assumed P_1 of 20 mm Hg, τ_{exp} at $1920^{\circ}K$ is 202 μs

and at $1834^{\circ}K$ is 217 μs.   Increasing pressure and density in the

relaxation region compensate for the increase in relaxation time

associated with decreasing temperature so that the resultant

increase in τ_{exp} is only 7%.   This small change would not be

expected to make an appreciable change to the usual plot of

emission against time.

4.11 Errors in the Calculated Shock Conditions due to Non-ideal Flow

The effect of boundary layer growth in a shock tube was discussed qualitatively in section 1.3: it causes the shock wave to attenuate. A direct result of this will be that the temperature of the relaxed gas will be lower the further downstream it is. The density and pressure will also be affected.

Belford and Strehlow[115] have developed equations by which the magnitude of the effect can be calculated. The parameters needed are:

(a) the diameter of the shock tube - a measurable quantity.

(b) the initial downstream pressure - a measurable quantity.

(c) the hot flow time. Only the region in which measurements are made is important so it was taken from the infrared emission traces to be the time taken to reach equilibrium.

(d) the shock mach number - calculated from the shock speed.

(e) the ideal average shock temperature - calculated according to section 1.4.

(f) the ideal average shock density ratio - calculated according to section 1.4.

(g)   the velocity decrement. This was taken as 1% m^{-1}
       as the three light screens, set at intervals of
       50 cm, would have been able to detect a faster
       rate of attenuation.

The calculations were made using a computer program
developed by Millward.[116]

Over the operating range of mach numbers, the temperature
was too low by less than 1% and the density and pressure by less
than 2%. Since the errors are small, no corrections were generally
made to the conditions as calculated assuming ideal flow.

4.12   Comparison of Experimental Napier Times and Theoretical

  Collision Numbers

Theoretical considerations of relaxation phenomena calculate
the number of collisions required to achieve vibrational relaxation
and it is necessary to convert these collision numbers to relaxation
times so that comparison with experimental Napier times can be made.
The essential parameter is the time between collisions, τ_c.

There are two major ways to calculate τ_c. Firstly one
can consider the molecules as solid spheres of diameter σ moving
with a mean speed Ω which is calculated from collision theory. The
number of collisions that one molecule undergoes each second, Z, is
given for a pure gas by (reference 33, equations 3.5 and 3.9)

$$Z = P\sigma^2 \sqrt{\frac{16\pi}{mkT}} \qquad\qquad 4.25$$

($\sqrt{\frac{16\pi}{mkT}}$ is the mean relative velocity)

If the gas, instead of being pure, contains one molecule of an
impurity (diameter σ_1, mass m_1) the equation for the number of
collisions suffered by the impurity is

$$Z = P\left(\frac{\sigma_1+\sigma_2}{2}\right)^2 \sqrt{\frac{8\pi}{\frac{m_1 m_2}{(m_1+m_2)} \cdot kT}} \qquad\qquad 4.26$$

(reference 33, equation 3.5)

If $m_1 = m_2$ and $\sigma_1 = \sigma_2$, equation 4.26 reduces to equation 4.25. The collision frequency given by equation 4.26 is the same as that which would be experienced in a hypothetical pure gas of molecules mass $2m_1 m_2/(m_1+m_2)$ and molecular diameter $(\sigma_1+\sigma_2)/2$. The equation for gas mixtures is the more general form and it is this one that is used in the calculations.

In either case, the time between collisions is the reciprocal of Z.

The second method of calculating τ_c tries to make allowance for non-idealities by using a measured parameter which is related to τ_c. (Viscosity, n, is chosen as values of σ and ε/k that are used in theoretical calculations are derived from viscosity measurements). The relationship is given in reference 15 (equation 36 - 3):

$$\eta \quad = \quad 1.271 \, P \, \tau_c \qquad\qquad 4.27$$

The value of the viscosity at any temperature is calculated using the equations of Hirschfelder, Curtiss and Bird.[91] For a pure gas,

$$\eta \quad = \quad \frac{26.693 \sqrt{MT}}{\sigma^2 \Omega^{(2,2)*}(T^*)} \qquad \mu \, \text{Poise} \qquad 4.28$$

(reference 91, equations 8.2 - 18).

where M is the molecular weight and $\Omega^{(2,2)*}(T^*)$ is the value of $\Omega^{(2,2)*}$, a correction parameter, at T^* where $T^* = kT/\varepsilon$.

(σ is in $\overset{o}{A}$)

Figure 4.10 Experimental and Calculated Viscosity of CO
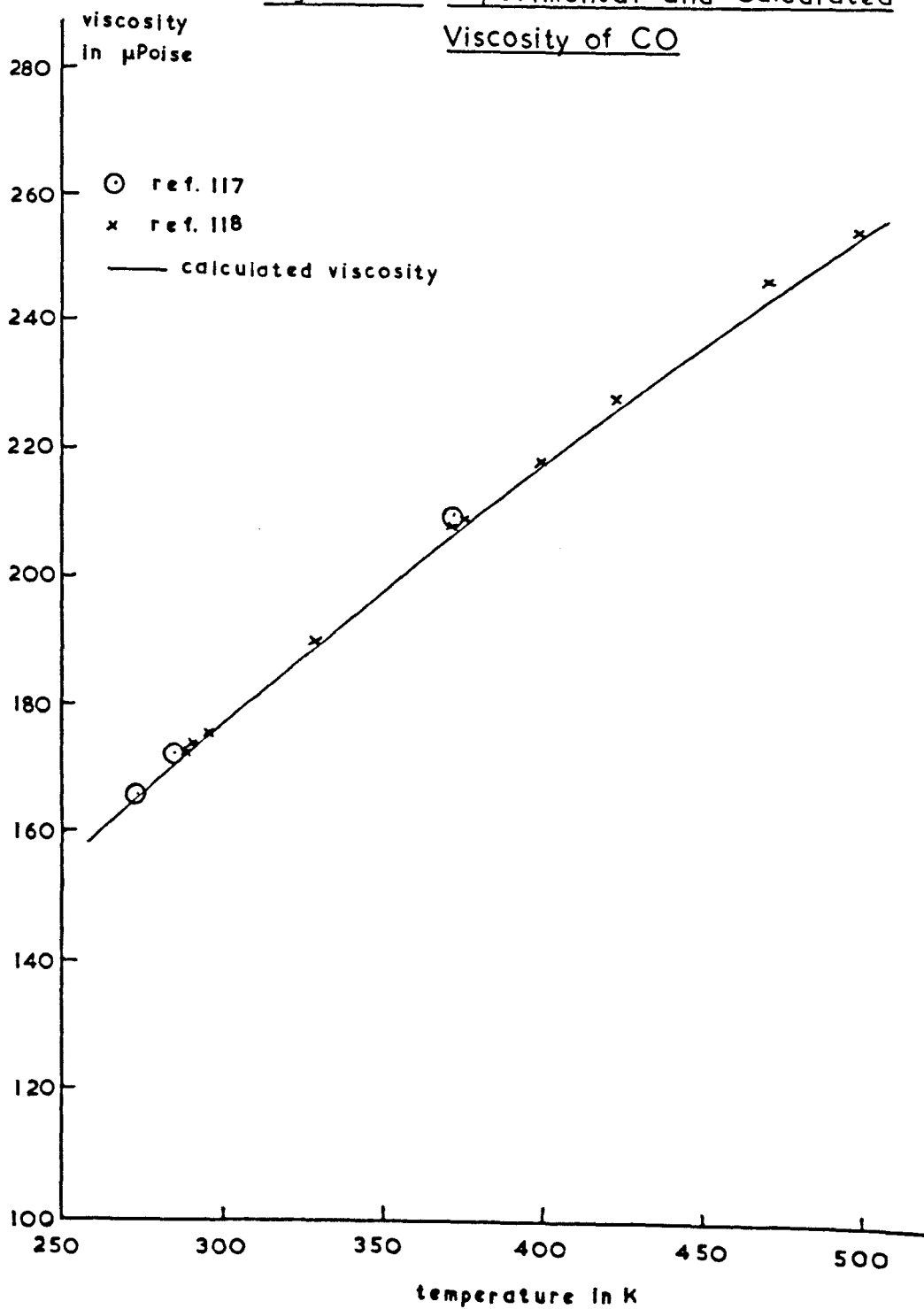
For a gas mixture

$$\eta = \frac{26.693 \sqrt{2M_1 M_2/(M_1+M_2)T}}{\sigma_{12}^2 \; \Omega_{1,2}^{(2,2)*} \; (T_{1,2}^*)} \quad \mu \text{ Poise} \qquad 4.29$$

(reference 91, equation 8.2 - 21)

which is the value for a hypothetical pure gas of molecular weight $2M_1 M_2/(M_1+M_2)$, cross sectional diameter $(\sigma_1+\sigma_2)/2$ and intermolecular potential $\epsilon_1 \epsilon_2$. If $M_1 = M_2$, $\sigma_1 = \sigma_2$, $\epsilon_1 = \epsilon_2$, 4.29 reduces to 4.28. Its similarity with equation 4.26 means that the second form of the viscosity, 4.29, is suitable for use when considering the hypothetical case of the relaxation of a single molecule of impurity in an otherwise pure gas.

The accuracy with which equation 4.29 represents viscosity is shown for CO, N_2, HCl and HBr by figures 4.10 to 4.13. Over the limited temperature ranges, the agreement between experimental and calculated viscosities is very good for CO and N_2 but less good for HCl and HBr. This could be anticipated for a simple spherical Lennard-Jones 12-6 potential cannot adequately represent the intermolecular potential between polar molecules. Also the paucity of viscosity measurements for HBr (Fig. 4.13) means that σ and ϵ/k may not be accurate. Indeed, Hirschfelder, Curtiss and Bird[91] do not list any and those used were obtained as shown in Appendix C.

Figure 4.11 Experimental and Calculated Viscosity of N₂
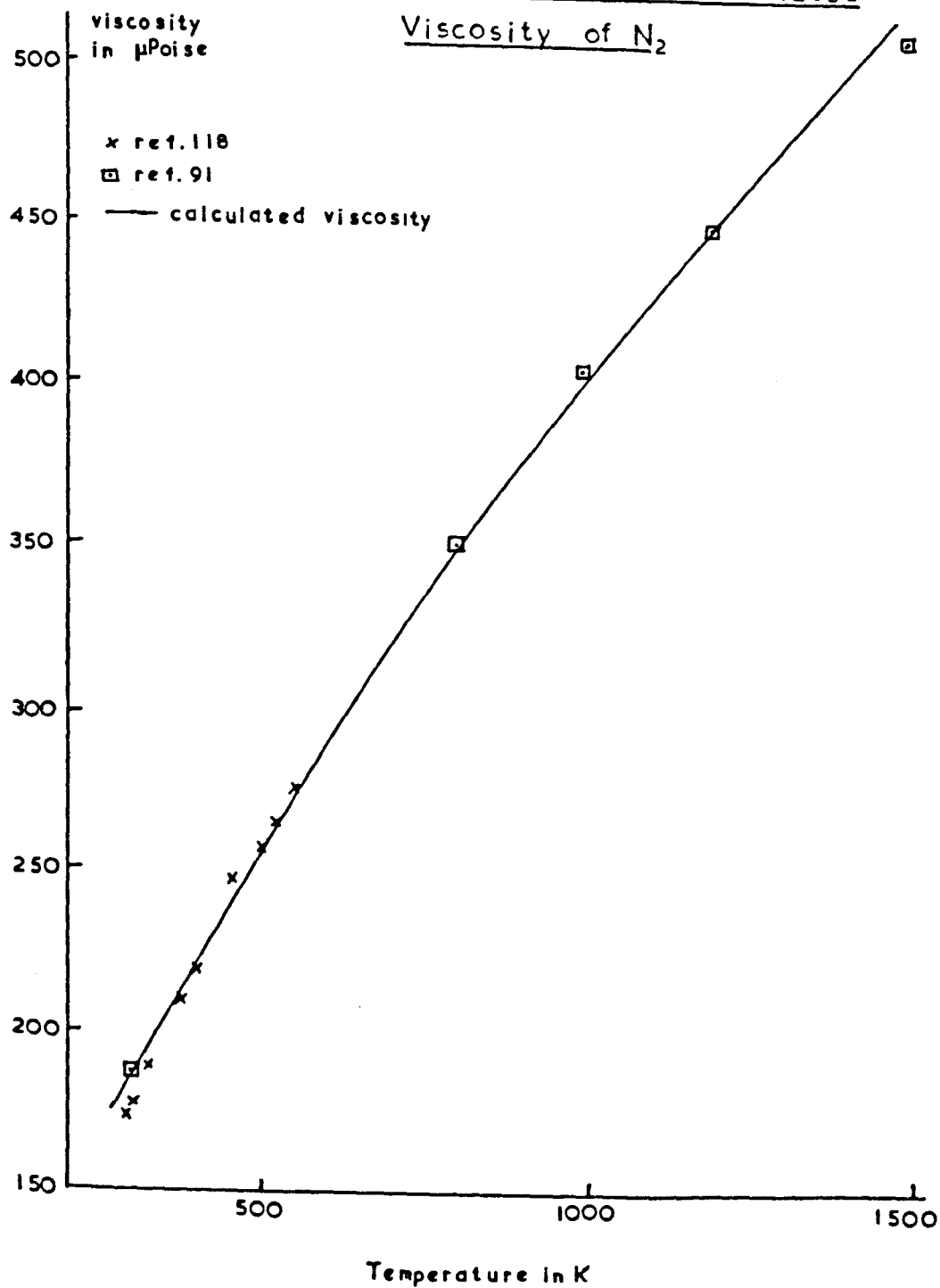
Figure 4.12 Experimental and Calculated Viscosity of HCl
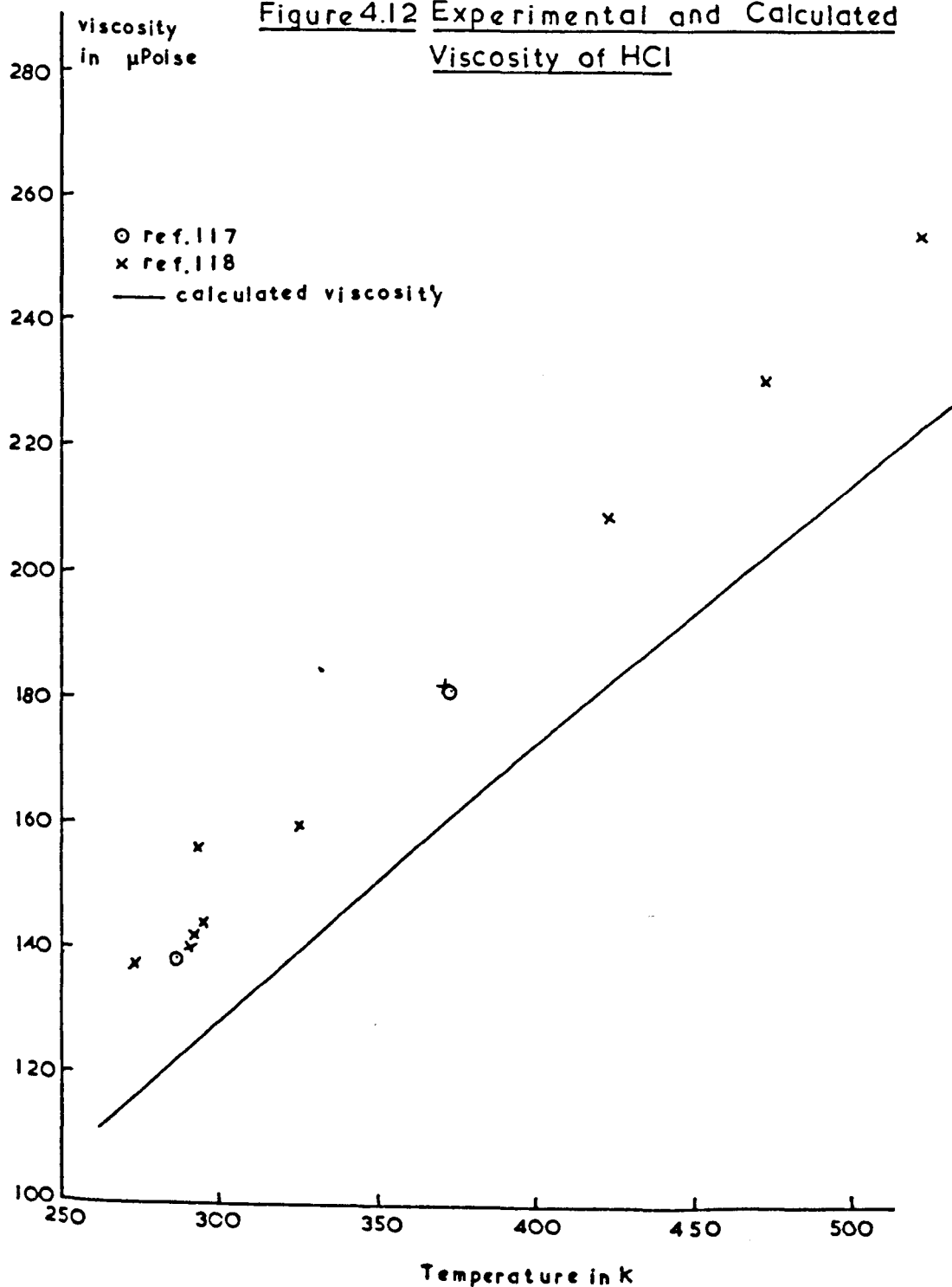
Figure 4.13 Experimental and Calculated Viscosity of HBr
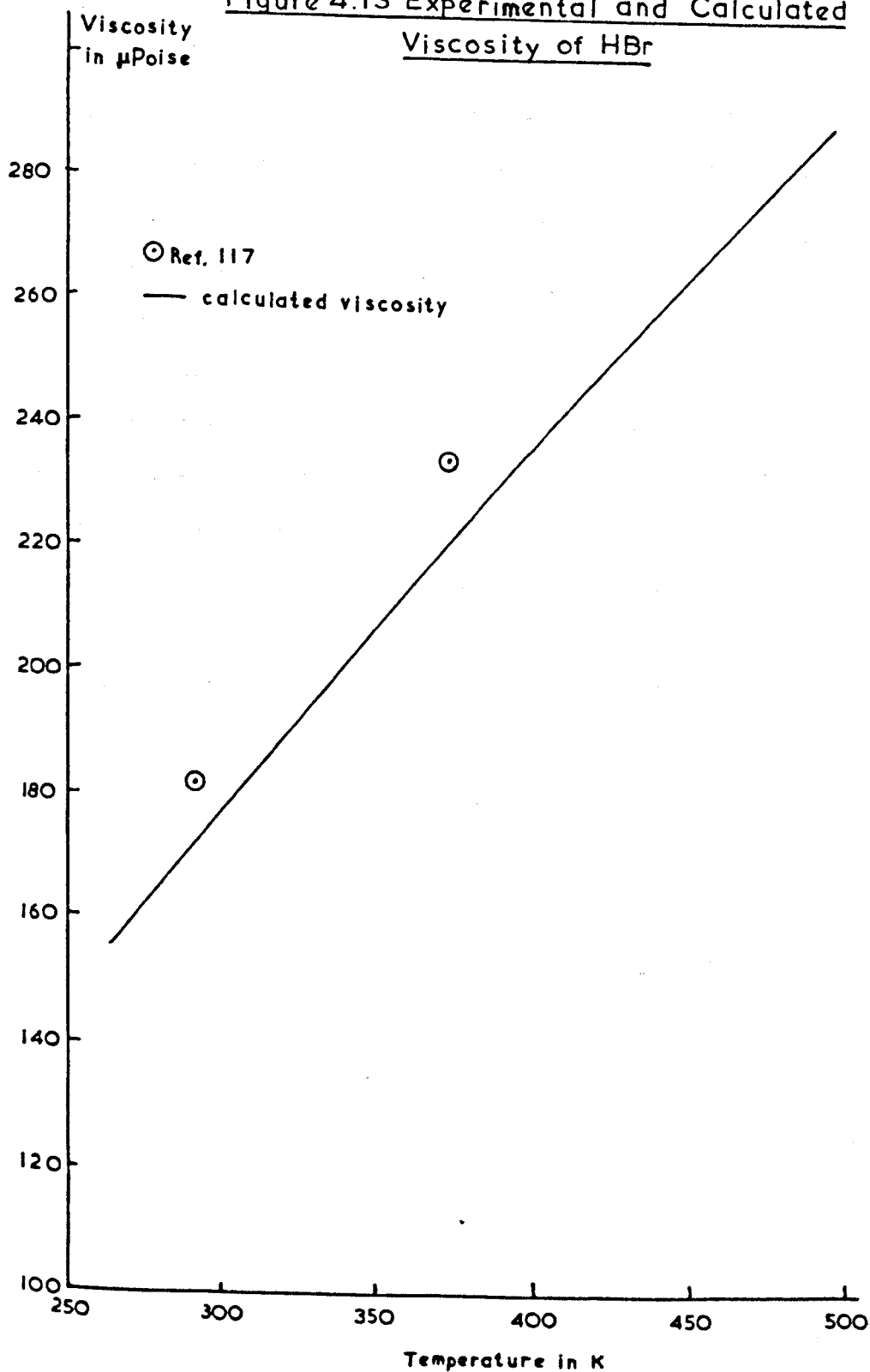
Monchick and Mason[119] suggest that more accurate values for
transport properties are obtained for polar molecules by using
a Stockmeyer 12-6-3 potential but for relaxation measurements,
this refinement seems unnecessary especially since the disagreement
in viscosity was not great and the SSH theory of vibrational
relaxation assumes a Lennard-Jones 12-6 intermolecular potential.

Collision times were obtained from calculated viscosity
and collision theory do not seriously conflict (Table 4.4). The
former method was adopted for converting collision numbers to
relaxation times since the molecular constants, which are needed
for both methods, are derived from viscosity measurements (Appendix
C). All molecules were treated in this way for although the results
for polar molecules may not be as accurate as for N_2 and CO there
is no reason to suppose that the alternative procedure is better.

Table 4.4   Time Between Collisions

Temp. $^{\circ}K$	HCl		HBr		CO		N_2	
	$\tau_c(z)$	$\tau_c(\eta)$	$\tau_c(z)$	$\tau_c(\eta)$	$\tau_c(z)$	$\tau_c(\eta)$	$\tau_c(z)$	$\tau_c(\eta)$
300	101	126	138	168	138	99	138	101
400	134	146	184	194	169	115	170	117
600	197	178	269	238	223	141	225	143
800	252	206	343	275	270	162	272	165
100	302	230	409	307	311	182	314	184
1200	347	252	487	337	348	190	351	202
1400	388	272	524	364	385	215	388	218
1600	427	291	576	389	422	230	425	233
1800	463	309	624	412	457	244	461	247
2000	498	326	671	435	488	257	493	261

Time measured in ps

5. DISCUSSION

5.1 Napier Times of Pure Gases and Gases with a Monatomic Diluent

Considerations relevant to the systems of pure HCl, pure HBr, pure CO and HCl in Ar are discussed in section 5.1.1. Each system is then treated separately from an experimental standpoint: the results obtained from this study are summarised and then compared with previous and subsequently published values. Theoretically predicted Napier times are compared with the experimental values in section 5.1.6.

5.1.1 Relationship between Population and Energy

In general, the emission observed emanated from the
second vibrational level. The exception was pure HCl for which
some measurements were made using emission from the third
vibrational level. For all cases, the intensity of the emission
was taken to be proportional to the population of the level
being monitored. To deduce Napier times from these observations,
it is necessary to relate changes in population to changes in
energy for the basic equation describing relaxation of the
vibrational mode at constant temperature is

$$\frac{dE}{dt} = \frac{E_\infty - E}{\tau} \qquad\qquad 5.1$$

where E is the vibrational energy at time t

E_∞ is the equilibrium vibrational energy at the new
temperature.

τ is the vibrational relaxation time.

Statistical mechanics gives the population, n_i, of the
ith vibrational level of energy ϵ_i, as

$$n_i = N\exp(-\epsilon_i/kT)/p.f. \qquad\qquad 3.5$$

where p.f. $= \exp(-\epsilon/2kT)/(1 - \exp(-\epsilon/kT)) \qquad\qquad 3.6$

The energy of a particular vibrational level of an harmonic
oscillator is given by

$$\epsilon_i \quad = \quad (v_i + \tfrac{1}{2})h\nu \qquad\qquad 5.2$$

where v_i is the vibrational quantum number of the ith level

ν is the frequency of the $v = 1 \rightarrow 0$ transition.

The total vibrational energy of a mole of gas is given by

$$E \quad = \quad \frac{\epsilon}{2} \quad + \quad \frac{\epsilon \, \exp(-\epsilon/kt)}{1 - \exp(-\epsilon/kt)} \qquad\qquad 5.3$$

$$= \quad \sum_{i=1}^{\infty} n_i \epsilon_i (v_i + \tfrac{1}{2})h\nu \qquad\qquad 5.4$$

Application of these equations to HCl at 300 K and 2000 K shows E_∞ increases from 34.5 to 44.5 kJ mole^{-1}. The population and energy changes are given in Table 5.1.

Table 5.1

Population and vibrational energy changes for HCl

Vibrational State	% population at 300 K	% population at 2000 K	% increase in vibrational energy
0	100	87.5	-
1	0	11.0	78.0
2	0	1.3	15.3
$\sum_{i=3}^{\infty} i$	0	0.2	6.7

Hence, to a first approximation,

$$\frac{dE}{dt} = \frac{d(n_1 \epsilon_1)}{dt} = \frac{dn_1}{dt} \qquad 5.5$$

but since the second level absorbs only 15.3% of the increase in energy, $\dfrac{d(n_2 \epsilon_2)}{dt}$ cannot be directly approximated to $\dfrac{dE}{dt}$. To use second level emission to measure Napier times, the mechanism by which E is related to n_2 must be known.

A possible mechanism for populating the second level of CO has already been postulated (Section 4.6). More generally, three distinct schemes can be written:

A. Direct Population

$$AB\ (v=0)\ +\ AB\ \underset{k_{20}}{\overset{k_{02}}{\rightleftarrows}}\ AB\ (v=2)\ +\ AB\ (T,\ R \rightarrow V) \qquad 5.6$$

B. Stepwise Population

$$AB\ (v=0)\ +\ AB\ \underset{k_{10}}{\overset{k_{01}}{\rightleftarrows}}\ AB\ (v=1)\ +\ AB\ (T,\ R \rightarrow V) \qquad 5.7$$

$$\text{and } AB\ (v=1)\ +\ AB\ \underset{k_{21}}{\overset{k_{12}}{\rightleftarrows}}\ AB\ (v=2)\ +\ AB\ (T,\ R \rightarrow V) \qquad 5.8$$

C. Stepwise Population with Resonance Exchange

$$AB\ (v=0)\ +\ AB\ \underset{k_{10}}{\overset{k_{01}}{\rightleftarrows}}\ AB\ (v=1)\ +\ AB\ (T,\ R \rightarrow V) \qquad 5.7$$

and AB (v=1) + AB (v=1) $\overset{e}{\underset{e}{\overset{\rightarrow}{\leftarrow}}}$ AB (v=2) + AB (v=0) ($\overset{resonance}{exchange}$) 5.9
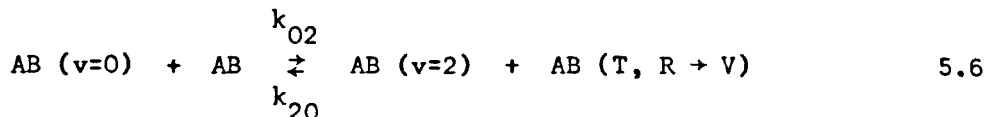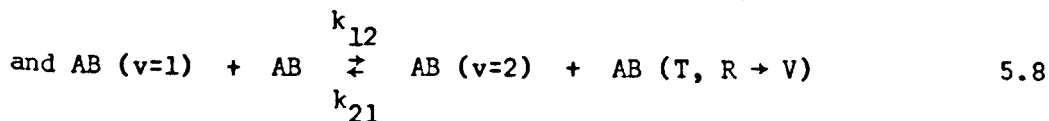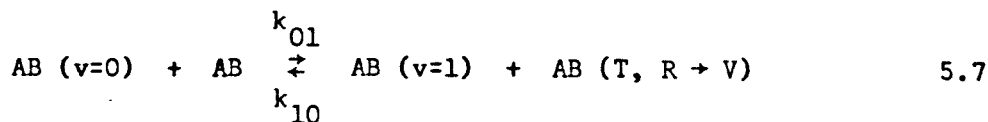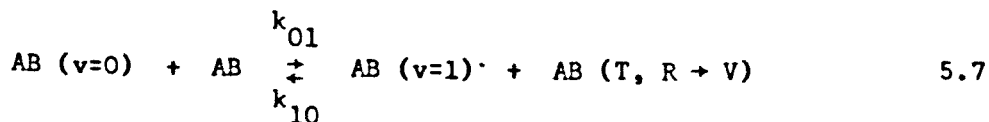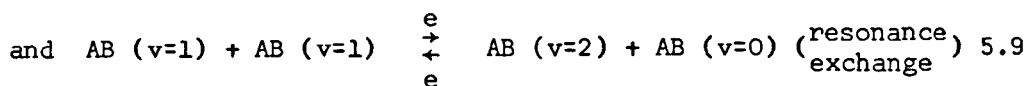
For gases in which there is a monatomic diluent, such as HCl with Ar, further schemes are possible:

A' Direct Population

AB (v=0) + M $\overset{\rightarrow}{\leftarrow}$ AB (v=2) + M (T → V)   5.10

B' Stepwise Population

AB (v=0) + M $\overset{\rightarrow}{\leftarrow}$ AB (v=1) + M (T → V)   5.11

and AB (v=1) + M $\overset{\rightarrow}{\leftarrow}$ AB (v=2) + M (T → V)   5.12

C' Stepwise Population with Resonance Exchange

AB (v=0) + M $\overset{\rightarrow}{\leftarrow}$ AB (v=1) + M   (T → V)   5.11

AB (v=1) + AB (v=1) $\overset{e}{\underset{e}{\overset{\rightarrow}{\leftarrow}}}$ AB (v=2) + AB (v=10) ($\overset{resonance}{exchange}$)5.9
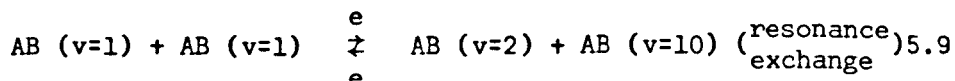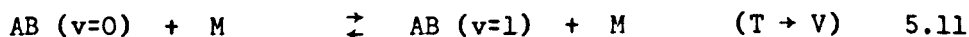
      The reactions in gases with diatomic diluents are considered in section 5.2.

      It has been shown in section 4.6 that when the experimental relaxation time was longer than the rise time of the system, the Napier time can be deduced from second level emission by making a suitable plot of emission intensity against time. Choice between a stepwise mechanism or direct transitions as a means of populating the upper level is made on the basis of which function of intensity plotted against time gives the more linear graph.

Figure 5.1 Napier Times of Pure HCl

SSH theory[15]

Quinn[120]

x $\Delta v = 3$, improvised cooler
⊙ $\Delta v = 3$, commercial cooler
⊡ $\Delta v = 2$, InSb detector

Breshears & Bird[121]

τ/atm μs

100

10

1

0.07   0.08   0.09

(temperature/ K)$^{-1/3}$
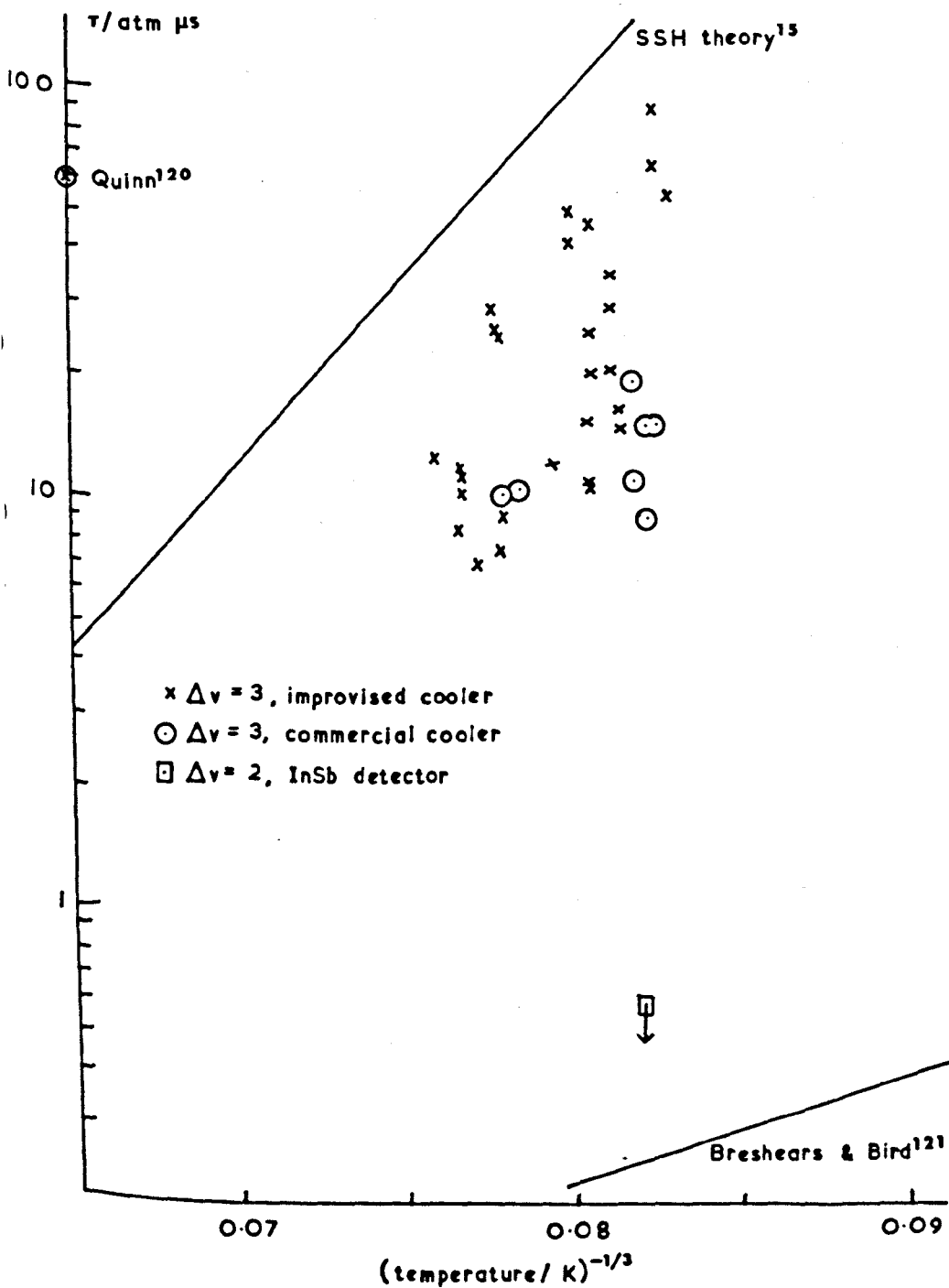
5.1.2   Relaxation Measurements for Pure HCl

In this study, HCl was observed to relax by
monitoring $\Delta v=3$ and $\Delta v=2$ emission. The former experiment gave
a Napier time of about 10 atm μs at 2000 K and the latter a value
of 0.6 atm μs at 1800 K (Sections 3.1.1 and 3.1.2). Borrell and
Gutteridge[105] reported the Napier times and later[106] discussed
them in relation to subsequently published values. As the
experimental relaxation times were close to the rise time of
the system, it was thought that the Napier times could only be
considered as upper limits and that the shape of the emission
did not signify the mechanism by which the second or third
vibrational level was populated. These limiting values will be
correlated initially with existing and then with subsequently
published measurements.

Previous high temperature measurements had been made
by Borrell[80] who reported a value of 8 atm μs at 2000 K, and
Quinn[120] who, using a microwave discharge, set a lower limit of
6.12×10^{4} for the collision number. This corresponds to a
Napier time of 60 atm μs for a temperature of 3646 K (Fig. 5.1).
Both these times are much too long to accord with the upper
limit of 0.6 atm μs at 1800 K set by this work.

Recent shock tube measurements on pure HCl have been
made by Breshears and Bird[121] who measured Napier times by a

Figure 5·2 Napier Times of Pure HCl
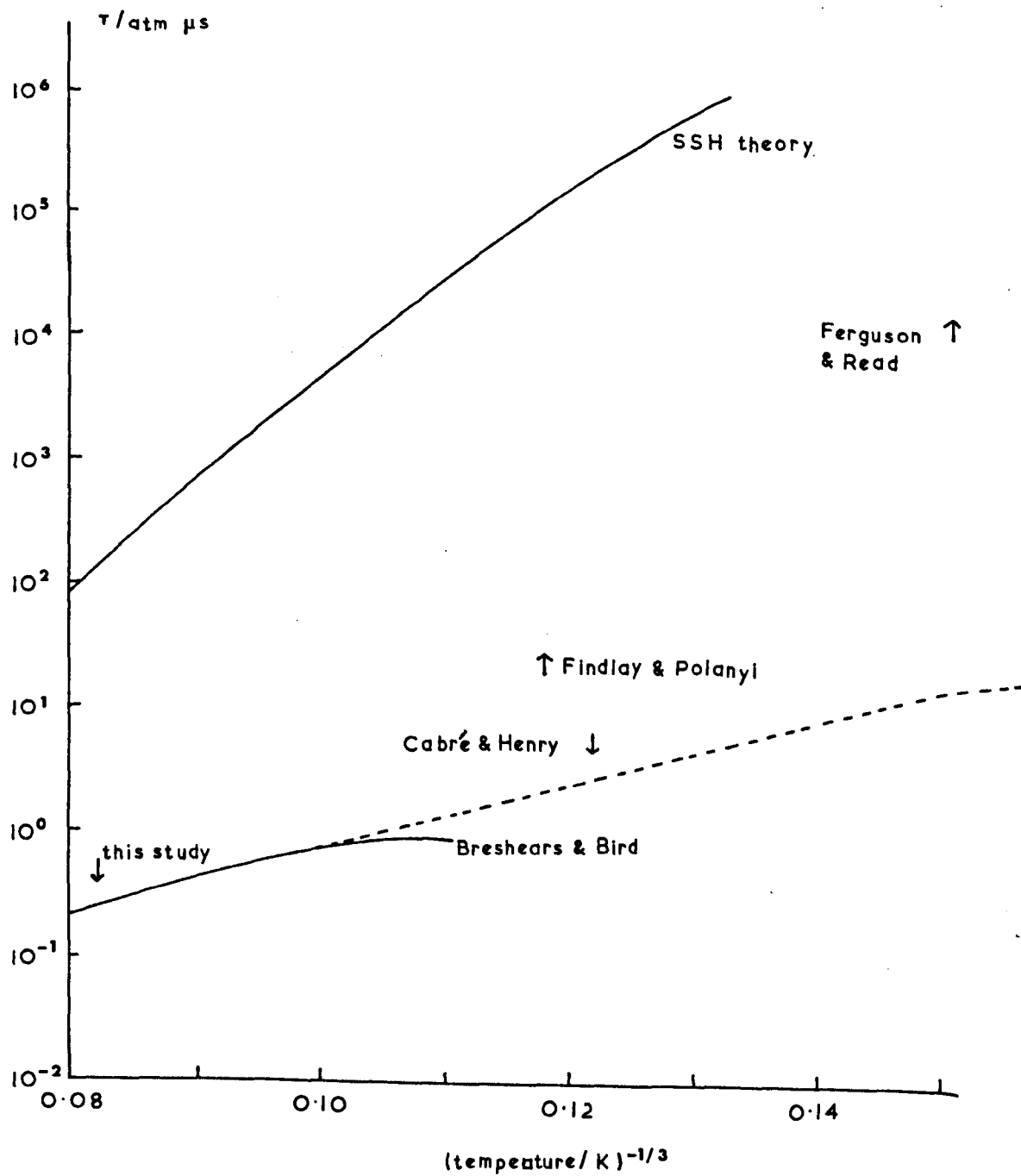
laser schlieren densitometry technique. Their times are much shorter than previous values (Fig. 5.2): at 1800 K it is 0.26 atm µs. Above 1000 K they show the normal $T^{-\frac{1}{3}}$ temperature dependence but below it there seems to be a maximum around 800 K. Clearly further measurements over the range 300 - 1000 K are very desirable. Measurements in the linear portion of the plot are supported by Bowman and Seery (Section 5.1.4) who worked with HCl diluted by argon.

Ferguson and Read[122] using a spectrophone set a shorter time limit for the Napier time at room temperature of 11 atm ms. This is much longer than expected by extrapolating the results of Breshears and Bird[121] (Fig. 5.2). Chen and Moore[123] have recently employed laser excited vibrational fluorescence to obtain a Napier time at room temperature of 1.6 atm µs. They suggest that the spectrophone measurements suffered seriously from the fact that the vibrational relaxation was several orders of magnitude faster than expected or measureable. Such a fast rate of relaxation they consider attributable to the depth of the attractive interaction potential well which has greater effect at low temperatures.

No measurements of τ_{HCl} are available at temperatures between 300 and 800 K but indications have been provided through work performed by Findlay and Polanyi[99] and Cabré and Henry[114]

on HCl produced chemically in a vibrationally excited state. Findlay and Polanyi thought that in 10^5 collisions at 600 K, the amount of vibrational energy lost by collisional deactivation was negligible compared with the loss by radiative transitions. This would correspond to a Napier time of >20 atm μs at 600 K. Cabré and Henry on the other hand measure experimental relaxation times of 4.2 ms for the first vibrational level at 550 K. They ascribe the relaxation, which occurred at a pressure of 1 mm Hg to both radiative transitions and collisional deactivation. We can write

$$\frac{1}{\tau_{exp}} = \frac{1}{\tau_{vib}} + \frac{1}{\tau_{rad}} \qquad 5.13$$

where τ_{vib} is the relaxation time due to collisional deactivation at that particular temperature and pressure, and if τ_{rad} = 0.03 s, then τ_{vib} = 4.9 ms so τ(1 atm) is 6.4 atm μs. This is rather more in keeping with the results of Breshears and Bird than is the measurement of Findlay and Polanyi (Fig. 5.2).

Apart from this study, only Cabré and Henry have observed the relaxation of individual vibrational levels of HCl. The results are interesting in that $\tau_{exp}(v=3) < \tau_{exp}(v=2) < \tau_{exp}(v=1)$ (Table 5.2).

Table 5.2

Vibrational Relaxation Times of HCl at 550 K

Measured by Cabré and Henry[114] at 1 mm Hg pressure.

Vibrational Level	τ_{exp}/ms
v=1	4.2
v=2	3.9
v=3	3.4

but this may be reflecting a shorter value of τ_{rad} (Section 4.4). Further investigation of the relaxation of individual levels should be worthwhile. Hence an assessment was made of the feasibility of modifying the experimental conditions used in the present set of experiments so that actual Napier times could be measured.

In this study, the upper limit for the Napier time (0.6 atm μs at 1800 K) for the second vibrational level of HCl was measured using an initial shock tube pressure, P_1, of 1.3 mm Hg and using τ_{exp} = 2 μs (the rise time of the detector). To measure the actual Napier time (0.26 atm μs) at this temperature a reduction in P_1 by a factor of 5 to 10 would be adequate but the

light screens would not operate at these pressures. Alternative
techniques for shock detection would need to be employed but
even if they were available, such low initial pressure in tubes
of 50 mm diameter would make the results suspect.[115] A second
possibility lies in the use of the reflected shock region where
there is no "time compression effect" and experimental relaxation
times are converted to Napier times by

$$\tau = \tau_{exp} \cdot \frac{P_1}{760} \cdot \frac{P_5}{P_1} \qquad 5.14$$

Calculation of conditions in the reflected region show that for a
given temperature, $P_5/P_1 \approx 2P_2/P_1$ therefore since $\rho_2/\rho_1 \approx 6$, the
gain in resolution is by a factor of 3. To make the experimental
relaxation time longer than the rise time of the detector, it would
still be necessary to reduce the initial pressure by a factor of
2 or 3. However it is undesirable to work at pressures below a
few millimetres of mercury in the reflected shock region.[9]
Therefore it does not appear possible to measure the relaxation
time of pure HCl spectroscopically unless there is available a
detector with a faster rise time or a system which can operate
at lower pressures.

Figure 5·3 Napier Times of Pure HBr
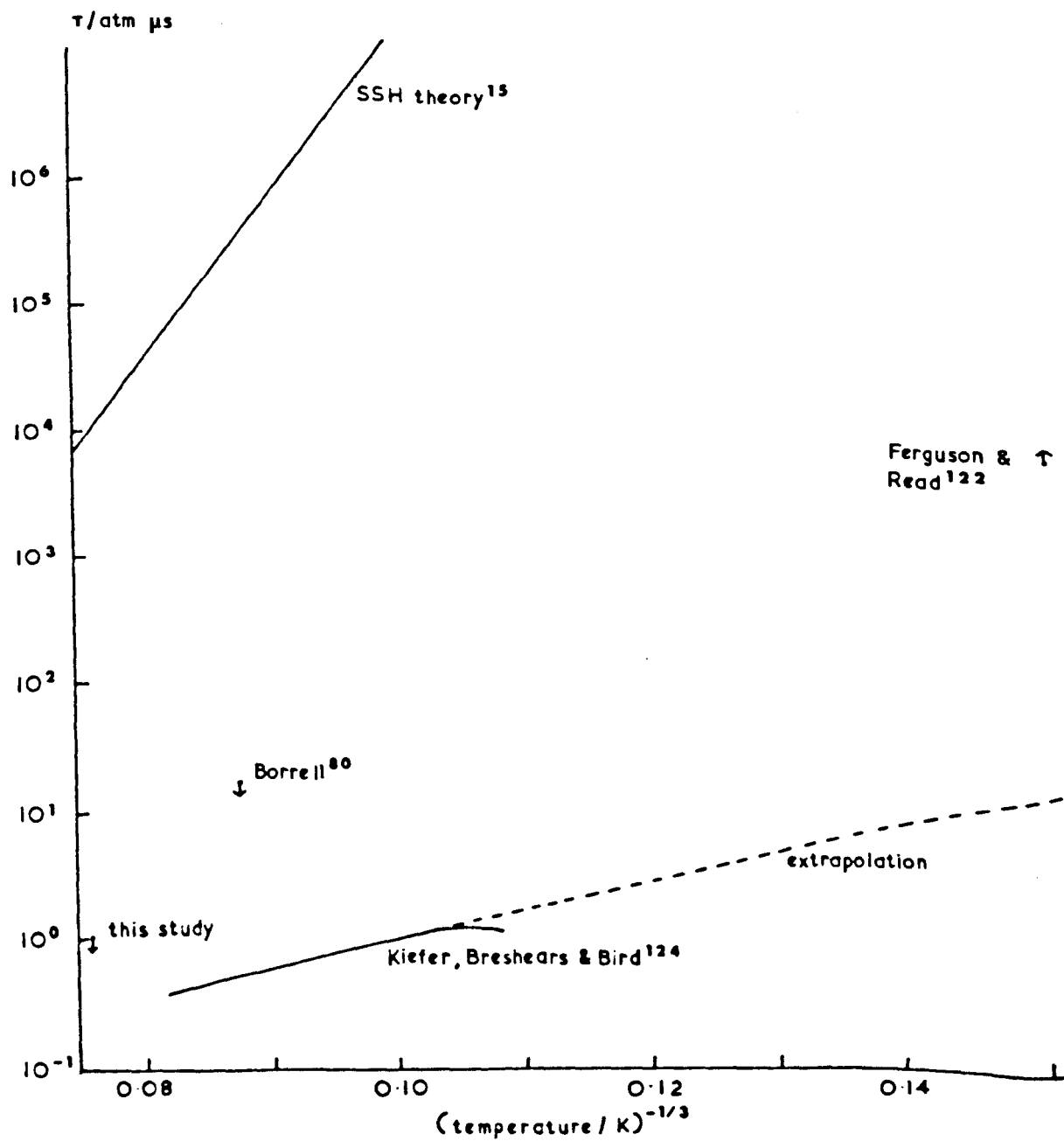
5.1.3   Relaxation Measurements of Pure HBr

This study set an upper limit for the Napier time of HBr at 2300 K of 1.0 atm μs (Section 3.1.3). As was the case with HCl, nothing could be deduced about the mechanism for populating the second vibrational level.

The previous measurements of 16 atm μs at 1000 K by Borrell[80] is now regarded as an upper limit.[106]

Subsequent measurements by Kiefer, Breshears and Bird[124] give a Napier time of 0.4 atm μs at 1800 K (Fig. 5.3). Linear extrapolation to low temperatures (Fig. 5.3) gives values which are much lower than the room temperature measurements of Ferguson and Read[122] who set a shorter limit of 1.5 atm ms (Fig. 5.3). It may be that their results suffer from errors similar to those experienced when observing HCl (Section 5.1.2).

Figure 3·7   Napier Times of Pure CO
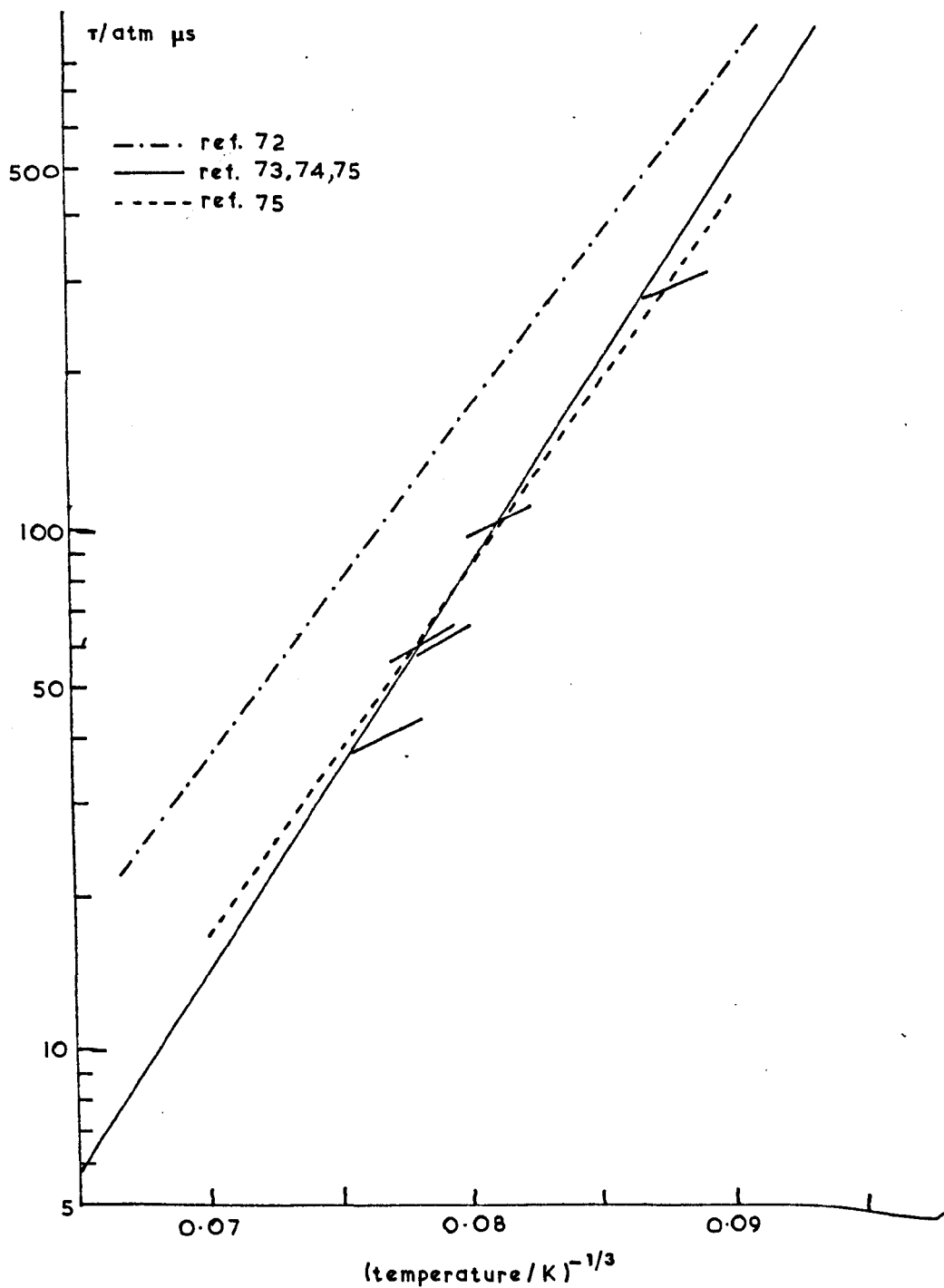
5.1.4   Relaxation Measurements of Pure CO

The Napier times of pure CO which were obtained in this study (Section 3.1.4) are not important in themselves but they were made to indicate whether the system was capable of handling a gas that is susceptible to low concentrations of impurities. Figure 3.7 (reproduced opposite) shows that the measurements are sufficiently close to the generally accepted values of Gaydon and Hurle,[74] Hooker and Millikan[75] and Matthews[73] to affirm this to be the case.

In this study, the experimental relaxation times were much longer than the rise time of the apparatus so it became possible to say from the shape of the trace something about the mechanism by which the second vibrational level was populated. In fact the deduced Napier times are based on the assumption of Windsor, Davidson and Taylor[72] that upper levels are populated by a stepwise mechanism (Section 5.1.1, schemes B or C). This assumption was investigated by Hooker and Millikan[75] who, by observing infrared radiation from both the first and second levels, deduced that more than 90% of molecules in the $v=2$ state obtained their energy by such a stepwise mechanism.

For the population to be due to direct excitation by a double quantum jump (Section 5.1.1, scheme A) the emission

would be of an exponential form and represented by equation 4.11. The traces however exhibit a "toe" (e.g. Fig. 3.6) and are found to be better represented by equation 4.17 which confirms the predominance of the stepwise mechanism.

5.1.5   Relaxation Measurements of HCl in Ar

A second method of finding the Napier time of HCl was tried by making measurements on HCl diluted by argon. With 5% HCl in Ar, the experimental relaxation times were longer than the rise time of the system (Table 3.4) but the intensity of the emission was so low that accurate measurements were not possible. Those that were made fell close to the recent lines of Bowman and Seery[125] (Fig. 3.10).

Even though measurements were not made for a range of concentrations, it is still possible to quote a shorter limit for $\tau_{HCl-HCl}$. The relaxation time for a mixture of HCl and Ar is given by

$$\frac{1}{\tau_{mix}} = \frac{1}{\tau_{HCl-HCl}} + \frac{1-x}{\tau_{HCl-Ar}} \qquad\qquad 5.15$$

where x is the mole fraction of HCl, $\tau_{HCl-HCl}$ the Napier time of the pure gas and τ_{HCl-Ar} an hypothetical Napier time for 1 molecule of HCl in pure Ar. By assuming $\tau_{HCl-Ar} = \infty$, a shorter limit for $\tau_{HCl-HCl}$ is found. If we use the results of run number 399 (Table 3.4) where $\tau_{mix} = 4.0$ atm μs at 1926 K and x = 0.05, then $\tau_{HCl-HCl} > 0.2$ atm μs at 1926 K. Coupled with the result for pure HCl (Section 5.1.2), the indication is that the true value for the Napier time of HCl is in the region 0.2

to 0.6 atm μs around 1850 K.

It is possible to suggest the part of the range in which the value probably lies by inserting into equation 5.17 a calculated value for τ_{HCl-Ar}. This is derived by SSH theory as the energy transfer must be between translational and vibrational modes. At 1870 K, τ_{HCl-Ar} is calculated to be 303 atm μs which leads to a value of $\tau_{HCl-HCl}$ of 0.202 atm μs giving close agreement with the measured value of Breshears and Bird (0.25 atm μs). Closer agreement would not be expected considering the accuracy of the measurements and calculations.

Figure 5.4 Napier Times of Pure HCl
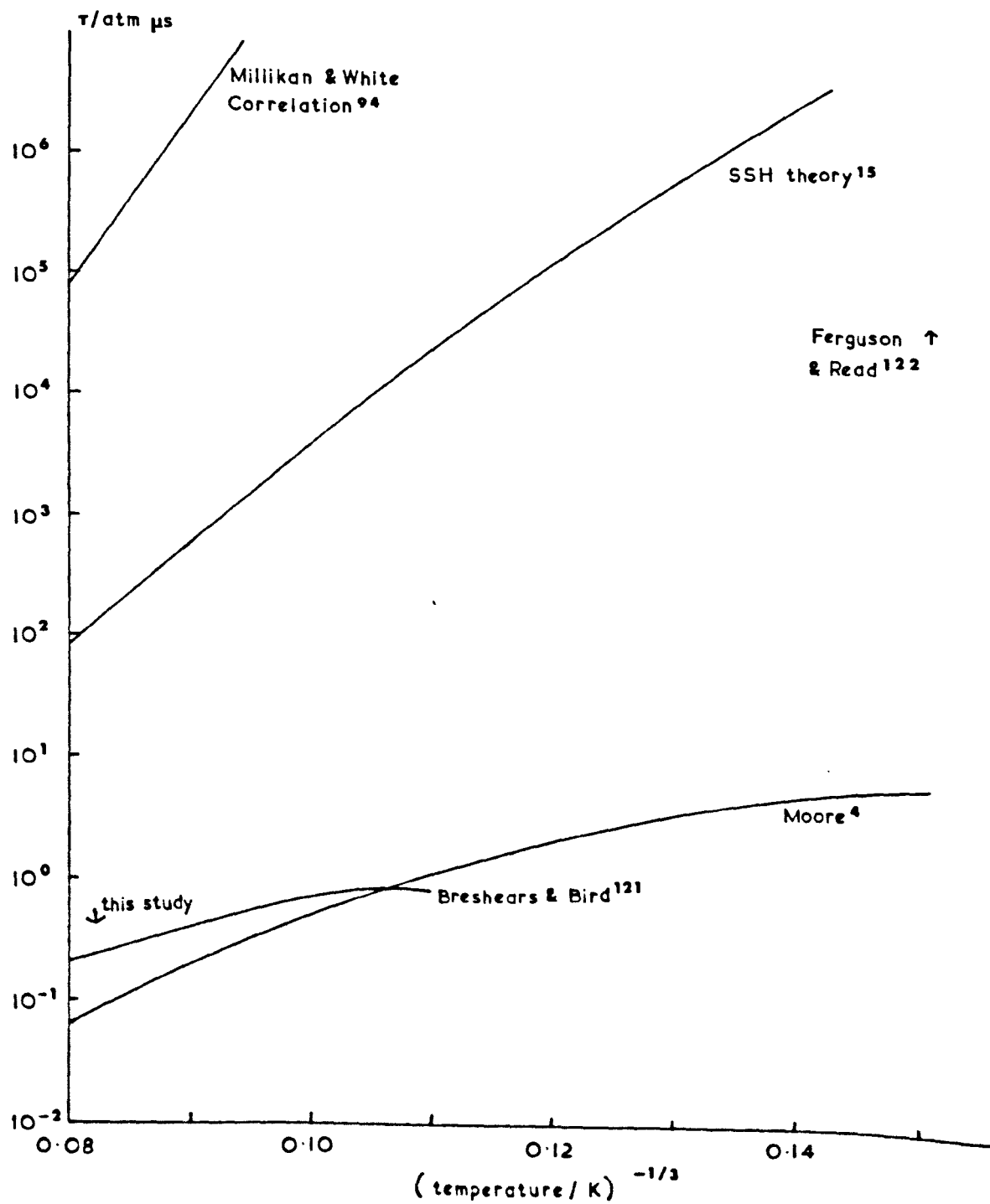
5.1.6   Comparison of Observations with Theory

Of the systems so far discussed, only pure CO exhibited a relaxation time that was much longer than the rise time of the system and hence only for CO is it possible to comment on the mechanism by which the second vibrational level was populated. The shape of the CO trace (Fig. 3.6) is consistent with the stepwise mechanism (equations 5.7 and 5.8 or 5.9) which had been demonstrated by Hooker and Millikan.[75]

Napier times are usually compared with the predictions of SSH theory[15] and often with the Millikan and White correlation[94] Millikan[60] took failure of the correlation as possibly indicating a mechanism different from the T → V energy transfer assumed in SSH theory. One alternative mechanism was considered by Moore[4] who calculated Napier times for energy transfer between rotational and vibrational modes. He thought that hydrogen halides, with their low moments of inertia and a peripheral atom of high velocity, would be molecules in which R → V energy transfer would be operative.

The three figures (5.4, 5.5 and 5.6) show measured and theoretical Napier times. Only that of CO is close to the prediction of SSH theory. Why it fails for HCl and HBr could be that the parameters used in the Lennard-Jones 12-6 equation do not adequately represent the intermolecular potential. De Wette

Figure 5.5 Napier Times of Pure HBr
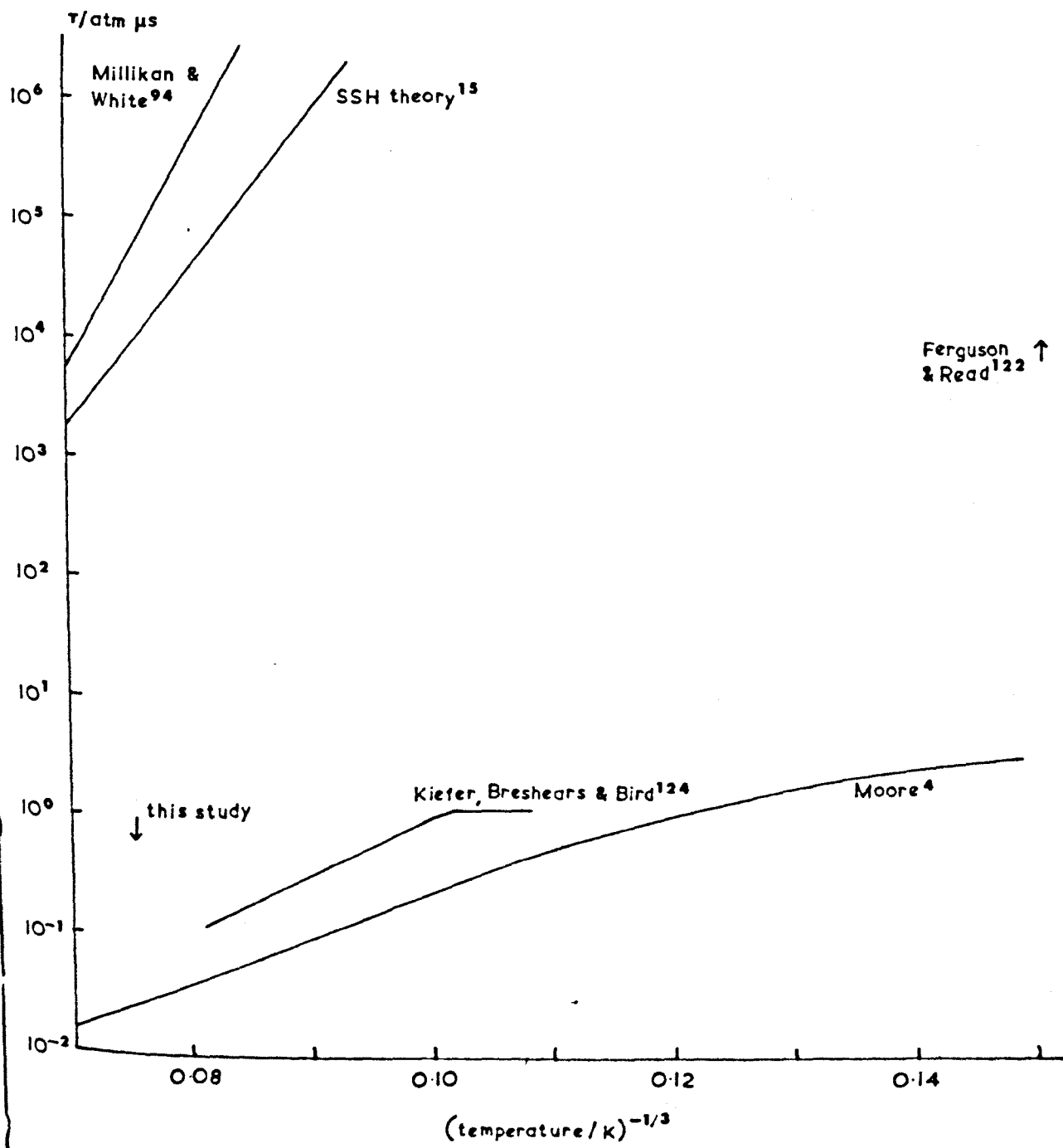
Figure 5.6 Napier Times of Pure CO
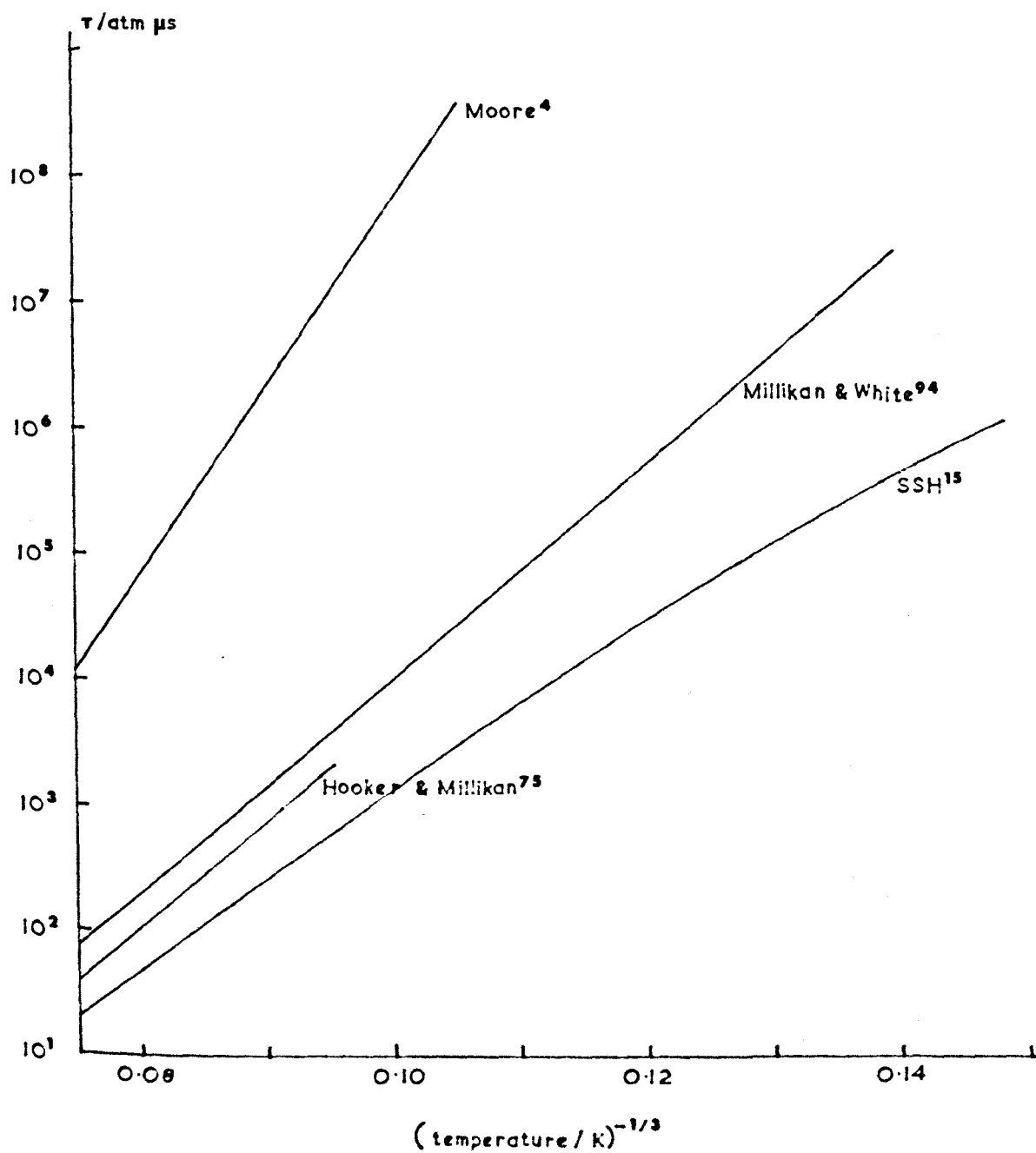
and Slawsky[126] have investigated the effect of dipole-dipole interaction concluding that for HCl, T → V transfer is four times more likely than the predictions of the usual SSH theory equations (the ones used in the above calculations). Such considerations do not substantially alter the poor correlation of experimental and theoretical Napier times for HCl and DCl. It seems more likely, considering the relative success of Moore's theory that the basic assumption of T → V energy transfer is incorrect and that R → V energy transfer is important.

Moore's failure to predict accurately could be due to his treating rotational energy levels as continuous and not quantised. The large gaps between the rotational energy levels of hydrogen halides would be expected to reduce the efficiency of R → V transfer but if this were the only cause, the discrepancy between theory and experiment should be greatest for HCl and least for HI. The reverse order is found in practice.[127] Part of the error is liable to arise from the intermolecular potential parameter which Moore takes as constant, being the average for many molecules in which the R → V mechanism is probable.[4] This is improbable for the hydrogen halides and points to the need for a more rigorous quantum mechanical treatment, such as the one by Sharma.[128]

Additional support to Moore's assumption of R → V

energy transfer is given by the deuterated halides which all have Napier times longer than their hydrogen analogue.[127] This behaviour is predicted by Moore contrasting sharply with the predictions of SSH theory.

In summary it can be said that the short Napier times found by this study are consistent with R → V energy transfer being important for HCl and HBr.

5.2   Relaxation of Bimolecular Mixtures of Diatomic Molecules

5.2.1   Introduction

Three systems in this category were investigated: HCl in N_2, HCl in CO and HBr in CO. These will be considered separately and then related to each other and more recent results will be discussed.

A problem in monitoring the emission of the last two pairs of molecules is that both components radiate. Experience with HCl in N_2 showed that the contribution of the minor component to the total monitored emission would be negligible. Temperatures in excess of 2000 K were needed for infrared radiation to be observed and only at 2500 K was it appreciable. In the mixtures with CO, temperatures were kept below 2000 K.

5.2.2 Reaction Scheme

A diatomic diluent can act in the same way as a monatomic diluent (Section 5.1) and by exchanging vibrational energy with the other diatomic molecule. For a pair of two state components, A and B, five reactions are possible.

$$A + A_0 \underset{k_1}{\overset{k_1}{\rightleftarrows}} A + A_1 \qquad\qquad 5.16$$

$$B + A_0 \underset{k_2}{\overset{k_2}{\rightleftarrows}} B + A_1 \qquad\qquad 5.17$$

$$A + B_0 \underset{k_3}{\overset{k_3}{\rightleftarrows}} A + B_1 \qquad\qquad 5.18$$

$$B + B_0 \underset{k_4}{\overset{k_4}{\rightleftarrows}} B + B_1 \qquad\qquad 5.19$$

$$A_0 + B_1 \underset{k_5}{\overset{k_5}{\rightleftarrows}} A_1 + B_0 \qquad\qquad 5.20$$

For multistate systems, the number of possible reactions is very much larger. However it is assumed that the Napier times measured using second level emission are the same as would be obtained if it were first level emission that were monitored. Verification of this would be valuable.

5.2.3 Relaxation Equations

Bauer[129] has shown that the reaction scheme in Section 5.2.1 can be represented by the equation

$$\left\{ \frac{1}{\tau} - (1 + \frac{c_{A1}}{c_{A0}}) \left[k_1' X_A + (k_2' + \frac{k_5'}{1+c_{B1}/c_{B0}}) X_B \right] \right\}$$

$$\times \left\{ \frac{1}{\tau} - (1 + \frac{c_{B1}}{c_{B0}}) \left[(k_3' + \frac{k_5}{1+c_{A1}/c_{A0}}) X_A + k_4' X_B \right] \right\}$$

$$- k_5 k_5' X_A X_B = 0 \qquad\qquad 5.21$$

τ is the measured relaxation time

X_A, X_B are the mole fractions of A and B

c_{A1}, c_{A0} are the concentrations of A in states
        1 and 0 respectively.

The equation is a quadratic in $\frac{1}{\tau}$ and the mole fraction X_A or X_B. Since $X_A + X_B = 1$, equation 5.21 represents a conic section. The end points are for the pure gases:

for pure A, $X_B \to 0$

$$\tau_{AA}^{-1} = (1 + c_{A1}/c_{A0})k_1' \qquad\qquad 5.22$$

$$\tau_{BA}^{o \; -1} = (1 + c_{B1}/c_{B0})[k_3' + k_5/(1 + c_{A1}/c_{A0})] \qquad\qquad 5.23$$
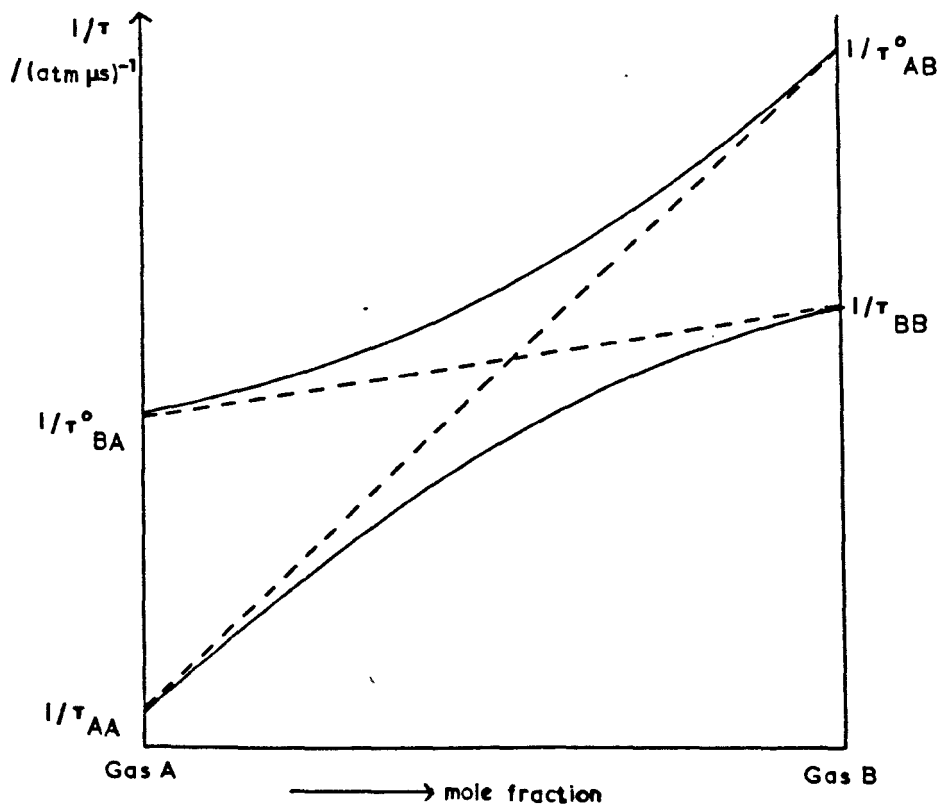
Figure 5.7 A Typical Conic Section

for pure B, $X_A \to 0$

$$\tau_{AB}^{o\ -1} = (1 + c_{A1}/c_{A0})[k_2' + k_5' (1 + c_{B1}/c_{B0})] \qquad 5.24$$

$$\tau_{BB}^{-1} = (1 + c_{B1}/c_{B0})k_4' \qquad 5.25$$

where τ_{AA}, τ_{BB} are the relaxation times for the pure gases and τ_{AB}^{o} is the relaxation time for 1 molecule of A in pure B and includes relaxation by T, R $\to$ V and V $\to$ V processes. Hence it differs from τ_{AB} which is a hypothetical value involving only T, R $\to$ V processes.

The four expressions (5.22 to 5.25) can be substituted in equation 5.21 to give

$$[\frac{X_A}{\tau_{AA}} + \frac{X_B}{\tau_{AB}^o} - \frac{1}{\tau}]\ [\frac{X_B}{\tau_{BA}^o} + \frac{X_B}{\tau_{BB}} - \frac{1}{\tau}]\ - k_5 k_5' X_A X_B = 0 \qquad 5.26$$

A typical conic section given by 5.21 is shown in figure 5.7.

For $k_5 = 0$ when there is no V-V exchange and equation 5.26 gives a degenerate conic section viz. the pair of straight lines

$$\frac{1}{\tau_1} = \frac{X_A}{\tau_{AA}} + \frac{X_B}{\tau_{AB}} \qquad 5.27$$

$$\frac{1}{\tau_2} = \frac{X_A}{\tau_{BA}} + \frac{X_B}{\tau_{BB}} \qquad 5.28$$

In this case, $\tau_{AB} = \tau_{AB}^{o}$ and $\tau_{BA} = \tau_{BA}^{o}$. Both molecules approach equilibrium exponentially and with their own relaxation time.

The other extreme case is when the V-V process is extremely
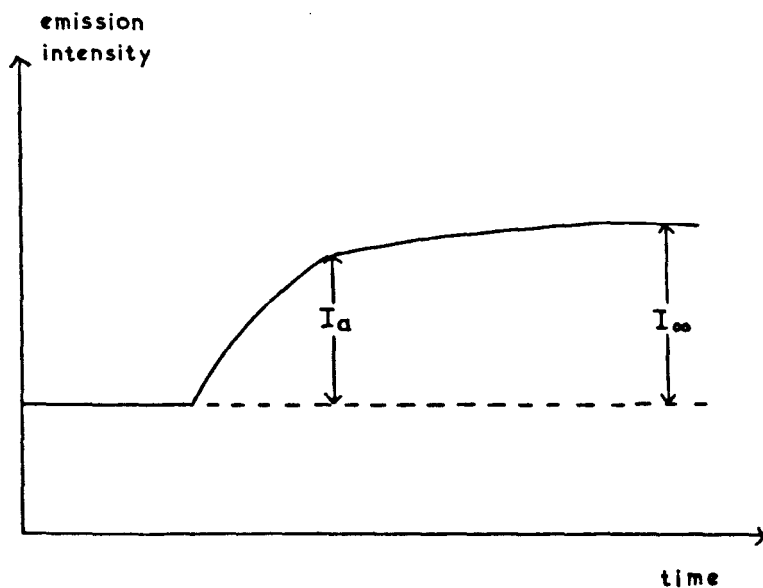
Figure 5.8 Schematic Oscillogram for the Faster Relaxing Component in a Bimolecular Gas Mixture. $a = I_a/I_\infty$

efficient i.e. $k_5 \rightarrow \infty$. Sato, Tsuchiya and Kuratani (STK)[130] shows that in this case, both molecules approach equilibrium with the same relaxation time, τ, and this is given by

$$\tau^{-1} = X_A \tau_{AA}^{-1} + X_B \tau_{BB}^{-1} \qquad 5.29$$

Apart from these two extreme cases, the relaxation of each molecule cannot be defined by a single relaxation time but may be regarded as a coupled case of two relaxation processes. STK[130] have shown that for the slow relaxing gas, the difference between the theoretical behaviour and a simple relaxation process is small so that in practice it can be missed. This was the case with Taylor, Camac and Feinberg (TCF)[85] in their work on N_2/NO and CO/NO mixtures. The coupling of two relaxation processes is more marked for the faster relaxing component and a schematic emission trace is shown in figure 5.8. TCF define a parameter α as indicated in the caption. STK have shown that

$$\alpha = 1/(1 + r) \qquad 5.30$$

where

$$r = (a'' + b')/(\tau_B^{-1} - \tau_A^{-1}) \tau_{AB}^v \exp(\theta_B - \theta_A) \qquad 5.31$$

$$a'' = X_A \exp(\theta_B - \theta_A) [1 - \exp(-\theta_B)]/[1 - \exp(-\theta_A)] \qquad 5.32$$

$$b' = X_B [1 - \exp(-\theta_A)]/[1 - \exp(-\theta_B)] \qquad 5.33$$

$$\tau_B^{-1} = X_A \tau_{BA}^{-1} + X_B \tau_{BB}^{-1} \qquad 5.34$$

$$\tau_A^{-1} = X_A \ \tau_{AA}^{-1} + X_B \ \tau_{AB}^{-1} \qquad\qquad 5.35$$

τ_{AB}^v is the relaxation time for the V-V process 5.20. Hence by knowing or assuming the necessary parameters, it is possible to obtain a value for τ_{AB}^v from α. This is done for the measurements of HCl in N_2.

Often it is only possible to make measurements near one end of the curve e.g. when a small amount of diluent greatly increases the rate of relaxation. This was the case for the CO/HCl and CO/HBr mixtures. For these situations, it is convenient to use a Taylor series expansion of the conic section in that range.[131] For small X_B

$$\frac{1}{\tau} = \frac{1}{\tau_{AA}} + W_1 X_B + W_2 X_B^2 + \ldots \qquad\qquad 5.36$$

where

$$W_1 = k_2' - k_1' + [k_5 k_3'/(k_5' + k_3')] \qquad\qquad 5.37$$

$$W_2 = k_5 k_5' (k_4' - W_1)/(k_5' + k_3')^2 \qquad\qquad 5.38$$

This expansion was used for the mixtures of HCl in CO and HBr in CO.

5.2.4   The Relaxation of Hydrogen Chloride Diluted by Nitrogen

Hydrogen chloride was expected to speed up the relaxation of N_2 by causing HCl $\rightarrow$ N_2 collisions which would, considering the relaxation of pure HCl, be more effective than N_2 $\rightarrow$ N_2 collisions in converting translational or rotational to vibrational energy. By comparison with pure N_2, N_2 $\rightarrow$ HCl collisions will be less effective than HCl $\rightarrow$ HCl collisions and hence the relaxation of HCl will be slowed down. The possibility of vibrational energy exchange from the fast relaxing HCl to the slow relaxing N_2 would emphasise these tendencies.

The results show that 10% HCl in N_2 still relaxes too fast (section 3.3.1) for precise measurements to be made. Figure 3.11 shows that the relaxation of HCl is rapid initially but slower to achieve equilibrium than when a pure gas. This could be due to V$\rightarrow$V energy exchange; similar featured traces are observed by TCF for NO/N_2 and NO/CO mixtures.

Table 5.3

Values of α for pairs of relaxing molecules
($\sim$10% molecule 1 in molecule 2, $\tau \overset{\sim}{\sim} 2300^{\circ}$K).

Molecule 1	Molecule 2	$\Delta\bar{\upsilon}/cm^{-1}$	α	Reference
NO	CO	267	0.1	85
NO	N_2	456	0.6	85
HCl	N_2	556	0.9	this study

The experimental value of α (see Figure 5.8) found in this study (Table 5.3) correlates with the large $\Delta\bar{\nu}$ and ~~infers~~ *implies* relatively inefficient V→V energy transfer. This is in agreement with the fact that dilution by N_2 fails to drastically increase the relaxation time of HCl.

Recent work by Breshears and Bird[132] and Chen and Moore[123] suggests that some of the foregoing assumptions are incorrect and that the relaxation of N_2 by HCl will be slow but of HCl by N_2 fast. They suggest that it is the rotational motion of the activated vibrator which results in some systems relaxing much more rapidly than SSH theory predicts.

To obtain an idea of the order of magnitude of the V→V relaxation process at 2300°K, equation 5.26 was used taking $\tau_{N_2-N_2}$ as 309 µs and $\tau_{HCl-HCl}$ as 0.16 µs. By analogy with the work on HI/N_2, it was assumed that $\tau_{N_2-HCl} \to \infty$ and $\tau_{N_2-HCl}/\tau_{HCl-HCl} = \tau_{N_2-HI}/\tau_{HI-HI}$. This lead to a value for τ_{N_2-HCl} of 8 atm µs which is roughly the same of that for the HI/N_2 system (8.3 atm µs) measured by Breshears and Bird.[132] A slightly longer time would be expected because of the larger energy gap between the pairs of molecules but errors in experimental measurements and in the assumptions made could well mask such an effect.

Figure 5.9 Reciprocal Napier Times for HCl / CO Mixtures
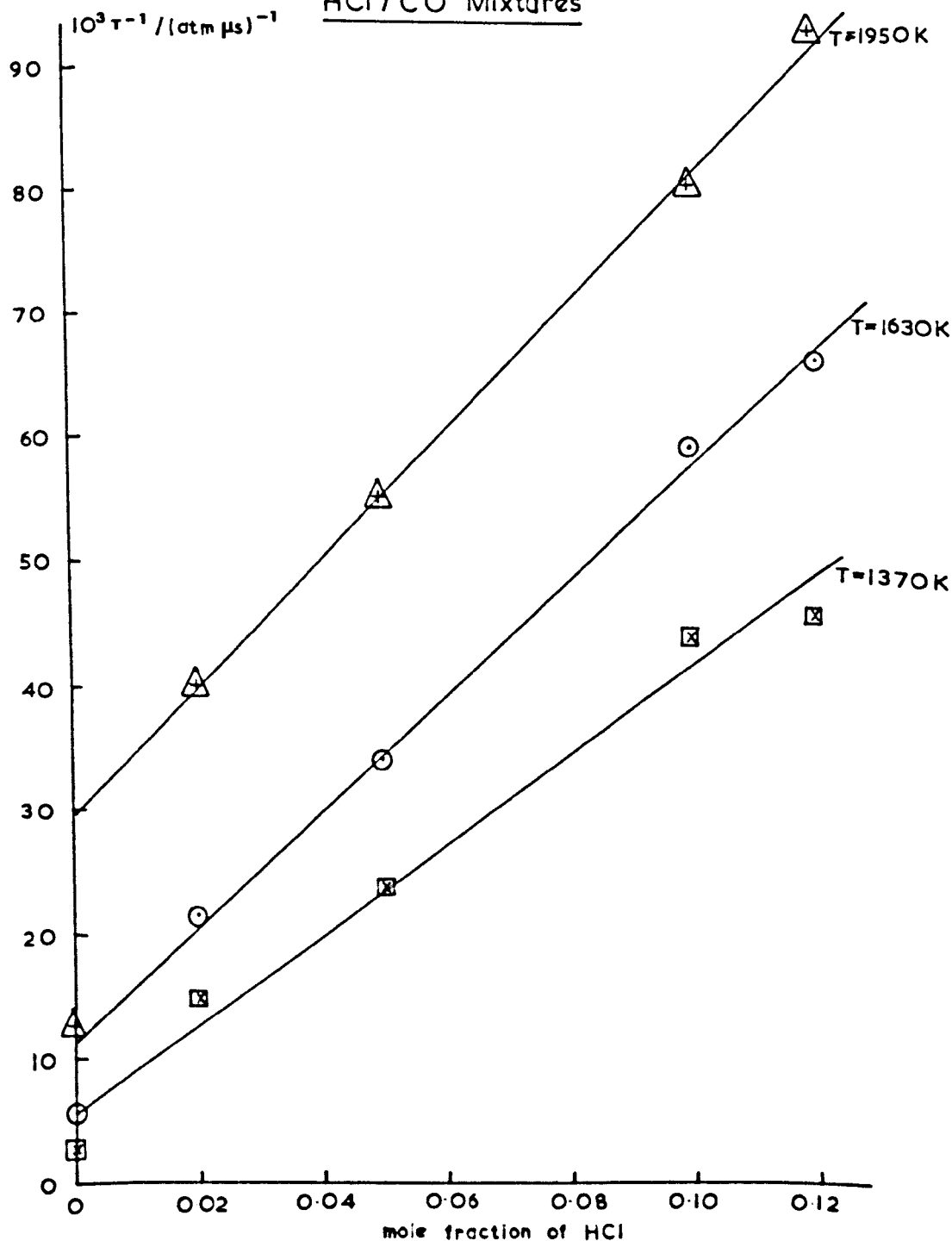
The relaxation measurements for 10% HCl were made in collaboration with P.M. Borrell.

5.2.5 The Relaxation of CO with Added HCl

In these gas mixtures, CO was the predominant component and
the observations made were taken as showing the relaxation of CO
in the presence of small amounts of HCl.

The measurements show (Figures 3.14 to 3.18 and Tables 3.6
to 3.10) that only small amounts of the halide are needed to
considerably accelerate the rate at which CO relaxes. The graphs
for the low concentration of HCl exhibit some curvature but if a
straight line is drawn through the points, the results can be
represented by the following equations over the temperature range
1300-2000 K.

2%   HCl in CO: $\log_{10} \tau$ (atm s) = 40.7 $T^{-\frac{1}{3}}$ - 7.82   5.39

5%   HCl in CO: $\log_{10} \tau$ (atm s) = 35.8 $T^{-\frac{1}{3}}$ - 7.57   5.40

10% HCl in CO: $\log_{10} \tau$ (atm s) = 24.0 $T^{-\frac{1}{3}}$ - 6.80   5.41

Such fast relaxation times could result from efficient T→V, R→V or
V→V processes.

Section 5.2.3 shows that if V→V energy transfer occurs, then
a plot of the reciprocal relaxation time versus the mole fraction of
HCl should be curved. Values of τ at 3 temperatures, 1950, 1630 and
1370 K (corresponding to $T^{-\frac{1}{3}}$ = 0.080, 0.085 and 0.090 respectively)
were taken from Figures 3.14, 3.15 and 3.17 and plotted against
x_{HCl} (Figure 5.9).

The points for $x_{HCl} > 0$ lie on fairly good straight lines and these were drawn in. In subsequent calculations it can be seen that it is the gradient of the graph which is the important parameter and it was felt that drawing these lines would represent the situation better than including the point for $x_{HCl} = 0$ (i.e. pure CO). It was believed that the difference in the two positions reflected the result of impurity which had entered the system in spite of the precautions taken. Its effect should remain small compared with the effect due to HCl.

There was no curvature in the expected direction which signifies (i) there is no V→V exchange or (ii) the range of x_{HCl} over which measurements were taken is too small to show up the curvature. The two cases are considered.

(i) No V→V exchange

In this case, the form of the line should be given by equation 5.27 viz.

$$\frac{1}{\tau} = \frac{1-x}{\tau_{CO-CO}} + \frac{x}{\tau_{CO-HCl}}$$

(x is the mole fraction of HCl)

which can be rearranged to give

$$\frac{1}{\tau} = x \left[\frac{1}{\tau_{CO-HCl}} - \frac{1}{\tau_{CO-CO}} \right] + \frac{1}{\tau_{CO-CO}} \qquad 5.42$$

Knowing τ_{CO-CO}, τ_{CO-HCl} was calculated from the gradients. The results are given in Table 5.4.

<div align="center">Table 5.4</div>

Napier times for CO/HCl mixtures assuming no V→V exchange

$(T/K)^{-\frac{1}{3}}$	T/K	τ_{CO-HCl}/atm μs
0.080	1950	2.0
0.085	1630	2.2
0.090	1370	2.7

These fast relaxation times would explain the observations and would be expected on a mechanistic basis by comparison with the results for pure HCl (Figure 5.4). Calculations using Moore's theory[4] also indicate that τ_{CO-HCl} will be fast. However these results are unlikely to represent the situation for V→V transfer is probable. Recent work[132] would support this and further suggest that τ_{CO-HCl} will be long and τ_{HCl-CO} short.

For a straight line, w_1 = gradient and w_2 = 0. Hence from equation 5.37,

gradient $= w_1 = k_2' - k_1' + [k_5 k_5'/(k_5' + k_3')]$

In this sytem $k_1 = k_{CO-CO}$ (T,R→V), $k_2 = k_{CO-halide}$ (T,R→V)

Figure 5.10 Graph of k_3' v. k_5 for Mixtures of HCl with CO at 1950 K

$k_3'/(atm \, \mu s)^{-1}$

assymptotes

$k_5/(atm \, \mu s)^{-1}$
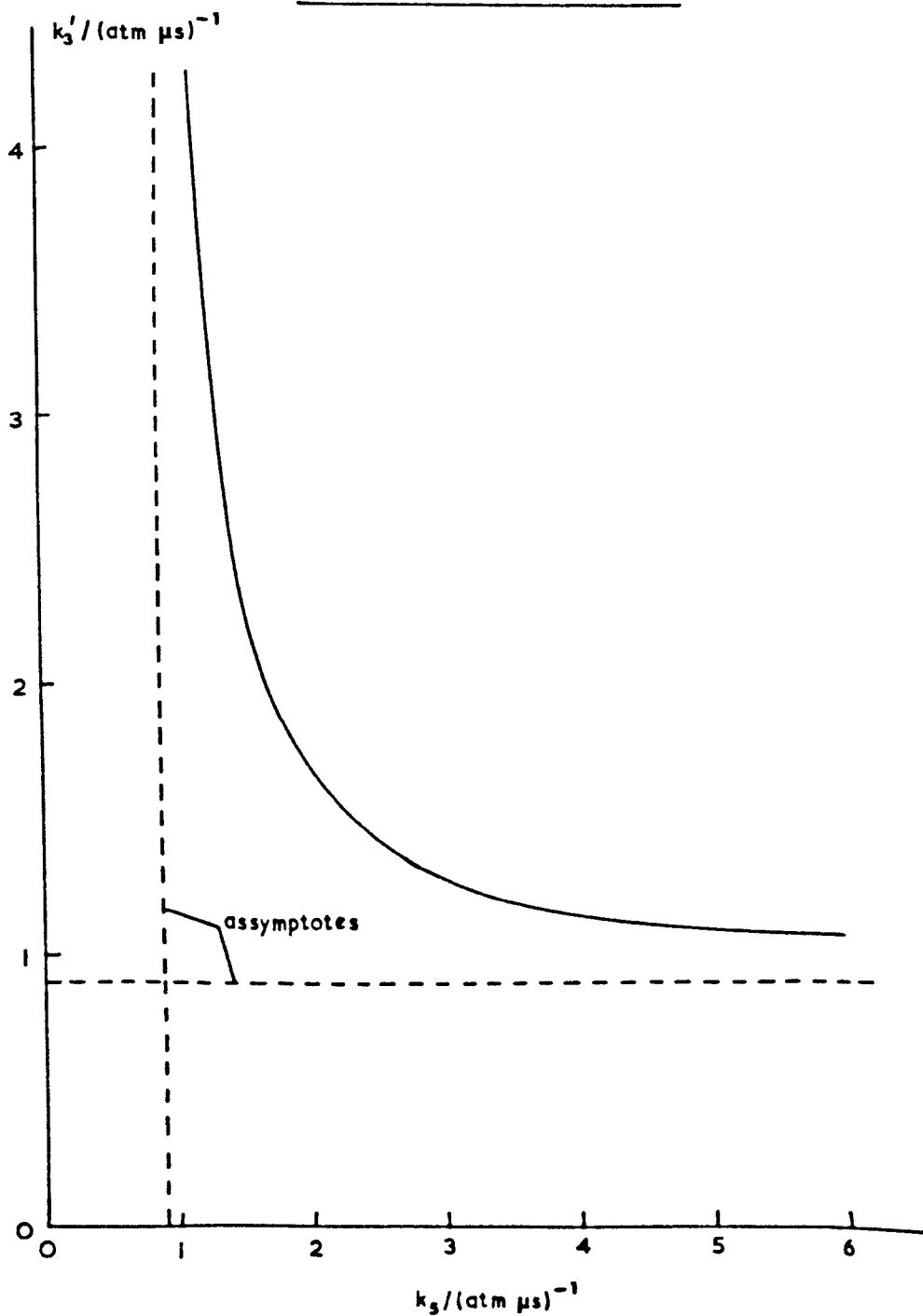
$k_3 = k_{halide-CO}$ $(T,R{\rightarrow}V)$, $k_4 = k_{halide-halide}$ $(T,R{\rightarrow}V)$ $k_5 = k_{halide-CO}$ $(V{\rightarrow}V)$.

From the work of Breshears and Bird[132] it seems reasonable to assume that since $k_2' \sim k_1' \ll [k_5 k_5'/(k_5' + k_3')]$ and

$$k_5' = k_5 \exp [-hc (\bar{\nu}_2 - \bar{\nu}_1)/kT] = yk_5$$

then equation 5.37 can be rearranged to give

$$k_5 = \frac{w_1 k_3'}{yk_3' - w_1} \qquad\qquad 5.43$$

Hence a range of corresponding values of k_5 and k_3' can be calculated. These have been plotted for one temperature (1950 K), (Figure 5.10). The assymptotes give the values of the alternative rate constant as $k_3' \rightarrow \infty$ and $k_5 \rightarrow \infty$. The asymptotic values of k_3' and k_5 are equal.

At lower temperatures, the graph of k_3' vs. k_5 has the same shape but displaced, together with its assymptotes, towards the origin. For T = 1950 K, the assymptotic values are 0.90 $(atm\ \mu s)^{-1}$, at T = 1630 K 0.88 $(atm\ \mu s)^{-1}$, and at 1370 K 0.80 $(atm\ \mu s)^{-1}$.

The upper limit for k_3' is taken to be equal to k_4' as it seems more reasonable that HCl will relax in the presence of CO more slowly than with itself.

A lower limit for k_3' can be set by considering the maximum value of w_2 which is insufficient to show curvature. Nonlinearity

would have been observed if the final value of $\frac{1}{\tau}$ was 0.01 above the line and this would be the value of

$$w_2 x^2 \quad (x = 0.12) \quad \text{[eqn. 5.36]}$$

Therefore $\quad w_2 x^2 < 0.01$

so $\quad w_2 \quad < 0.695$

But $w_2 = k_5 k_5' (k_4' - w_1)/(k_5' + k_3')^2$ $\qquad\qquad$ 5.38

and $\quad k_5' = y k_5$

so $\qquad \dfrac{y (k_4' - w_1)}{(y + \dfrac{k_3'}{k_5})^2} \quad < \quad 0.695$

which yields

$$\frac{k_3'}{k_5} \quad > \quad \sqrt{\frac{y(k_4' - w_1)}{0.695}} \quad - \quad y$$

But since $\quad k_5 = \dfrac{w_1 k_3'}{y k_3' - w_1}$, limiting values of

k_3' and k_5 can be calculated.

Figure 5.11 Napier Times for HCl / CO Mixtures
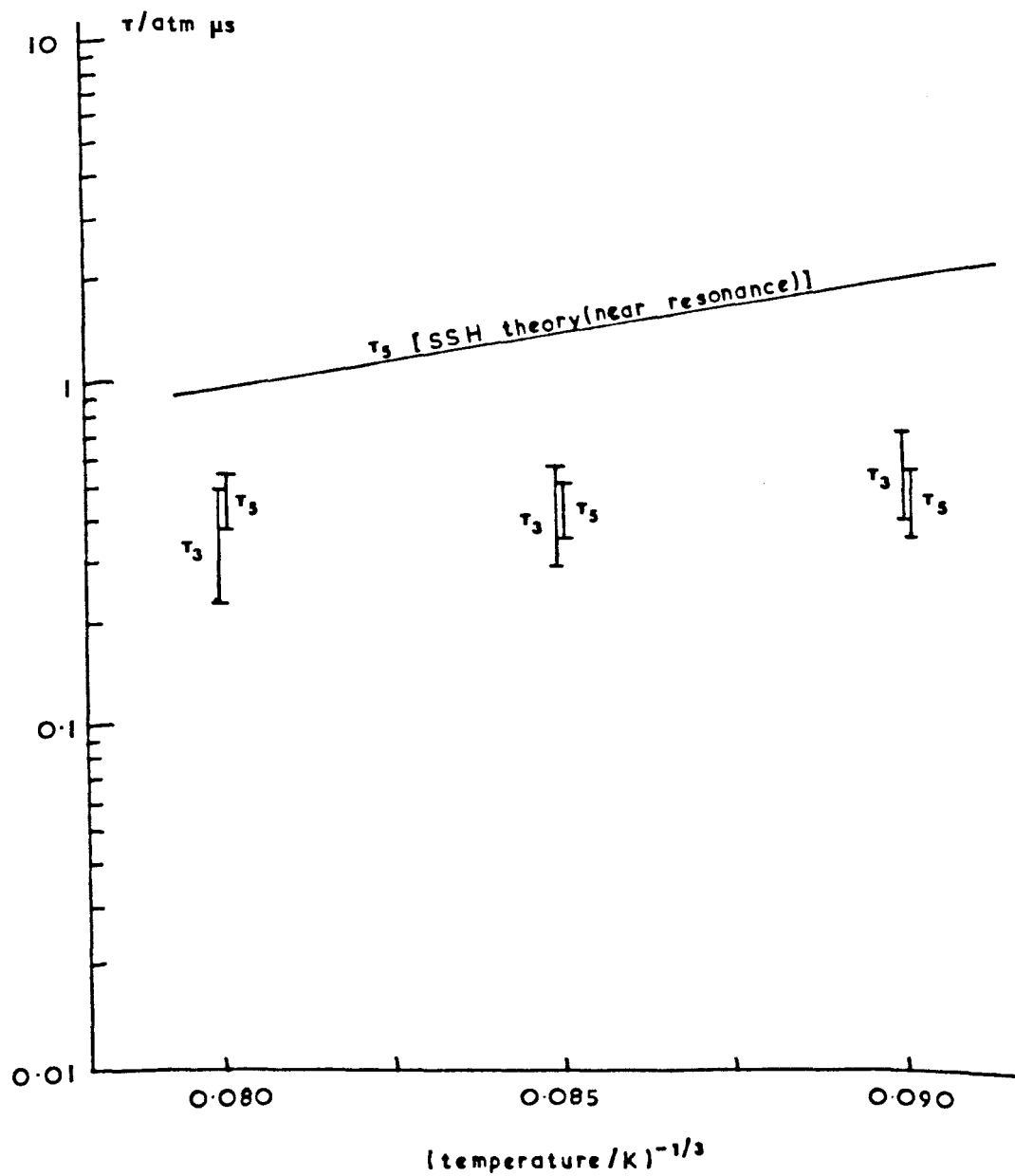
Table 5.5

Limiting Values of k_3' and k_5

T/K	$k_3'/(atm\ \mu s)^{-1}$	$k_5/(atm\ \mu s)^{-1}$
1950	2.0 – 4.4	1.6 – 1.1
1630	1.7 – 3.4	1.8 – 1.2
1370	1.4 – 2.5	1.9 – 1.2

Table 5.6

Napier times derived from the rate constants in Table 5.5

T/K	$\tau_3/atm\ \mu s$	$\tau_5/atm\ \mu s$	$\tau_5/atm\ \mu s$ (SSH theory)
1950	0.50 – 0.23	0.38 – 0.56	1.0
1630	0.58 – 0.30	0.36 – 0.53	1.4
1370	0.72 – 0.40	0.36 – 0.58	2.0

The usual relaxation time versus temperature graph (Figure 5.11) does show whether the temperature dependence of $\log \tau_3$ or $\log \tau_5$ is either positive or negative. It can be seen however that the temperature

dependence of either is not great and for τ_5 must be slightly less than predicted by SSH theory using the equations suitable for near resonance conditions. The theory does predict a slower relaxation rate than the experiments indicate and this could be due to the assumption that the vibrational energy difference between the two molecules is converted into translational motion. For this to be true, the speed of the molecules after the collision would need to be very high. In the reaction

$$HCl* \ + \ CO \ \rightarrow \ CO* \ + \ HCl \ + \ \Delta E \qquad\qquad 5.44$$

some energy could be converted into rotational motion of the halide which could well be an easier process. On the whole agreement is reasonable.

Theoretical predictions of τ_3 (τ_{HCl-CO}) are not good. The failure of SSH theory could be due to their only considering T$\rightarrow$V energy transfer whereas the velocity of the hydrogen atom in HCl is greater than that of the molecule as a whole. On the other hand, Moore's theory may fail (τ_3 = 342 atm s at 1370 K, τ_3 = 5.5 atm s at 1950 K) because he only considers the rotational velocity of the activating molecule. Experiments have indicated[123,132] that it may be the rotational motion of the activated molecule which has a greater effect.

Figure 5.12 Reciprocal Napier Times for
HBr/CO Mixtures
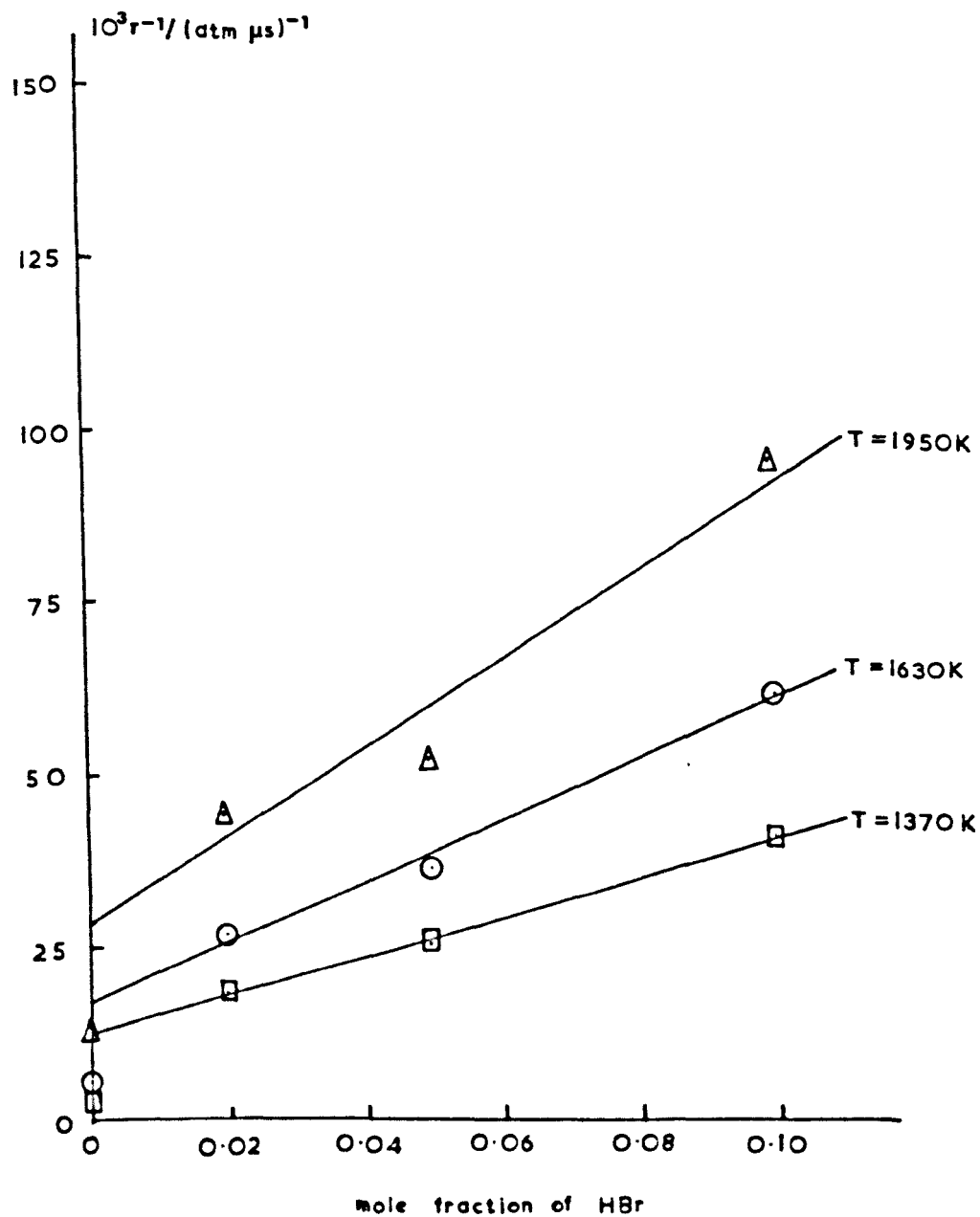
5.2.6   The Relaxation of CO with added HBr

In these gas mixtures CO was the predominant component and the observations made were taken as showing the relaxation of CO in the presence of small amounts of HBr.

The measurements (Figures 3.20 to 3.22 and Tables 3.11 to 3.13) show that only small amounts of HBr are needed to accelerate considerably the rate at which CO relaxes. The results are summarised below.

% HBr in CO	Temperature range: 1300-2000 K	
0	$\log \tau(\text{atm s}) = 69.5\ T^{-\frac{1}{3}} - 9.65$	5.45
2	$\log \tau(\text{atm s}) = 33.6\ T^{-\frac{1}{3}} - 7.31$	5.46
5	$\log \tau(\text{atm s}) = 31.8\ T^{-\frac{1}{3}} - 7.27$	5.47
10	$\log \tau(\text{atm s}) = 32.0\ T^{-\frac{1}{3}} - 7.50$	5.48

Such an increase in the rate of relaxation could be due to efficient $T \rightarrow V$, $R \rightarrow V$ or $V \rightarrow V$ processes.

Analysis of the results followed a pattern similar to that used for CO/HCl mixtures. Figure 5.12 corresponds to Figure 5.9 in the CO/HCl measurements.

(i)   Assuming no $V \rightarrow V$ exchange

Table 5.7

Napier times for CO/HBr mixtures assuming no V→V exchange

$(T/K)^{-\frac{1}{3}}$	T/K	τ_{CO-HBr}/atm µs
0.080	1950	1.5
0.085	1630	2.3
0.090	1370	3.5

As for CO/HCl mixtures, these fast relaxation times would account for the fast relaxation of CO in the presence of HBr and they would be expected from Moore's theory.[4] Reference to recent work[132] would again suggest that V→V transfer will occur, τ_{CO-HBr} being long and τ_{HBr-CO} short.

(ii) With V→V exchange

Following the analysis used for CO/HCl mixtures leads again to equation 5.43 viz.

$$k_5 = \frac{w_1 k_3'}{y k_3' - w_1}$$

Plotting values of k_3' versus k_5 calculated from it gives curves the same shape as that for CO/HCl (Figure 5.10) but with the following assymptotes: for T = 1950 K at 0.85 (atm µs)$^{-1}$, for

T = 1630 K at 0.62 (atm μs)$^{-1}$, for T = 1370 K at 0.44 (atm μs)$^{-1}$.

Upper and lower limits for k_3' were set using the criteria adopted previously and these, together with the corresponding values of k_5 are given in Table 5.8

Table 5.8

Limiting Values of k_3' and k_5

T/K	$k_3'/$(atm μs)$^{-1}$	$k_5/$(atm μs)$^{-1}$
1950	1.4 - 2.5	2.1 - 1.3
1630	1.0 - 2.2	1.6 - 0.9
1370	0.7 - 1.7	1.3 - 0.6

Table 5.9

Napier times derived from the above rate constants

T/K	$\tau_3/$atm μs	$\tau_5/$atm μs	$\tau_5/$atm μs (SSH theory)
1950	0.70 - 0.40	0.27 - 0.44	0.22
1630	0.99 - 0.46	0.37 - 0.68	0.29
1370	1.52 - 0.59	0.47 - 1.04	0.39

Figure 5.13 Napier Times for HBr/CO Mixtures
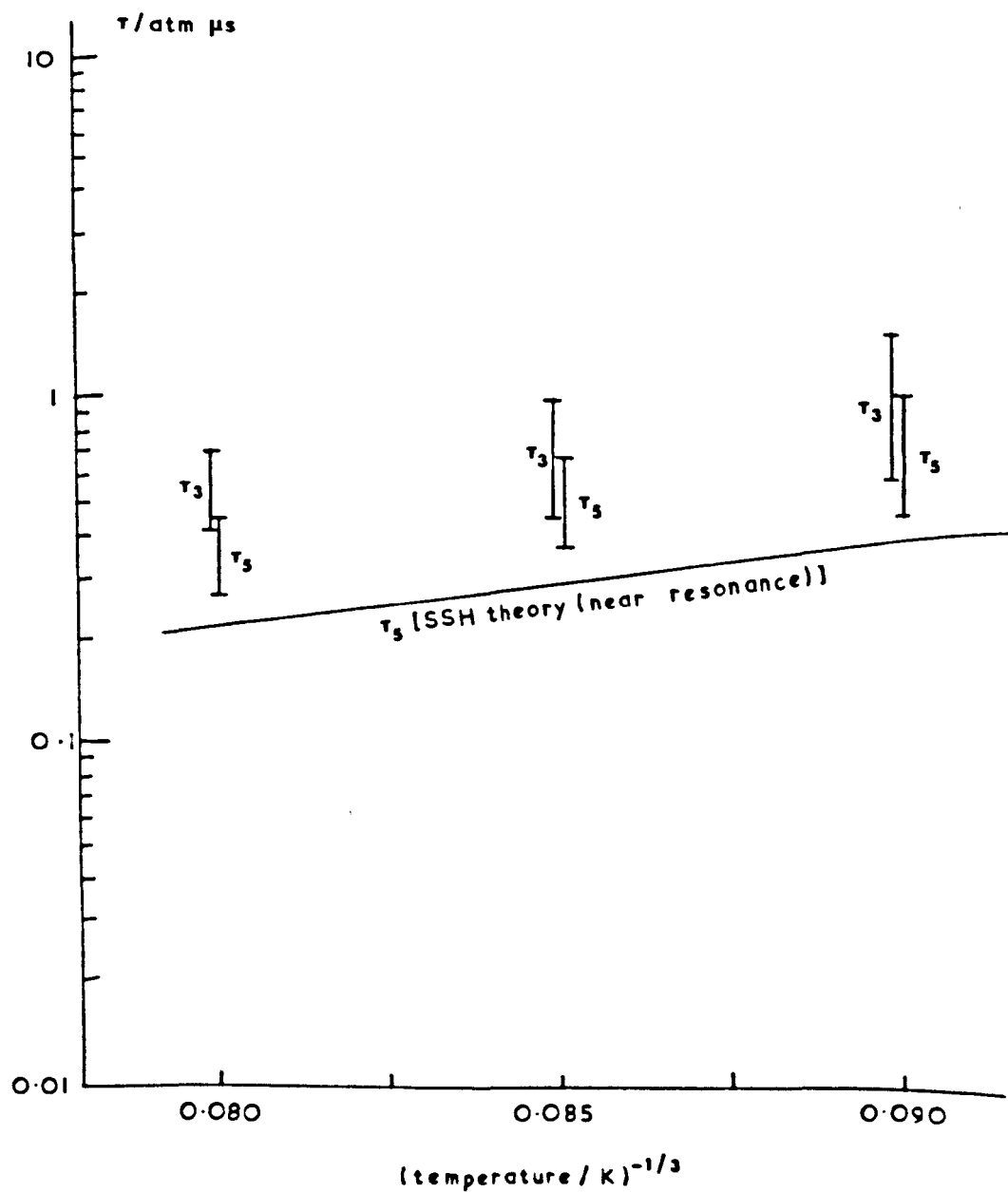
The graph of relaxation time versus temperature (Figure 5.13) shows that there is an increase of τ_5 with decreasing temperature. However the temperature dependence of τ_3 is uncertain but it is probably similar.

Calculations of τ_5 by SSH theory using the conditions for near resonance gives good values for this system. Experimental values show a variation with temperature very similar to that of the theory and although the latter values are a little shorter, the difference is not significant considering the approximations made.

Theoretical predictions of τ_3 are again very poor (Moore's theory gives a values of 2.7 atm s at 1630 K) and the reasons suggested for the CO/HCl system could well apply here.

Figure 5.14 Reciprocal Napier Times for HI/CO Mixtures
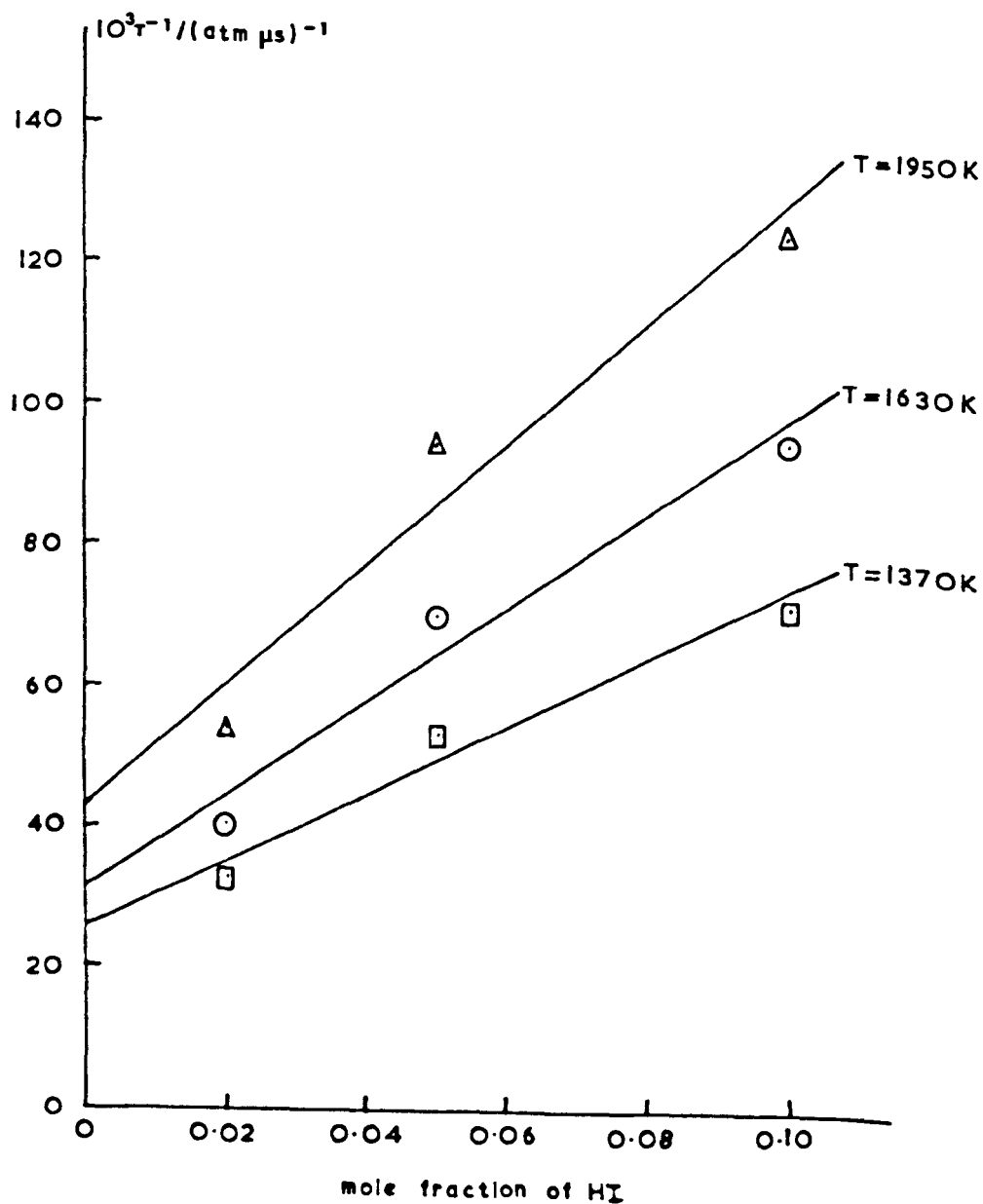
5.2.7 The Relaxation of CO with added HI or DCl

The measurements summarised below were made in collaboration with P.M. Borrell.

As with the previous CO-halide mixtures, the emission monitored was from both components. The traces obtained were very similar to those for CO/HCl and CO/HBr mixtures and the observed Napier times are described by equations 5.49 to 5.54.

% HI in CO	Temperature Range: 1400-2000 K	
2	$\log \tau(\text{atm s}) = 21.4 \, T^{-\frac{1}{3}} - 6.45$	5.49
5	$\log \tau(\text{atm s}) = 24.7 \, T^{-\frac{1}{3}} - 6.95$	5.50
10	$\log \tau(\text{atm s}) = 24.1 \, T^{-\frac{1}{3}} - 7.82$	5.51

% DCl in CO	Temperature Range: 1400-2000 K	
2	$\log \tau(\text{atm s}) = 42.8 \, T^{-\frac{1}{3}} - 8.20$	5.52
5	$\log \tau(\text{atm s}) = 44.7 \, T^{-\frac{1}{3}} - 8.67$	5.53
10	$\log \tau(\text{atm s}) = 44.0 \, T^{-\frac{1}{3}} - 8.78$	5.54

Analysis of the traces was the same as for previous mixtures but for these, scatter precluded evaluating an upper limit for w_2 (equation 5.38) and so the lower limit for τ_5 is zero. The results are given in Figures 5.14 and 5.15 and Tables 5.10 to 5.13.

Figure 5.15 Reciprocal Napier Times for DCI/CO Mixtures
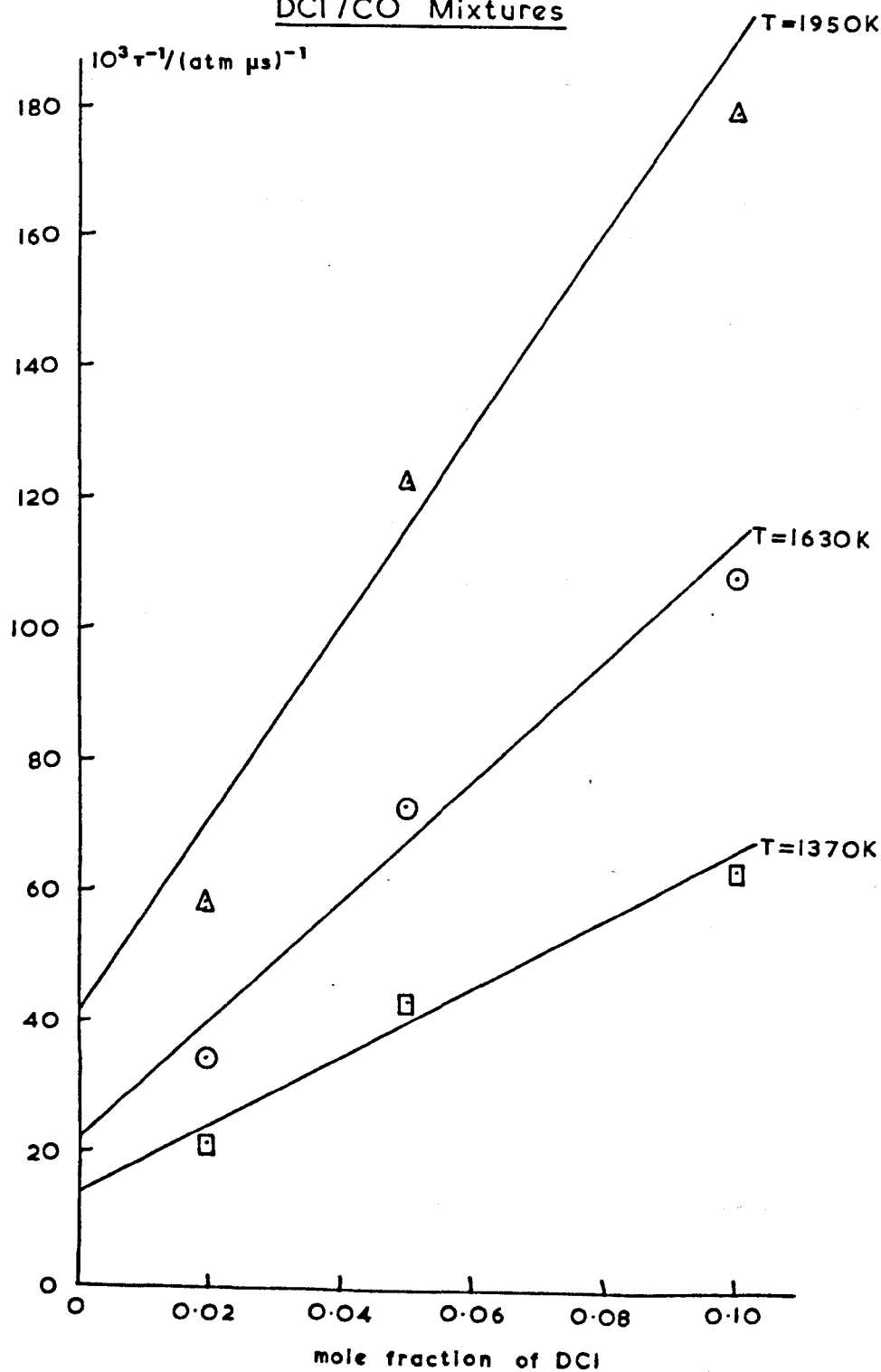
Table 5.10

Limiting Values of k_3' and k_5 for CO/HI mixtures

T/K	$k_3'/(\text{atm } \mu s)^{-1}$	$k_5/(\text{atm } \mu s)^{-1}$
1950	1.0 - 3.7	∞ - 1.4
1630	1.0 - 2.9	∞ - 1.5
1370	0.8 - 2.3	∞ - 1.1

Table 5.11

Napier times derived from the above rate constants

T/K	$\tau_3/\text{atm } \mu s$	$\tau_5/\text{atm } \mu s$	$\tau_5(\text{SSH})/\text{atm } \mu s$
1950	1.01 - 0.27	0 - 0.39	0.064
1630	1.02 - 0.34	0 - 0.41	0.062
1370	1.32 - 0.43	0 - 0.54	0.060

Table 5.12

Limiting Values of k_3' and k_5 for CO/DCl mixtures

T/K	$k_3'/(\text{atm } \mu s)^{-1}$	$k_5/(\text{atm } \mu s)^{-1}$
1950	1.5 - 3.2	∞ - 3.1
1630	1.0 - 2.0	∞ - 1.9
1370	0.6 - 1.4	∞ - 0.9

Table 5.13

Napier times derived from the above rate constants

T/K	τ_3/atm µs	τ_5/atm µs	τ_5(SSH)/atm µs
1950	0.66 - 0.31	0 - 0.17	0.26
1630	1.04 - 0.50	0 - 0.28	0.27
1370	1.79 - 0.71	0 - 0.55	0.28

Figure 5.16   Overall (measured) Napier Times for Mixtures of CO with 10% Hydrogen Halide
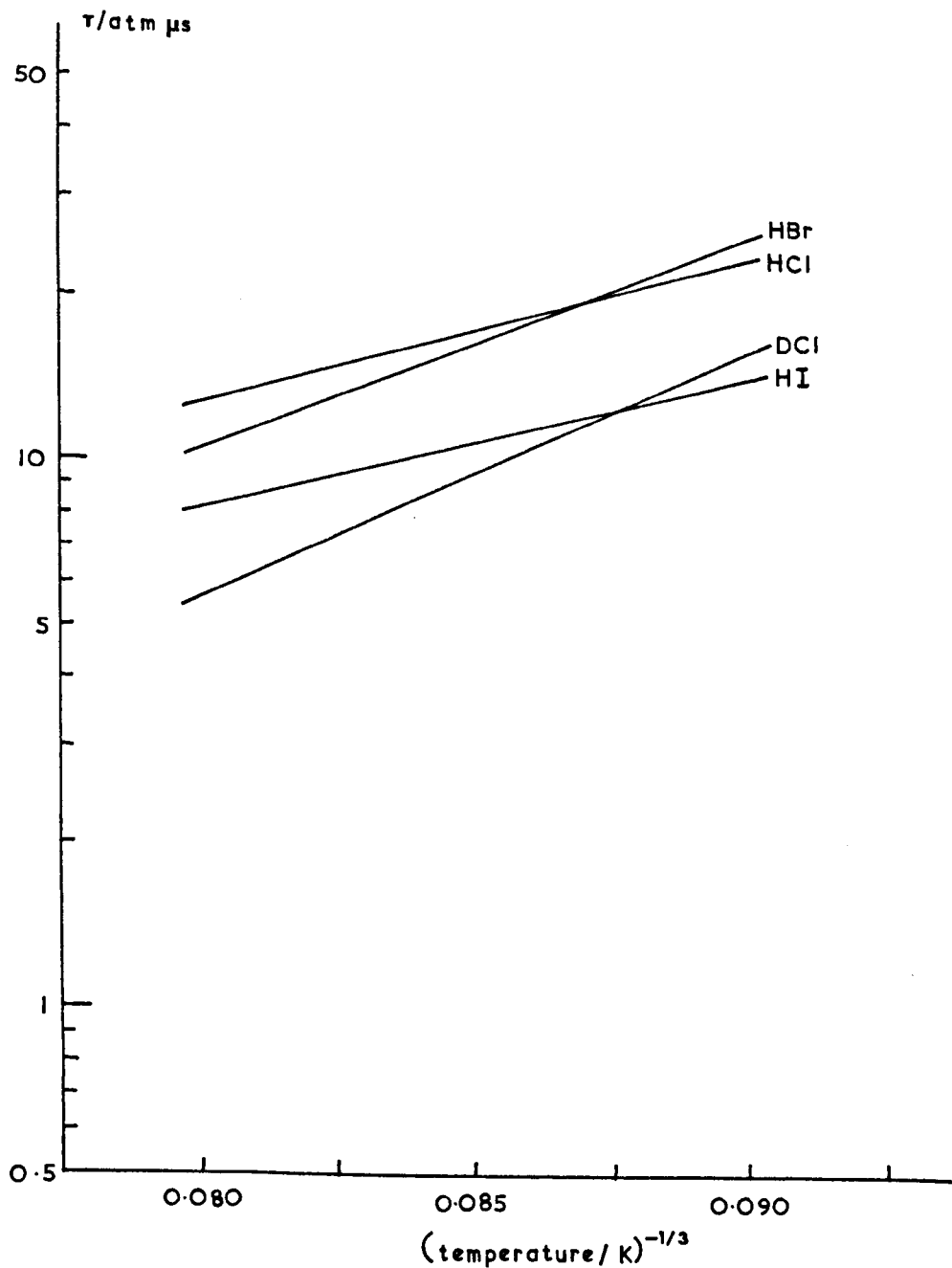
5.2.8 Comparison of the Measurements for CO/Halide Mixtures

(a) Overall Napier Times

A summary of the Landau-Teller plots for one particular composition (10% halide) is made in Figure 5.16. The results for mixtures with 2% and 5% halide show similar features. In all cases the Napier times for CO/HBr are about equal to those for CO/HCl and a little longer than for CO/HI. The shortest Napier times are for CO/DCl at the high temperatures but for CO/HI at the lowest temperatures.

The order found for the mixtures is expected considering the results for the pure gases[121,124,127] and the energy difference between the pairs of molecules (Table 5.14).

Table 5.14

Comparison of Napier times at 1630 K with Energy Difference

molecule A	molecule B	τ_{BB} /atm µs	τ_{BA} /atm µs	$\Delta\bar{\nu}$ /cm^{-1}
CO	HCl	0.28	18	743
CO	HBr	0.42	17	416
CO	HI	0.33	10	87
CO	DCl	0.49	9	52

It can be seen that whereas $\tau_{HI-HI} \sim \tau_{HCl-HCl}$, $\tau_{CO-HI} < \tau_{CO-HCl}$ and this correlates with the energy difference between CO and HI being much less than between CO and HCl so offering a greater opportunity for V→V transfer. A similar explanation can be advanced for τ_{CO-HBr} being approximately equal to τ_{CO-HCl} whereas $\tau_{HBr-HBr} > \tau_{HCl-HCl}$.

The Napier time for the CO/DCl system can also be compared with those for other mixtures in a similar way for the greatest shortening in Napier time corresponds to the smallest energy difference.

However the final order of $\tau_{CO-HCl} > \tau_{CO-HBr} > \tau_{CO-HI} > \tau_{CO-DCl}$ need not be solely a reflection of $\Delta\bar{v}$ as the observed Napier time is dependent on τ_3 ($\tau_{halide-CO}$). These would also be expected to decrease in the same order for it corresponds to that for the vibrational frequencies. Of interest therefore would be measurements for other deuterated halides, especially those for DBr for $\Delta\bar{v}_{CO-DBr} \sim \Delta\bar{v}_{CO-HBr}$ so any difference in the rates of relaxation can be ascribed to an isotopic effect.

The comparatively steep temperature dependence for the CO/DCl system at first sight is surprising, but probably arises from the different ways in which τ_3 and τ_5 vary with temperature (subsections 5.2.8a and 5.2.8b). Two cases are possible: firstly where both Napier times decrease as temperature increases and secondly where one exhibits this behaviour while the other increases

as temperature increases i.e. one has a positive and the other a

negative gradient. An example of both types of behaviour is found

in the work of Breshears and Bird[132] who found that for N_2/DI

both τ_3 and τ_5 decrease with increasing temperature but for N_2/HI,

τ_3 behaves as above but τ_5 has the opposite temperature dependence.

Breshears and Bird found that the gradient of the Landau-Teller plot

for the overall Napier time was greater for the deuterated halide

mixture as was found here with CO/DCl and CO/HCl mixtures. By

comparing the two studies, it seems reasonable to suppose that for

CO/DCl, τ_3 and τ_5 vary similarly with temperature whereas for

CO/HCl, they vary in opposing ways.

(b)   T,R→V (halide-CO) Napier Times

       When dealing with individual processes, a common practice

is to quote collision numbers. The Napier times previously quoted

(Tables 5.6, 5.9, 5.11, 5.13) are converted to collision numbers

in Table 5.15. The equations used are those employed in Appendix A,

Program 3 where relaxation times are calculated using SSH theory.

Table 5.15

Collision numbers for vibrational energy transfer in

CO-HCl, CO-HBr, CO-HI and CO-DCl systems

	1950 K	1630 K	1370 K
$Z(HCl, CO)$	450 - 970	670 - 1090	980 - 1760
$Z(CO^{01}, HCl^{10})$ exptl.	740 - 1090	830 - 1220	880 - 1420
$Z(CO^{01}, HCl^{10})$ calc.	1829	3028	5000
$Z(HBr, CO)$	760 - 1330	980 - 2100	1400 - 3610
$Z(CO^{01}, HBr^{10})$ exptl.	510 - 830	790 - 1440	1110 - 2470
$Z(CO^{01}, HBr^{10})$ calc.	426	632	936
$Z(HI, CO)$	540 - 2020	760 - 2260	1080 - 3310
$Z(CO^{01}, HI^{10})$ exptl.	<780	<920	<1350
$Z(CO^{01}, HI^{10})$ calc.	122	140	160
$Z(DCl, CO)$	600 - 1280	1080 - 2280	1720 - 4300
$Z(CO^{01}, DCl^{10})$ exptl.	<330	<610	<1330
$Z(CO^{01}, DCl^{10})$ calc.	553	592	634

Since in this subsection T,R→V processes are being considered, it is expected that the collision numbers would increase with decreasing temperatures. This can be seen for HCl-CO, HBr-CO and DCl-CO and it is probably true for HI-CO.

From Table 5.15 it can also be seen that the T,R→V process is approximately as efficient as the V→V process for CO-HCl and CO-HBr and possibly for CO-HI and CO-DCl. Thus T,R→V energy transfer is important to the relaxation of the mixture as a whole.

In all cases, the number of collisions needed for relaxation to occur is much fewer than the predictions of the Moore and SSH theories for the latter neglects rotational motion completely and the former only considers the rotation of the activating molecule. Relaxation is also likely to be more rapid than the theory suggests on account of dipole-dipole interaction[126] which would explain why the value of τ_{CO-HI} is about four times less than τ_{N_2-HI}[132]. although the energy gap of the two pairs is approximately equal (87 and 101 cm^{-1} respectively).

c)   <u>V→V transfer Napier times</u>

The numerical values of τ_5 (Tables 5.6, 5.9, 5.11 and 5.13) have a range such that is not possible to assign a positive or negative sign to the temperature dependence of the Napier times for the various systems. However the indications are that τ_{CO-HBr}^v is

shorter than τ^v_{CO-HCl} with τ^v_{CO-HI} and τ^v_{CO-DCl} shorter still. This would be expected considering the energy differences (Table 5.14).

It is useful to compare the magnitude of the experimental values for τ_5 with those for N_2-HI mixtures. The values of $\tau^v_{CO-halide}$ are all several times shorter than $\tau^v_{N_2-HI}$ [132] and $\tau^v_{N_2-HCl}$ (Section 5.2.4) even though the energy difference of some is greater (cp. Table 5.14 with $\Delta\bar{\nu}$ (N_2/HCl) = 555 cm^{-1}, $\Delta\bar{\nu}$ (N_2/HI) = 101 cm^{-1}).

Probably the dipole moment of CO is at least partly the cause of the rapid relaxation of these mixtures, an effect that has been theoretically discussed by Mahan.[133] Chen and Moore[134] notice this effect in their room temperature work on V→V exchange between HCl and several collision partners. They noticed that the rate of transfer is greater than between HCl and N_2 if the colliding partner contains hydrogen, such as CH_4, or has a dipole moment, such as CO or HBr.

Considering the limitations for Z_5 (Z for the V→V process) agreement between experimental and calculated values is quite good for all the systems. Several reasons can be suggested as to why agreement for CO-HCl is worse than for CO-HBr. Firstly it is clear (Table 5.14) that the energy difference between the former pair is greater and it may be that it is too great for the near resonance theory of SSH to be directly applicable. Secondly it may be that

the energy difference, $h(\nu_{halide} - \nu_{CO})$ is changed to rotational rather than to vibrational energy as SSH suppose. This factor could be of greater importance for CO-HCl seeing that $(\nu_{HCl} - \nu_{CO}) >$ $(\nu_{HBr} - \nu_{CO})$. A third possibility seems more likely: the agreement would be better for both systems if dipole-dipole interactions were included in the calculations since the dipole moment of HCl is greater than for HBr.

If the third suggestion is true, the closeness of the overall agreement shows that SSH near resonance theory is applicable for quite large energy differences and that the rotational motion of molecules has little effect on the rate of V→V energy exchange.

5.3 General Reflections on the Work

It has not been possible to solve all the problems it was hoped to when this study was commenced. It was possible to ascribe upper limits for the Napier times of pure HCl and HBr which were significantly lower than previously available values but the time resolution of the apparatus prevented determination of their actual size. Even so these limits for the rate of the T,R→V process were much faster than the T→V rates predicted by SSH theory and closer to the values predicted by Moore's theory so giving clear support to his suggestion that for molecules containing hydrogen, R→V energy transfer is important.

The problem of time resolution was a limiting factor throughout the work. At 2 μs it was as good as the rise time of infrared detectors available at the commencement of this study. Developments since then, particularly the laser beam deflection technique for high temperatures and the laser-excited vibrational fluorescence technique for room temperature work, have improved the time resolution. If available at the time, they would obviously have been considered for this study and could be very useful for extension of it.

In spite of this limitation, some conclusions have been drawn. It can be seen from observations on mixtures that the relaxation of CO is accelerated considerably by small amounts of

hydrogen halides. Analysis of the emission indicates that CO excites the halides rapidly by a T,R→V process. The experimentally determined Napier times for this mechanism differ considerably from the theoretical predictions of Moore and SSH, both of whom neglect the rotation of the activated molecule.

That CO is activated by the halide to a considerable extent by a rapid V→V process is demonstrated for all the mixtures. These rates are similar to those for the corresponding halide-CO T,R→V process so neither mechanism dominates the overall relaxation rates. The collision numbers for the V→V process are predicted quite well by the SSH near resonance theory.

Throughout the present work, a basic assumption has been that the Napier times deduced from second level emission are equal to those which would have been obtained using first level emission. This is a point which could be confirmed experimentally for these mixtures using the present apparatus with infrared transmitting windows in the shock tube.

To obtain more precise data about the temperature dependence of the various rate constants it would be desirable to extend the range of temperatures and concentrations over which measurements are made. In this case it would be essential to use an alternative technique; the laser beam deflection technique would be very useful for this purpose with its having such a short rise-time.

An obvious extension of this work would be to the other deuterated halides and to the halides with nitrogen. Comparing the results for CO/HBr and CO/DBr could be particularly interesting as the energy gaps are approximately equal and so the differences in behaviour will be mainly due to the isotopic effect.

With laser-excited vibrational fluorescence it should be possible to conduct similar experiments at around room temperature. Such a wide temperature range would give a crictical test to any relaxation theory.

APPENDIX A.   COMPUTER PROGRAMS

Computer calculations have now become an integral part
of shock tube experiments and the programs used in this present
study are set out below. They are compiled from a user's
standpoint and it is not intended that their operation should be
explained in detail.

Language:	Fortran IV
Computer:	Elliot 4130
Plotter:	Elliot; 13 inches wide, 200 divisions per inch
Pencil Follower:	d-mac Ltd., Type PF1000 (the instrument is generally referred to as the D-Mac) with keyboard for punching characters onto tape. 200 divisions per inch
Tape Punch:	Westrex
Source Program:	Cards unless otherwise stated
Devices:	2 printer
	3 tape reader
	7 card reader
	9 plotter

A.1 Curve Fitter

This program was written by W.R. Graves.

A.1.1 Function and Limitations

Coefficients are found for the equation

$$Y = a_o + a_1X + a_2X^2 + \ldots\ldots a_nX^n$$ which is chosen to
represent a set of points $(X(I), Y(I))$. The value of n $(\leqslant 15)$
can be nominated.

Care needs to be exercised when the equation is
used to extrapolate beyond the range of given points.

A.1.2   The Program

```
&LIST:
   1•     ' 1 FORMAT(26H POLOYNOMIAL CURVE FITTING)
   2•         DIMENSION X(100),Y(100),A(16,16),SUMX(31),SUMY(15)
   3•         H(AJOULE)=AJOULE/4.184
   4•         WRITE(2,1)
   5•       9 FORMAT(I2)
   6• C  SENSE SWITCHES 3 AND 4 ARE REPRESENTED BY VALUES OF JSSW
   7• C  AND KSSW.
   8•      26 READ(7,9) LAST,JSSW,KSSW
   9•         READ(7,3) N
  10•       3 FORMAT (I3)
  11•         READ(7,4) (X(I),Y(I),I=1,N)
  12•       4 FORMAT(F7.1,F10.2)
  13•         IF (JSSW.EQ.0) GO TO 27
  14•      28 DO 29 I=1,N
  15•         Y(I)=Y(I)*X(I)
  16•      29 Y(I)=H(Y(I))
  17•      27 CONTINUE
  18•         SUMX(1)=N
  19•         SUMX(2)=0.0
  20•         SUMX(3)=0.0
  21•         SUMY(1)=0.0
  22•         SUMY(2)=0.0
  23•         DO 10 I=1,N
  24•         SUMX(2)=SUMX(2)+X(I)
  25•         SUMX(3)=SUMX(3)+X(I)*X(I)
  26•         SUMY(1)=SUMY(1)+Y(I)
  27•      10 SUMY(2)=SUMY(2)+Y(I)*X(I)
  28•         NORD=1
  29•      25 L=NORD+1
  30•         KK=L+1
  31•         DO 11 I=1,L
  32•         DO 12 J=1,L
  33•         IK=J-1+I
  34•      12 A(I,J)=SUMX(IK)
  35•      11 A(I,KK)=SUMY(I)
  36•         DO 15 I=1,L
  37•         A(KK,I)=-1.0
  38•         KKK=I+1
  39•         DO 13 J=KKK,KK
  40•      13 A(KK,J)=0.0
  41•         C=1.0/A(1,1)
  42•         DO 14 II=2,KK
  43•         DO 14 J=KKK,KK
  44•      14 A(II,J)=A(II,J)-A(1,J)*A(II,1)*C
  45•         DO 15 II=1,L
  46•         DO 15 J=KKK,KK
  47•         A(II,J)=A(II+1,J)
  48•      15 CONTINUE
  49•         S2=0.0
  50•         DO 16 J=1,N
```

```
51•        S1=0.0
52•        S1=S1+A(1,KK)
53•        DO 17 I=1, NORD
54•     17 S1=S1+A(I+1,KK)*X(J)**I
55•     16 S2=S2+(S1-Y(J))*(S1-Y(J))
56•        R=N-L
57•        S2=S2/R
58•        WRITE (2,5) NORD,S2,N
59•      5 FORMAT(7H ORDER=,I2,11H    (S2)**2=,E16.8,6H    N=,I3)
60•        DO 18 I=1,L
61•        J=I-1
62•     18 WRITE (2,6) J,A(I,KK)
63•      6 FORMAT(15H COEFFICIENTS  ,I3,E18.8)
64•        IF (KSSW.EQ.1) GO TO 50
65•     51 IF (NORD-LAST)52,50,52
66•     52 IF(S2)21,50,21
67•     50 WRITE (2,8)
68•      8 FORMAT(6H   X(I),8X,4HY(I),10X,8HY(CURVE))
69•  •     DO 19 I=1,N
70•        S1=0.0
71•        S1=A(1,KK)
72•        DO 20 J=1,NORD
73•     20 S1=S1+A(J+1,KK)*X(I)**J
74•     19 WRITE (2,7) X(I),Y(I),S1
75•      7 FORMAT(1H ,F7.2,E16.8,E16.8)
76•        IF(NORD-LAST)39,40,40
77•     39 IF(S2)21,40,21
78•     21 NORD=NORD+1
79•        J=2*NORD
80•        SUMX(J)=0.0
81•        SUMX(J+1)=0.0
82•        SUMY(NORD+1)=0.0
83•        DO 22 I=1,N
84•        SUMX(J)=SUMX(J)+X(I)**(J-1)
85•        SUMX(J+1)=SUMX(J+1)+X(I)**J
86•     22 SUMY(NORD+1)=SUMY(NORD+1)+Y(I)*X(I)**NORD
87•        GO TO 25
88•     40 PAUSE
89• C   SENSE SWITCH 2 IS REPRESENTED BY VALUE OF ISSW.
90•        READ (7,9) ISSW
91•        IF (ISSW.EQ.1) GO TO 26
92•        STOP
93•        END
```

A.1.3 Input Data

Card	Format	Name	Comment
1	I2	LAST	required order of equation ($\leqslant 15$)
2	I2	JSSW	=0 if Y(I) is enthalpy; $\neq$ 0 if $Y(I) = $ enthalpy x temperature^{-1}
3	I2	KSSW	=1 if print out is to contain coefficients for trial equations of orders 1,2 ... LAST. $\neq$ 1 if only equation of order LAST is printed
4	I3	N	number of data points (<100)
5 to N+4	F7.1 / F10.2	X(I) / Y(I)	temperature /$^{\circ}$K enthalpy/kcal mole^{-1} or enthalpy x temperature^{-1}/kcal mole^{-1} $^{\circ}$K^{-1}
N+5	I2	ISSW	=1 if another equation to be found (Needs another set of data cards)

A.1.4 Output

Line	Statement	Format	Name	Comment
1	1	H		
2	5	I2	NØRD	order of equation tried by computer
		H		
		E16.8	S2	x^2 test for fit of equation to data; the lower the value of S2 the better the fit
		H		
		I3	N	the number of data points
3 to NØRD+3	6	H		
		I3	J	index of X in equation (J=0→NØRD)
		E16.8	A(I,KK)	coefficient of X of index J
NØRD+4	8	H		
NØRD+5 to NØRD+N+4	7	H		
		F7.2	X(I)	temperature $/^{\circ}K$
		E16.8	Y(I)	as input Y(I)
		E16.8	S1	calculated enthalpy $/kcal\ mole^{-1}$

If KSSW ≠ 1, lines 3 → (NØRD+2) omitted

If ISSW = 1, lines 2 → end repeated

A.2   Incident Shock Wave Parameters

The program, written by R. Millikan (135), was adapted by Mrs P.M. Borrell.

A.2.1   Function and Limitation

For a range of shock speeds, the density, pressure and temperature ratios across the shock front are calculated for a single gas or a mixture of gases. Two states are distinguished: state A where all the energy is either translational or rotational and state 2 where selected molecules contain vibrational energy. Electronic excitation and dissociation are not considered.

The program has been shown to be only accurate when one constituent is present in much greater preponderance over the others. A modification is being prepared by G.E. Millward[116] to make it suitable for a wider range of mixtures.

A.2.2   The Program

```
'LIST;
  1•       1 FORMAT(55H MAIN PROGRAMME FOR NORMAL SHOCK MIXTURES FROM MILLIKAN)
  2•         DIMENSION FJ(5),ZJK(5,5),AJ(5),BJ(5),CJ(5),DJ(5),THETJ(5),XMWJ(5),
  3•        1SHJ(5),HJ(5),ANJ(5),X(5)
  4•         COMMON FJ,ZJK,AJ,BJ,CJ,DJ,THETJ,XMWJ,SHJ,HT1,HJ,ANJ,X,T,HT,T1,XMW,
  5•        1VELT1,SH,IS
  6•         WRITE(2,1)
  7•         READ(7,3)IS,XMS,XME,XMI,T1,HDEL,IMIX
  8•       3 FORMAT(I2,3F6.3,2F6.1,I2)
  9•         WRITE(2,3)IS,XMS,XME,XMI,T1,HDEL,IMIX
 10•         DO 12 J=1,IS
 11•         READ(7,5)ANJ(J),X(J),XMWJ(J),SHJ(J)
 12•         READ(7,4)THETJ(J),AJ(J),BJ(J),CJ(J),DJ(J)
 13•         WRITE(2,5)ANJ(J),X(J),XMWJ(J),SHJ(J)
 14•      12 WRITE(2,4)THETJ(J),AJ(J),BJ(J),CJ(J),DJ(J)
 15•         WRITE(2,20)
 16•       5 FORMAT(2F3.0,2F6.2)
 17•       4 FORMAT(5E11.4)
 18•      20 FORMAT(2X,3HVEL,6X,5HMACHN,3X,5HTA/T1,2X,5HPA/P1,2X,8HRHOA/RHO,3X,
 19•        15HT2/T1,3X,5HP2/P1,2X,9HRHO2/RHO1,2X,2HTA,5X,2HT2,5X,3HTAV,2X,
 20•        28H T(-1/3),3X,5HERROR,3X,5HHDIFF)
 21•         DO 40 M=1,IMIX
 22•         WRITE(2,1001)
 23•    1001 FORMAT(1H0)
 24•         READ(7,6)(FJ(J),J=1,IS)
 25•       6 FORMAT(5F10.5)
 26•         XMW=0.0
 27•         SH=0.0
 28•         DO 13 J=1,IS
 29•         XMW=XMW+FJ(J)*XMWJ(J)
 30•      13 SH=SH+FJ(J)*SHJ(J)
 31•         VELT1=1./10.*SQRT(SH*0.8313*T1/XMW)
 32•         T=T1
 33•         CALL H SHOCK
 34•         HT1=HT
 35•         XM=XMS
 36•      30 U=XM*VELT1
 37•         Y=XM**2
 38•         PRESR=(2.*SH*Y-(SH-1.))/(SH+1.0)
 39•         RHORA=((SH+1.)*Y)/((SH-1.)*Y+2.)
 40•         TRA=PRESR/RHORA
 41•         TA=TRA*T1
 42•         T=TA
 43•         PREST=PRESR
 44•         RHOT=RHORA
 45•      31 CALL H SHOCK
 46•         HDIFT=HT-HT1
 47•         HDIFF=119.503*(U**2)*(1.-(1./RHOT)**2)*XMW
 48•         ERROR=HDIFT-HDIFF
 49•         ERR=ABS(ERROR)
 50•         IF (HDEL-(ERR))32,33,33
```

```
51·      32 T=T-ERROR/10.0
52·         RHOT=PREST*(T1/T)
53·         PREST=1.0+(120.274*XMW*(U**2)*(1.0-(1.0/RHOT)))/T1
54·         RHOT=PREST*(T1/T)
55·         GO TO 31
56·      33 TAV=0.5*(TA+T)
57·         TROOT=TAV**(-.33333)
58·         TR2=T/T1
59·         ITAV=TAV
60·         IT=T
61·         ITA=TA
62·         JERROR=ERROR
63·         WRITE(2,7)U,XM,TRA,PRESH,RHORA,TR2,PREST,RHOT,ITA,IT,ITAV,TROOT,IE
64·        1RROR,NDIFF
65·       7 FORMAT(F7.4,3X,F6.3,1X,F7.3,1X,F6.2,3X,F6.3,2X,F7.3,2X,F6.2,2X,F6.
66·        13,3X,I5,2X,I5,2X,I5,2X,F8.5,4X,I2,3X,F7.0)
67·         XM=XM+XMI
68·         IF(XM-XME)30,30,40
69·      40 CONTINUE
70·         STOP
71·         END


1·          SUBROUTINE N SHOCK
2·          DIMENSION FJ(5),ZJK(5,5),AJ(5),BJ(5),CJ(5),DJ(5),THETJ(5),XMWJ(5),
3·         1SHJ(5),HJ(5),ANJ(5),X(5)
4·          COMMON FJ,ZJK,AJ,BJ,CJ,DJ,THETJ,XMWJ,SHJ,HT1,HJ,ANJ,X,T,HT,T1,XMW,
5·         1VELT1,SH,IS
6·          Q=T**2
7·          R=T**3
8·          Y=T**4
9·          HT=0.0
10·         S=1.9872*T
11·         DO 10 J=1,IS
12·         IF(X(J))11,11,12
13·      11 HJ(J)=S*(2.5*(ANJ(J)-1.0))
14·         GO TO 10
15·      12 HJ(J)=THETJ(J)+AJ(J)*T+BJ(J)*Q+CJ(J)*R+DJ(J)*Y
16·      10 HT=HT+FJ(J)*HJ(J)
17·         RETURN
18·         END
```

A.2.3 Input Data

Card	Format	Name	Comment
1	I2	IS	number of gases ($\leqslant 5$)
	F6.3	XMS	initial mach no.
	F6.3	XME	final mach no.
	F6.3	XMI	incremental steps of mach no.
	F6.1	T1	initial temperature, $T_1/^{\circ}K$
	F6.1	HDEL	accuracy to which enthalpy /kcal mole^{-1} is calculated (usually set equal to 10.0)
	I2	IM1X	no. of gas mixtures for which the calculations are to be performed
2	F3.0	ANJ(J)	no. of atoms in gas
	F3.0	X(J)	= 1.0 if gas is vibrationally relaxed in state 2
	F6.2	XMWJ(J)	molecular wt. of gas
	F6.2	SHJ(J)	$= {}^{C}P/C_v$ (at initial temperature)
3	E11.4	THETJ(J)	coefficient in ethalpy equation of X^0
	E11.4	AJ(J)	'' '' '' '' '' X^1
	E11.4	BJ(J)	'' '' '' '' '' X^2
	E11.4	CJ(J)	'' '' '' '' '' X^3
	E11.4	DJ(J)	'' '' '' '' '' X^4

Cards 2 and 3 are included for J = 1,2 ... IS

i.e. a pair for each constituent of the gas mixture

Card	Format	Name	Comment
2IS + 1	5F10.5	FJ(J)	mole fraction in first mixture of gas 1,2, ... IS
			A similar card for each gas mixture

A.2.4 Output

Line	Statement	Format	Name	Comment
1	1	H		
2	3	I2	IS	As input card 1
		F6.3	XMS	ditto
		F6.3	XME	ditto
		F6.3	XMI	ditto
		F6.1	TI	ditto
		F6.1	HDEL	ditto
		I2	IM1X	ditto
3	5	F3.0	ANJ(J)	As input card 2
		F3.0	X(J)	ditto
		F6.2	XMJ(J)	ditto
		F6.2	SHJ(J)	ditto
4	4	E11.4	THETJ(J)	As input card 3
		E11.4	AJ(J)	ditto
		E11.4	BJ(J)	ditto
		E11.4	CJ(J)	ditto
		E11.4	DJ(J)	ditto

Output lines 3 and 4 printed for J = 1,2 ... IS

Line	Statement	Format	Name	Comment
2IS+2	20	H		
2IS+3	7	F7.4	U	shock velocity /km s^{-1}
		F6.3	XM	mach no.
		F7.3	TRA	T_A/T_1

Line	Statement	Format	Name	Comment
		F6.2	PRESR	P_A/P_1
		F6.3	RHØRA	P_A/P_1
		F7.3	TR2	T_2/T_1
		F6.2	PREST	P_2/P_1
		F6.3	RHØT	P_2/P_1
		I5	ITA	$T_A/^{\circ}K$
		I5	IT	$T_2/^{\circ}K$
		I5	ITAV	$(T_2+T_A)/2$
		F8.5	TRØØT	$(T_2)^{-\frac{1}{3}}/(^{\circ}K)^{-\frac{1}{3}}$
		I2	IERRØR	closeness of trial enthalpy /cal mole^{-1} to correct value, must be >HDEL
		F7.0	HD1FF	enthalpy/cal mole^{-1} of shocked gas

A.3 Napier Times by SSH Theory, Method B

The main program was written jointly by R. Gutteridge and G.E. Millward, subroutine LOOKUP by Mrs P.M. Borrell.

A.3.1 Function and Limitation

SSH theory is used to calculate the number of collisions required to relax a vibrationally excited molecule by vibration → translation energy transfer. The general case is of a hard sphere A colliding with a vibrating molecule BC. However when A is a molecule as opposed to an atom, there can be vibration → vibration resonant energy transfer and the rate at which this occurs is calculated. For the situation where the vibrational frequencies of A and BC are not identical, vibration → vibration energy transfer may only possess near resonant character and suitable calculations are performed when appropriate.

Collision numbers are converted to relaxation times using times between collisions deduced from calculated viscosities.

A limitation placed by this program is that BC must be a diatomic gas and A must be either an atom or diatom.

The equations on which this treatment is based are set out in Section A.3.5.

A.3.2 The Program

```
&LIST:
 1•          DIMENSION TEMP(100),ZED(100),EXPEK(100),ETHETA(100),ZTRAN(100),X(1
 2•      100),Y(100),GAMA(100),TAUC(100),TAU(100),L(20),BL(100),ZEK(100),
 3•      2T3(100),Z(100),CTAU(100),ZEKBC(100),ZEKA(100),ZEKABC(100),ZEKBCA(
 4•      3100),ZOS(100),ZTRA(100),Z10NR(100),ZTR(100),ZEX(100)
 5•          COMMON M,X,Y
 6•    1 FORMAT(73H CALCULATION OF Z10 FOR VIBRATIONAL RELAXATION IN GAS MI
 7•      1XTURES. METHOD B        )
 8•    3 FORMAT(33H0GAS A  DEACTIVATING  GAS BC                    )
 9•    4 FORMAT(76H0CONSTANTS USED  F=PI     BK=BOLTZ.    INIT.LO  LO INC. A
10•      1N=AVAGAD C(CM/SEC)                )
11•          WRITE(2,1)
12•          WRITE(2,3)
13•          WRITE(2,4)
14•    5 FORMAT(F7.4,E12.4,2F10.5,3E10.3)
15•          READ(7,5)F,BK,BL(1),BLI,AN,CE,H
16•   41 FORMAT(15X,F7.4,1PE12.4,0P2F10.5,1P3E10.3)
17•          WRITE(2,41)F,BK,BL(1),BLI,AN,CE,H
18•    6 FORMAT(29H0MOLECULAR CONSTANTS       EPS/K,7X,2HRO,5X,39HMOL.WT.   AT
19•      1.WT.B   AT.WT.C   NUBAR          )
20•    9 FORMAT(F5.2)
21•          READ(7,9)ZEDO
22•          READ(7,170)M
23•  170 FORMAT(I3)
24•  171 FORMAT(12F0.0)
25•          READ(7,171) (X(J),Y(J),J=1,M)
26•  101 FORMAT(I2)
27•  108 READ(7,101)N
28•  111 READ(7,109)(TEMP(I),I=1,N)
29•  109 FORMAT(F7.1)
30•  501 WRITE(2,6)
31•    7 FORMAT(5A4,6F10.4)
32•          READ(7,7) (L(I),I=1,5),CQA,DRA,XMA,XMA1,XMA2,XNUA
33•          WRITE(2,7)(L(I),I=1,5),CQA,DRA,XMA,XMA1,XMA2,XNUA
34•          DR=(DRA+DRBC)/2.
35•          CQ=SQRT(CQA+CQBC)
36•   20 FORMAT(20H AVERAGE FOR A & BC ,2F10.4)
37•          WRITE(2,20)CQ,DR
38•   16 FORMAT(1H0,19X,7HT(DEGK),3X,5HEM/EP,7X,4HRO/L,6X,5HRO/RC,8X,3HL,A,
39•      18X,6HTHETAD,7X,6HMV(2,2),2X,22HEXP(-EP/KT)       1-EXP)
40•          WRITE(2,16)
41•          XMW=XMA*XMBC/((XMA+XMBC)*AN)
42•          THETA=XNU*H*CE/BK
43•          THETAA=XNUA*H*CE/BK
44•          DO 30 I=1,N
45•          BL(I)=0.15
46•   15 AL=2.0*F*BL(I)
47•          ZEK(I)=XMW*(2.0*CE*F/10.0**8*XNU*AL)**2/BK
48•          ZEMK=TEMP(I)/2.0*(ZEK(I)/TEMP(I))**0.33333
49•          ZEMKA=ZEMK/CQ
50•          BLC=DR*(1.-(0.5*(1.+SQRT(ZEMKA+1.)))**(-.16667))/(ALOG(ZEMKA+1.))
```

```
51•        IF(BLC-BL(I))104,104,22
52•     22 BL(I)=BL(I)+BLI
53•        IF(0.2500-BL(I))27,27,15
54•     27 WRITE(2,24)
55•     24 FORMAT(43HOBL LESS THAN 0.1500 OR GREATER THAN 0.2500)
56•        GO TO 26
57•     31 GO TO 15
58•    104 DROC=(0.5•(1.+SQRT(ZEMKA+1.)))••0.16667
59•        ROL=DR/BL(I)
60•        BLN=BL(I)
61•        Y22=0.76•(1.+(1.1•CQ/TEMP(I)))
62•        IF(0.7-TEMP(I)/ZEK(I))28,29,29
63•     28 WRITE(2,10)
64•     10 FORMAT(21H KT/EPSILON TOO SMALL)
65•        GO TO 26
66•     29 CONTINUE
67•        IF(10.0-TEMP(I)/ZEK(I))11,13,13
68•     11 WRITE(2,12)
69•     12 FORMAT(21H KT/EPSILON TOO LARGE)
70•        GO TO 26
71•     13 EXPEK(I)=EXP(-CQ/TEMP(I))
72•        ZOSC=(XMB•XMC•(XMA+XMBC)•ZEK(I))/((XMB••2+XMC••2)•XMA•F••2•THETA)
73•        ETHETA(I)=1./(1.-EXP(-THETA/TEMP(I)))
74•        ZTRAN(I)=((F•THETA/ZEK(I))••2)•(SQRT(1.5/F))•((TEMP(I)/ZEK(I))••0.
75•    116667)•(EXP((1.5•(ZEK(I)/TEMP(I))••0.33333)-(THETA/(2•TEMP(I)))))
76•        ZED(I)=1.017•DROC••2•Y22•ETHETA(I)•ZEDO•ZOSC•ZTRAN(I)•EXPEK(I)
77•        WRITE(2,17)TEMP(I),ZEMKA,ROL,DROC,BLN,ZEK(I),Y22,EXPEK(I),ETHETA(I
78•    1)
79•     17 FORMAT(1HO,19X,F7.1,4X,F6.2,5X,F6.2,5X,F6.3,5X,F8.5,3X,1PE10.3,5X,
80•    10PF6.3,4X,F7.4,8X,F7.4)
81•        BL(I)=BLN
82•     30 CONTINUE
83•     94 FORMAT(1HO,23X,92H•••••• VIBRATIONAL-TRANSLATIONAL ENERGY TRANSFER
84•    1--COLLISION NUMBERS--RELAXATION TIMES ••••••)
85•        WRITE(2,94)
86•     93 FORMAT(1HO,19X,7HT(DEGK),4X,7HT(-1/3),5X,2HZO,6X,4HZOSC,9X,5HZTRAN
87•    1,12X,3HZ10,10X,4HTAUC,10X,3HTAU)
88•        WRITE(2,93)
89•        DO 50 I=1,N
90•        T3(I)=1.0/TEMP(I)••0.33333
91•        Z(I)=1.013249E-10•DRA••2•SQRT(16•AN•F/XMA/BK/TEMP(I))
92•        CTAU(I)=ZED(I)/Z(I)
93•        XX=TEMP(I)/CQ
94•        CALL LOOKUP(XX,YY)
95•        GAMA(I)=(266.93•SQRT(2•XMA•XMBC•TEMP(I)/(XMA+XMBC)))/((DR••2.)•YY•
96•    1(10.0••7.0))
97•        TAUC(I)=GAMA(I)/1.271/1.013249E6
98•        TAU(I)=ZED(I)•TAUC(I)
99•        WRITE(2,51)TEMP(I),T3(I),ZEDO,ZOSC,ZTRAN(I),ZED(I),TAUC(I),TAU(I)
100•    51 FORMAT(1HO,19X,F7.1,3X,F8.5,3X,F4.1,4X,F6.1,6X,1PE10.3,5X,E11.4,4X
101•    1,1PE11.5,4X,1PE11.5)
102•    50 CONTINUE
103•        IF(XNUA.EQ.0.0)GO TO 26
104•        DO 61 I=1,N
105•        ZEKBC(I)=16.0•F••4•XMBC/AN/2.0•(BL(I)/10.0••8•XNU•CE)••2/BK
106•        ZEKA(I)=16.0•F••4•XMA/AN/2.0•(BL(I)/10.0••8•XNUA•CE)••2/BK
107•        ZEKABC(I)=16.0•F••4• XMW•(BL(I)••2/10.0••16)•CE••2•(XNU-XNUA)••2
108•    1/BK
109•        ZEKBCA(I)=16.0•F••4•XMW•(BL(I)••2/10.0••16)•CE••2•((XMB+XMC)••2)/4
110•    1.0
```

```
111•        ZOS(I)=((4.0•XMA1• XMA2)/(XMA1••2+XMA2••2))/4.0/F••4•((4.0•XMB•XMC
112•       1)/(XMB••2+XMC••2))•ZEKA(I)/THETAA•ZEKBC(I)/THETA
113•    61 CONTINUE
114•       ZONR=9.0
115•       IF (ZEKABC(1).EQ.0.0) GO TO 98
116•    95 FORMAT(1H0,24X,88H•••••• VIBRATIONAL-VIBRATIONAL ENERGY TRANSFER--
117•       1NEAR RESONANCE--COLLISION NUMBERS ••••••)
118•       WRITE(2,95)
119•       WRITE(2,96)
120•    96 FORMAT(1H0,32X,7HT(DEGK),4X,7HT(-1/3),5X,2HZO,10X,4HZOSC,10X,5HZTR
121•       1AN,9X,9HZ10(N.R.))
122•       DO 73 I=1,N
123•       ZTRA(I)=(F••2)•(SQRT(3.0/2.0/F))•((TEMP(I)/ZEKABC(I))••0.16667)
124•       1•(((THETA-THETAA)/ZEKABC(I))••2)•EXP(1.5•((ZEKABC(I)/TEMP(I))••
125•       20.33333)-(ABS(THETA-THETAA)/2.0/TEMP(I))-(CQ/TEMP(I)•BK))
126•       Z10NR(I)=ZONR•ZOS(I)•ZTRA(I)
127•       WRITE(2,97)TEMP(I),T3(I),ZONR,ZOS(I),ZTRA(I),Z10NR(I)
128•    97 FORMAT(1H0,32X,F7.1,3X,F8.5,3X,F4.1,4X,E12.5,4X,E12.5,4X,E12.5)
129•    73 CONTINUE
130•    98 FORMAT(1H0,24X,89H•••••• VIBRATIONAL-VIBRATIONAL ENERGY TRANSFER--
131•       1EXACT RESONANCE--COLLISION NUMBERS ••••••)
132•       WRITE(2,98)
133•    99 FORMAT(1H0,32X,7HT(DEGK),4X,7HT(-1/3),5X,2HZO,10X,4HZOSC,10X,5HZTR
134•       1AN,9X,9HZ10(E.R.))
135•       WRITE(2,99)
136•       DO 75 I=1,N
137•       ZTR(I)=(H••2)/(64.0•F••2•XMW•(BL(I)•2.0/10.0••16.0)•BK•TEMP(I))
138•       1•EXPEK(I)
139•       7EX(I)=ZONR•ZOS(I)•ZTR(I)
140•   100 FORMAT(1H0,32X,F7.1,3X,F8.5,3X,F4.1,4X,E12.5,4X,E12.5,4X,E12.5)
141•       WRITE(2,100)TEMP(I),T3(I),ZONR,ZOS(I),ZTR(I),ZEX(I)
142•    75 CONTINUE
143•    26 CONTINUE
144•       READ(7,500)IPW
145•   500 FORMAT(I2)
146•       IF(IPW.EQ.1)GO TO 501
147•       STOP
148•       END


  1•       SUBROUTINE LOOKUP(XX,YY)
  2•       DIMENSION X(100),Y(100)
  3•       COMMON M,X,Y
  4•       DO 178 J=1,M
  5•       IF(XX.GT.X(J))GO TO 178
  6•       IF(XX.EQ.X(J))GO TO 177
  7•       IF(.NOT.(J.EQ.1))GO TO 181
  8•       WRITE(2,179)
  9•       YY=(XX-X(J))•((Y(J+1)-Y(J))/(X(J+1)-X(J)))+Y(J)
 10•       RETURN
 11•   177 YY=Y(J)
 12•       RETURN
 13•   178 CONTINUE
 14•       WRITE(2,180)
 15•   179 FORMAT(/39H POINT BELOW TABLE LIMITS-EXTRAPOLATION)
 16•   180 FORMAT(/39H POINT ABOVE TABLE LIMITS-EXTRAPOLATION)
 17•   181 YY=(XX-X(J))•((Y(J)-Y(J-1))/(X(J)-X(J-1)))+Y(J)
 18•       RETURN
 19•       END
```

A.3.3 Input Data

Card	Format	Name	Comment
1	F7.4	F	π
	E12.4	BK	Boltzmann's Constant/erg deg^{-1}
	F10.5	BL(1)	initial 1/A$^{\circ}$ (0.15)
	F10.5	BLI	increment of 1/A$^{\circ}$ in loop (usually 0.0001)
	E10.3	AN	Avagadro's Number/mole^{-1}
	E10.3	CE	velocity of light/cm s^{-1}
	E10.3	H	Planck's Constant/erg s^{-1}
2	F5.2	ZEDØ	constant Zo in equation (usually 3.0)
3	I3	M	no. of values of $\Omega^{(2,2)*}$ (see card 4)
4 to x+3	12F0.0	X(J) Y(J)	$\left. \begin{array}{l} T^* = kT/\varepsilon \\ \Omega^{(2,2)*} \end{array} \right\}$ Table 1-M of ref.[91] x depends on M; 6 pairs of X(J), Y(J) per card
x+4	I2	N	no. of temperatures at which calculations are to be made (<100)
x+5 to x+N+4	F7.1	TEMP(I)	temperatures/$^{\circ}$K, one per card

Card	Format	Name	Comment
x+N+5	5A4	L(I),I=1,5	name of A-deactivator
	F10.4	CQA	ϵ/k (for A)/degree^{-1}
	F10.4	DRA	σ (for A)/A$^{\circ}$
	F10.4	XMA	mol. wt. A
	F10.4	XMA1	at. wt. of atom 1 of A (if A is a molecule)
	F10.4	XMA2	at. wt. of atom 2 of A (if A is a molecule)
	F10.4	XNUA	vibrational frequency (of A)/cm^{-1} (if A is a molecule)
x+N+6	5A4	L(I),I=6,10	name of BC- vibrator being deactivated
	F10.4	CQBC	ϵ/k (for BC)/degree^{-1}
	F10.4	DRBC	σ (for BC)/A$^{\circ}$
	F10.4	XMBC	mol. wt. BC
	F10.4	XMB	mol. wt. B
	F10.4	XMC	mol. wt. C
	F10.4	XNU	vibrational frequency (of BC)/cm^{-1}
x+N+7	I2	IPW	= 1 for iteration, then another set of (x+N+5), (x+N+6) and (x+N+7) last IPW = 0 (say)

A.3.4   Output

N.B.   N is the number of temperatures for which the calculations
are performed.

Line	Statement	Format	Name	Comment
1	1	H		
2	3	H		
3	4	H		
4	41	F7.4	F	As input card 1
		1PE12.4	BK	ditto
		OPF10.5	BL(1)	ditto
		F10.5	BLI	ditto
		1PE10.3	AN	ditto
		1PE10.3	CE	ditto
		1PE10.3	H	ditto
5	6	H		
6	7	5A4	L(I),I=1,5	As input card (x+N+5)
		F10.4	CQA	ditto
		F10.4	DRA	ditto
		F10.4	XMA	ditto
		F10.4	XMA1	ditto
		F10.4	XMA2	ditto
		F10.4	XNUA	ditto

Line	Statement	Format	Name	Comment
7	8	5A4	L(I),I=6,10	As input card (x+N+6)
		F10.4	CQBC	ditto
		F10.4	DRBC	ditto
		F10.4	XMBC	ditto
		F10.4	XMB	ditto
		F10.4	XMC	ditto
		F10.4	XNU	ditto
8	20	F10.4	CQ	geometric mean of $\varepsilon/k/$ degree^{-1} for A and BC
		F10.4	DR	arithmetic mean of σ/A° For A and BC
9	16	H		
10 to N+9	17	F7.1	TEMP(I)	temperature/$^{\circ}$K,T (see A3.3)
		F6.2	ZEMKA	E_m/ε
		F6.2	RØL	$\sigma/1(=r_0/1)$(see A3.4)
		F6.3	DRØC	$\sigma/r_c(=r_0/r_c)$(see A3.6)
		F8.5	BLN	$1(BLN=BL(I)/A^{\circ}$
		1PE10.3	ZEK(I)	$\varepsilon'/k/$degree^{-1} (see A3.2)
		OPE6.3	Y22	$Y(2,2)$ (see A3.10)
		F7.4	EXPEK(I)	$\exp(-\varepsilon/kT)$
		F7.4	ETHETA(I)	$\{1- \exp(-\theta/T)\}^{-1}$(see A3.11)
N+10	94	H		
N+11	93	H		

Line	Statement	Format	Name	Comment
N+12 to 2N+11	51	F7.1	TEMP(I)	temperature/$^\circ$K,T
		F8.5	T3(I)	$T^{-\frac{1}{3}}$
		F4.1	ZEDØ	Zo (usually 3.0)(see A3.7)
		F6.1	ZØSC	Zosc (see A3.8)
		1PE10.3	ZTRAN(I)	$Z_{tr}{}'$ (see A3.9)
		E11.4	ZED(I)	collision no., Z (see A3.5)
		1PE11.5	TAUC(I)	τ_c (time between collisions)/s
		1PE11.5	TAU(I)	calculated vibrational relaxation time = $Z\tau_c$/s

There is more output if A is not an atom.

If vibrational frequencies of A and B are the same, lines

(2N+12) to (3N+13) are omitted.

Line	Statement	Format	Name	Comment
2N+12	95	H		
2N+13	96	H		
2N+14 to 3N+13	97	F7.1	TEMP(I)	temperature/$^\circ$K,T
		F8.5	T3(I)	$T^{-\frac{1}{3}}$
		F4.1	ZØNR	Zo (set at 9.0)(see A3.14)
		E12.5	ZØS(I)	Zosc (see A3.15)
		E12.5	ZTRA(I)	$Z_{tr}{}'$ (see A3.16)
		E12.5	Z1ONR(I)	collision number (see A3.13)
3N+14	98	H		
3N+15	99	H		

Line	Statement	Format	Name	Comment
3N+16 to 4N+15	100	F7.1	TEMP(I)	temperature/$^\circ$K,T
		F8.5	T3(I)	$T^{-\frac{1}{3}}$
		F4.1	ZØNR	Zo (set at 9.0)(see A3.14)
		E12.5	ZØS(I)	Zosc (see A3.15)
		E12.5	ZTR(I)	Z_{tr}' (see A3.20)
		E12.5	ZEX(I)	collision number (see A3.13)

If IPW = 1, i.e. calculations are performed for a second pair of molecules, lines 3 to (4N+15) are repeated.

A.3.5 Comments

The collision numbers were calculated using the equations below which are obtained from Herzfeld and Litovitz (15).

The molecular constants, $^\epsilon/k$ and σ, were taken from Hirschfelder, Curtiss and Bird (91). For pairs of molecular, $^\epsilon/k$ was taken as the geometric mean and σ as the arithmetic mean of the values for the pure gases.

Notation: Herzfeld uses r_o instead of σ.

The intermolecular parameter 1 was calculated by an iterative procedure.

Herzfeld

choose $1 = 0.1500$

57-11/12 $\qquad 1' = 2\pi 1 \qquad$ A3.1

56-6' $\qquad \epsilon' = \dot{m}(2\pi\nu 1')^2 \qquad$ A3.2

56-6''' $\qquad Em = \dfrac{kT}{2}\left(\dfrac{\epsilon'}{kT}\right)^{\frac{1}{3}} \qquad$ A3.3

This value of Em inserted into

56-10'' $\qquad \dfrac{\sigma}{1} = \left[\ln\left(\dfrac{Em}{\epsilon} + 1\right)\right]\left\{1 - \left[\dfrac{1}{2}\left(1 + \sqrt{\dfrac{Em}{\epsilon} + 1}\right)\right]^{-\frac{1}{6}}\right\}^{-1}$ A3.4

(note last index which is omitted in printing the book)
From this is obtained a value of 1 which is usually higher
than 0.1500. If this is so, the chosen value of 1 is
incremented and the calculations repeated. Iteration is
continued until the chosen 1 and the 1 from A3.4 are equal.

* * * * * * * * *

When A is treated as a solid sphere, the collision number is
calculated from:

62-16 $Z = 1.017\left(\dfrac{\sigma}{r_c}\right)^2 Z_o\, Z_{osc}\, Z_{tr}'\, Y(2,2)\exp(-\epsilon/kT)\{1-\exp(-\theta/T)\}^{-1}$ A3.5

59-3' $\dfrac{\sigma}{r_c} = \left\{\dfrac{1}{2}\left[1 + \sqrt{\dfrac{Em}{\epsilon} + 1}\right]\right\}^{\frac{1}{6}}$ A3.6

Sec. 58,66 Z_o is taken as 3.0 A3.7

62-16 $Z_{osc} = \dfrac{M_B\, M_C(M_A + M_B + M_C)}{(M_B{}^2 + M_C{}^2)M_A}\ \dfrac{1}{\pi^2}\ \dfrac{\theta'}{\theta}$ A3.8

62-16'' $Z_{tr}' = \pi^2\left(\dfrac{\theta}{\theta'}\right)^2\left(\dfrac{3}{2\pi}\right)^{\frac{1}{2}}\left(\dfrac{T}{\theta'}\right)^{\frac{1}{6}}\exp\left[\dfrac{3}{2}\left(\dfrac{\theta'}{T}\right)^{\frac{1}{3}} - \dfrac{\theta}{2T}\right]$ A3.9

62-14 $Y(2,2) = 0.76\left(1 + 1.1\dfrac{\epsilon}{kT}\right)$ A3.10

58-9 $\theta = \dfrac{h\nu}{k}$ A3.11

58-9' $\theta' = \dfrac{\epsilon'}{k} = \dfrac{16\pi^4\, \bar{m}\, 1^2\nu^2}{k}$ A3.12

* * * * * * * * *

When A is a diatomic molecule and near resonant vibrational
energy transfer takes place, the equations become.

$$Z = Zo \ Zosc \ Z_{tr}' \qquad\qquad \text{A3.13}$$

There is no obvious justification for using this but it is used
for exact resonance (see below) and equation A3.5 is approximately
equal to A3.13.

65-14' $\qquad\qquad Zo = 9.0 \qquad\qquad$ A3.14

65-14 $\quad Zosc = \dfrac{1}{4\pi^4}\left(\dfrac{4M_B M_C}{M_B^2 + M_C^2}\right)_1 \left(\dfrac{4M_B M_C}{M_B^2 + M_C^2}\right)_2 \dfrac{\theta_1'}{\theta} \dfrac{\theta_2'}{\theta} \qquad$ A3.15

65-9 $Z_{tr}' = \pi^2 \left(\dfrac{3}{2\pi}\right)^{\frac{1}{2}} \left(\dfrac{T}{\theta_{12}'}\right)^{\frac{1}{6}} \left(\dfrac{\theta_1 - \theta_2}{\theta_{12}'}\right)^2 \exp\left[\dfrac{3}{2}\left(\dfrac{\theta_{12}'}{T}\right)^{\frac{1}{3}} - \dfrac{|\theta_1 - \theta_2|}{T} - \dfrac{\varepsilon}{T}\right]$ A3.16

Sec 65d $\qquad \theta_1' = \dfrac{16\pi^4 \bar{m}_1 1^2 \nu_1^2}{k} \qquad\qquad$ A3.17

Sec 65d $\qquad \theta_2' = \dfrac{16\pi^4 \bar{m}_2 1^2 \nu_2^2}{k} \qquad\qquad$ A3.18

65-10 $\qquad \theta_{12}' = \dfrac{16\pi^4 \bar{m}_{12} 1^2 (\nu_1 - \nu_2)^2}{k} \qquad\qquad$ A3.19

N.B.   Only one value of 1 is used and this is calculated in
        usual way.

* * * * * * * * *

For exact resonance:

67-1 $Z = Z_o \, Z_{osc} \, Z_{tr}'$ A3.13

            $Z_o = 9.0$ (by analogy with near resonance case)   A3.14

65-14 Z_{osc} as for near resonance   A3.15
67-1

65-12 $Z_{tr}' = \dfrac{h^2}{64\pi^2 \hat{m} l^2 kT} \exp(-\epsilon/kT)$ A3.20
67-1

A.4 Napier Times by the Theory of Moore

The program was written by R. Gutteridge.

A.4.1 Function and Limitation

Moore's theory (4) is used to calculate the number of collisions required to effect vibrational relaxation by a rotation → vibration energy transfer mechanism. All three of Moore's equations (4, 8 and 9) are employed with the appropriate constants that he empirically derived.

The program is only suitable for treating a diatomic molecule which relaxes by collision with a rotating diatomic molecule.

A.4.2   The Program

```
RLIST:
  1•         DIMENSION TEMP(100),T3(100),Z104(100),Z108(100),Z109(100),Z(100),
  2•        1GAMA(100),TAUC(100),TAU4(100),TAU8(100),TAU9(100),L(20),CTAU4(100)
  3•        2,CTAU8(100),CTAU9(100),X(100),Y(100)
  4•         COMMON M,X,Y
  5•       1 FORMAT(87H CALCULATION OF VIBRATIONAL RELAXATION TIMES CONSIDERING
  6•         1 VIBRATION-ROTATION TRANSITIONS)
  7•       2 FORMAT(42H SEE MOORE J. CHEM. PHYS. 43(9),2979,1965.)
  8•         WRITE(2,1)
  9•         WRITE(2,2)
 10•       4 FORMAT(15H0CONSTANTS USED,7X,4HF =PI,6X,8HBK=BOLTZ,4X,8HH=PLANCK,
 11•        13X,12HCE=LIGHT VEL,2X,9HAN=AVAGAD,3X,8HGAS CON.)
 12•         WRITE(2,4)
 13•       5 FORMAT(F10.4,5(1PE10.4))
 14•         READ(7,5)F,BK,H,CE,AN,R
 15•      19 FORMAT(17X,F10.4,5(3X,1PE10.4))
 16•         WRITE(2,19)F,BK,H,CE,AN,R
 17•         READ(7,170)M
 18•     170 FORMAT(I3)
 19•         READ(7,171)(X(J),Y(J),J=1,M)
 20•     171 FORMAT(12F0.0)
 21•      40 FORMAT(75H0CONSIDER MOLECULE AB (VIBRATOR) BEING DEACTIVATED BY MO
 22•        1LECULE CD (ROTATOR))
 23•         WRITE(2,40)
 24•       6 FORMAT(16H0PARAMETERS USED,6X,10HEQUATION 4,8X,10HEQUATION 8,8X,
 25•        110HEQUATION 9)
 26•         WRITE(2,6)
 27•       7 FORMAT(20X,5HALPHA,5X,2HZ0,5X,5HALPHA,5X,1HC,6X,5HALPHA,5X,2HZ0)
 28•         WRITE(2,7)
 29•       8 FORMAT(20X,F4.2,5X,F4.2,4X,F4.2,5X,F4.2,5X,F4.2,3X,F4.2)
 30•         READ(7,8)ALP4,Z04,ALP8,C8,ALP9,Z09
 31•         WRITE(2,8)ALP4,Z04,ALP8,C8,ALP9,Z09
 32•         READ(7,14)N
 33•         READ(7,16)(TEMP(I),I=1,N)
 34•      16 FORMAT(F7.1)
 35•       9 FORMAT(20H1MOLECULAR CONSTANTS,2X,8HMA OR MC,3X,8HMB OR MD,6X,2HR0
 36•        1,6X,5HNUBAR,4X,5HSIGMA,4X,5HEPS/K)
 37•      20 WRITE(2,9)
 38•      10 FORMAT (5A4,6F10.4)
 39•         READ(7,10) (L(I),I=1,5),XMA,XMB,R01,XNU1,DRA1,CQA1,
 40•         WRITE(2,10)(L(I),I=1,5),XMA,XMB,R01,XNU1,DRA1,CQA1
 41•         READ(7,10) (L(I),I=6,10),XMC,XMD,R02,XNU2,DRA2,CQA2
 42•         WRITE(2,10)(L(I),I=6,10),XMC,XMD,R02,XNU2,DRA2,CQA2
 43•         DRA=(DRA1+DRA2)/2
 44•         CQA=SQRT(CQA1*CQA2)
 45•         IF(XMC-XMD)12,12,13
 46•      13 Q=XMD
 47•         XMD=XMC
 48•         XMC=Q
 49•      12 CONTINUE
```

```
50•         D=(RO2•XMD)/(XMC+XMD)
51•      14 FORMAT(I2)
52•         XM=XMA•XMB/(XMA+XMB)
53•         DO 15 I=1,N
54•         Z(I)=1.012349E-10•DRA••2•SQRT(16•AN•F/((XMA+XMB)•(XMC+XMD)/
55•      1(XMA+XMB+XMC+XMD))/BK/TEMP(I))
56•         XX=TEMP(I)/CQA
57•         CALL LOOKUP(XX,YY)
58•         GAMA(I)= 266.93•SQRT(2•(XMA+XMB)•(XMC+XMD)•TEMP(I)/(XMA+XMB
59•      1+XMC+XMD))/((DRA••2)•YY•(10.••7)))
60•         T3(I)=1./TEMP(I)••0.33333
61•         TAUC(I)=GAMA(I)/1.271/1.013249E6
62•      15 CONTINUE
63•         XIA=XMC•D••2+XMD•(RO2-D)••2
64•         C1=17.1
65•         C2=3•(2.0•CE••2•F••4/AN/10.0••16/BK)••0.33333
66•         C3=H•CE/BK/2.0
67•         FA=32.0•F••4•(2.0•F)••0.16667/3.0••0.5•(CE••1.33333)•2.0•F/
68•      1(BK••0.166667)/H/(AN••1.16667)/(10.0••18.66667)
69•      17 FORMAT(30H0CALCULATIONS USING EQUATION 4)
70•         WRITE(2,17)
71•         DO 24 I=1,N
72•         D41=C1•XIA••2.16667•XNU1••1.33333/D••4.33333/TEMP(I)••0.16667
73•      1/XM/ALP4••2.33333
74•         D42=EXP(-(C2•((XIA/TEMP(I)•((XNU1/D/ALP4)••2))••0.33333)))
75•         D43=EXP(C3•XNU1/TEMP(I))
76•         Z104(I)=Z04/D41/D42/D43
77•         TAU4(I)=Z104(I)•TAUC(I)
78•         CTAU4(I)=Z104(I)/Z(I)
79•      51 FORMAT(3X,F6.1,4X,F8.5,6(4X,1PE11.5))
80•         WRITE(2,51)TEMP(I),T3(I),Z104(I),Z(I),CTAU4(I),TAUC(I),TAU4(I)
81•      24 CONTINUE
82•      21 FORMAT(30H0CALCULATIONS USING EQUATION 8)
83•         WRITE(2,21)
84•         DO 31 I=1,N
85•         D82=EXP(-(C2•((XIA/TEMP(I)•((XNU1/D/ALP8)••2))••0.33333)))
86•         Z108(I)=C8/D82
87•         CTAU8(I)=Z108(I)/Z(I)
88•         TAU8(I)=Z108(I)•TAUC(I)
89•         WRITE(2,51)TEMP(I),T3(I),Z108(I),Z(I),CTAU8(I),TAUC(I),TAU8(I)
90•      31 CONTINUE
91•      22 FORMAT(30H0CALCULATIONS USING EQUATION 9)
92•         WRITE(2,22)
93•         DO 23 I=1,N
94•         D91=C1•XIA••2.16667•XNU1••1.33333/D••4.33333/TEMP(I)••0.16667/XM/
95•      1ALP9••2.3333
96•         D92=EXP(-(C2•((XIA/TEMP(I)•((XNU1/D/ALP9)••2))••0.33333)))
97•         Z109(I)=Z09/D91/D92
98•         CTAU9(I)=Z109(I)/Z(I)
99•         TAU9(I)=Z109(I)•TAUC(I)
100•        WRITE(2,51)TEMP(I),T3(I),Z109(I),Z(I),CTAU9(I),TAUC(I),TAU9(I)
101•     23 CONTINUE
102•        READ(7,3)ISSW
103•      3 FORMAT(I2)
104•        IF(ISSW.EQ.1) GO TO 20
105•        STOP
106•        END

  1•        SUBROUTINE LOOKUP(XX,YY)
```

```
 2•        COMMON M,X,Y
 3•        DIMENSION X(100),Y(100)
 4•        DO 178 J=1,M
 5•        IF(XX.GT.X(J))GO TO 178
 6•        IF(XX.EQ.X(J))GO TO 177
 7•        IF(.NOT.(J.EQ.1))GO TO 181
 8•        WRITE(2,179)
 9•        YY=(XX-X(J))*((Y(J+1)-Y(J))/(X(J+1)-X(J)))+Y(J)
10•        RETURN
11•   177 YY=Y(J)
12•        RETURN
13•   178 CONTINUE
14•        WRITE(2,180)
15•   179 FORMAT(/39H POINT BELOW TABLE LIMITS-EXTRAPOLATION)
16•   180 FORMAT(/39H POINT ABOVE TABLE LIMITS-EXTRAPOLATION)
17•   181 YY=(XX-X(J))*((Y(J)-Y(J-1))/(X(J)-X(J-1)))+Y(J)
18•        RETURN
19•        END
```

A.4.3 Input Data

Card	Format	Name	Comment
1	F10.4	F	π
	1PE10.4	BK	Boltzmann's Constant, k/erg deg^{-1}
	1PE10.4	H	Planck's Constant, h/erg s^{-1}
	1PE10.4	CE	velocity of light/cm s^{-1}
	1PE10.4	AN	Avagadros No./mole^{-1}
	1PE10.4	R	Gas Constant/erg deg^{-1} mole^{-1}
2	I3	M	no. of $\Omega^{(2,2)*}$ (see card 3)
3 to x+2	12F0.0	X(J) X(J)	$\left.\begin{array}{l} T^* \\ \Omega^{(2,2)*} \end{array}\right\}$ see A3.3, card 4
x+3	20X		
	F4.2	ZLP4	α (potential energy range parameter) /A$^{\circ}$ $^{-1}$ eqn. 4 (2.94 A$^{\circ}$ $^{-1}$)
	5X		
	F4.2	ZO4	Zo, steric factor, eqn. 4 (4.97)
	4X		
	F4.2	ZLP8	α/A$^{\circ}$ $^{-1}$ for eqn. 8 (8.04 A$^{\circ}$ $^{-1}$)
	5X		
	F4.2	C8	constant (which includes Zo) for eqn. 8 (0.13)
	5X		
	F4.2	ALP9	α/A$^{\circ}$ $^{-1}$ for eqn. 9 (3.80 A$^{\circ}$ $^{-1}$)
	3X		
	F4.2	ZO9	Zo for eqn. 9 (6.75)

Card	Format	Name	Comment
x+4	I2	N	no. of temperatures at which calculations are performed (<100)
x+5 to N+x+5	F7.1	TEMP(I)	temperatures/$^{\circ}$K, one per card
N+x+5	5A4	L(I),I=1,5	name of vibrator
	F10.4	XMA	at. wt. of one atom of vibrator
	F10.4	XMB	at. wt. of other atom of vibrator
	F10.4	RO1	internuclear distance/A°
	F10.4	XNU1	vibration frequency/cm^{-1}
	F10.4	DRA1	σ/A°
	F10.4	CQA1	$\varepsilon/k/degree^{-1}$
N+x+6	5A4	L(I),I=6,10	name of rotator
	F10.4	XMC	at. wt. of one atom of rotator
	F10.4	XMD	at. wt. of other atom of rotator
	F10.4	RO2	internuclear distance/A°
	F10.4	XNU2	vibration frequency/cm^{-1}
	F10.4	DRA2	σ/A°
	F10.4	CQA2	$\varepsilon/k/degree^{-1}$
N+x+7	I2	ISSW	if = 1, iterate program. Need to insert another 3 cards equivalent to (N+x+5), (N+x+6) and (N+x+7). if $\neq$ 1, program ends.

A.4.4   Output

N.B.   N is the number of temperatures for which the collision number is calculated.

Line	Statement	Format	Name	Comment
1	1	H		
2	2	H		
3	4	H		
4	19	F10.4	F	As input card 1
		1PE10.4	BK	ditto
		1PE10.4	H	ditto
		1PE10.4	CE	ditto
		1PE10.4	AN	ditto
		1PE10.4	R	ditto
5	40	H		
6	6	H		
7	7	H		
8	8	F4.2	ALP4	As input card (x+3)
		F4.2	ZO4	ditto
		F4.2	ALP8	ditto
		F4.2	C8	ditto
		F4.2	ALP9	ditto
		F4.2	ZO9	ditto

Line	Statement	Format	Name	Comment
9	9	H		
10	10	5A4	L(I),I=1,5	As input card (N+x+5)
		F10.4	XMA	ditto
		F10.4	XMB	ditto
		F10.4	RO1	ditto
		F10.4	XNU1	ditto
		F10.4	DRA1	ditto
		F10.4	CQA1	ditto
11	11	5A4	L(I),I=1,5	As input card (N+x+6)
		F10.4	XMC	ditto
		F10.4	XMD	ditto
		F10.4	RO2	ditto
		F10.4	XNU2	ditto
		F10.4	DRA2	ditto
		F10.4	CQA2	ditto
12	17	H		
13 to N+12	51	F6.1	TEMP(I)	temperature/$^\circ$K,T
		F8.5	T3(I)	$T^{-\frac{1}{3}}$
		1PE11.5	Z104(I)	collision no. (equation 4)
		1PE11.5	Z(I)	rate of collisions (kinetic theory)
		1PE11.5	CTAU4(I)	Napier time,τ, from Z(I) (equation 4)

Line	Statement	Format	Name	Comment
		1PE11.5	TAUC(I)	τ_c, time between collisions, from
		1PE11.5	TAU4(I)	$\tau = Z10(I)*\tau_c$ (equation 4)
N+13	21	H		
N+14 to 2N+13	51	F6.1	TEMP(I)	
		F8.5	T3(I)	
		1PE11.5	Z108(I)	
		1PE11.5	Z(I)	As for output lines 13 to (N+12) but using equation 8 rather than 4
		1PE11.5	CTAU8(I)	
		1PE11.5	TAUC(I)	
		1PE11.5	TAU8(I)	
2N+14	22	H		
2N+15 to 3N+14	51	F6.1	TEMP(I)	
		F8.5	T3(I)	
		1PE11.4	Z109(I)	
		1PE11.4	Z(I)	As for output lines 13 to (N+12) but using equation 9 rather than 4
		1PE11.4	CTAU9(I)	
		1PE11.4	TAUC(I)	
		1PE11.4	TAU9(I)	

A.4.5 Comments

The intermolecular parameters ϵ/k and σ were obtained as for SSH theory (Section A.3.5).

The four equations of Moore are:

Equation 4:
$$\frac{1}{Z_{10}} = \frac{1}{Z_0} \frac{17.1 \; I^{13/6} \upsilon^{4/3}}{d^{13/3} T^{1/6} M \alpha^{7/3}} \exp\left[-1.78\left(\frac{I\upsilon^2}{d^2 \alpha^2 T}\right)^{\frac{1}{3}} \right]$$

$$x \quad \exp \frac{0.7194\upsilon}{T} \qquad\qquad\qquad A4.1$$

where Z_0 = 4.97 $\qquad\qquad\qquad\qquad$ A4.2

α = $2.94\text{A}^{\circ -1}$ $\qquad\qquad\qquad\qquad$ A4.3

T is temperature

I is moment of inertia in a.m.u. $\text{A}^{\circ 2}$

d is internuclear distance in A°

υ is vibrational frequency in cm^{-1}

Equation 8: Z_{10}^{-1} = $C^{-1} \exp -1.78(I\upsilon^2 \; d^2 \; \alpha^2 T)^{\frac{1}{3}}$ $\qquad$ A4.4

where C = 0.13 $\qquad\qquad\qquad\qquad$ A4.5

α = $8.04\text{A}^{\circ -1}$

d, I, T and υ as for equation 4

Equation 9: $Z_{10}^{-1} = Z_0^{-1} \dfrac{17.1 \; I^{13/6} \; \bar{\nu}^{-4/3}}{d^{13/3} T^{1/6} M_\alpha^{7/3}} \exp\left[-1.78 \left(\dfrac{I^{-2}}{d^2 \alpha^2 T} \right)^{\frac{1}{3}} \right]$ A.47

where $Z_0 = 6.75$ A4.8

$\alpha = 3.80 \mathring{A}^{-1}$ A4.9

d, I, T and $\bar{\nu}$ as for equation 4
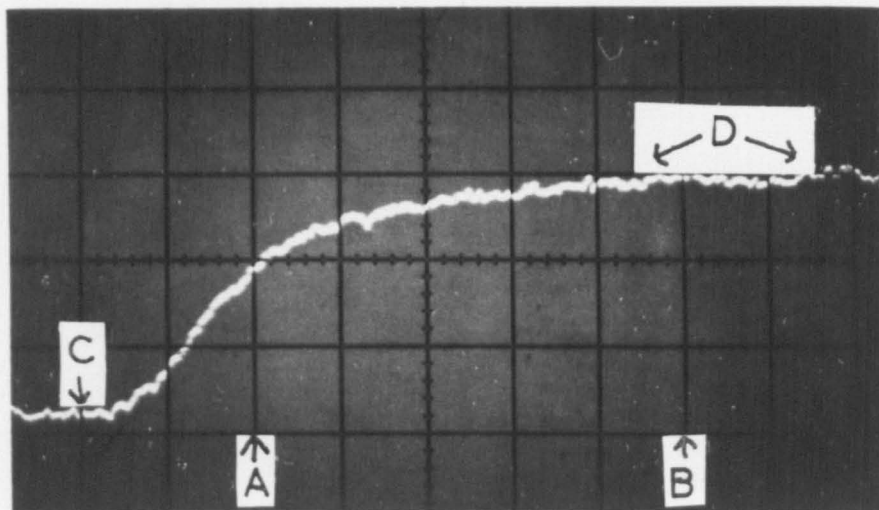
Figure A5·1 Trace of Second level Emission
            for Analysis by Computer
            Plotting

            Typical points for the D-Mac:
            A & B first and second
            C origin
            D region for 5 values of I_∞

A.5   D-Mac with Relaxation Calculations and Graph Plotting

The main program and subroutine SCREW were written by R. Gutteridge and G.E. Millward; the basic plotting routine by R.D. Dowsing.

A.5.1   Function

The coordinates of points on an oscilloscope trace are found and calculations performed on them. Plots are made of the computed functions.

The photograph of a typical trace for which the program is suitable is shown in figure A3.1. Points are read from the trace in D-Mac coordinates and then, using the graticule as a scale, converted to oscilloscope coordinates (relative to a chosen origin) in terms of cm or μs and mV. The functions plotted are YCØRD 1 $(= -\ln(1-I/I_\infty))$ vs t and YCØRD 2 $(= -\ln\{1-(I/I_\infty)^{\frac{1}{2}}\})$ vs t

where I is the height of the trace at time t and I_∞ is the equilibrium value of I. The former function gives a straight line if the trace is represented by $I = I_\infty (1 - \exp(-t/\tau))$ while the latter gives a straight line if $I = I_\infty (1 - \exp(-t/\tau))^2$

The program illustrates a novel use of the plotting routine: two graphs are plotted on a single pair of axes.

It is not suitable for negative values of I_∞. If all positive values of I are smaller in magnitude than I_∞, then the program

can be adapted by changing statement 11 for

11   IF(ABS(YINFP-YP(I)). LE. 0.05)G∅   T∅   26

A.5.2 The Program

```
&LIST:
   1•          DIMENSION YCORD1(610),YCORD2(610)
   2•          COMMON YP(300),XPC(310),YPC(300),YINFP,YINFPC,J,MPHOTO
   3•          EQUIVALENCE (YCORD1(301),YCORD2(1))
   4•        2 CONTINUE
   5•          CALL SCREW
   6•          READ(3,1)ISSW
   7•        1 FORMAT(I1)
   8•       10 FORMAT(15H0PHOTOGRAPH NO.,I4)
   9•          WRITE(2,10)MPHOTO
  10•          WRITE(2,19)
  11•       19 FORMAT(22H0   X-COORD-TIMES USECS,2X,26HY-COORD EXPONENTIAL GROWTH,
  12•          12X,23HY-COORD STEPWISE GROWTH)
  13•          XPC(1)=0.0
  14•          YCORD1(1)=0.0
  15•          YCORD2(1)=0.0
  16•          XPC(2)=0.0
  17•          YCORD1(2)=0.0
  18•          YCORD2(2)=0.0
  19•          WRITE(2,22)(XPC(I),YCORD1(I), YCORD2(I),I=1,2)
  20•          JX=2
  21•          DO 90 I=3,J
  22•          JX=JX+1
  23•          IF(ABS(YINFP-YP(I)).LE.0.05) GO TO 26
  24•          YCORD1(I)=-ALOG(1-YPC(I)/YINFPC)
  25•          YCORD2(I)=-ALOG(1-(YPC(I)/YINFPC)**0.5)
  26•       22 FORMAT(6X,F10.4,15X,F10.4,12X,F10.4)
  27•          WRITE(2,22)XPC(I),YCORD1(I),YCORD2(I)
  28•       90 CONTINUE
  29•       26 CONTINUE
  30•       12 FORMAT(15H PHOTOGRAPH NO.,I4)
  31•          DO 4 I=JX,300
  32•          XPC(I)=0.0
  33•          YCORD1(I)=0.0
  34•          YCORD2(I)=0.0
  35•        4 CONTINUE
  36•          CALL ORIGIN(0,0)
  37•          CALL ORIGIN(200,0)
  38•          CALL MOVE(200,1900)
  39•          CALL WAY (0,8)
  40•          WRITE(9,12)MPHOTO
  41•          CALL CENCH (1)
  42•          CALL WAY (0,4)
  43•          CALL MOVE (1200,1700)
  44•          CALL MOVE(1250,1790)
  45•       13 FORMAT (10H -LN(1-I/I)
  46•          WRITE(9,13)
  47•          CALL WAY(0,2)
  48•       14 FORMAT (3HINF)
  49•          WRITE(9,14)
  50•          CALL WAY (0,4)
```

```
51·     15 FORMAT (1H))
52·        WRITE(9,15)
53·        CALL MOVE ( 1200,1700)
54·        CALL CENCH(3)
55·        CALL MOVE(1250,1690)
56·     16 FORMAT (11H -LN(1-(1/1)
57·        WRITE(9,16)
58·        CALL WAY(0,2)
59·        WRITE(9,14)
60·        CALL WAY (0,4)
61·        WRITE(9,15)
62·        CALL MOVE(1580,1706)
63·        CALL WAY(0,2)
64·     17 FORMAT (3H1/2)
65·        WRITE(9,17)
66·        CALL MOVE(1630,1690)
67·        CALL WAY (0,4)
68·        WRITE(9,15)
69·        CALL MOVE( 200,0)
70·        CALL DRAW( 200,1600)
71·        CALL MOVE( 600,0)
72·        CALL DRAW( 600,1600)
73·        CALL MOVE(1000,0)
74·        CALL DRAW(1000,1600)
75·        CALL MOVE(1600,0)
76·        CALL DRAW(1600,1600)
77·        CALL SCALE (XPC,8.0,300,1,302)
78·        CALL SCALE(YCORD1,8.0,600,1,602)
79·        CALL AXIS (0.0,0.0,11,8.0,1.0,XPC(301),XPC(302))
80·        CALL AXIS (0.0,0.0,6,8.0,0.0,YCORD1(601),YCORD1(602))
81·        CALL LINE (XPC,YCORD1,JX,1,-1,1,310,610)
82·        CALL LINE (XPC,YCORD2,JX,1,-1,3,310,610)
83·        CALL MOVE(2500,2500)
84·     18 CONTINUE
85·        IF (ISSW.EQ.1) GO TO 2
86·        STOP
87·        END


 1·        SUBROUTINE SCREW
 2·        DIMENSION IX(300),IY(300),XT(300),YT(300),XTC(300),YTC(300)
 3·       1,XP(300),X(300),Y(300)
 4·        COMMON YP(300),XPC(310),YPC(300),YINFP,YINFPC,J,MPHOTO
 5·        READ(3,1)MPHOTO
 6·      1 FORMAT(I4)
 7·     10 FORMAT(15H0PHOTOGRAPH NO.,I4)
 8·        WRITE(2,10)MPHOTO
 9·        READ(3,3)XQ,YQ
10·      3 FORMAT(2F0.0)
11·        K=0
12·        DO 12 I=1,300
13·        K=K+1
14·        READ(3,2)IX(I),IY(I)
15·      2 FORMAT(1X,I4,2X,I4)
16·     11 IF(IX(I).EQ.0)GO TO 13
17·     12 CONTINUE
18·     13 CONTINUE
19·        J=K-1
20·        DO 14 I=1,J
21·        X(I)=IX(I)
```

```
22•         Y(I)=IY(I)
23•      14 CONTINUE
24•         THETA=ATAN((Y(2)-Y(1))/(X(2)-X(1))          )
25•         CM=SQRT ((Y(2)-Y(1))**2+(X(2)-X(1))**2)/5.0
26•      16 FORMAT(1H0,5X,5HD-MAC,12X,2HXP,8X,2HYP,8X,3HXPC,7X,3HYPC)
27•      17 FORMAT(4X,2HIX,5X,2HIY,10X,2HCM,8X,2HCM,7X,4HUSEC,6X,5HMVOLT)
28•         WRITE(2,16)
29•         WRITE(2,17)
30•       4 FORMAT(2(3X,I4))
31•         WRITE(2,4)IX(1),IY(1)
32•         WRITE(2,4)IX(2),IY(2)
33•         DO 15 I=3,J
34•         XT(I)=X(I)-X(3)
35•         XTC(I)=ABS(XT(I)*COS(THETA)+YT(I)*SIN(THETA)
36•         YT(I)=Y(I)-Y(3)
37•         YTC(I)=ABS(YT(I)*COS(THETA)-XT(I)*SIN(THETA)
38•         YP(I)=YTC(I)/CM
39•         XP(I)=XTC(I)/CM
40•         XPC(I)=XP(I)*X0
41•         YPC(I)=YP(I)*Y0
42•      20 FORMAT(2(3X,I4),3X,4F10.3)
43•         WRITE(2,20)IX(I),IY(I),XP(I),YP(I),XPC(I),YPC(I)
44•      15 CONTINUE
45•      18 FORMAT(12H0    X0=SPEED,2X,8HYQ=SENS.,3X,5HYINFP,4X,6HYINFPC)
46•       9 FORMAT(4X,7HUSEC/CM,4X,5HMV/CM,6X,2HCM,7X,5HMVOLT)
47•         WRITE(2,18)
48•         WRITE(2,9)
49•         YINF=(YTC(J)+YTC(J-1)+YTC(J-2)+YTC(J-3)+YTC(J-4))/5.0
50•         YINFP=YINF/CM
51•         YINFPC=YINFP*Y0
52•         WRITE(2,21)X0,Y0,YINFP,YINFPC
53•      21 FORMAT(4(3X,F8.4))
54•         RETURN
55•         END


 1•         SUBROUTINE LINE(X,Y,N,K,J,L,IX,IY)
 2•         DIMENSION X(IX),Y(IY)
 3•         M=0
 4•         DO 2 I=1,N,K
 5•         M=M+1
 6•         IX=IFIX(X(I))
 7•         IY=IFIX(Y(I))
 8•         IF(I.NE.1) GO TO 5
 9•         CALL MOVE(IX,IY)
10•       5 CONTINUE
11•         IF(J.GE.0) GO TO 4
12•         CALL MOVE (IX,IY)
13•         A=M/J
14•         MB=A
15•         F=A-FLOAT(MB)
16•         IF(F.GT.0.001) GO TO 2
17•         CALL CENCH (L)
18•         GO TO 2
19•       4 CALL DRAW(IX,IY)
20•         IF(J.EQ.0) GO TO 1
21•         A=M/J
22•         MB=A
23•         F=A-FLOAT(MB)
24•         IF(F.GT.0.001) GO TO 1
```

```
25•          CALL CENCH(L)
26•       1 IF((I+K).GT.N) GO TO 3
27•       2 CONTINUE
28•       3 RETURN
29•         END


 1•         SUBROUTINE SCALE(A,B,N,M,IA)
 2•         DIMENSION A(IA)
 3•         E=A(1)
 4•         D=A(1)
 5•         DO 2 I=2,N,M
 6•         IF(A(I).LT.D) D=A(I)
 7•         IF(A(I).GT.E) E=A(I)
 8•         IA=I+M
 9•       2 IF(IA.GT.N) GO TO 3
10•       3 F=E-D
11•         A(N+1)=D
12•         A(N+2)=F/B
13•         L=0
14•         DO 1 I=1,N,M
15•         L=L+1
16•         A(L)=B*(A(I)-D)/F
17•       1 A(L)=IFIX(200.*A(L))
18•         RETURN
19•         END


 1•         SUBROUTINE AXIS(A,B,NC,S,IT,PAGE,Z,ZA)
 2•         DIMENSION JX(10)
 3•         INTEGER PAGE
 4•         X1=IFIX(200.*A)
 5•         Y1=IFIX(200.*B)
 6•         X2=X1
 7•         Y2=Y1
 8•         CALL MOVE(X2,Y2)
 9•         X3=Y1+IFIX(200.*S)
10•         Y3=X1+IFIX(200.*S)
11•         F=ZA*S
12•         N=0
13•     204 IF(ABS(F)-10.)201,201,202
14•     201 IF(ABS(F).LT.1.) GO TO 203
15•         IX=Z*10.**(-N)+1.0
16•         X=IX-Z*10.**(-N)
17•         F=F*10.**N
18•         ZC=200.*X*10.**N*S/F
19•         GO TO 4
20•     202 N=N+1
21•         F=0.1*F
22•         GO TO 204
23•     203 N=N-1
24•         F=10.*F
25•         GO TO 204
26•       4 IF(IT.EQ.1) GO TO 1
27•         X2=X1
28•         Y2=X3
29•         NI=Y2
30•         MI=X2
31•         CALL DRAW(MI,NI)
32•         JA=S
```

```
33•          X2=X1
34•          Y2=Y1+ZC
35•          NI=Y2
36•          MI=X2
37•          CALL MOVE(MI,NI)
38•          X2=X1-10.
39•          Y2=Y1+ZC
40•          NI=Y2
41•          MI=X2
42•          CALL DRAW(MI,NI)
43•          X2=X1-50.
44•          Y2=Y1+ZC
45•          NI=Y2
46•          MI=X2
47•          CALL MOVE(MI,NI)
48•          CALL WAY(0,4)
49•          WRITE(9,1001) IX
50•    1001 FORMAT(I2)
51•          DO 10 IN=1,10
52•          ZC=200.•(X+FLOAT(IN))•10.••N•S/F
53•          IX=IX+1
54•          ZN=(Z+F)•10.••(-N)
55•          IF(IX.GT.ZN) GO TO 3
56•          Y2=Y1+ZC
57•          X2=X1
58•          NI=Y2
59•          MI=X2
60•          CALL MOVE(MI,NI)
61•          X2=X1-10.
62•          Y2=Y1+ZC
63•          NI=Y2
64•          MI=X2.
65•          CALL DRAW(MI,NI)
66•          X2=X1-50.
67•          Y2=Y1+ZC
68•          NI=Y2
69•          MI=X2
70•          CALL MOVE(MI,NI)
71•          WRITE(9,1001) IX
72•      10 CONTINUE
73•       1 X2=Y3
74•          Y2=Y1
75•          NI=Y2
76•          MI=X2
77•          CALL DRAW(MI,NI)
78•          JA=S
79•          X2=X1+ZC
80•          Y2=Y1
81•          NI=Y2
82•          MI=X2
83•          CALL MOVE(MI,NI)
84•          X2=X1+ZC
85•          Y2=Y1-10.
86•          NI=Y2
87•          MI=X2
88•          CALL DRAW(MI,NI)
89•          X2=X1+ZC
90•          Y2=Y1-50.
91•          MI=X2-15.
92•          NI=Y2
```

```
93•        CALL MOVE(MI,NI)
94•        CALL WAY(0,4)
95•        WRITE(9,1001) IX
96•        DO 11 IN=1,10
97•        ZC=200.•(X•IN)•10.••N•S/F
98•        IX=IX+1
99•        ZN=(Z+F)•10.••(-N)
100•       IF(IX.GT.ZN) GO TO 3
101•       X2=X1+ZC
102•       Y2=Y1
103•       MI=X2
104•       NI=Y2
105•       CALL MOVE(MI,NI)
106•       X2=X1+ZC
107•       Y2=Y1-10.
108•       NI=Y2
109•       MI=X2
110•       CALL DRAW(MI,NI)
111•       X2=X1+ZC
112•       Y2=Y1-50.
113•       NI=Y2
114•       MI=X2-15.
115•       CALL MOVE(MI,NI)
116•       WRITE(9,1001) IX
117•    11 CONTINUE
118•     3 N2=100.•S-12.•FLOAT(NC)
119•       IF(IT.EQ.0) GO TO 5
120•       N3=Y1-100.
121•       CALL WAY(0,4)
122•       N4=Y1+0.5•(200.•S-FLOAT(NC•5•4))
123•       CALL MOVE (N4,N3)
124•       LX=NC/4+1
125•   999 FORMAT(14H TIME IN USECS)
126•       WRITE(9,999)
127•       WRITE(9,1002)
128•  1002 FORMAT(10HSCALE • 10)
129•       N3=Y1-80.
130•       N4=Y1+0.5•(200.•S-FLOAT(NC•5•4))
131•       CALL WAY(0,2)
132•       WRITE(9,1003)N
133•  1003 FORMAT(I2)
134•       GO TO 7
135•     5 N3=X1-100.
136•       CALL WAY(3,4)
137•       N4=X3-0.5•(200.•S-FLOAT(NC•5•4))
138•       CALL MOVE(N3,N4)
139•       LX=NC/4+1
140•   998 FORMAT(7H Y-AXIS)
141•       WRITE(9,998)
142•       WRITE(9,1002)
143•       N3=X1-80.
144•       N4=X3-0.5•(200.•S-FLOAT(NC•5•4))
145•       CALL WAY(3,2)
146•       WRITE(9,1003)N
147•     7 RETURN
148•       END
```

A.5.3   Input Data (Tape)

The data tape is comprised of parameters punched into it and coordinates read by the D-Mac and automatically punched into the tape. The characters in inverted commas are those typed on the key board (CR LF is carriage return, line feed).

Type number of photograph, MPHØTØ, in I4 format, then "CR LF"

Type oscilloscope sweep speed µs cm^{-1}, XQ, in F0.0 format, then ","

Type oscilloscope sensitivity mV cm^{-1}, YQ, in F0.0 format, then ", CR LF"

Points then taken by D-Mac (format 1X, I4, 2X, I4)

Points 1 and 2 are on a line parallel to the x-axis a distance apart equal to 50 mm on the oscilloscope (5 graticule divisions on the photograph)

Point 3 is the chosen origin which must be on the trace (or I_∞ will be wrong) and if the plot is to go through the origin, point 3 should be where the emission starts.

Points 4 → points on the trace with the last 5 points at $I = I_\infty$ (I_∞ should not be negative with respect to the origin. Maximum number of points: 299.

Type "X0000 space Y0000   CR   LF"

Type cycle repeater, ISSW in Il format, then "CR LF"

    If ISSW = 1, the whole of the above data input is repeated

    for the next photograph.

    If ISSW $\neq$ 1, program stops.

A.5.4 Output

a) Printer Output

N.B. S preceeding a statement number means it occurs in subroutine SCREW.

J is total number of points.

Line	Statement	Format	Name	Comment	
1	S10	H			
		I4	MPHØTØ	photograph number	
2	S16	H			
3	S17	H			
4	S4	I4	IX(I)	D-Mac x-coordinate, I = 1	
		I4	IY(I)	D-Mac y-coordinate, I = 1	
5	S4	I4	IX(I)	D-Mac x-coordinate, I = 2	
		I4	IY(I)	D-Mac y-coordinate, I = 2	
6 to J+3	S20	I4	IX(I)	D-Mac x-coordinate	
		I4	IY(I)	D-Mac y-coordinate	
		F10.3	XP(I)	x-coordinate of oscilloscope trace/cm	I=3,J
		F10.3	YP(I)	y-coordinate of oscilloscope trace/cm	

Line	Statement	Format	Name	Comment
		F10.3	XPC(I)	x-coordinate of oscilloscope trace/μs
		F10.3	YPC(I)	y-coordinate of oscilloscope trace/mV
J+4	S18	H		
J+5	S9	H		
J+6	S21	F8.4	XQ	oscilloscope sweep speed/μs cm^{-1}
		F8.4	YQ	oscilloscope sensitivity/mV cm^{-1}
		F8.4	YINFP	$I_\infty/cm = \sum_{I=(J-4)}^{J} YP(I)/5$
		F8.4	YINFPC	$I_\infty/mV = \sum_{I=(J-4)}^{J} YPC(I)/5$
J+7	10	H		
		I4	MPHØTØ	photograph number
J+8	19	H		
J+9 to x	22	F10.4	XPC(I)	time/μs
		F10.4	YCØRD1(I)	YCØRD1 (see sec. A.5.5)
		F10.4	YCØRD2(I)	YCØRD2 (ditto)

The I=3,J applies to XPC(I) and YPC(I) at the top.

XPC(1), XPC(2), YCØRD1(1), YCØRD1(2), YCØRD2(1), YCØRD2(2) defined
to be 0.0 XPC(3), YCØRD1(3), YCØRD2(3) chosen to be 0.0 as they are
at the origin. x depends on the shape of the curve, calculations
stop when (YINFP - YP(I)) < 0.05 i.e. when I is close to I_∞.
If ISSW = 1, the whole of the output is repeated.

b) Plotter output

> Title - photograph number
>
> Meaning of symbols used in plotting
>
> Pair of labelled and graduated axes
>
> Four lines parallel to the y axis
>
> Points (XPC(I), YCØRD1(I)) plotted with symbol +
>
> Points (XPC(I), YCØRD2(I)) plotted with sumbol x
>
> If ISSW = 1, whole of output repeated.

A.5.5   Comments

a) Main Program

The only feature of interest is the use of the D-Mac points. The first two are used to calculate the angle of the photograph to the D-Mac table and also to scale the points. As they are not for plotting, coordinates which would be derived from them (XPC(I), YCØRD1(I), YCØRD2(I), I = 1,2) are defined as zero.

$$YCØRD1(I) = -\ln(1- YPC(I)/YINFPC) = -\ln(1- {}^{I}/I_\infty)$$
$$YCØRD2(I) = -\ln(1-(YPC(I)/YINFPC)^{\frac{1}{2}}) = -\ln\{1-({}^{I}/I_\infty)^{\frac{1}{2}}\}$$

b)   Basic Plotting Routine

This is made up of a main program and three subroutines:

SCALE, AXIS, LINE. In the conventional use, the only difference
from the subroutines as written is in AXIS.

Statement 999 has replaced

999 FØRMAT (40 H←——————40 spaces——————→)

    READ (7,999)

and statement 998 has replaced

998 FØRMAT (40 H←——————40 spaces——————→)

    READ (7,998)

Two cards are read in for each graph (after reading in the data).
The first contains the name for the x-axis and the second the name
for the y-axis. Both must be less than 40 characters long.

      The main program is constructed from:

DIMENSIØN   variables with the size of the array at least two
              greater than the number of points

READ   variables

CALL ØRIGIN (0,0) sets plotter pen at centre of paper

CALL ØRIGIN (200,0) sets origin 200 divisions (1") from L.H.S. of paper

CALL SCALE (x,w,n,k,i)

        x is the name of the array to be plotted

        w is the maximum distance in inches over which the points
        are to be plotted

        n is the number of data points in the array

        k is the repeat cycle; of k = 1, each point plotted

        i is the size of the array plus 2.

CALL SCALE (x,w,n,k,i)

for second variable to be plotted

CALL AXIS $(xa,ya,nc,sl,it,page,a,b)$

xa,ya are page coordinates in inches of the starting point of the axis relative to the origin

nc is the number of characters in the label of the axis

sl is the length of the axis in floating point inches

it: it = 1 draws x axis, it = 0 draws y axis

page: page = 0, x axis across the paper, y axis up

page = 1, axes rotated by -90°

a: a = n + 1
b: b = n + 2 $\Big\}$ n defined in subroutine SCALE

CALL AXIS $(xa,ya,nc,sl,it,page,a,b)$

for second axis

CALL LINE (x,y,n,k,j,l,i,i_2)

n,k as in SCALE

j repeat cycle for plotting

j = 0, line plot;negative j, no line just points

l CENCH symbol which is plotted $(1 \to 10)$

i_1,i_2 dimensions of arrays as in DIMENSIØN statement

STØP

END

c) Plotting Routine Modification

The plotting routine was modified so that two sets of coordinates could be plotted to the same scale on one pair of axes. In this instance, the coordinates were for two values of y (YCØRD1(I) and YCØRD2(I)) for each value of x (XPC(I)) but it can easily be extended for a more general case.

To use one scale, all values of y must be scaled together so use an equivalence statement

EQUIVALENCE (YCØRD1(301),YCØRD2(1))

   but there is only J values of each variable so it is
   necessary to set a value to the missing points; 0.0 chosen

DØ 4   I = JX,300

XPC(I) = 0.0

YCØRD1(I) = 0.0

YCØRD2(I) = 0.0

CØNTINUE

   where JX = J + 1

Scaling is for 300 values of XPC(I), 600 values of YCØRD1(I).
Plotting is of JX values of each variable so the large number of points at the origin are not plotted. Subroutine LINE is therefore called twice, once for YCØRD1 and once for YCØRD2. A second graph is plotted by trying to move the point off the R.H.S. of the paper but further up.
CALL MØVE (2500,2500) pen moves to R.H.S. of paper, $12\frac{1}{2}$ inches in
   y-direction.

Appendix B. Calculation of the Refractive Index across the

        Shock Front

    The refractive index calculated is for a typical shock wave into nitrogen with initial pressure 10 mm Hg and density ratio (ρ_2/ρ_1) of 5.5.

    The absolute refractive index (A.R.I.) of nitrogen is given as 1.000 276 at 273 K and 1 atmosphere pressure.

    Glasstone-Dale's Law states $(n-1) \alpha \rho$ where n is the refractive index of a gas with density ρ.

    Therefore the A.R.I. of the downstream gas, n_1, is given by

$$n_1 = 1 + [(n-1) \times \frac{273}{300} \times \frac{10}{760}] \qquad \text{(for a room temperature of 300 K).}$$

$$= 1.000\ 003\ 3$$

The A.R.I. of the shocked gas, n_2, is given by

$$n_2 = 1 + \frac{\rho_2}{\rho_1} (n_1 - 1)$$

$$= 1.000\ 018\ 2$$

Therefore the refractive index across the shock front (n_2/n_1) is 1.000 015.

Appendix C.   Calculation of ε/k and σ

Reference: Hirschfelder, Curtiss and Bird.[91]

For HBr, no value for ε/k was tabulated in Hirschfelder, Curtiss and Bird. It can however be derived from the two viscosity measurements available:[117]   181.9 µPoise at 18.7°C, 234.4 µPoise at 100.2°C.

A parameter, k_η, can be defined by

$$k_\eta = \frac{\eta(T_2)}{\eta(T_1)} \, (\frac{T_1}{T_2})^{\frac{1}{2}} \qquad\qquad C.1$$

k_η can hence be calculated using the above experimental data.

To a first approximation, we can use the equation for viscosity (4.28) to obtain

$$k_\eta = \frac{\Omega^{(2,2)*}(T_1^*)}{\Omega^{(2,2)*}(T_2^*)} \qquad\qquad C.2$$

By choosing a value of ε/k, values of T_1^* and T_2^* can be calculated (T_1^* and T_2^* are the values of T^* (= kT/ε) for the two temperatures of the experimental data). Hence $\Omega^{(2,2)*}$ (T_1^*) and $\Omega^{(2,2)*}$ (T_2^*) can be found from table I-M of reference 91. The value of k_η thus calculated will usually differ from that derived by using equation C.1. The process is repeated until the value of ε/k which gives the closest value is found.

A useful starting point is to take $\varepsilon/k = 1.15$ Tb where Tb

is the boiling point.

Once ε/k has been found, σ can be calculated from equation 4.28 using either experimental value for the viscosity.

A quicker method for HBr is to try a value of ε/k which is an arithmetical average for HCl and HI. When it is used to substitute values in equation C.2, the value of k_η obtained closely agrees with that derived from equation C.1 using experimental data. This was the value of ε/k used in all the calculations.

REFERENCES

1. P. Vielle, *Compt. Rend. Acad. Sci., Paris*, 129, 1228 (1899).

2. R.N. Schwartz, Z.I. Slawsky and K.F. Herzfeld, *J. Chem. Phys.*, 20, 1591 (1952).

3. T.L. Cottrell, R.C. Dobbie, J. McLain and A.W. Read, *Trans. Faraday Soc.*, 60, 241 (1964).

4. C.B. Moore, *J. Chem. Phys.*, 43, 2979 (1965).

5. A.W. Read, *Progress in Reaction Kinetics*, 3, 203, Pergamon Press Limited, Oxford (1965).

6. R.G. Gordon, W. Klemperer and J.I. Steinfeld, *Ann. Rev. Phys. Chem.*, 19, 215 (1968).

7. P. Borrell, *Transfer and Storage of Energy by Molecules, Vol. 2 Vibrational Energy* (edited by G.M. Burnett and A.M. North) Wiley-Interscience, London (1969).

8. R. Becker, *Z. Phys.*, 8, 321 (1922).

9. A.G. Gaydon and I.R. Hurle, *The Shock Tube in High Temperature Chemical-Physics*, Chapman and Hall Limited, London (1963).

10. E.F. Greene and J.P. Toennies, *Chemical Reactions in Shock Waves*, Edward Arnold Limited, London (1964).

11. J.N. Bradley, *Shock Waves in Chemistry and Physics*, Methuen and Company Limited, London (1962).

12. JANAF *Thermochemical Tables*, The Dow Chemical Company, Midland, Michigan (1965).

13.   R.A. Strehlow, *Aeronautical and Astronautical Engineering Department, Technical Report AAE 68-1*, University of Illinois (February 1968).

14.   S.H. Bauer, *Ann. Rev. Phys. Chem.*, $\underline{16}$, 245 (1965).

15.   K.F. Herzfeld and T.A. Litovitz, *Absorption and Dispersion of Ultrasonic Waves*, Academic Press, New York (1959).

16.   T.L. Cottrell and J.C. McCoubrey, *Molecular Energy Transfer in Gases*, Butterworths, London (1961).

17.   K. Takayanagi, *Prog. Theoretical Phys. (Kyoto)*, Suppl. No. 25, 1 (1963).

18.   K. Takayanagi, *Adv. Atomic and Molecular Physics*, $\underline{1}$, 149, Academic Press, New York (1965).

19.   A.B. Callear, *Appl. Optics*, Suppl. 2, 145 (1965).

20.   B. Stevens, *Collisional Activation in Gases, Vol. 3 of Topic 19 of the International Encylopedia of Phys. Chem. and Chem. Phys.*, Pergamon Press Limited, Oxford (1967).

21.   P. Borrell, *Advances in Molecular Relaxation Processes*, $\underline{1}$, 69 (1967).

22.   M. Kohler, *Z. Physik*, $\underline{125}$, 715 (1948). cf. ref. 15, p. 195.

23.   H.M. Mott-Smith, *Phys. Rev.*, $\underline{82}$, 885 (1951).

24.   K. Zoller, *Z. Phys.*, $\underline{130}$, 1 (1951).

25.   W.A. Gustafson, *Phys. of Fluids*, $\underline{3}$, 732 (1960).

26.   D. Gilbarg and D. Paolucci, *J. Rat. Mech. Anal.*, $\underline{2}$, 617 (1953).

27. W.H. Andersen and D.F. Hornig, *Molecular Physics*, 2, 49 (1959).

28. M. Linzer and D.F. Hornig, *Phys. Fluids*, 6, 1661 (1963).

29. C. Muckenfuss, *Phys. Fluids*, 5, 1325 (1962).

30. R.J. Cross Jr. and D.R. Herschbach, *J. Chem. Phys.*, 43, 3530 (1965).

31. C.A. Brau and R.M. Jonkman, *J. Chem. Phys.*, 50, 1041 (1969).

32. G. Herzberg, *Molecular Spectra and Molecular Structure. I Spectra of Diatomic Molecules*, (2nd edit.) Van Nostrand, New York (1966).

33. G.L. Pratt, *Gas Kinetics*, John Wiley and Sons Limited, London (1969).

34. L.M. Raff, *J. Chem. Phys.*, 46, 520 (1967).

35. L.M. Raff, *J. Chem. Phys.*, 47, 1884 (1967).

36. F.J. Zeleznik, *J. Chem. Phys.*, 47, 3410 (1967).

37. G.C. Berend and S.W. Benson, *J. Chem. Phys.*, 47, 4199 (1967).

38. T.G. Winter and G.L. Hill, *J. Acoust. Soc. Am.*, 42, 848 (1967).

39. E.H. Carnevale, C. Carey and G. Larson, *J. Chem. Phys.*, 47, 2829 (1967).

40. B.N. Srivastava and A.D. Gupta, *Phys. Fluids*, 9, 722 (1966).

41. C.B. Baker and N. De Haas, *Phys. Fluids*, 7, 1400 (1964).

42. C.E. Baker and R.S. Brokaw, *J. Chem. Phys.*, 40, 1523 (1964).

43. C.E. Baker and R.S. Brokaw, *J. Chem. Phys.*, 43, 3519 (1965).

44. C.E. Baker, *J. Chem. Phys.*, 46, 2846 (1967).

45. A.K. Barua, A. Manna and P. Mukhopadhyay, *J. Chem. Phys.*, 49, 2422 (1968).

46. A.J. Zmuda, *J. Acoust. Soc. Am.*, 23, 472 (1951).

47. J.G. Parker, C.E. Adams and R.M. Stavseth, *J. Acoust. Soc. Am.*, 25, 263 (1953).

48. W. Tempest and H.D. Parbrook, *Acustica*, 7, 354 (1957).

49. G. Sessler, *Acustica*, 31, 155 (1959).

50. M. Greenspan, *J. Acoust. Soc. Am.*, 31, 155 (1959).

51. Y. Fugi, R.B. Lindsay and K. Urushihara, *J. Acoust. Soc. Am.*, 35, 961 (1963).

52. R. Holmes, G.R. Jones, N. Pusat and W. Tempest, *Trans. Faraday Soc.*, 58, 2342 (1962).

53. L. O'Neil and R.S. Brokaw, *Phys. Fluids*, 6, 1675 (1963).

54. E.A. Mason, *J. Chem. Phys.*, 39, 522 (1963).

55. A.P. Malinauskas, *J. Chem. Phys.*, 44, 1196 (1966).

56. A. Tip, J. Los and A.E. de Vries, *Physica*, 35, 489 (1967).

57. D.R. Miller and R.P. Andres, *J. Chem. Phys.*, 46, 3418 (1967).

58. H.-J. Bauer and H. Kosche, *Acustica*, 17, 96 (1966).

59. M.A. Breazeale and H.O. Kneser, *J. Acoust. Soc. Am.*, 32, 885 (1960).

60. R.C. Millikan, *Chem. Soc. (London)*, Spec. Publ. 20 (1966), p. 219.

61. M.C. Henderson, *Phys. Today*, 16, No. 1, 84 (1963).

62. J.K. Bhangu, *J. Fluid Mech.*, 25, 817 (1966).

63. N.H. Johannesen, H.K. Zienkiewicz, P.A. Blythe and J.H. Gerrard, *J. Fluid Mech.*, 13, 213 (1962).

64. H.K. Zienkiewicz and N.H. Johannesen, *J. Fluid Mech.*, 17, 499 (1963).

65. J.G. Parker, *J. Chem. Phys.*, <u>45</u>, 3641 (1966).

66. P.W. Huber and A. Kantrowitz, *J. Chem. Phys.*, <u>15</u>, 275 (1947).

67. V. Blackman, *J. Fluid Mech.*, <u>1</u>, 61 (1956).

68. I.R. Hurle, *J. Chem. Phys.*, <u>41</u>, 3911 (1964).

69. I.R. Hurle, *Recent Advances in Aerothermochemistry*, Conference Proceedings 12, AGARD, Paris (1967) p. 125, 130.

70. R.C. Millikan and D.R. White, *J. Chem. Phys.*, <u>39</u>, 98 (1963).

71. B.P. Levitt and D.B. Sheen, *Chem. Soc. (London)*, Spec. Publ. <u>20</u> (1966), p. 269.

72. M.H. Windsor, N. Davidson and R. Taylor, *7th Symposium on Combustion*, Butterworths, London (1959) p. 80.

73. D.L. Matthews, *J. Chem. Phys.*, <u>34</u>, 639 (1961).

74. A.G. Gaydon and I.R. Hurle, *8th Symposium on Combustion*, Williams and Wilkins, Baltimore (1962) p. 309.

75. W.J. Hooker and R.C. Millikan, *J. Chem. Phys.*, <u>38</u>, 214 (1963).

76. R.C. Millikan, *J. Chem. Phys.*, <u>40</u>, 2594 (1964).

77. C.W. von Rosenberg, Jr., R.L. Taylor and J.D. Teare, *J. Chem. Phys.*, <u>48</u>, 5731 (1968).

78. R.C. Millikan, *J. Chem. Phys.*, <u>38</u>, 2855 (1963).

79. D.R. White, *J. Chem. Phys.*, <u>45</u>, 1257 (1966).

80. P. Borrell, *Chem. Soc. (London)*, Spec. Publ. <u>20</u> (1966) p. 263.

81. D.R. White and R.C. Millikan, *AIAA Journal*, <u>2</u>, 1844 (1964).

82. N. Basco, A.B. Callear and R.G.W. Norrish, *Proc. Roy. Soc. (London)* <u>A260</u>, 459 (1961).

83. N. Basco, A.B. Callear and R.G.W. Norrish, *Proc. Roy. Soc. (London)* A269, 180 (1962).

84. A.B. Callear, *Discussions Faraday Soc.*, 33, 28 (1962).

85. R.L. Taylor, M. Camac and R.M. Feinberg, *11th Int. Symposium on Combustion*, Berkeley, California (1966).

86. A. Euken and R. Becker, Z. *phys. Chem.*, 27B, 235 (1934).

87. C.F. Zitlau and W.M. Moore, *J. Chem. Phys.*, 49, 1255 (1968).

88. C.C. Chow and E.F. Greene, *J. Chem. Phys.*, 43, 324 (1965).

89. D. Rapp and T. Kassal, *Chem. Rev.*, 69, 61 (1969).

90. L.D. Landau and E. Teller, *Z. Phys. Sowjetunion*, 10, 34 (1936).

91. J.O. Hirschfelder, C.F. Curtiss and R.B. Bird, *Molecular Theory of Gases and Liquids*, John Wiley and Sons, Inc., (1954).

92. T.L. Cottrell and A.J. Matheson, *Trans. Faraday Soc.*, 58, 2336 (1962).

93. T.L. Cottrell and A.J. Matheson, *Trans. Faraday Soc.*, 59, 824 (1963).

94. R.C. Millikan and D.R. White, *J. Chem. Phys.*, 39, 3209 (1963).

95. Pirani-Penning Vacuum Gauge, Instructions MO7621/1, Edwards High Vacuum Limited (December 1963).

96. W. Bleakney, 159-163, *Physical Measurement in Gas Dynamics and Combustion, Vol IX High Speed Aerodynamics and Jet Propulsion*, London, Oxford University Press (1955).

97. J. Sharpe, *Dark Current in Photomultiplier Tubes*, Report C.P. 5475, E.M.I. Electronics Limited (1964).

98. Data Sheet for Photoconductive Cell RPY36, *Mullard* (May 1966).

99. F.D. Findlay and J.C. Polanyi, *Can. J. Chem.*, 42, 2176 (1964).

100. D.R. Corson and P. Lorrain, *Electromagnetic Fields and Waves*, Freeman, San Francisco (1970).

101. D.W. Holder and R.J. North, *Notes on Applied Science No. 31: Schlieren Methods*, H.M.S.O., London (1963).

102. I. Simon, *Infrared Radiation*, Van Nostrand momentum books No. 12, Princeton, N.J. (1966).

103. S.L. Ridgway, *Design Electronics*, 20 (September 1970).

104. F.A. Jenkins and H.E. White, *Fundamentals of Optics*, 3rd edit., McGraw-Hill Book Co., Inc., London (1957).

105. P. Borrell and R. Gutteridge, *Recent Advances in Aerothermochemistry*, Conference Proceedings 12, AGARD, Paris (1967).

106. P. Borrell and R. Gutteridge, *J. Chem. Phys.*, 50, 2273 (1969).

107. A.R. Fairbairn, *Proc. Roy. Soc.*, (London) Ser. A, 312, 207 (1969).

108. N.V. Sidgwick, *The Chemical Elements and their Compounds*, Oxford University Press, Oxford (1950).

109. A.C.G. Mitchell and M.W. Zemansky, *Resonance Radiation and Excited Atoms*, Cambridge University Press (1961) 2nd impression.

110. S.S. Penner, *Quantitative Molecular Spectroscopy and Gas Emissivities*, Pergamon Press, London (1959).

111. W.S. Benedict, R. Herman, G.E. Moore and S. Silverman, *J. Chem. Phys.*, 26, 1671 (1957).

112. P. Jouve, *Compt. Rend.* Ser. B 263, 155 (1966).

113.   L. Doyennette, M. Margottin-Maclou and L. Henry, *J. Chim. Phys.*, 64, 33 (1967).

114.   F. Cabré and L. Henry, *J. Chim. Phys.*, 64, 119 (1967).

115.   R.L. Belford and R.A. Strehlow, *Ann. Rev. of Phys. Chem.*, 20, 247 (1969).

116.   G.E. Millward, *Ph.D. Thesis*, Keele University, 1970.

117.   *International Critical Tables of Numerical Data, Physics, Chemistry and Technology*, Vol. V, p. 5, National Research Council of the U.S.A., McGraw-Hill Inc., New York (1929).

118.   *Landolt-Bornstein, Zahlenwerte und Funktionen aus Physik, Chemie, Astronomie, Geophysik, Technik*, p. 7, II Band, 5 Teil, Springer-Verlag, Heidelberg (1969).

119.   L. Monchick and E.A. Mason, *J. Chem. Phys.*, 35, 1676 (1961).

120.   J.W. Quinn, Res. Rept. AFCRL-64-559 (1964).

121.   W.D. Breshears and P.F. Bird, *J. Chem. Phys.*, 50, 333 (1969).

122.   M.G. Ferguson and A.W. Reed, *Trans. Faraday Soc.*, 63, 61 (1967).

123.   H.-L. Chen and C.B. Moore, *J. Chem. Phys.*, 54, 4072 (1971).

124.   J.H. Kiefer, W.D. Breshears and P.F. Bird, *J. Chem. Phys.*, 50, 3641 (1969).

125.   C.T. Bowman and D.J. Seery, *J. Chem. Phys.*, 50, 1904 (1969).

126.   F.W. de Wette and Z.I. Slawsky, *Physica*, 20, 1178 (1954).

127.   W.D. Breshears and P.F. Bird, *J. Chem. Phys.*, 52, 999 (1970).

128.   R.D. Sharma, *J. Chem. Phys.*, 50, 919 (1969).

129. H.-J. Bauer, *Physical Acoustics*, (Academic Press, London) 1965, Vol. II-A, 47.

130. Y. Sato, S. Tsuchiya and K. Kuratani, *J. Chem. Phys.*, 50, 1911 (1969).

131. H.-J. Bauer and R. Schotter, *J. Chem. Phys.*, 51, 3261 (1969).

132. W.D. Breshears and P.F. Bird, *J. Chem. Phys.*, 54, 2968 (1971).

133. B. Mahan, *J. Chem. Phys.*, 46, 98 (1967).

134. H.-L. Chen and C.B. Moore, *J. Chem. Phys.*, 54, 4080 (1971).

135. R.C. Millikan, General Electric Research Report, No. 64-RL-3700C Schenectaday, New York (July 1964).